

Nonreciprocity and noise in few-mode bosonic systems

Master Thesis



Submitted by
Danial Chughtai

Assessors
Prof. Dr. Patrick Potts
Dr. Matteo Brunelli

Department of Physics
University of Basel

July 8, 2024

“Only when a system behaves in a sufficiently random way may the difference between past and future, and therefore irreversibility, enter its description.”

– Ilya Prigogine, *Order Out of Chaos: Man’s New Dialogue with Nature*

Abstract

This thesis investigates the influence of nonreciprocity on directional transport and thermal noise in few-mode bosonic systems. A system is called nonreciprocal if transmission features are altered under an exchange of source and detector. Recent advances revealed that dissipative quantum systems can break reciprocity if coherent and dissipative interactions are balanced out, which causes destructive interference in only one transport direction. This approach generalizes the theory of cascaded quantum systems and is based on reservoir engineering, where the dissipative coupling between two resonators is achieved by the addition of an auxiliary element. This auxiliary element can be just another dissipative resonator. The underlying system is based on a minimal model of three coherently coupled dissipative resonators, subject to thermal noise, arranged in an Aharonov-Bohm ring. Similar to the Aharonov-Bohm effect, gauge-invariant phases appear in the three-mode configuration, enforcing nonreciprocal transport for nontrivial values. To investigate the role of (non)reciprocity on thermal noise, we developed a theoretical framework centered on gauge-invariant phases for bilinear systems using input-output theory. The effect of different transport limits on scattering probabilities and thermal noise at output-ports is compared across multiple linearly coupled models in the mode and quadrature basis. We show that the noise solely depends on the phases, while scattering additionally varies depending on the chosen basis. Our approach reveals that (non)reciprocity influences how noise is redistributed at outputs, and that such systems act as frequency filters for incident noise. Correlations between output-modes become complex outside the unidirectional limit, thus clearly indicating the transport regime of the system. Building on this analysis, we propose an expanded four-resonator design that offers enhanced control over directional transport. This system resembles a directional transistor with full bias-control, achieved only by tuning gauge-invariant phases. This thesis advances our understanding of nonreciprocity in bosonic systems and their influence on thermal noise. Our findings introduce new possibilities for manipulating quantum signals and noise in applications ranging from quantum information processing to quantum-limited communication networks.

Disclaimer: AI was only used to increase legibility of the text. We used DeepL Translator, ChatGPT, TeXGPT, and Claude AI, to enhance grammar, orthography and stylistic choices. Nothing in terms of the content itself was generated by any LLM or AI in general.

Contents

I. Introduction	1
II. Theoretical Background	6
A. Nonreciprocity	6
B. Review of the Aharonov-Bohm effect	6
C. States of the quantized electromagnetic field	8
1. Multi-mode number states	8
2. Coherent states	9
3. Squeezed states and two-mode squeezing	10
4. Thermal states	13
5. Gaussian states	14
D. Frequency space representation of operators	14
E. Coupling isolated systems to reservoirs - Open quantum systems	15
1. Input-output theory	15
2. The Langevin equation	19
III. System and model	21
A. Hamiltonian of the general three-cavity ring	21
1. Derivation of the interaction picture Hamiltonian	22
B. Dissipative three-cavity ring	25
1. Equations of motion for the expectation values of modes	25
2. Expressing the system in terms of synthetic fluxes	26
3. Properties of quadratic Bogoliubov-de-Gennes Hamiltonians	29
C. Quadrature representation	32
D. Heisenberg-Langevin equation in frequency space	33
E. Reservoir engineering and the nonreciprocal two-mode model	34
1. Markovian effective model via adiabatic elimination - the brute force way	35
2. Non-Markovian effective model via elimination by Fourier transforming - the gentle way	36
F. When is the system nonreciprocal?	40
1. Optical isolator - effective model without squeezing	41
2. Parametrically driven directional amplifier	42
G. Energy spectrum of the system	43
1. Energy spectrum of the dissipative ring	43
2. Energy spectrum of the optical isolator	45
IV. Scattering Matrix	46
A. Derivation of the S-Matrix using I/O theory	46
1. Differences of the S-matrix between the bases	47

B. Properties of the S-matrix and non-unitarity	48
C. Scattering behaviour of the optical isolator and maximizing power transfer	50
V. Noise and diffusion	54
A. Derivation of the output-noise	54
1. Output-noise in the quadrature basis	54
2. Output-noise in the mode basis	57
B. Analytical properties of the output-noise spectrum	60
C. Noise spectral density of the optical isolator in the mode basis	62
VI. Analysis of thermal noise and transport for selected models	65
A. Dissipative three-mode ring	65
1. S-matrix of the dissipative ring in the mode basis	65
2. S-matrix of the dissipative ring in the quadrature basis	70
3. Output-noise spectrum of the dissipative ring	73
B. Dissipative directional transistor	78
1. Scattering and noise of the directional transistor	81
VII. Discussion	84
VIII. Conclusion and further outlook	86
References	87
APPENDIX	A. 1
A. THEORETICAL BACKGROUND	A. 1
B. SYSTEM AND MODEL	B. 1
1. Isolating the gauge-invariant phases	B. 1
2. Counting the number of interactions for a general bilinear system	B. 1
3. Understanding the outer-product of non-Hermitian vectors	B. 2
4. Generalizing the transformation matrix	B. 3
5. Dynamical matrix of the dissipative ring in the quadrature representation	B. 4
6. Dynamical matrix of the optical isolator in the mode representation	B. 5
7. Dynamical matrix of the optical isolator in the quadrature representation	B. 5
8. Derivation of the energies by transforming the system to momentum space	B. 5
9. Fourier-transform and convolution theorem	B. 7
a. Proof of convolution theorem	B. 7
b. Fourier-transforming the equations of motion of the optical isolator from frequency to time	B. 7
C. S-MATRIX	C. 1
1. Proof of transformation formula	C. 1

2. Alternative way of enforcing non-Markovianity to the susceptibility matrix and the S-matrix	C. 1
3. Expressing the S-matrix in terms of damping rates	C. 2
4. Non-Markovian S-matrix for the optical isolator	C. 3
5. Scattering behaviour of the optical isolator for quadratures	C. 4
D. NOISE SPECTRAL DENSITY	D. 1
1. Explicit form of the input-correlation matrix in the quadrature basis	D. 1
2. Explicit form of the output-correlation matrix in the mode basis	D. 1
3. Proof of transformation formula between the mode and the quadrature basis of the output-noise	D. 1
4. Output-noise in the reciprocal limit of the optical isolator	D. 2
5. Output-noise spectrum of the optical isolator for quadratures	D. 2
6. Output-noise spectrum of the optical isolator for asymmetric dissipation rates	D. 3
E. DIFFUSION BEHAVIOUR OF SELECTED MODELS	E. 1
1. Dissipative three-mode ring	E. 1
a. Heatmaps of scattering probabilities for different cases	E. 1
b. S-matrix coefficients for asymmetric damping rates	E. 2
c. S-matrix coefficients in the quadrature basis	E. 3
d. Composition of the output-noise in the quadrature representation by scattering probabilities	E. 4
e. Expressing output-noise in the mode basis by elements of the quadrature representation	E. 4
f. Rectification	E. 6
2. Dissipative directional transistor	E. 7
a. Isolating the gauge-invariant phases for the directional transistor	E. 7
b. Derivation of the effective model of the transistor and explicit formulas	E. 8
c. Different scattering probabilities for the directional transistor	E. 9
d. Comparison scattering between two-ports with the noise of all ports for the directional transistor	E. 10

I. Introduction

Nonreciprocity in dissipative bosonic systems has become a pivotal concept in quantum optics, revolutionizing our way of manipulating light-matter interactions [1–4]. The classical notion, after Lorentz’s reciprocity theorem, states that the transmission features of a system remain invariant under an exchange of source and detector [5]. Recent developments demonstrate that dissipative quantum systems can violate reciprocity, establishing such systems as promising candidates for a wide range of applications in modern photonics [1, 6, 7]. The advent of nonreciprocal devices, such as isolators, circulators, and directional amplifiers, has led to significant advancements in signal processing, communication networks, and the control of signal flow [8, 9]. Building quantum analogues facilitates the operation of quantum signals, such as the readout of superconducting qubits [10], with a precision approaching fundamental limits, ideally by minimizing noise to the greatest possible extent [11, 12]. In general, transport in nonreciprocal systems can reach various operating limits, i.e. the fully symmetric *reciprocal limit*, the *unidirectional limit* with maximized directionality, or *amplification limits*. Metelmann and Clerk (2015) [1] introduced a versatile approach for designing nonreciprocal quantum systems. They proposed a model involving two coherently coupled dissipative resonators that also interact with a shared reservoir. As they illustrate, interference between coherent and suitable dissipative interactions results in nonreciprocity - a technique known as *reservoir engineering*. The strength of this approach lies in its ability to achieve nonreciprocity using only dissipative couplings without the need for a pre-designed nonreciprocal element. Hence, achieving nonreciprocity in a system still has a cost: the addition of a dissipative element. Due to its broad applicability, reservoir engineering has garnered significant attention in recent years for creating nonreciprocal quantum devices [1, 2, 13, 14]. A way the shared reservoir can be realized is via an auxiliary resonator acting as the dissipative element. The proposed model consists of three coupled dissipative resonators, which are arranged in an Aharonov-Bohm ring [15, 16]. Much like the Aharonov-Bohm effect, phase-shifts between traversable paths in a closed loop can accumulate to a single gauge-invariant phase. Tuning this phase to a non-trivial value enforces nonreciprocity. Since each of the resonators is in contact to a local thermal environment, it opens up the exploration of the system’s influence on thermal noise and directional transport in general.

The aim of this thesis is to uncover the precise impact of nonreciprocity on thermal noise, an area that has yet to be fully explored. Here we not only show that nonreciprocity redistributes noise and acts as a frequency-filter, but also that a greater control of directional transport can be achieved by expanding the system design. In order to understand nonreciprocal physics in more detail, we explored the theoretical underpinnings and implementations of nonreciprocity in different few-mode bosonic systems. Note that the presence of linear and parametric processes inside a given system vastly complicates the identification of gauge-invariant phases. To address this, we found a way to analyze these phases pictorially. This approach can become useful for understanding more extensive systems. We describe elements of our system, like the scattering matrix or the noise spectral density, in terms of these phases. This has the additional benefit of giving us a greater appreciation for intermediate values between the extremes of the reciprocal and unidirectional limits. The effect of nonreciprocity on the scattering matrix and noise was then compared across different models in the mode and the quadrature basis. This distinction in representations is particularly useful for describing parametric processes. We found that the variances of the output-noise are unaffected by our choice of basis and depend solely on the phase. This is different for scattering probabilities, which are significantly influenced by the chosen representation, especially for the reciprocal limit. Additionally, the focus on phases aids the search for a broader class of nonreciprocal systems, which was illustrated by expanding the basic three-resonator model to a four-resonator configuration. This proposed configuration not only effectively reproduces known unidirectional transport, but also offers novel limits, where any transport between a given pair of resonators can be fully suppressed - resembling a directional transistor. This four-resonator extension achieves complete bias control simply by tuning phases and without altering any other system-specific parameters like coupling strengths or dissipation rates.

Our results successfully demonstrate how the emphasis on noise and gauge-invariant phases can be used to construct more complex and sophisticated control systems [17]. Thus, we expect this thesis to motivate future research in the field of directional thermal systems and their ability to redistribute and filter noise.

This thesis is organized as follows: Section II briefly provides a theoretical background for many concepts relevant to this thesis. First, we discuss how nonreciprocity has to be understood (Sec. II A and II B), continue by presenting different ways of expressing quantum states of light (Sec. II C), and finish this Section with the input-output formalism for open systems (Sec. II E). Section III delves into theoretical underpinnings of the system itself. We do this as a step-wise addition of features, where we start at the bare isolated system and work our way up to a more faithful description of the dissipative system. First, we introduce a general time-dependent Hamiltonian of the three-mode system (Sec. III A) and demonstrate a way to (experimentally) introduce phase-shifts between interaction parameters (Sec. III A 1). This gives us the time-independent Hamiltonian for the isolated system. Then we couple resonators to reservoirs (Sec. III B) using the Heisenberg-Langevin equation, yielding equations of motion for the resonators (Sec. III B 1). The equations of motion are then expressed in terms of Aharonov-Bohm phases (Sec. III B 2), which

are compactly written using an extension of the Bogoliubov-de-Gennes formalism for open bosonic systems (Sec. III B 3). After that, we introduce the quadrature representation (Sec. III C), which is frequently used when dealing with squeezed states or two-mode squeezing interactions, and finish the three-mode model by expressing everything in frequency space (Sec. III D). Section III E introduces the effective two-mode model already known from Metelmann and Clerk (2015) [1]. This toy-model can be understood as a limit of the general three-mode model and gives us a greater appreciation for different transport limits and how to achieve maximized power-transfer. Section III F, builds up on this effective model and shows us which conditions are necessary to achieve nonreciprocal transport by (partially) decoupling one mode from other (in one direction), either for a model with only beam-splitter interactions (*optical isolator*), and another with parametric interactions (*parametrically driven directional amplifier*). Note, the provided conditions are not yet sufficient for unidirectional transport without power-loss. The last aspect of the system, see Sec. III G, takes a deeper look at the energy-spectrum of the *dissipative three-mode ring* and the optical isolator (both models are only linearly coupled). Section IV is about the scattering matrix and transmission features. First, we derive the S-matrix in Sec. IV A, and compare properties of the S-matrix for reciprocal to nonreciprocal systems, see Sec. IV B. After that, we take a look at scattering features of the optical isolator in Sec. IV C, where we find the sufficient criterion for unidirectional transport with maximized power. In Section V we derive an expression for the noise-spectral density for output-fields of the reservoir. This will give us an understanding how the system filters and redistributes thermal noise. Again, this is exemplified by the optical isolator (Sec. V C). Section VI analyzes the scattering and noise behaviour for the dissipative three-mode ring, and the four-mode extension, the *dissipative directional transistor*. The main results are discussed in Sec. VII, and the thesis is concluded in Sec. VIII, where we also provide a further outlook.

Table of symbols and results

Symbol	Definition ($\hbar = 1$). All symbols with $\tilde{\cdot}$ are in the mode-basis.
$\Re(z), \Im(z)$	Real and imaginary parts of a complex number $z \in \mathbb{C}$, defined as $\Re(z) = (z^* + z)/2$ and $\Im(z) = i(z^* - z)/2$
<i>Fourier transform conventions.</i>	
$f[\omega]$	Fourier transform of an operator-valued function $f(t)$, defined as $f[\omega] = \mathcal{F}\{f(t)\}[\omega] = \frac{1}{\sqrt{2\pi}} \int_{-\infty}^{\infty} dt f(t) e^{-i\omega t}$
$f^\dagger[\omega]$	Fourier transform of adjoint operators $f^\dagger[\omega] = \frac{1}{\sqrt{2\pi}} \int_{-\infty}^{\infty} dt f^\dagger(t) e^{-i\omega t} = (f[-\omega])^\dagger$
$\delta_{ij}, \delta(t - t')$	Kronecker delta, and Fourier transform relation of the Dirac delta function $\delta(t - t') = \frac{1}{2\pi} \int_{-\infty}^{\infty} d\omega e^{-i\omega(t-t')}$
<i>Operator representations with $i, j = 1, \dots, N$.</i>	
$a_i (a_i^\dagger)$	Bosonic annihilation (creation) operator of cavity i , with $[a_i, a_j^\dagger] = \delta_{ij}$, $[a_i, a_j] = [a_i^\dagger, a_j^\dagger] = 0$
x_i, p_i	Quadrature operators $x_i = \frac{1}{\sqrt{2}}(a_i^\dagger + a_i)$, $p_j = \frac{i}{\sqrt{2}}(a_j^\dagger - a_j)$, with $[x_i, p_j] = i\delta_{ij}$, $[x_i, x_j] = [p_i, p_j] = 0$
$\langle a \rangle$	Expectation value of an operator $\langle a \rangle = \text{Tr}\{a\rho\}$, where ρ is the density matrix of the system
<i>Three-mode system with $i \neq j = 1, 2, 3$.</i>	
J_{ij}, λ_{ij}	Beam-splitter $J_{ij} = J_{ij} e^{i\alpha_{ij}}$, and two-mode squeezing $\lambda_{ij} = \lambda_{ij} e^{i\beta_{ij}}$ amplitudes, with phase α_{ij} , and β_{ij}
H_{hop}	Beam-splitter Hamiltonian in the interaction picture $H_{\text{hop}} = J_{12}a_1^\dagger a_2 + J_{31}a_3^\dagger a_1 + J_{32}a_3^\dagger a_2 + \text{H.c.}$
H_{sq}	Two-mode squeezing Hamiltonian in the interaction picture $H_{\text{sq}} = \lambda_{12}a_1^\dagger a_2^\dagger + \lambda_{31}a_3^\dagger a_1^\dagger + \lambda_{32}a_3^\dagger a_2^\dagger + \text{H.c.}$
H_{sys}	System Hamiltonian in interaction picture $H_{\text{sys}} = H_{\text{hop}} + H_{\text{sq}}$
$\Phi, \vartheta_1, \vartheta_2$	Gauge-invariant phases $\Phi \equiv \alpha_{12} + \alpha_{31} - \alpha_{32} \pmod{2\pi}$, $\vartheta_1 \equiv \beta_{12} - \beta_{31} + \alpha_{32} \pmod{2\pi}$, $\vartheta_2 \equiv -\beta_{12} - \alpha_{31} + \beta_{32} \pmod{2\pi}$
κ_i	Damping rate of the cavity i to its respective reservoir
$\phi_{\text{R,L}}$	Maximally nonreciprocal values of the gauge-invariant phase Φ with $\phi_{\text{R,L}} \equiv \pm \frac{\pi}{2} \pmod{2\pi}$
ϕ_0	Reciprocal values of the gauge-invariant phase Φ with $\phi_0 \in \{0, \pm\pi\} \pmod{2\pi}$
<i>Bogoliubov-de-Gennes extension for open systems with N modes.</i>	
Λ_i	Extended Pauli matrices $\Lambda_i = \sigma_i \otimes \mathbb{1}_N$, with $i = x, y, z$
\mathbf{a}	Vector of bosonic operators $\mathbf{a} \equiv (a_1, \dots, a_N, a_1^\dagger, \dots, a_N^\dagger)^T$
\mathbf{a}^\dagger	Adjoint vector $\mathbf{a}^\dagger \equiv (a_1^\dagger, \dots, a_N^\dagger, a_1, \dots, a_N)$, the vector fulfills $[\mathbf{a}_i, \mathbf{a}_j^\dagger] = (\Lambda_z)_{ij}$, $[\mathbf{a}_i, \mathbf{a}_j] = i(\Lambda_y)_{ij}$
\mathbf{a}^\ddagger	Column vector with adjoint elements $\mathbf{a}^\ddagger \equiv \Lambda_x \mathbf{a}$
\mathbf{H}	Hamiltonian matrix in BdG form $\mathbf{H} = \begin{pmatrix} \mathbf{h}_1 & \mathbf{h}_2 \\ \mathbf{h}_2^* & \mathbf{h}_1^* \end{pmatrix}$, with $\mathbf{h}_1 = \begin{pmatrix} 0 & J_{12} & J_{31}^* \\ J_{12}^* & 0 & J_{32}^* \\ J_{31} & J_{32} & 0 \end{pmatrix}$, and $\mathbf{h}_2 = \begin{pmatrix} 0 & \lambda_{12} & \lambda_{31} \\ \lambda_{12} & 0 & \lambda_{32} \\ \lambda_{31} & \lambda_{32} & 0 \end{pmatrix}$
\mathbf{A}	Dynamical matrix of the closed system $\mathbf{A} = -i\Lambda_z \mathbf{H}$
$\tilde{\mathbf{K}}$	Matrix of damping rates $\tilde{\mathbf{K}} = \mathbb{1}_2 \otimes \text{diag}(\kappa_1, \dots, \kappa_N)$
\mathbf{D}	Dynamical matrix of the open system $\mathbf{D} = \mathbf{A} - \frac{1}{2}\tilde{\mathbf{K}}$
\mathbf{v}	Vector of quadrature operators $\mathbf{v} = (x_1, p_1, \dots, x_N, p_N)^T$, the vector fulfills $[\mathbf{v}_i, \mathbf{v}_j] = i\Omega_{ij}$, with $\Omega = \mathbb{1}_N \otimes i\sigma_y$
\mathbf{T}	Unitary transformation matrix between mode and quadrature basis, with $\mathbf{v} = \mathbf{T} \mathbf{a}$
\mathbf{M}	Dynamical matrix of the open system in the quadrature representation $\mathbf{M} = \mathbf{T} \mathbf{D} \mathbf{T}^\dagger$

Symbol	Definition ($\hbar = 1$). All symbols with $\tilde{\cdot}$ are in the mode-basis.
<i>Effective two-mode model.</i>	
J, λ	Interaction parameters $J := J_{12}$, $\lambda := \lambda_{12}$
u_j, v_j, μ, ν	Effective unit-less interaction strengths $u_j := J_{3j}/J$, $v_j := \lambda_{3j}/J$, $\mu = v_1 v_2^* - u_2 u_1^*$, $\nu = v_1 u_2^* - v_2 u_1^*$
$ \mu_{1,2} , \nu_{1,2} $	Abbreviations $ \mu_1 := \lambda_{31} \lambda_{32} $, $ \mu_2 := J_{32} J_{31} $, and $ \nu_1 := \lambda_{31} J_{32} $, $ \nu_2 := \lambda_{32} J_{31} $
$\Gamma[\omega]$	Non-Markovian effective reservoir $\Gamma[\omega] := 2 J ^2/(i\omega + \kappa_3/2)$, here $\Gamma_0 \equiv \Gamma[0] = 4 J ^2/\kappa_3$ is the Markovian limit
$\Gamma_j[\omega]$	Scaled effective reservoir $\Gamma_j[\omega] := \Gamma[\omega](u_j ^2 - v_j ^2)$
\mathbf{a}_{eff}	Vector of bosonic modes in the effective model $\mathbf{a}_{\text{eff}} = (a_1, a_2, a_1^\dagger, a_2^\dagger)^T$
\mathbf{v}_{eff}	Vector of quadratures in the effective model $\mathbf{v}_{\text{eff}} = \mathbf{T}_{\text{eff}} \mathbf{a}_{\text{eff}}$, where \mathbf{T}_{eff} is the effective transformation matrix
$\mathbf{A}_{\text{eff}} (\mathbf{D}_{\text{eff}}[\omega])$	Dynamical matrix of the closed (open) effective model
$\mathbf{M}_{\text{eff}}[\omega]$	Dynamical matrix of the open effective model in the quadrature basis, with $\mathbf{M}_{\text{eff}}^*[0] = \mathbf{M}_{\text{eff}}[0]$ only for $\omega = 0$
$\vartheta_{1,\mp}, \vartheta_{1,0}$	Nonreciprocal limits for the phase ϑ_1 with $\vartheta_{1,\mp} \equiv \mp \frac{\pi}{2} \pmod{2\pi}$, and phase-sensitive quasi-reciprocal limits $\vartheta_{1,0} \in \{0, \pm\pi\} \pmod{2\pi}$, for the parametrically driven amplifier
<i>Energy spectrum.</i>	
H_k	Diagonal Hamiltonian in momentum space of the dissipative ring (with $N = 3$) $H_k = \sum_{m=0,\pm 1} \bar{\omega}_m b_m^\dagger b_m$, with energies $\bar{\omega}_m = \sum_m 2 J \cos((\Phi - 2\pi m)/3)$, quasi-momentum eigenstates $b_m^\dagger = \frac{1}{\sqrt{N}} \sum_j e^{i\frac{2\pi m j}{3}} a_j^\dagger$
\mathbf{H}_k	Diagonal Hamiltonian matrix in momentum space
\mathbf{A}_k	Diagonal dynamical matrix of the closed system $\mathbf{A}_k = -i\mathbf{\Lambda}_z \mathbf{H}_k = -i \text{diag}(\bar{\omega}_{-1}, \bar{\omega}_0, \bar{\omega}_1, -\bar{\omega}_{-1}, -\bar{\omega}_0, -\bar{\omega}_1)$
\mathbf{D}_k	Diagonal dynamical matrix of the open system $\mathbf{D}_k = \mathbf{A}_k - \frac{1}{2}\tilde{\mathbf{K}}$
<i>Scattering matrix.</i>	
$\mathbf{a}_{\text{in}}[\omega], \mathbf{a}_{\text{out}}[\omega]$	Reservoir input/output field vector in the mode basis
$\mathbf{v}_{\text{in}}[\omega], \mathbf{v}_{\text{out}}[\omega]$	Reservoir input/output field vector in the quadrature basis
$\tilde{\chi}[\omega]$	Susceptibility matrix in mode basis $\tilde{\chi}[\omega] = (i\omega \mathbf{1} - \mathbf{D})^{-1}$, with $\tilde{\chi}^*[\omega] = \mathbf{\Lambda}_x \tilde{\chi}[-\omega] \mathbf{\Lambda}_x$
$\chi[\omega]$	Susceptibility matrix in quadrature basis $\chi[\omega] = (i\omega \mathbf{1} - \mathbf{M})^{-1}$, with $\chi^*[\omega] = \chi[-\omega]$
	Basis transform $\tilde{\chi}[\omega] = \mathbf{T}^\dagger \chi[\omega] \mathbf{T}$
$\tilde{\mathbf{S}}[\omega]$	S-matrix in mode basis $\tilde{\mathbf{S}}[\omega] = \mathbf{1} - \sqrt{\tilde{\mathbf{K}}} \tilde{\chi}[\omega] \sqrt{\tilde{\mathbf{K}}}$, with $\mathbf{a}_{\text{out}}[\omega] = \tilde{\mathbf{S}}[\omega] \mathbf{a}_{\text{in}}[\omega]$, and $\tilde{\mathbf{S}}^*[\omega] = \mathbf{\Lambda}_x \tilde{\mathbf{S}}[-\omega] \mathbf{\Lambda}_x$
	Note, $\mathbf{a}_{\text{out}}^\dagger[\omega] = \mathbf{a}_{\text{in}}^\dagger[\omega] \tilde{\mathbf{S}}^\dagger[-\omega]$, and $\mathbf{a}_{\text{out}}^\dagger[\omega] = \tilde{\mathbf{S}}^*[-\omega] \mathbf{a}_{\text{in}}^\dagger[\omega]$
$\mathbf{S}[\omega]$	S-matrix in quadrature basis $\mathbf{S}[\omega] = \mathbf{1} - \sqrt{\tilde{\mathbf{K}}} \chi[\omega] \sqrt{\tilde{\mathbf{K}}}$, with $\mathbf{S}^*[\omega] = \mathbf{S}[-\omega]$
	Basis transform $\tilde{\mathbf{S}}[\omega] = \mathbf{T}^\dagger \mathbf{S}[\omega] \mathbf{T}$
$\mathbf{S} = \mathbf{S}^T$	Symmetric S-matrix for an reciprocal system
\mathcal{C}_j	Cooperativity $\mathcal{C}_j \equiv \Gamma_j[0]/\kappa_j$
$\Gamma_j[0] = \kappa_j$	Impedance matching condition $\Gamma_j[0] = \kappa_j \implies 4 J_{3j} ^2 = \kappa_j \kappa_3$
<i>Noise and Diffusion.</i>	
\bar{n}_j	Temperature-dependent Bose-Einstein occupations of the input-modes
\mathbf{n}_{th}	Vector of thermal occupations in the quadrature basis $\mathbf{n}_{\text{th}} \equiv (\bar{n}_1, \bar{n}_1, \dots, \bar{n}_N)^T$

Symbol	Definition ($\hbar = 1$). All symbols with $\tilde{\cdot}$ are in the mode-basis.
$\mathbf{C}_{\text{non-sym}}$	Non-symmetrized covariance matrix for quadratures $\mathbf{C}_{\text{non-sym}} = \langle\langle \mathbf{v}\mathbf{v}^T \rangle\rangle \equiv \langle \mathbf{v}\mathbf{v}^T \rangle - \langle \mathbf{v} \rangle \langle \mathbf{v}^T \rangle$
\mathbf{C}_{sym}	Sym. covariance matrix $\mathbf{C}_{\text{sym}} = \frac{1}{2}(\mathbf{C}_{\text{non-sym}} + \mathbf{C}_{\text{non-sym}}^T)$
$\mathbf{C}_{\text{in}}^{\text{non-sym}}[\omega, \omega']$	Non-sym. input-covariance matrix $\mathbf{C}_{\text{in}}^{\text{non-sym}}[\omega, \omega'] = \langle\langle \mathbf{v}_{\text{in}}[\omega] \mathbf{v}_{\text{in}}^T[\omega'] \rangle\rangle$
$\mathcal{S}_{\text{in}}^{\text{non-sym}}$	Non-sym. input-noise with $\mathbf{C}_{\text{in}}^{\text{non-sym}}[\omega, \omega'] = \delta(\omega + \omega') \mathcal{S}_{\text{in}}^{\text{non-sym}}$, and $\mathcal{S}_{\text{in}}^{\text{non-sym}} = \bigoplus_{j=1}^N [(\bar{n}_j + \frac{1}{2}) \mathbf{1}_2 - \frac{1}{2} \sigma_y]$
$\mathbf{C}_{\text{in}}[\omega, \omega']$	Input-covariance $\mathbf{C}_{\text{in}}[\omega, \omega'] = \delta(\omega + \omega') \mathcal{S}_{\text{in}}(\mathbf{n}_{\text{th}})$
$\mathcal{S}_{\text{in}}(\mathbf{n}_{\text{th}})$	Input-noise $\mathcal{S}_{\text{in}}(\mathbf{n}_{\text{th}}) = \bigoplus_{j=1}^N (\bar{n}_j + \frac{1}{2}) \mathbf{1}_2$
$\mathbf{C}_{\text{out}}[\omega, \omega']$	Output-covariance $\mathbf{C}_{\text{out}}[\omega, \omega'] = \delta(\omega + \omega') \mathcal{S}_{\text{out}}[\omega]$
$\mathcal{S}_{\text{out}}[\omega]$	Output-noise $\mathcal{S}_{\text{out}}[\omega] = \Re\{\mathbf{S}[\omega] \mathcal{S}_{\text{in}} \mathbf{S}^\dagger[\omega]\}$
\mathcal{S}_0	Vacuum-input $\mathcal{S}_0 \equiv \mathcal{S}_{\text{in}}[0] = \mathbf{1}_{2N}/2$
\mathcal{S}_{vac}	Vacuum-output $\mathcal{S}_{\text{vac}} = \mathcal{S}_0$
$\mathcal{S}_{\text{th}}[\omega]$	Thermal-output $(\mathcal{S}_{\text{th}}[\omega])_{ij} = \sum_k^{2N} \bar{n}_{\lceil k/2 \rceil} \Re\{(\mathbf{S}[\omega])_{ik} (\mathbf{S}^\dagger[\omega])_{kj}\}$
$\tilde{\mathbf{C}}_{\text{in}}[\omega, \omega']$	Input-covariance $\tilde{\mathbf{C}}_{\text{in}}[\omega, \omega'] = \frac{1}{2} \langle\langle \{\mathbf{a}_{\text{in}}[\omega], \mathbf{a}_{\text{in}}^\dagger[\omega']\} \rangle\rangle$ in the mode basis
$\tilde{\mathcal{S}}_{\text{in}}$	Input-noise $\tilde{\mathcal{S}}_{\text{in}} = \left[\bigoplus_{j=1}^N (\bar{n}_j + \frac{1}{2}) \right] \otimes \mathbf{1}_2$ in the mode basis
$\tilde{\mathbf{C}}_{\text{out}}[\omega, \omega']$	Output-covariance $\tilde{\mathbf{C}}_{\text{out}}[\omega, \omega'] = \delta(\omega + \omega') \tilde{\mathcal{S}}_{\text{out}}[\omega]$ in the mode basis
$\tilde{\mathcal{S}}_{\text{out}}[\omega]$	Output-noise $\tilde{\mathcal{S}}_{\text{out}}[\omega] = \frac{1}{2} (\tilde{\mathbf{S}}[\omega] \tilde{\mathcal{S}}_{\text{in}} \tilde{\mathbf{S}}^\dagger[\omega] + \tilde{\mathbf{S}}[-\omega] \tilde{\mathcal{S}}_{\text{in}} \tilde{\mathbf{S}}^\dagger[-\omega])$ in the mode basis
$\mathcal{S}_{a_i^\dagger a_j}[\omega]$	Element of the output-noise $\mathcal{S}_{a_i^\dagger a_j}[\omega] \equiv (\tilde{\mathcal{S}}_{\text{out}}[\omega])_{ij} = (\tilde{\mathcal{S}}_{\text{out}}[\omega])_{ji}$, with $\mathcal{S}_{a_i^\dagger a_j}[\omega] = \mathcal{S}_{a_j a_i^\dagger}[\omega]$
$\tilde{\xi}_{a_i a_j}[\omega]$	Scattering rectification $\tilde{\xi}_{a_i a_j}[\omega] = (\tilde{\mathbf{S}}_{a_j a_i} ^2 - \tilde{\mathbf{S}}_{a_i a_j} ^2) / (\tilde{\mathbf{S}}_{a_j a_i} ^2 + \tilde{\mathbf{S}}_{a_i a_j} ^2)$ in the mode basis
$\tilde{\zeta}_{ij}[\omega]$	Noise rectification $\tilde{\zeta}_{ij}[\omega] = (\tilde{\mathcal{S}}_{a_i^\dagger a_i}^{\text{out}} ^2 - \tilde{\mathcal{S}}_{a_j^\dagger a_j}^{\text{out}} ^2) / (\tilde{\mathcal{S}}_{a_i^\dagger a_i}^{\text{out}} ^2 + \tilde{\mathcal{S}}_{a_j^\dagger a_j}^{\text{out}} ^2)$ in the mode basis
<i>Dissipative directional transistor</i>	
H_{T}	Hamiltonian of the directional transistor $H_{\text{T}} = J_{12} a_1^\dagger a_2 + J_{31} a_3^\dagger a_1 + J_{32} a_3^\dagger a_2 + J_{41} a_4^\dagger a_1 + J_{42} a_4^\dagger a_2 + J_{43} a_4^\dagger a_3 + \text{H.c.}$
\mathbf{a}_{T}	Vector of bosonic modes $\mathbf{a}_{\text{T}} := (a_1, \dots, a_4, a_1^\dagger, \dots, a_4^\dagger)^T$
$\tilde{\mathbf{A}}_{\text{T}}$	Dynamical matrix of the isolated system $\tilde{\mathbf{A}}_{\text{T}} = -i \mathbf{\Lambda}_z \mathbf{H}_{\text{T}}$
$\tilde{\mathbf{K}}_{\text{T}}$	Damping rate matrix $\tilde{\mathbf{K}}_{\text{T}} = \mathbf{1}_2 \otimes \text{diag}(\kappa_1, \dots, \kappa_4)$
$\tilde{\mathbf{D}}_{\text{T}}$	Dynamical matrix of the open system $\tilde{\mathbf{D}}_{\text{T}} = \tilde{\mathbf{D}}_{\text{T}} - \frac{1}{2} \tilde{\mathbf{K}}_{\text{T}}$
τ_1, τ_2, τ_3	Gauge-invariant phases $\tau_1 = \alpha_{31} - \alpha_{41} + \alpha_{43} \pmod{2\pi}$, $\tau_2 = -\alpha_{32} + \alpha_{42} - \alpha_{43} \pmod{2\pi}$, and $\tau_3 = \alpha_{12} + \alpha_{41} - \alpha_{42} \pmod{2\pi}$
$ \delta $	Effective coupling strength $ \delta := J_{12} $
$\chi_i[\omega]$	Effective susceptibility to the auxiliary reservoirs $\chi_i[\omega] := 1/(i\omega + \kappa_i/2)$, with $i = 3, 4$
$\bar{\chi}[\omega]$	Shared effective susceptibility $\bar{\chi}[\omega] := \chi_3[\omega] \chi_4[\omega]$
$\bar{d}[\omega]$	Unit-less scaling factor $\bar{d}[\omega] := 1/(1 + \bar{\chi}[\omega] J_{43} ^2)$
$\lambda_1[\omega], \lambda_2[\omega]$	Dissipative interaction parameters $\lambda_1[\omega] := \chi_3[\omega] \bar{d}[\omega] J_{31} J_{32} $, and $\lambda_2[\omega] := \chi_4[\omega] \bar{d}[\omega] J_{41} J_{42} $ (analogous to $\Gamma[\omega]$ of the optical isolator)
$\mu_1[\omega], \mu_2[\omega]$	Effective renormalized interaction parameters $\mu_1[\omega] := \bar{d}[\omega] J_{31} J_{42} J_{43} $, and $\mu_2[\omega] := \bar{d}[\omega] J_{41} J_{32} J_{43} $
$\bar{\sigma}_i[\omega]$	Effective interaction strength of the complex damping rate $\bar{\sigma}_i[\omega] := 2\bar{\chi}[\omega] \bar{d}[\omega] J_{3i} J_{4i} J_{43} $, with $i = 1, 2$
$\bar{\gamma}_i[\omega]/2$	Effective damping rate $\bar{\gamma}_i[\omega]/2 := (\kappa_i + 2\chi_3[\omega] \bar{d}[\omega] J_{3i} ^2 + 2\chi_4[\omega] \bar{d}[\omega] J_{4i} ^2)/2$, with $i = 1, 2$
$\bar{\chi}[0] = 1$	Impedance matching condition $\bar{\chi}[0] = 1 \implies \kappa_3 \kappa_4 = 4$ in units of $\kappa \equiv \kappa_i/2$, with $i = 1, \dots, 4$

II. Theoretical Background

In the following, we will lay down a succinct and brief introduction to many theoretical concepts relevant to this thesis. This will specify a common ground of the optical properties of open systems in general and help us to further expand our understanding of nonreciprocity in later Sections.

A. Nonreciprocity

“What is Nonreciprocity?” is the first question we need to consider in this thesis. Luckily for us, this is also the title of the publication from Caloz *et al.* [18]. Etymologically, *nonreciprocity* is the lack of *reciprocity*, having Latin roots in the word *reciprocus* [18]. Here, two prefixes *re-* (backwards) and *pro-* (forward) give rise to *reque proque*, meaning “going backward as forward” [18]. Thus, as Ref. [18] explains, “A *nonreciprocal/reciprocal system is defined as a system that exhibits different/same received-transmitted field ratios when its source(s) and detector(s) are exchanged*”. The notion of *ratios* is very useful for us, since we consider open systems in this work, and (non)reciprocity can be adequately characterized by ratios of scattering probabilities. This sounds awfully similar to time-reversal symmetry (breaking) [18–22] at first, however, there is some nuance to it. As Caloz *et al.* [18] and Carminati *et al.* [20] both point out, the concepts *reciprocity* and *time-reversal symmetric* are indifferent for closed systems. Nonetheless, both publications mention the sufficiently confusing discussion about the precise definition of reciprocity in open systems. As both explain, an open system can be reciprocal, while still being able to break time-reversal symmetry. However, we will defer from that particular detail and just use the definition of reciprocity provided above, where transport between given ports remains invariant upon an exchange of source and detector, see Fig 1.

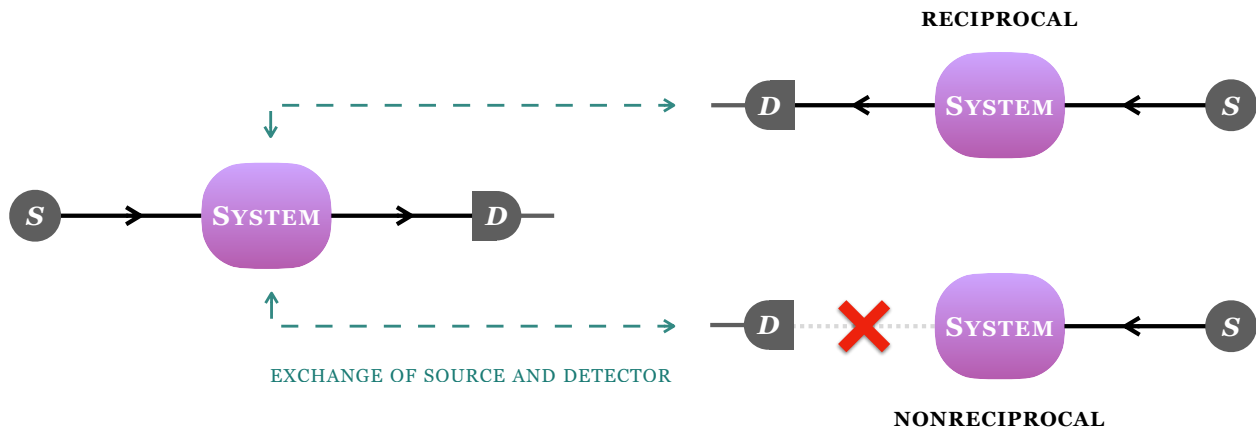


FIG. 1. Comparison between a reciprocal and a nonreciprocal system. In the left figure, a source (S) sends out a signal and meets a detector (D) after interacting with the system. Upon change of source and detector (teal dashed lines), a reciprocal system will behave the same (upper right), whereas a nonreciprocal system has either partially suppressed (grey dashed lines), fully suppressed (red crosses) or amplified transport in the opposite direction (lower right).

B. Review of the Aharonov-Bohm effect

To understand nonreciprocal transport, we will first review the Aharonov-Bohm (AB) effect. The Aharonov-Bohm effect, initially proposed as a thought experiment in the seminal paper *Significance of Electromagnetic Potentials in the Quantum Theory* by Y. Aharonov and D. Bohm in 1959 [15], represents a pivotal moment in the understanding of quantum mechanics. This theoretical prediction, which shows the physical significance of electromagnetic potentials, was experimentally verified by Peshkin in 1989 [16]. The publication by Aharonov and Bohm sparked considerable debate, initially questioning the effects validity and subsequently exploring its practical implications [16, 23–25]. There is even substantial philosophical literature on the AB effect, mainly focused on the nature of *non-locality* and “*reality*” of physical quantities, see Liu [26]. Today, the Aharonov-Bohm effect can be seen as a special case of a broader class of physical theories, namely, the study of geometric phases and topology in physics. Note, that the following is based upon the book by Lancaster and Blundell [27].

To understand this thought experiment, we consider a modified double slit experiment, see Fig. 2. A coherent beam of particles, where $|\Psi\rangle$ is the state of a particle with charge q , are emitted from a source S . The beam is then split into two distinct parts $|\Psi_1\rangle$ and $|\Psi_2\rangle$, before coming together at the detector D , measuring their interference pattern. A thin, long solenoid, with a constant magnetic flux Φ_B , is placed after the double slit and between the two beams. There is no magnetic field outside the solenoid. Thus, the particles never experience the magnetic field. Surprisingly, the presence of the magnetic field does change the interference pattern at the detector! So why does this effect occur? There are several ways to understand this, but we can just look at the probabilities to understand it in an effective manner: The probability to measure the state in a double-split experiment is given by the modulus squared

$$|\Psi|^2 = |\Psi_1|^2 + |\Psi_2|^2 + (\langle\Psi_1|\Psi_2\rangle + \langle\Psi_2|\Psi_1\rangle), \quad (2.1)$$

where the latter two terms are the interference terms of the waves at the detector D . Not the magnetic field $\mathbf{B} = \nabla \times \mathbf{A}$ itself, but its vector potential \mathbf{A} shifts the phases of the propagating waves. This is since plane-waves $|\Psi_{1,2}\rangle \propto e^{i\mathbf{p}\mathbf{r}}$, and \mathbf{A} change the momentum $\mathbf{p} \rightarrow \mathbf{p} - q\mathbf{A}$. This implies, that $|\Psi_{1,2}\rangle$ acquires an additional phase $|\Psi_{1,2}\rangle \rightarrow |\tilde{\Psi}_{1,2}\rangle \equiv e^{i\alpha_{1,2}}|\Psi_{1,2}\rangle$, where $\alpha_{1,2} = -\frac{q}{\hbar} \int \mathbf{A} \cdot d\mathbf{r}$. Now, one could think that this problem could be just *gauged away* by applying $\mathbf{A} \rightarrow \mathbf{A} + \nabla\chi$. However, since we are interested in the phase difference between the paths, namely $\delta \equiv \alpha_1 - \alpha_2$, it implies

$$\delta = \alpha_1 - \alpha_2 = -\frac{q}{\hbar} \int_{S \rightarrow 1 \rightarrow D} \mathbf{A} \cdot d\mathbf{r} + \frac{q}{\hbar} \int_{S \rightarrow 2 \rightarrow D} \mathbf{A} \cdot d\mathbf{r} = \frac{q}{\hbar} \oint \mathbf{A} \cdot d\mathbf{r}, \quad (2.2)$$

where the last integral is evaluated anticlockwise around the trajectories. Since the path is a closed circle, Stokes' theorem gives us

$$\delta = \frac{q}{\hbar} \oint \mathbf{A} \cdot d\mathbf{r} = \frac{q}{\hbar} \int \nabla \times \mathbf{A} \cdot d\mathbf{S} = \frac{q}{\hbar} \int \mathbf{B} \cdot d\mathbf{S} = \frac{q}{\hbar} \Phi_B, \quad (2.3)$$

where the result $\delta = \frac{q}{\hbar} \Phi_B$ is in units of the flux quantum [28]. Applying a gauge transformation does not save us from this effect, since the shift of the vector potential vanishes $\oint \nabla\chi \cdot d\mathbf{r} = 0$. This means, that even though the particles see no explicit magnetic field, there still appears a *gauge invariant* local phase between the paths, which changes the interference pattern. Calculating the probabilities of the new waves gives us

$$|\Psi|^2 = |\Psi_1|^2 + |\Psi_2|^2 + 2|\Psi_1||\Psi_2| \cos \delta, \quad (2.4)$$

where the interference pattern is now shifted by the phase $\delta = \frac{q}{\hbar} \Phi_B$.

All considerations we have made thus far hold only for charged particles, which are influenced by a magnetic vector potential. Nonetheless, similar effects can even occur without *physically observable* magnetic fields for chargeless particles such as photons. As already mentioned, Aharonov-Bohm phases are today understood as a specific instance of more generalized phases. These so-called *geometric (Berry) phases* have become a recurring area of interest, as they can explain the occurrence and the impact of topological defects in systems, most famously for the quantum Hall effect [29, 30]. To understand how gauge-invariant phases arise in our system, we make a quick remark about geometric

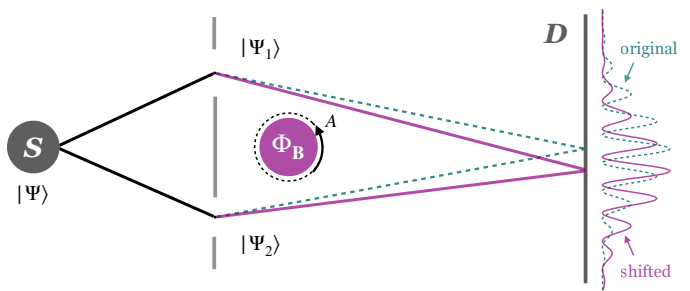


FIG. 2. Schematic of the Aharonov-Bohm effect. A split beam of particles with charge q is sent from the source S to the detector D . An encapsulated solenoid with constant magnetic flux Φ_B shifts the interference pattern at the detector, even though the beams feel no magnetic field, as $\mathbf{B} = 0$ outside the solenoid. The interference pattern is shifted due to the vector potential $\mathbf{A} \neq 0$ creating a phase difference $\delta = \frac{q}{\hbar} \Phi_B$ between the paths.

phases, see Refs. [31, 32]. For this, consider a cyclic adiabatic evolution of a Hamiltonian in some parameter-space. This evolution can lead to a gauge-dependent *Berry potential*. Since this potential is gauge-dependent (and can be simply *gauged away*), it is not physically observable. This artificial potential then gives rise to an artificial magnetic monopole, close in spirit to the physical observable magnetic field of the AB effect. However, integrating the Berry potential over a closed path yields gauge-independent geometric phases, which are observable and change the topology of the system for appropriate non-trivial values. Even though geometric phases are more general than AB phases, there is still a common theme for both, which applies to our system: *Since our resonators have multiple interactions that form closed paths, excitations traversing these interactions pick up relative phase-shifts, which accumulate to gauge-invariant phases. These then enforce nonreciprocal transport for non-trivial values.* The specifics for this will be touched upon in Section III B 2 and III F.

C. States of the quantized electromagnetic field

In this section, we briefly introduce states of the quantized electromagnetic field that are appropriate for expressing optical fields. For a single-mode (monochromatic) field, dynamics can be described using *Fock (number) states* [33], which are eigenstates of the quantum harmonic oscillator [33]. If the system would be in contact with a finite-temperature reservoir, we could adequately describe the dynamics using single-mode *thermal states* (after reaching thermal equilibrium) [34]. Note, that multi-mode fields can be expressed using number states. Nonetheless, since most optical fields are either superposed or mixed number states, we can find a different way of expressing such fields. A suitable description are *coherent states*, which have an indefinite number of photons. However, they have an important property, making them very suitable for describing quantized light fields: Coherent states equally minimize the Heisenberg uncertainty in amplitude and phase, which makes them the closest analogues to classical electromagnetic fields, with the lowest amount of quantum noise in phase space. Coherent states are already sufficient for many applications and are frequently used in Laser physics [33, 34]. However, this is not the end of the story. For this, consider the uncertainty relation $\sigma_A \sigma_B \geq \hbar/2$ for two self adjoint operators \hat{A} and \hat{B} . This formula has only one requirement: That the *product* of their standard deviations is subject to a lower bound. Therefore, one can consider a broader class of uncertainty-minimizing states, where the uncertainty in one observable is reduced at the expense of an increased uncertainty in the other, while the integrity of the uncertainty relation is still maintained. These more general states are called *squeezed states*, which can be used for precise quantum measurements, as they reduce the amount of noise below the standard “shot noise limit” of the vacuum state [35]. All states mentioned above (except non-vacuum number states), can be classified as *Gaussian states*, which are frequently used in the context of quantum optics and offer useful statistical properties, see Refs. [35, 36]. Thus, the last part of this section about field quantization will be dedicated on the physics of Gaussian states.

To define minimal-uncertainty coherent states, it is useful to first take a look at number states. Note, that the subsequent sections roughly follow Meystre [34], and Walls and Milburn [33].

1. Multi-mode number states

Consider a cavity, enclosed by lossless reflecting mirrors, where we want to quantize a multi-mode field. Using Maxwell’s equations, we can find the Hamiltonian of this system, expressed as a sum of N single-mode harmonic oscillators

$$\hat{H} = \sum_s^N \hat{H}_s, \quad \text{with} \quad \hat{H}_s = \hbar\omega_s \left(\hat{a}_s^\dagger \hat{a}_s + \frac{1}{2} \right), \quad (2.5)$$

where ω_s is the frequency of a single-mode field, \hat{a}_s^\dagger (\hat{a}_s) are *creation (annihilation)* operators, and the last term is the contribution of the so-called *zero-point energy*. For clarity, all operators are denoted by $\hat{\cdot}$ in this section. The bosonic creation (annihilation) operators fulfill the following commutation relations

$$[\hat{a}_s, \hat{a}_{s'}^\dagger] = \delta_{s,s'}, \quad [\hat{a}_s, \hat{a}_{s'}] = [\hat{a}_s^\dagger, \hat{a}_{s'}^\dagger] = 0, \quad (2.6)$$

where the commutator of two operators \hat{A} and \hat{B} is defined as

$$[\hat{A}, \hat{B}] \equiv \hat{A}\hat{B} - \hat{B}\hat{A}.$$

Here, we introduced the Kronecker delta

$$\delta_{kl} = \begin{cases} 1, & \text{if } k = l, \\ 0, & \text{otherwise.} \end{cases} \quad (2.7)$$

The eigenstates of the Hamiltonian are then the product of single-mode eigenstates

$$|n_1\rangle \otimes \cdots \otimes |n_N\rangle = |n_1, \cdots, n_N\rangle \equiv |\{n\}\rangle \in \mathcal{H}^{\otimes N}, \quad (2.8)$$

with $n_k \in \mathbb{N}_{>0}$, which builds up our orthogonal $\langle n_k | n_l \rangle = \delta_{kl}$, and complete basis of the Fock space $\mathcal{H}^{\otimes N}$. The creation (annihilation) operators act on the number state $|\{n\}\rangle$ as

$$\hat{a}_k^\dagger |\{n\}\rangle = \sqrt{n_k + 1} |n_1, \cdots, n_k + 1, \cdots, n_N\rangle, \quad \hat{a}_k |\{n\}\rangle = \sqrt{n_k} |n_1, \cdots, n_k - 1, \cdots, n_N\rangle, \quad (2.9)$$

which creates (annihilates) an excitation inside $|\{n\}\rangle$. This implies, that we can identify $\hat{a}_k^\dagger \hat{a}_k = \hat{n}_k$ inside the Hamiltonian as the number operator, giving us the particle number n_k of oscillator k when acted upon the number state $\hat{n}_k |\{n\}\rangle = n_k |\{n\}\rangle$. Thus, the average number of particles of an oscillator k is $\langle \hat{n}_k \rangle = \langle \{n\} | \hat{n}_k | \{n\} \rangle = n_k$. Note that there is a lower bound. Annihilating the lowest occupied state of an oscillator k , gives us the vacuum state with $\hat{a}_k |1\rangle = |0\rangle$. For completeness, we will also quickly mention the energies of the quantum oscillator. To calculate the energies E_{n_k} of oscillator k , we act with \hat{n}_k on a state $|n_k\rangle$, and get from the time-independent Schroedinger equation the following expression

$$\hat{H}_k |n_k\rangle = E_{n_k} |n_k\rangle \implies E_{n_k} = \hbar\omega_k \left(n_k + \frac{1}{2} \right). \quad (2.10)$$

This implies that the zero-point energy of a vacuum state $|0\rangle$ is

$$E_{0_k} = \frac{\hbar\omega_k}{2}.$$

Now we are equipped to introduce coherent states.

2. Coherent states

There are many ways of constructing coherent states $|\alpha\rangle$, here we stay in the single-mode picture, and introduce them as right eigenstates of the annihilation operator

$$\hat{a} |\alpha\rangle = \alpha |\alpha\rangle, \quad (2.11)$$

where α is a parameter characteristic to the coherent state. This implies, that acting with \hat{a} on $|\alpha\rangle$ does not change the coherent state. Due to this stability, coherent states are highly practical in experimental settings [33, 34]. If we

express $|\alpha\rangle$ in terms of number states

$$|\alpha\rangle = e^{-|\alpha|^2/2} \sum_n \frac{\alpha^n}{\sqrt{n!}} |n\rangle, \quad (2.12)$$

it shows that acting with \hat{a} on the state gives us an additional factor of α , but leaves the sum invariant. Note, that two coherent states $|\alpha\rangle, |\beta\rangle$ are not orthogonal $\langle\beta|\alpha\rangle = \exp(-\frac{1}{2}(|\alpha|^2 + |\beta|^2 - 2\alpha^*\beta))$, and thus form an *overcomplete basis*, see Meystre [34]. However, if α gradually deviates from β , they increasingly become orthogonal.

The probability of finding n photons in the coherent state is given by the Poisson distribution

$$p_n = |\langle n|\alpha\rangle|^2 = e^{-|\alpha|^2} \frac{|\alpha|^{2n}}{n!}, \quad (2.13)$$

This gives us the average photon number and variance

$$\langle\hat{n}\rangle = e^{-|\alpha|^2} \sum_{n=0}^{\infty} n \frac{|\alpha|^{2n}}{n!} = |\alpha|^2, \quad \text{and} \quad \sigma_{\hat{n}}^2 = \langle\hat{n}^2\rangle - \langle\hat{n}\rangle^2 = |\alpha|^2, \quad (2.14)$$

where the Poisson distribution of the photon number converges to a Gaussian distribution for large values of $\langle\hat{n}\rangle$, see Loudon [37]. Since we can write $(\hat{a}^\dagger)^n |0\rangle = \sqrt{n!} |n\rangle$, it follows that $|\alpha\rangle$ can be expressed in terms of the vacuum state. With the Baker-Campbell-Hausdorff formula

$$e^{\hat{A}+\hat{B}} = e^{\hat{A}} e^{\hat{B}} e^{-[\hat{A},\hat{B}]},$$

we get

$$|\alpha\rangle = \hat{D}(\alpha)|0\rangle, \quad \text{with} \quad \hat{D}(\alpha) \equiv e^{\alpha\hat{a}^\dagger - \alpha^*\hat{a}}, \quad (2.15)$$

where we call $\hat{D}(\alpha)$ the *displacement operator*. Note, that this has implications on the vacuum state, as they are non-displaced states for the limit $\alpha = 0$. This makes vacuum states unique, as they are zero-occupation Fock states $|0\rangle$, but also minimal uncertainty eigenstates of the annihilation operator $\hat{a}|0\rangle = 0|0\rangle$. More formally, we can apply the displacement operator $\hat{D}(\alpha = 0)$ to $|0\rangle$, and get $\hat{D}(0)|0\rangle = e^{0\hat{a}^\dagger - 0\hat{a}}|0\rangle = |0\rangle$. This again shows that coherent states are displaced vacuum states.

In optical phase space, vacuum states can be expressed by quasi-probability distributions centered at the origin. If we plot the in-phase and out-of-phase components of the state (its *quadratures*, see Sec. II C 3), the distribution has a circular shape with equally minimized uncertainty or quantum *noise* in both components. Thus, the amount of noise is encoded by the size of its distributions radius. The variance of the vacuum photon number is 1/2, see Ref. [35]. By applying the displacement operator on the vacuum, the state is displaced in phase space without changing the amount of noise. Recall, that classical states have no uncertainty with a point-like distribution in phase space. Thus, since the noise of a coherent state has the lowest possible quantum value, they are indeed characterized as the closest analogue to classical states.

3. Squeezed states and two-mode squeezing

For ease of notation, we set $\hbar = 1$ in this section. Consider a single-mode field described by the operator \hat{a} (\hat{a}^\dagger). We can decompose this field into two Hermitian *quadrature* operators

$$\hat{a}(\phi) = \frac{1}{\sqrt{2}}(\hat{x}(\phi) + i\hat{p}(\phi)), \quad \text{and} \quad \hat{a}^\dagger(\phi) = \frac{1}{\sqrt{2}}(\hat{x}(\phi) - i\hat{p}(\phi)), \quad (2.16)$$

or written equivalently

$$\hat{x}(\phi) = \frac{1}{\sqrt{2}}(\hat{a}^\dagger(\phi) + \hat{a}(\phi)), \quad \text{and} \quad \hat{p}(\phi) = \frac{i}{\sqrt{2}}(\hat{a}^\dagger(\phi) - \hat{a}(\phi)), \quad (2.17)$$

where the fields depend on an additional phase ϕ . The creation (annihilation) operators are then given by

$$\hat{a}^\dagger(\phi) \equiv e^{-i\phi} \hat{a}^\dagger, \quad \hat{a}(\phi) \equiv e^{i\phi} \hat{a}, \quad (2.18)$$

and the quadratures fulfill following canonical commutation relations

$$[\hat{x}(\phi), \hat{p}(\phi)] = i, \quad \text{and} \quad [\hat{x}(\phi), \hat{x}(\phi)] = [\hat{p}(\phi), \hat{p}(\phi)] = 0. \quad (2.19)$$

The quadratures would correspond to the position and momentum of a classical oscillator. For the quantum case however, they are real and imaginary parts of creation (annihilation) operators, and correspond to *in-phase* and *out-of-phase* components of quantized fields, see Ref. [38].

By finding the phase ϕ which minimizes the variances of quadratures, the uncertainty relation becomes an elliptic equation

$$\sigma_x \sigma_p = \frac{1}{4} \sqrt{(1 + 2\langle \hat{a}^\dagger \hat{a} \rangle - 2|\langle \hat{a}^2 \rangle|)(1 + 2\langle \hat{a}^\dagger \hat{a} \rangle + 2|\langle \hat{a}^2 \rangle|)} \geq \frac{1}{4}. \quad (2.20)$$

This gives us

$$\sigma_x \sigma_p \geq \frac{1}{4}, \quad (2.21)$$

for a coherent state with $|\langle \hat{a}^2 \rangle| = 0$. Squeezing happens, when $|\langle \hat{a}^2 \rangle| \neq 0$. In that case, σ_x (σ_p) drops below $1/2$, where the other variance increases by the same amount above $1/2$. Thus, the uncertainty relation of the product is still fulfilled, even though one of the variances is less noisy. As this equation is an elliptic equation, the squeezed state becomes an ellipse in phase space. In practical terms, squeezing is often used to make either the amplitude or the phase of a mode less noisy. This is particularly useful for quantum measurements, namely in heterodyne or homodyne detection schemes, see Meystre [34], Walls and Milburn [33].

As before, we can also define a *squeeze operator*

$$\hat{S}(\zeta) \equiv e^{\zeta \hat{a}^{\dagger 2} - \zeta^* \hat{a}^2}, \quad \text{with} \quad \zeta \equiv \frac{r}{2} e^{-2i\phi}, \quad (2.22)$$

where ζ is the *squeezing parameter*. Applying this on a displaced state gives us a *squeezed coherent state*

$$|\alpha, \zeta\rangle \equiv \hat{S}(\zeta)|\alpha\rangle = \hat{S}(\zeta)\hat{D}(\alpha)|0\rangle, \quad (2.23)$$

which is again a minimal-uncertainty state. For $\alpha = 0$ we get the *squeezed vacuum state*

$$|\zeta\rangle \equiv \hat{S}(\zeta)|0\rangle. \quad (2.24)$$

Note, that squeezing and displacement operators almost commute, but commuting changes the argument of the displacement operator $\hat{D}(\alpha)\hat{S}(\zeta) = \hat{S}(\zeta)\hat{D}(\gamma)$, with $\gamma = \alpha \cosh r + \alpha^* e^{i\phi} \sinh r$. The mean photon number for a squeezed vacuum state $|\zeta\rangle$ is

$$\langle \hat{n} \rangle_{\text{sq}} = \sinh^2 r. \quad (2.25)$$

This implies the following mean photon number for squeezed coherent state $|\alpha, \zeta\rangle$

$$\langle \hat{n} \rangle_{\text{sq, coh}} = \langle \hat{n} \rangle_{\text{coh}} + \langle \hat{n} \rangle_{\text{sq}} = |\alpha|^2 + \sinh^2 r. \quad (2.26)$$

Squeezing can also be generalized to multi-mode fields. Here, squeezing reduces the noise between quadratures of different modes, which is essentially nothing more than redistributing noise between given modes. For the simplest case with $N = 2$, we can define the *two-mode squeeze operator* as

$$\hat{S}_2(\zeta) = e^{\zeta \hat{a}_1^\dagger \hat{a}_2^\dagger - \zeta^* \hat{a}_1 \hat{a}_2}. \quad (2.27)$$

When this operator is acted upon the vacuum $|0, 0\rangle$, this gives us the *two-mode squeezed vacuum state*

$$|TMSV\rangle \equiv \hat{S}_2(\zeta)|0, 0\rangle = \frac{1}{\cosh r} \sum_n (-e^{-2i\phi} \tanh r)^n |n, n\rangle. \quad (2.28)$$

Note, that we will not consider any squeezed-light input in this thesis, but only consider thermal vacuum states, see Sec. IIC4. However, two-mode squeezing is still relevant to us, since it can be understood as arising from an interaction between two different resonators. To understand this, we consider a four-wave mixing interaction with a *parametric pump laser*, see Meystre [34]. Here, two incident photons of the pump, each with frequency ω_p , interact with two resonators. This will result in a signal photon with frequency ω_s , and an idler photon with ω_i . This process can be described by the following effective Hamiltonian (again with $\hbar = 1$)

$$\hat{H}_{4\text{-wave-mix}} = \omega_s \hat{a}_s^\dagger \hat{a}_s + \omega_i \hat{a}_i^\dagger \hat{a}_i + i\lambda \hat{a}_s^\dagger \hat{a}_i^\dagger - i\lambda^* \hat{a}_s \hat{a}_i, \quad (2.29)$$

where the coupling strength λ is proportional to the pump-laser amplitude $E_p^2(\omega_p)$. The time-evolution operator (properly defined in Sec. IIE2) becomes

$$\hat{U}(t) \equiv \hat{S}_2(\zeta), \quad \text{with} \quad \zeta = -\lambda t \quad (2.30)$$

which is exactly the two-mode squeeze operator from above! For the degenerate case with $\omega \equiv \omega_s = \omega_i$, and $\hat{a} \equiv \hat{a}_s = \hat{a}_i$, the time-evolution reduces to the single-mode squeeze operator $\hat{U}(t) \equiv \hat{S}(\zeta)$.

4. Thermal states

For simplicity, we will only consider a single-mode field with the Hamiltonian $\hat{H} = \hbar\omega(\hat{a}^\dagger\hat{a} + 1/2)$, fully thermalized to an external reservoir with temperature T . The average energy of \hat{H} is the only thing that can be known and is given by

$$\langle\hat{H}\rangle_{\text{th}} = \text{Tr}\left\{\hat{H}\hat{\rho}_{\text{th}}\right\}, \quad (2.31)$$

where $\hat{\rho}_{\text{th}}$ is the density matrix of the thermalized system state, and the average of an operator \hat{A} for a system state $\hat{\rho}$ is $\langle\hat{A}\rangle = \text{Tr}\{\hat{A}\hat{\rho}\}$. The thermalized system state can be found by invoking the *maximum entropy principle* using the von Neumann entropy $S = -k_B\text{Tr}\{\hat{\rho}_{\text{th}}\ln\hat{\rho}_{\text{th}}\}$, where k_B is the Boltzmann factor and “ln” the natural logarithm, which can be identified as a Gibbs state:

$$\hat{\rho}_{\text{th}} = \frac{\exp(-\beta\hat{H})}{Z}, \quad \text{with} \quad Z \equiv \text{Tr}\left\{\exp(-\beta\hat{H})\right\}. \quad (2.32)$$

Here, $\beta \equiv 1/k_B T$ is the unit-less inverse temperature, and Z the thermodynamic partition function. Using this state, we can find an explicit form of the average energy

$$\langle\hat{H}\rangle_{\text{th}} = \hbar\omega\left(\langle\hat{n}\rangle_{\text{th}} + \frac{1}{2}\right), \quad \text{with} \quad \bar{n} \equiv \langle\hat{n}\rangle_{\text{th}} = \frac{1}{e^{\hbar\omega/k_B T} - 1}, \quad (2.33)$$

where the mean number of photons \bar{n} for a temperature T is given by the Bose-Einstein occupation. Consider now limiting cases of the average energy. The oscillator reaches its ground state at absolute zero for $T = 0$, since only the zero-point energy $\langle\hat{H}\rangle_{\text{th}} = \hbar\omega/2$ remains. These zero-temperature fluctuations are unique for the quantum mechanical oscillator and cannot be found in classical systems. However, for sufficiently high temperatures $k_B T \gg \hbar\omega$, the average energy of the quantum oscillator will approach the result of a classical oscillator $\langle\hat{H}\rangle_{\text{th}} \rightarrow \langle\hat{H}\rangle_{\text{cl}} = k_B T$.

Note, that we have only demonstrated the single-mode field case here. The generalization is more technical for multi-modal fields and can be found in Olivares [39]. The precise construction of thermal coherent states is achieved by displacing a thermal vacuum state with the displacement operator, giving us

$$\hat{\rho}_{\text{th}}(\alpha) = \hat{D}(\alpha)\hat{\rho}_{\text{th}}\hat{D}^\dagger(\alpha). \quad (2.34)$$

Which has implications on the mean photon number $\langle\hat{n}\rangle_{\text{th, coh}}$ of a thermal coherent state

$$\langle\hat{n}\rangle_{\text{th, coh}} = \text{Tr}\{\hat{n}\hat{\rho}_{\text{th}}(\alpha)\} = |\alpha|^2 + \langle\hat{n}\rangle_{\text{th}}, \quad (2.35)$$

as the mean photon number now depends on the displacement parameter and the thermal occupations. The variance also increases

$$\sigma_{\text{th, coh}}^2 = \langle\hat{n}^2\rangle_{\text{th, coh}} - \langle\hat{n}\rangle_{\text{th, coh}}^2 = \sigma_{\text{th}}^2 + |\alpha|^2(1 + 2\langle\hat{n}\rangle_{\text{th}}), \quad \text{with} \quad \sigma_{\text{th}}^2 = \langle\hat{n}^2\rangle_{\text{th}} - \langle\hat{n}\rangle_{\text{th}}^2, \quad (2.36)$$

meaning that the thermal state has a now a bigger amount of noise, depending on the temperature T . In turn, coherent states are just displaced thermal states for $T = 0$ K.

We can now make a few general remarks about (thermal) vacuum states. Since we will only consider thermal vacuum states for the rest of this thesis, we view them as thermal coherent states with $\alpha = 0$, and an average photon occupation

equal to the thermal occupation $\langle \hat{n} \rangle_{\text{vac}} = \langle \hat{n} \rangle_{\text{th}}$. But, different to non-thermal vacuum states, the variance of thermal vacuum states is broadened in phase space, as the uncertainty is now higher and the state has more noise.

5. Gaussian states

In general, the term *Gaussian state* refers to any state in phase space, where its Wigner function (quasiprobability distribution, see Refs. [33–36]) can be adequately described by a Gaussian function. We can write this Gaussian function as

$$f(x) = ae^{-\frac{(x-b)^2}{2c^2}}, \quad (2.37)$$

which is symmetrically peaked at position b , has height a , width c , and rapidly falls off towards $\pm\infty$. Vacuum, coherent, squeezed, and even thermal states can all be classified as Gaussian. As mentioned above, this is not the case for number states (except the vacuum). The reason for that is simple: Every Gaussian state can be sufficiently described by a thermal state if the only actions on it are *Gaussian unitaries* (displacement, squeezing, rotation), see Weedbrook *et al.* [35]. Thus, a single thermal state can be viewed as the most fundamental Gaussian state [35]. Bilinear systems (like the one we will consider) only act via Gaussian unitaries and thus preserve “*Gaussianity*”, since any incoming Gaussian wave packet leaves the system still as a Gaussian [35]. More formally, we assume a general bilinear Hamiltonian

$$\hat{H}_{\text{bi-lin}} = \hbar \left(\sum_s \omega_s \hat{a}_s^\dagger \hat{a}_s + i\nu_s \hat{a}_s^\dagger \hat{a}_s^\dagger + \sum_{i,j} J_{ij} \hat{a}_i^\dagger \hat{a}_j + i\lambda_{ij} \hat{a}_i^\dagger \hat{a}_j^\dagger \right) + \text{H.c.}, \quad (2.38)$$

for $s = 1, \dots, N$, $i \neq j = 1, \dots, N$, where ω_s is the frequency of a single resonator, ν_s the squeezing interaction strength, J_{ij} the beam-splitter coupling between different modes and λ_{ij} the coupling between different modes via two-mode squeezing. By writing it in the BdG-form (see Sec. III B 3 for more)

$$\hat{H}_{\text{bi-lin}} = \sum_{i,j} \hat{\mathbf{a}}_i^\dagger \mathbf{H}_{ij} \hat{\mathbf{a}}_j, \quad (2.39)$$

with $\hat{\mathbf{a}} \equiv (\hat{a}_1, \dots, \hat{a}_N, \hat{a}_1^\dagger, \dots, \hat{a}_N^\dagger)^T$, we find that the thermal state of this bilinear Hamiltonian becomes

$$\rho = \frac{e^{-\beta \hat{H}_{\text{bi-lin}}}}{Z} = \frac{\exp\left(-\beta \sum_{i,j} \hat{\mathbf{a}}_i^\dagger \mathbf{H}_{ij} \hat{\mathbf{a}}_j\right)}{Z}. \quad (2.40)$$

Any state, which can be written in the form above, is *always* guaranteed to be Gaussian, see [35, 36, 39, 40]. This is reasonable as a Gaussian function can be written as $f(x) \propto \exp(-x^2)$ in general. Gaussian states have useful properties, since they can be fully determined by their first and second statistical moments [35]. Thus, knowing the expectation values and variances of operators is sufficient enough to fully understand the physics of Gaussian states, where higher statistical moments can always be decomposed into first and second moments.

D. Frequency space representation of operators

In this thesis we will heavily use the frequency space representation of operators as this gives us a clear understanding of several things; mainly how incoming states are scattered depending on frequency, and additionally, how the system filters frequencies of the noise of incoming Gaussian states. For this, we use the *Fourier transform*, which can transform a given function between two dual representations. In our case, applying the Fourier transform to a complex valued

function (i.e. an operator $\hat{a}(t)$), will decompose the function into its constituent frequencies and amplitudes. For this, we introduce the following convention for the backward and forward Fourier transform

$$\hat{f}(t) = \mathcal{F}^{-1}\{\hat{f}[\omega]\}(t) = \frac{1}{\sqrt{2\pi}} \int_{-\infty}^{\infty} d\omega \hat{f}[\omega] e^{i\omega t}, \quad \text{and} \quad \hat{f}[\omega] = \mathcal{F}\{\hat{f}(t)\}[\omega] = \frac{1}{\sqrt{2\pi}} \int_{-\infty}^{\infty} dt \hat{f}(t) e^{-i\omega t}, \quad (2.41)$$

where $\mathcal{F}\{\cdot\}$ is the Fourier transform operator acting on an arbitrary operator-valued function \hat{f} . For clarity of notation, all functions in time space are denoted by round brackets (\cdot) , whereas in frequency-space we will use square brackets $[\cdot]$. The adjoint of an operator is transformed using the convention

$$\hat{f}^\dagger[\omega] = \mathcal{F}\{\hat{f}^\dagger(t)\}[\omega] = \frac{1}{\sqrt{2\pi}} \int_{-\infty}^{\infty} dt \hat{f}^\dagger(t) e^{-i\omega t} \implies \hat{f}^\dagger[\omega] = (\hat{f}[-\omega])^\dagger, \quad (2.42)$$

see Clerk *et al.* [41] for additional details. This is only a convention, however, this notion seems intuitive and acts the same way as applying the complex-conjugation to a general complex-valued function. By using the Fourier transform, we are enabled to use the subsequent well-known relation

$$\mathcal{F}\{\dot{\hat{f}}(t)\}[\omega] = \frac{1}{\sqrt{2\pi}} \int_{-\infty}^{\infty} dt \dot{\hat{f}}(t) e^{-i\omega t} = \frac{1}{\sqrt{2\pi}} \lim_{a \rightarrow \infty} \underbrace{\left[\hat{f}(t) e^{-i\omega t} \right]_{-a}^a}_{= 0, \text{ since } \lim_{t \rightarrow \pm\infty} \hat{f}(t) = 0} - (-i\omega) \frac{1}{\sqrt{2\pi}} \int_{-\infty}^{\infty} dt \hat{f}(t) e^{-i\omega t}, \quad (2.43)$$

implying

$$\mathcal{F}\{\dot{\hat{f}}(t)\}[\omega] = i\omega \hat{f}[\omega] \iff \mathcal{F}\{\hat{f}^\dagger(t)\}[\omega] = i\omega \hat{f}^\dagger[\omega], \quad (2.44)$$

which essentially gets rid of bothersome time derivatives in frequency space, and instead of solving non-trivial differential equations, we are left with a set of algebraic equations. Note that the inverse of the above equation is also true. Trivially, the same relation also holds for expectation values of operators

$$\mathcal{F}\{\langle \dot{\hat{f}}(t) \rangle\}[\omega] = i\omega \langle \hat{f}[\omega] \rangle. \quad (2.45)$$

E. Coupling isolated systems to reservoirs - Open quantum systems

1. Input-output theory

The following is based on the online appendices of Clerk *et al.* [41].

Usually, fields external to the cavity are modeled as a passive heat bath, exchanging heat and particles with the system until the system state eventually equilibrates. Often, this is done with finding an appropriate Lindblad master equation and solving it for the system state, see Appendix A. However, in the input-output formalism (I/O), we will approach this differently. The reservoir is treated as an external field (i.e. a Gaussian state) that interacts with the intracavity field and leaves the system as a new external field. The environment then either drives or probes the system. Thus, we need a joint formalism accounting for system-reservoir interactions, and can not simply trace out the reservoir.

To see how this is done, consider a system composed of a simple harmonic oscillator \hat{H}_{sys} , which is coupled to a discretized continuum of external reservoir modes \hat{H}_{res} , and interacts with the external modes \hat{H}_{int} . This gives us the total Hamiltonian

$$\hat{H}_{\text{tot}} = \hat{H}_{\text{sys}} + \hat{H}_{\text{res}} + \hat{H}_{\text{int}}. \quad (2.46)$$

The system itself is described by a single intracavity field mode with ($\hbar = 1$)

$$\hat{H}_{\text{sys}} = \omega_s \hat{a}^\dagger \hat{a}, \quad (2.47)$$

where ω_s is the frequency of that mode, \hat{a} (\hat{a}^\dagger) is a bosonic annihilation (creation) operator, and we dismissed the zero-point energy by rescaling. The Hamiltonian for the reservoir is

$$\hat{H}_{\text{res}} = \sum_q \omega_q \hat{b}_q^\dagger \hat{b}_q, \quad (2.48)$$

where we assume the reservoir to have a really wide frequency band, similar to the theory of spontaneous emission from Weisskopf and Wigner [33, 42]. Here, \hat{b}_q is a bosonic field operator and q its quantum number. The bosonic fields fulfill

$$[\hat{b}_q, \hat{b}_{q'}^\dagger] = \delta_{q,q'}. \quad (2.49)$$

The reservoir modes must terminate at the system, which implies that there is no translational invariance and q is not a real wave-vector. The modes are then stationary waves, reasonably assumed to be non-propagating close to the system and only varying in time. The interaction Hamiltonian, by employing the *rotating-wave approximation* (RWA), becomes

$$\hat{H}_{\text{int}} = -i \sum_q \left(g_q \hat{a}^\dagger \hat{b}_q - g_q^* \hat{b}_q \hat{a} \right), \quad (2.50)$$

where g_q is the coupling strength between the system and the reservoir modes. The avid reader might see how any parametric coupling terms drop out. This comes from the RWA, where we neglect high oscillating terms inside the approximation. The dynamics of the cavity and reservoir operators are given by the Heisenberg equation (see Refs. [43–45])

$$\frac{d}{dt} \hat{a} = i[H_{\text{sys}}, \hat{a}] - \sum_q g_q \hat{b}_q, \quad (2.51a)$$

$$\frac{d}{dt} \hat{b}_q = i[\hat{H}_{\text{tot}}, \hat{b}_q] = -i\omega_q \hat{b}_q + g_q^* \hat{a}. \quad (2.51b)$$

The equation of motion (EOM) for the reservoir operators can be solved, since this is a linear system. For $t_0 < t$ in the past before a wave packet has reached the cavity at time t , the solution for the reservoir EOM (2.51b) becomes

$$\hat{b}_q(t) = e^{-i\omega_q(t-t_0)} \hat{b}(t_0) + g_q^* \int_{t_0}^t d\tau e^{-i\omega_q(t-\tau)} \hat{a}(\tau) \equiv \hat{b}_{\text{free}}(t_0, t) + \hat{b}_{\text{radiated}}(t_0, t), \quad (2.52)$$

The first term $\hat{b}_{\text{free}}(t_0, t)$ of the RHS is the free evolution of the mode, where the second term $\hat{b}_{\text{radiated}}(t_0, t)$ describes

the coupling between the intracavity field to the reservoir with frequency ω_q . We can also write an analogous expression for later times $t_1 > t$

$$\hat{b}_q(t) = e^{-i\omega_q(t-t_1)}\hat{b}(t_1) - g_q^* \int_t^{t_1} d\tau e^{-i\omega_q(t-\tau)}\hat{a}(\tau) \equiv \hat{b}_{\text{free}}(t_1, t) - \hat{b}_{\text{radiated}}(t, t_1). \quad (2.53)$$

By substituting the first solution of the reservoir fields (2.52) into the cavity EOM (2.51a), we get for the second term

$$\sum_q g_q \hat{b}_q = \sum_q g_q e^{-i\omega_q(t-t_0)}\hat{b}_q(t_0) + \sum_q |g_q|^2 \int_{t_0}^t d\tau e^{-i(\omega_q-\omega_s)(t-\tau)} \left(e^{i\omega_s(\tau-t)}\hat{a}(\tau) \right), \quad (2.54)$$

where we inserted an additional factor of $1 = e^{-i\omega_s(\tau-t)}e^{i\omega_s(\tau-t)}$. The last term inside the brackets is assumed to vary slowly in τ . By only considering a single decay channel of the cavity oscillator from an excited state to the ground state $n = 1 \rightarrow n = 0$, we can relate the *decay probability* to the system-reservoir coupling using *Fermi's golden rule* [46]. For this, recall that Fermi's golden rule is a first-order perturbation, where the transition probability for an initial state $|i\rangle$ (of an unperturbed Hamiltonian), to another state $|j\rangle$ (of a weakly perturbed Hamiltonian), is essentially constant. This decay probability is thus related to the inverse of the mean lifetime within the (decay) rate equation. This gives us

$$\kappa(\omega_s) = 2\pi \sum_q |g_q|^2 \delta(\omega_s - \omega_q), \quad (2.55)$$

where

$$\delta(x) = \begin{cases} \infty, & x = 0, \\ 0, & x \neq 0, \end{cases} \quad \text{with} \quad \int_{-\infty}^{\infty} dx \delta(x) = 1, \quad (2.56)$$

is the Dirac delta function. This can be re-written as

$$\frac{1}{2\pi} \int_{-\infty}^{\infty} d\nu \kappa(\omega_s + \nu) e^{-i\nu(t-\tau)} = \sum_q |g_q|^2 e^{-i(\omega_q-\omega_s)(t-\tau)}. \quad (2.57)$$

Via the *Markov approximation*, which says that the coupling is constant $\kappa(\nu) \approx \kappa$ over the relevant frequency range of the cavity, we get

$$\sum_q |g_q|^2 e^{-i(\omega_q-\omega_s)(t-\tau)} = \kappa \delta(t - \tau), \quad (2.58)$$

where we used

$$\delta(t - t') = \frac{1}{2\pi} \int_{-\infty}^{\infty} d\omega e^{-i\omega(t-t')}. \quad (2.59)$$

By integrating from the past at $t = -\infty$ to $t = t_0$, we get

$$\int_{-\infty}^{t_0} dt \delta(t - t_0) = \frac{1}{2}, \quad (2.60)$$

where it follows for the cavity EOM

$$\frac{d}{dt} \hat{a}(t) = i[\hat{H}_{\text{sys}}, \hat{a}] - \frac{\kappa}{2} \hat{a} - \sum_q g_q e^{-i\omega_q(t-t_0)} \hat{b}_q(t_0). \quad (2.61)$$

Looking closer at our result, the field radiated out from the resonator to the reservoir can be simply seen as a linear damping of the intracavity field. We can introduce the coupling constant $g \equiv \sqrt{|g_q|^2}$ and define the density of states

$$\rho = \sum_q \delta(\omega_s - \omega_q), \quad (2.62)$$

which implies for Fermi's golden rule

$$\kappa = 2\pi g^2 \rho. \quad (2.63)$$

This finally gives us an useful expression for the reservoir *input-field*

$$\hat{a}_{\text{in}}(t) \equiv \frac{1}{\sqrt{2\pi\rho}} \sum_q e^{-i\omega_q(t-t_0)} \hat{b}_q(t_0), \quad (2.64)$$

and the cavity EOM reads

$$\frac{d}{dt} \hat{a} = i[\hat{H}_{\text{sys}}, \hat{a}] - \frac{\kappa}{2} \hat{a} - \sqrt{\kappa} \hat{a}_{\text{in}}(t), \quad (2.65)$$

which is also called the *Heisenberg-Langevin equation*. This EOM is the famous result of I/O theory and relates the dynamics of the intracavity field to input modes coming from the reservoir. This equation tells us, how a wave-packet coming from the reservoir evolves freely, till it reaches the cavity, interacts, and drives the system. Hence, the wave-packet \hat{a}_{in} can indeed be appropriately identified as the input-field to our cavity, reminiscent of classical I/O theory for a driven oscillator and a transmission line, see Ref. [41]. Note however, that modes $\hat{a}_{\text{in}}(t)$ and $\hat{a}_{\text{in}}(t')$ for different times are completely different modes in general! Our system will interact at time t with $\hat{a}_{\text{in}}(t)$, then after some time $t' > t$, when the next mode is incident, interact with $\hat{a}_{\text{in}}(t')$. Note, that we will only consider incident *white noise* [41] later, which is a constant field in frequency space.

If we now focus on the second solution for the reservoir-fields (2.53), we get the *output-field*

$$\hat{a}_{\text{out}}(t) \equiv \frac{1}{\sqrt{2\pi\rho}} \sum_q e^{-i\omega_q(t-t_1)} \hat{b}_q(t_1), \quad (2.66)$$

for $t_1 > t > t_0$. Which is essentially the free evolving reservoir mode from the future (after interacting) back to the present. We can write down the cavity EOM in terms of output-fields as

$$\frac{d}{dt}\hat{a}(t) = i[\hat{H}_{\text{sys}}, \hat{a}] + \frac{\kappa}{2}\hat{a} - \sqrt{\kappa}\hat{a}_{\text{out}}(t). \quad (2.67)$$

By subtracting Eq. (2.67) from Eq. (2.65), we find the so-called *input-output relation*

$$\hat{a}_{\text{out}}(t) = \hat{a}_{\text{in}}(t) + \sqrt{\kappa}\hat{a}(t). \quad (2.68)$$

This simple equation is a highly useful result, because it directly relates intracavity fields to input- and output-fields of the reservoir.

2. The Langevin equation

The resulting stochastic differential equation of the cavity can be seen as a linear process with constant diffusion. Thus, we can identify equation (2.65) as the quantum analogue of the classical Langevin equation, see Lemons and Gythiel [47], Einstein [48], Gardiner and Collett [49], Zwanzig [50]. To understand this, we first look at the classical Langevin equation describing *Brownian motion* of a viscous thermal fluid.

a. Brownian motion of a classical fluid

Consider a velocity vector $\mathbf{v} = (v_1, \dots, v_N)^T$ for N particles with mass m , a diagonal matrix encoding the damping coefficients $(\mathbf{A})_{ii} = -\lambda_i$ (or sometimes called the inverse of the particles *mobility*), and a vector $\boldsymbol{\xi}(t) = (\xi_1(t), \dots, \xi_N(t))^T$ encoding collisions with other particles (sometimes called *Langevin forces*). The equation for the total force is then

$$\mathbf{F}_{\text{tot}} = m\dot{\mathbf{v}} = \mathbf{A}\mathbf{v} + \boldsymbol{\xi}(t), \quad (2.69)$$

where the first term of the RHS describes the *drag* of a viscous fluid (from Stokes' law, see Zwanzig [50]), and the second term is a rapidly fluctuating *noise* term due to particle collisions. The stochastic noise term $\boldsymbol{\xi}(t)$ essentially drives the system and influences the trajectory of the particle. The resulting trajectory is often called a *random walk*. Mathematically, this type of noise is called a *Wiener process*, which has a Gaussian correlation function $\langle \xi_i(t)\xi_j(t') \rangle = 2B_i\delta_{ij}\delta(t-t')$, with proportionality constant B_i . By the *fluctuation-dissipation theorem*, we get

$$B_i = \lambda_i k_B T, \quad (2.70)$$

which relates the strength of fluctuations B_i , to the magnitude of the dissipation λ_i , see Ref. [50]. As this noise has an infinite variance at any time t , it is non-differentiable in general (see the Thesis of Kurt Jacobs [51] for more). However, by Fourier transforming the correlation function into frequency space, we find that the spectrum becomes flat [51]. This is what we call *white noise*, which is exactly the relevant type of noise for this thesis. Since $\boldsymbol{\xi}(t)$ is rapidly fluctuating over the time-scale of collisions, it has zero mean $\langle \boldsymbol{\xi}(t) \rangle = 0$.

b. Quantum Langevin equation

Here we restate the Heisenberg-Langevin equation (2.65)

$$\frac{d}{dt}\hat{a}(t) = i[\hat{H}_{\text{sys}}, \hat{a}(t)] - \frac{\kappa}{2}\hat{a}(t) - \sqrt{\kappa}\hat{a}_{\text{in}}(t), \quad (2.71)$$

for a single intracavity field $a(t)$, where the first term is the coherent evolution of the isolated system, the second term encodes dissipation due to the reservoir-coupling, and the last term is a fluctuating input-field. This essentially has the same effect as the classical Langevin force from before [34], but instead of being a real number, the Langevin

force is now operator-valued and stochastically “drives” the system. The Langevin force appears in the input-output formalism as the reservoir input-field

$$\hat{a}_{\text{in}}(t) = \langle \hat{a}_{\text{in}}(t) \rangle + \hat{\xi}(t), \quad (2.72)$$

which we can decompose as the mean $\langle \hat{a}_{\text{in}}(t) \rangle$ and the so-called *quantum noise operator* $\hat{\xi}(t)$. The noise operator is the fluctuating part of the input-field and vanishes by taking the expectation value $\langle \hat{\xi}(t) \rangle = 0$. Note, that vacuum-fields have an average of $\langle \hat{a}_{\text{in}}(t) \rangle = 0$, and thus also vanish when taking the expectation value

$$\frac{d}{dt} \langle \hat{a}(t) \rangle = i \langle [H_{\text{sys}}, \hat{a}(t)] \rangle - \frac{\kappa}{2} \langle \hat{a}(t) \rangle. \quad (2.73)$$

However, even though the mean noise for vacuum inputs is zero, the variances are not, just like for the classical case. More on that in Sec. V.

Now is a good time to make a few remarks about the I/O approach compared to the standard Lindblad master equation formalism. Note, that I/O theory already describes dynamics at the level of operators and not only their expectation values. We could also employ the Lindblad master equation to calculate the EOMs, see Appendix A, but we would need to include a coherent drive term inside the Hamiltonian to additionally describe an input. Without an input, the time-evolution for the mean can be calculated using the adjoint Liouvillian \mathcal{L}^\dagger inside the Heisenberg equation

$$\frac{d}{dt} \langle \hat{a}(t) \rangle = \langle \mathcal{L}^\dagger \hat{a}(t) \rangle = i \langle [H_{\text{sys}}, \hat{a}(t)] \rangle - \frac{\kappa}{2} \langle \hat{a}(t) \rangle. \quad (2.74)$$

Therefore, a coherent drive term inside the Hamiltonian is not needed in the I/O formalism. There are shortcomings of the I/O formalism however. Recall from Eq. (2.52), that $\hat{b}_j(t)$ depends on $\hat{a}(t)$, and even though the intracavity field and the reservoir fields as a whole commute for equal times $[\hat{a}(t), \hat{b}_j(t)] = 0$, the free part does not $[\hat{a}(t), \hat{b}_{\text{free}}(t_0, t)] \neq 0$, see Ref. [34]. Thus, interchanging reservoir and cavity operators is not possible without significant problems. This issue can be resolved by choosing an ordering convention from the start and adhering to it, with *normal-ordering* being the most commonly used standard, see Walls and Milburn [33], Meystre [34].

This concludes the theoretical background needed for this thesis and we can now look at the proposed system itself.

III. System and model

A. Hamiltonian of the general three-cavity ring

In this section, we will introduce the general setup of the system, which is based on Refs. [1, 14], and will be more thoroughly analyzed in the coming chapters of this thesis. At first, we will focus only on the coherent dynamics of the system and derive an expression of the Hamiltonian in the interaction picture. By going this route and starting from the time-dependent Hamiltonian in the laboratory frame and then moving to the time-independent representation, it becomes clear how local phases start to appear and accumulate to gauge-invariant phases. Tuning these phases enables varying dynamical behaviour of the model to different limiting regimes. Namely, either reciprocal or nonreciprocal transport of bosonic excitations becomes possible. By using the former established Heisenberg-Langevin equation we can then model dissipative currents in the following section. This is a key ingredient for achieving nonreciprocity, as coherent and dissipative couplings are balanced out and lead to a destructive interference in only one direction of transport. In the subsequent Sections, we will always use the convention “only people wear hats, not operators”, except when it is explicitly useful to do so. We will also always use natural units with $\hbar = c = 1$. This system of coupled bosonic resonators is described by assigning each resonator j a creation operator $\hat{a}_j^\dagger \equiv a_j^\dagger$. This creates a photon (or a phonon in an optomechanical setup) in the respective cavity of interest and fulfills the usual bosonic commutation relations $[a_j, a_k^\dagger] = \delta_{jk}$ and $[a_j, a_k] = [a_j^\dagger, a_k^\dagger] = 0$. We assume that each pair of resonators can interact via the following processes: 1. A *linear beam-splitter (BS) interaction* and 2. A *parametric two-mode squeezing (TMS) interaction*. The most general case, where each pair is coupled via a beam-splitter and two-mode squeezing interaction can be written as the time-dependent Hamiltonian (for $j, k, l = \{1, 2, 3\}$)

$$H(t) = H_0 + H_{\text{hop}}(t) + H_{\text{sq}}(t) = \sum_{j=1,2,3} \omega_j a_j^\dagger a_j + \sum_{k>l} \left(J_{kl}(t) a_k^\dagger a_l + \text{h.c.} \right) + \sum_{k>l} \left(\lambda_{kl}(t) a_k^\dagger a_l^\dagger + \text{h.c.} \right), \quad (3.1)$$

where ω_j is the cavity frequency with the simplifying assumption that the three modes are non-resonant, namely, $\omega_j \neq \omega_k$ for $k < l$. Here, the parameters $J_{kl}(t) \in \mathbb{R}$ ($\lambda_{kl}(t) \in \mathbb{R}$) are time-modulated matrix elements of beam-splitter (two-mode squeezing) interactions, and “h.c.” is the hermitian conjugate, see Fig 3.

For the interactions we assume time-varying harmonic functions of the kind (see Ref. [14])

$$J_{kl}(t) = 2|J_{kl}| \cos(\Delta_{kl}t - \alpha_{kl}), \quad \lambda_{kl}(t) = 2|\lambda_{kl}| \cos(\Delta'_{kl}t - \beta_{kl}), \quad (3.2)$$

where $|J_{kl}|$ ($|\lambda_{kl}|$) is the coupling strength, Δ_{kl} (Δ'_{kl}) is the modulation frequency and $\alpha_{kl} = -\alpha_{lk}$ ($\beta_{kl} = -\beta_{lk}$) is just a general phase shift, but contributes to the gauge-invariant phase later on. In the next subsection, we will derive an expression of the Hamiltonian in the interaction picture.

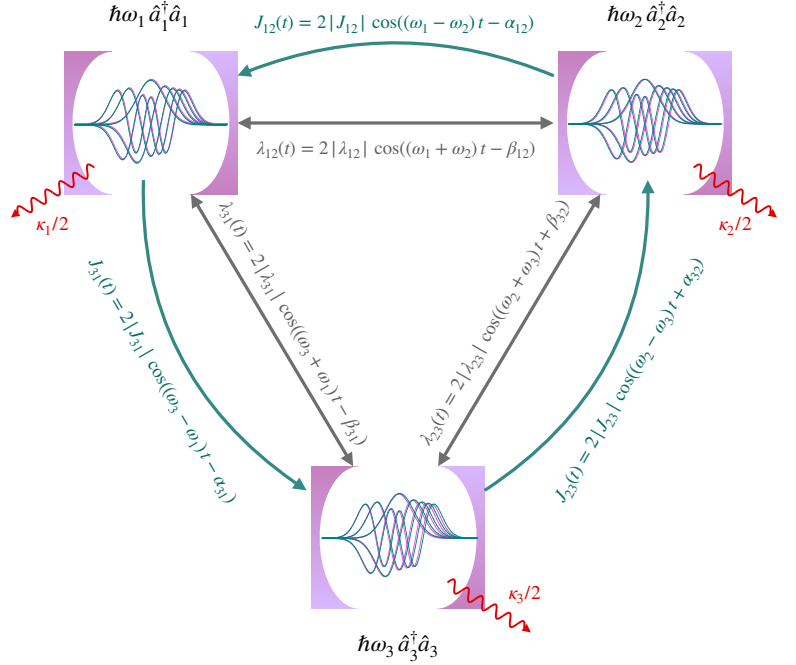


FIG. 3. Three cavities with Hamiltonian $\hbar\omega_i \hat{a}_i^\dagger \hat{a}_i$, are coupled either with linear beam-splitter (BS) interactions $J_{ij}(t)$, or (parametric) two-mode squeezing (TMS) interactions $\lambda_{ij}(t)$, for $i \neq j \in \{1, 2, 3\}$. Each resonator is also dissipatively coupled to a reservoir with strength $\kappa_i/2$. Here, the adjoint interactions $J_{ij}^*(t) = J_{ji}(t)$, and $\lambda_{ij}^*(t) = \lambda_{ji}(t)$ are not shown.

1. Derivation of the interaction picture Hamiltonian

Since we want to work in the interaction picture, we can use a unitary rotation

$$U_t \equiv e^{itH_0}, \quad (3.3)$$

which is just composed of the free harmonic term H_0 and apply the following transformation to the full Hamiltonian

$$H_{\text{int}}(t) \equiv U_t H(t) U_t^\dagger + i\dot{U}_t U_t^\dagger, \quad (3.4)$$

resulting in

$$H_{\text{int}}(t) = U_t H_0 U_t^\dagger + U_t H_{\text{hop}}(t) U_t^\dagger + U_t H_{\text{sq}}(t) U_t^\dagger + i\dot{U}_t U_t^\dagger. \quad (3.5)$$

Now, we will look at each term of equation above individually. For this, we note that the unitary U_t and the free Hamiltonian H_0 commute with $[U_t, H_0] = 0$, which implies for the first term

$$U_t H_0 U_t^\dagger = H_0. \quad (3.6)$$

Next, the last term of Eq. (3.5) can also be easily evaluated to be

$$i\dot{U}_t U_t^\dagger = i^2 H_0 \underbrace{e^{itH_0} e^{-itH_0}}_{\mathbb{1}} = -H_0, \quad (3.7)$$

which implies that only the remaining terms of eq (3.5) need to be considered. Let us focus on the hopping term

$$U_t H_{\text{hop}}(t) U_t^\dagger = \sum_{k>l} J_{kl}(t) e^{itH_0} a_k^\dagger a_l e^{-itH_0} + J_{kl}^*(t) e^{itH_0} a_l^\dagger a_k e^{-itH_0}, \quad (3.8)$$

where we can insert an identity between the operators to get

$$\sum_{k>l} J_{kl}(t) e^{itH_0} a_k^\dagger \mathbb{1} a_l e^{-itH_0} + J_{kl}^*(t) e^{itH_0} a_l^\dagger \mathbb{1} a_k e^{-itH_0} \quad (3.9)$$

$$= \sum_{k>l} J_{kl}(t) (e^{itH_0} a_k^\dagger e^{-itH_0}) (e^{itH_0} a_l e^{-itH_0}) + J_{kl}^*(t) (e^{itH_0} a_l^\dagger e^{-itH_0}) (e^{itH_0} a_k e^{-itH_0}) \quad (3.10)$$

$$= \sum_{k>l} J_{kl}(t) e^{it(\omega_k - \omega_l)} a_k^\dagger a_l + J_{kl}^*(t) e^{-it(\omega_k - \omega_l)} a_l^\dagger a_k. \quad (3.11)$$

For readability we introduce the short-hand $\omega_{kl} \equiv \omega_k - \omega_l$, where the BS Hamiltonian in the interaction picture is now written as follows

$$U_t H_{\text{hop}}(t) U_t^\dagger = \sum_{k>l} J_{kl}(t) e^{i\omega_{kl}t} a_k^\dagger a_l + J_{kl}^*(t) e^{-i\omega_{kl}t} a_l^\dagger a_k. \quad (3.12)$$

By now considering the case where the modulation frequency is equal to $\Delta_{kl} = \omega_{kl}$, we can expand (with $\alpha_{kl} = -\alpha_{lk}$)

$$J_{kl}(t) = 2|J_{kl}| \cos(\omega_{kl}t - \alpha_{kl}) = |J_{kl}| \left(e^{i(\omega_{kl}t - \alpha_{kl})} + e^{-i(\omega_{kl}t - \alpha_{kl})} \right), \quad (3.13)$$

$$J_{kl}^*(t) = J_{lk}(t) = 2|J_{kl}| \cos(\omega_{lk}t - \alpha_{lk}) = |J_{kl}| \left(e^{-i(\omega_{kl}t - \alpha_{kl})} + e^{i(\omega_{kl}t - \alpha_{kl})} \right), \quad (3.14)$$

and get

$$U_t H_{\text{hop}}(t) U_t^\dagger = \sum_{k>l} |J_{kl}| \left(e^{i\alpha_{kl}} a_k^\dagger a_l + e^{-i\alpha_{kl}} a_l^\dagger a_k \right) + |J_{kl}| \left(e^{2it\omega_{kl}} e^{-i\alpha_{kl}} a_k^\dagger a_l + e^{-2it\omega_{kl}} e^{i\alpha_{kl}} a_l^\dagger a_k \right). \quad (3.15)$$

If the coupling strength is set to a small value $|J_{kl}| \ll |\omega_k - \omega_l|$, see Ref. [14, 52], we can assume that the last term will become highly non-resonant and fast oscillating. Therefore, it is safe to assume that the last term will effectively average out and vanish in the rotating wave approximation. This implies,

$$U_t H_{\text{hop}}(t) U_t^\dagger \approx \sum_{k>l} |J_{kl}| \left(e^{i\alpha_{kl}} a_k^\dagger a_l + e^{-i\alpha_{kl}} a_l^\dagger a_k \right). \quad (3.16)$$

Using the same procedure, we can also approximate the TMS Hamiltonian. For this, we tune the modulation frequencies of the squeezing interactions to $\Delta'_{kl} = \omega_k + \omega_l \equiv \omega'_{kl}$, and expand

$$\lambda_{kl}(t) = 2|\lambda_{kl}| \cos(\omega'_{kl}t - \beta_{kl}) = |\lambda_{kl}| \left(e^{i(\omega'_{kl}t - \beta_{kl})} + e^{-i(\omega'_{kl}t - \beta_{kl})} \right), \quad (3.17)$$

$$\lambda_{kl}^*(t) = \lambda_{lk}(t) = 2|\lambda_{kl}| \cos(\omega'_{lk}t - \beta_{lk}) = |\lambda_{kl}| \left(e^{-i(\omega'_{kl}t - \beta_{kl})} + e^{i(\omega'_{kl}t - \beta_{kl})} \right). \quad (3.18)$$

After applying the RWA with $|\lambda_{kl}| \ll |\omega_k + \omega_l|$, this results in

$$U_t H_{\text{sq}}(t) U_t^\dagger = \sum_{k>l} \lambda_{kl}(t) e^{it(\omega_k + \omega_l)} a_k^\dagger a_l^\dagger + \lambda_{kl}^*(t) e^{-it(\omega_k + \omega_l)} a_l a_k \quad (3.19)$$

$$\approx \sum_{k>l} |\lambda_{kl}| \left(e^{i\beta_{kl}} a_k^\dagger a_l^\dagger + e^{-i\beta_{kl}} a_k a_l \right). \quad (3.20)$$

Finally, this gives us an expression of the total time-independent Hamiltonian in the interaction picture:

$$H_{\text{sys}} \equiv H_{\text{int}} = \sum_{k>l} |J_{kl}| \left(e^{i\alpha_{kl}} a_k^\dagger a_l + \text{h.c.} \right) + \sum_{k>l} |\lambda_{kl}| \left(e^{i\beta_{kl}} a_k^\dagger a_l^\dagger + \text{h.c.} \right). \quad (3.21)$$

The Hamiltonian (3.21) is now composed of only two parts

$$H_{\text{sys}} = H_{\text{hop}} + H_{\text{sq}}. \quad (3.22)$$

explicitly written out as, the beam-splitter Hamiltonian

$$H_{\text{hop}} = |J_{12}| e^{i\alpha_{12}} a_1^\dagger a_2 + |J_{31}| e^{i\alpha_{31}} a_3^\dagger a_1 + |J_{32}| e^{i\alpha_{32}} a_3^\dagger a_2 + \text{H.c.}, \quad (3.23)$$

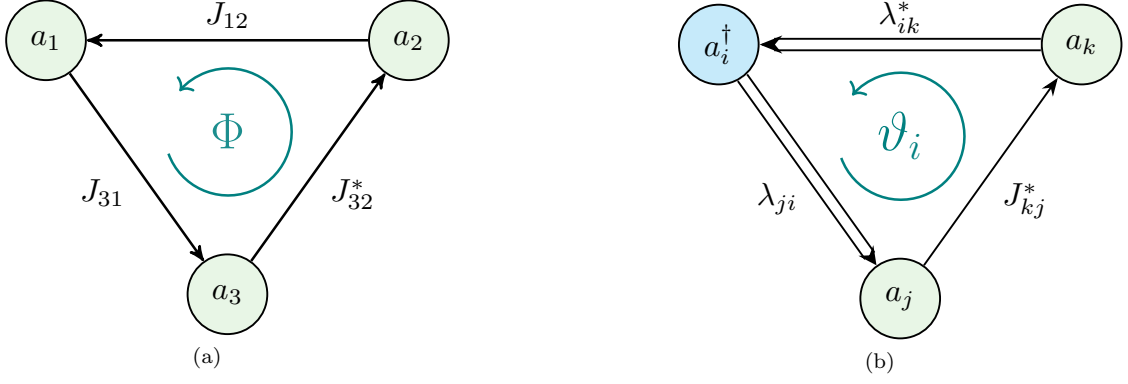


FIG. 4. Couplings for the three-cavity system and the appearance of gauge-invariant phases. Here we only show one direction for the interactions, where the complex conjugate constitutes for the opposite direction of the respective interaction. (a) In this Figure, each pair of bosonic modes (green) a_l and a_k is coupled via a beam-splitter interaction J_{kl} , allowing an excitation to tunnel from cavity $a_l \rightarrow a_k$. Since each coupling parameter J_{kl} has a local phase factor, an anti-clockwise closed loop results in a non-vanishing circulator flux $\Phi \equiv \alpha_{12} + \alpha_{31} - \alpha_{32} \pmod{2\pi}$ (teal). A clockwise loop would result in $-\Phi$, since we define anti-clockwise to be positive. Tuning this flux Φ results in the system being either nonreciprocal or reciprocal. (b) Illustrated here is a single closed loop via a two-mode squeezing interaction of mode a_i^\dagger (light blue) with either λ_{ji} to mode a_j (green) or λ_{ik}^* to mode a_k (green). When there is also tunneling between a_j and a_k , the loop closes, which results in a flux $\vartheta_i \equiv -\beta_{ik} + \beta_{ji} - \alpha_{kj} \pmod{2\pi}$ (teal). However, squeezing introduces a vast number of seemingly closed loops, and considering all possible fluxes needs a more careful treatment, which is done in Sec. III B 2.

and the two-mode squeezing Hamiltonian

$$H_{\text{sq}} = |\lambda_{12}| e^{i\beta_{12}} a_1^\dagger a_2^\dagger + |\lambda_{31}| e^{i\beta_{31}} a_3^\dagger a_1^\dagger + |\lambda_{32}| e^{i\beta_{32}} a_3^\dagger a_2^\dagger + \text{H.c.} . \quad (3.24)$$

As shown, the Hamiltonian becomes static in the rotating frame, and describes the system only by the interactions between different resonators. These interactions in the rotating frame are now complex numbers, with a coupling strength $|J_{kl}|$ (or $|\lambda_{kl}|$), and a complex phase α_{kl} (or β_{kl}). Note, that usually complex interactions are just assumed *ab initio*, in models like ours, see Ref. [1]. However, here they arise as a direct consequence of a time-modulation, which is procedurally closer to experimental realizations. Note, that there are alternate means of constructing complex interaction parameters, one way is by modulating the resonance frequencies of each resonator, see Ref. [14]. As already mentioned in Sec. II B, each individual phase by itself is gauge-dependent and thus not relevant. However, the accumulation of all individual phases into a single gauge-invariant phase is in-turn relevant, and changes the dynamics depending on its value. Nonreciprocal transport occurs for non-trivial values of the AB phase, see Fig. 4. Section III B 2 will talk about this more in-depth.

By introducing the short-hand notation (and suppressing the phases)

$$J_{kl} \equiv |J_{kl}| e^{i\alpha_{kl}} \quad \text{and} \quad \lambda_{kl} \equiv |\lambda_{kl}| e^{i\beta_{kl}} , \quad (3.25)$$

with $J_{kl}^* = J_{lk} \in \mathbb{C}$ ($\lambda_{kl}^* = \lambda_{lk} \in \mathbb{C}$), we can write down the system akin to a more standard beam-splitter

$$H_{\text{hop}} = J_{12} a_1^\dagger a_2 + J_{31} a_3^\dagger a_1 + J_{32} a_3^\dagger a_2 + \text{H.c.} , \quad (3.26)$$

and two-mode squeezing Hamiltonian

$$H_{\text{sq}} = \lambda_{12} a_1^\dagger a_2^\dagger + \lambda_{31} a_3^\dagger a_1^\dagger + \lambda_{32} a_3^\dagger a_2^\dagger + \text{H.c.} . \quad (3.27)$$

In the next chapter, we will add dissipative dynamics to the coherent (and still closed) system above, and derive equations of motion for the resonators coupled to bosonic reservoirs.

B. Dissipative three-cavity ring

1. Equations of motion for the expectation values of modes

The general goal of this section is to engineer nonreciprocal dynamics using the environment to our advantage. A valid starting point for deriving equations of motions is given by the quantum Langevin equation (see Sec. IIE 2), where the stochastic differential equation for operators can be seen as a linear process with constant diffusion. For this, we consider the Hamiltonian (3.22) and simply add dissipation to the Heisenberg equation. The expectation value of the intracavity field $\langle a_i(t) \rangle$ can then be written as

$$\frac{d}{dt} \langle a_i(t) \rangle = i \langle [H_{\text{sys}}, a_i(t)] \rangle - \frac{\kappa_i}{2} \langle a_i(t) \rangle, \quad (3.28)$$

where the first term is the coherent evolution and the second term is the dissipation due to the coupling to a local bosonic reservoir. Here, the expectation value of a system operator a_i is given by the trace

$$\langle a_i \rangle = \text{Tr} \{ a_i \rho \}, \quad (3.29)$$

with system state ρ . Equation (3.28) describes the full coherent and dissipative dynamics, see Fig. 5. This approach

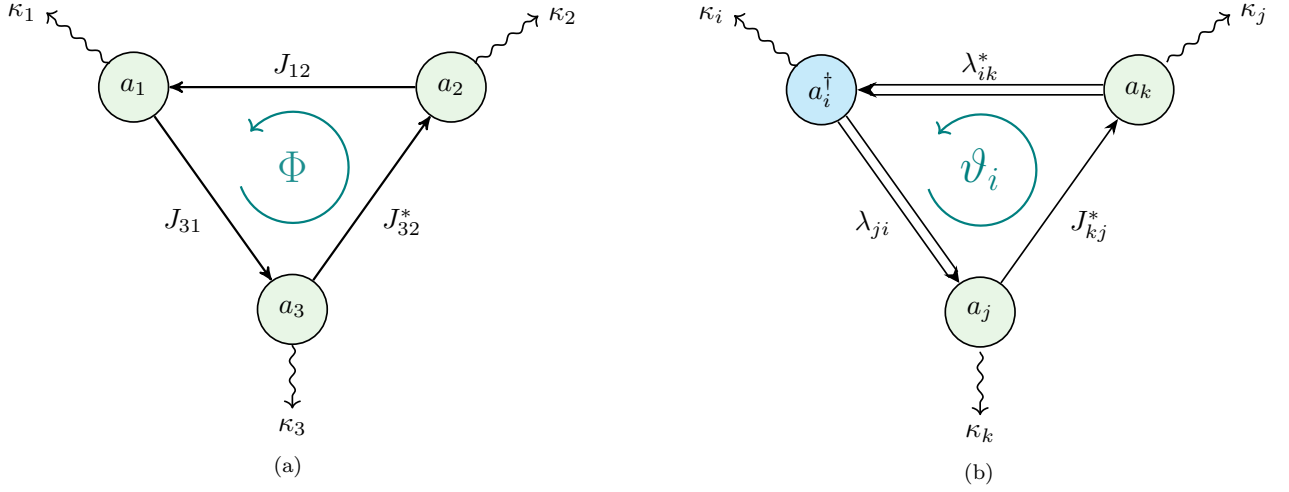


FIG. 5. Couplings for the three-cavity system, where each mode a_i (a_i^\dagger) is dissipatively coupled to a local reservoir with strength κ_i . (a) A closed loop with only BS interactions, resulting in a gauge-invariant phase Φ . (b) Shown is a single possible closed loop due to TMS between modes a_j^\dagger and a_j (resp. a_j^\dagger and a_k), and a single BS interaction between resonators a_j and a_k , resulting in a phase ϑ_i .

gives us the following differential equations for the expectation values

$$\langle \dot{a}_1 \rangle = -\frac{\kappa_1}{2} \langle a_1 \rangle - iJ_{12} \langle a_2 \rangle - iJ_{31}^* \langle a_3 \rangle - i\lambda_{12} \langle a_2^\dagger \rangle - i\lambda_{31} \langle a_3^\dagger \rangle, \quad (3.30a)$$

$$\langle \dot{a}_2 \rangle = -\frac{\kappa_2}{2} \langle a_2 \rangle - iJ_{12}^* \langle a_1 \rangle - iJ_{32}^* \langle a_3 \rangle - i\lambda_{12} \langle a_1^\dagger \rangle - i\lambda_{32} \langle a_3^\dagger \rangle, \quad (3.30b)$$

$$\langle \dot{a}_3 \rangle = -\frac{\kappa_3}{2} \langle a_3 \rangle - iJ_{31} \langle a_1 \rangle - iJ_{32} \langle a_2 \rangle - i\lambda_{31} \langle a_1^\dagger \rangle - i\lambda_{32} \langle a_2^\dagger \rangle, \quad (3.30c)$$

where we suppressed the explicit time-dependence of the operators for readability. This approach recovers the same result one would get using the Lindblad master equation. In general, we also have the adjoint counterparts for the equations of motion above. It is useful to understand what these equations of motion describe: A mode $\langle a_k \rangle$ is driven by mode $\langle a_l \rangle$ in two distinct ways: Either by a BS interaction with amplitude J_{kl} , or a TMS interaction via the adjoint mode $\langle a_l^\dagger \rangle$ and amplitude λ_{kl} . This implies, that setting $\lambda_{kl} = 0$, decouples the dynamics of modes from the dynamics of adjoint modes. Therefore, it becomes completely sufficient to only consider one set of differential equations (either of modes $\langle a_1 \rangle, \langle a_2 \rangle, \langle a_3 \rangle$ or their respective adjoints), for a full treatment. This three-mode model without squeezing will be denoted as the *dissipative ring*. The adjoint equations encode the same amount of information and describe the same (but opposite) dynamics. In the next chapter we will understand how Aharonov-Bohm like gauge-invariant phases arise, and how these equations of motion can be re-expressed in terms of these phases.

2. Expressing the system in terms of synthetic fluxes

Suppose, an excitation wants to propagate from a certain cavity to another. The excitation can then take several different paths to reach that other cavity. However, if the excitation traverses the system and ends up again in its original cavity, the path closes to a loop. All individual phases in that loop accumulate to a single unified Aharonov-Bohm-like phase. We will sometimes denote this phase as the *circulator flux/phase* hereafter. When this phase acquires a specific value, it will enforce a preferred direction of transport, due to destructive interference in the opposite direction, see Sec. III F. Consequently, the probability of a mode travelling the reverse direction becomes zero, resulting in a circulating vortex-like current of modes. The system reaches a limiting regime, where directional transport is protected by this circulator phase. Note that transport is then either unidirectional or amplified. Therefore, we must develop a method to identify all non-trivial loops within this system. Naturally, the following question arises: “When do we consider a closed loop to be non-trivial?” This question is not always easy to answer, as isolating phases becomes increasingly difficult for systems with many pathways. Nonetheless, the geometry of the system introduces constraints, which helps us to simplify the problem. These constraints yield a general assertion, that is, an enclosed loop is considered non-trivial if either (or both) of the following statements hold: 1. *Individual phases on the enclosed path do not trivially cancel each other out* (i.e. $\arg(J_{12}\lambda_{12}^*J_{12}^*\lambda_{12}) = 0$, which resembles the closed path $a_2 \rightarrow a_1 \rightarrow a_2^\dagger \rightarrow a_1^\dagger \rightarrow a_2$). 2. *A circulator phase cannot be written as the sum of remaining circulator phases*. Knowing all relevant phases is immensely useful for understanding the limiting cases and also the system-behaviour of in-between values. Thus, the ultimate goal of this Section is to re-express the equations of motion in terms of gauge-invariant phases.

Since our system with three modes has only six possible pathways, isolating all phases becomes straightforward by expressing the couplings as a (complex) directed graph, consider Fig. 6 (a). Notice, that only one direction for each coupling is shown, since conjugated amplitudes would just give us the same circulator phases with an opposite sign. For readability, we have also suppressed losses in this picture, which are implicitly assumed. By counting all non-trivial loops, we find three distinct phases

$$\Phi \stackrel{\text{def}}{=} \arg(J_{12}J_{31}J_{32}^*) \equiv +\alpha_{12} + \alpha_{31} - \alpha_{32} \pmod{2\pi}, \quad (3.31a)$$

$$\vartheta_1 \stackrel{\text{def}}{=} \arg(\lambda_{12}\lambda_{31}^*J_{32}) \equiv +\beta_{12} - \beta_{31} + \alpha_{32} \pmod{2\pi}, \quad (3.31b)$$

$$\vartheta_2 \stackrel{\text{def}}{=} \arg(\lambda_{12}^*J_{31}^*\lambda_{32}) \equiv -\beta_{12} - \alpha_{31} + \beta_{32} \pmod{2\pi}, \quad (3.31c)$$

where anti-clockwise phases are always defined to be positive. As mentioned earlier, the loop $a_1^\dagger \rightarrow a_2 \rightarrow a_1 \rightarrow a_2^\dagger \rightarrow a_1^\dagger$ vanishes and constitutes no new phase. Thus, one of the phases bordering that path is simply composed of the remaining phases and inherits no additional information. Note, that which phase we choose to express by other phases is just a matter of convention. Here we keep Φ , ϑ_1 and ϑ_2 . Plaquette $a_1^\dagger \rightarrow a_3 \rightarrow a_2^\dagger \rightarrow a_1^\dagger$ and its complex conjugate then has the phase $-(\Phi + \vartheta_1 + \vartheta_2)$. However, this logic holds true for all cases, as each phase of a plaquette is just the negative sum of enclosing phases, i.e. plaquette $a_2^\dagger \rightarrow a_3 \rightarrow a_1 \rightarrow a_2^\dagger$ gives us: $\vartheta_2 = -(\Phi + \vartheta_1 - (\Phi + \vartheta_1 + \vartheta_2))$. By a closer examination of Fig. 6 (a) it can also be understood as holographic projection of a (twisted) platonic octahedron, see Fig. 6 (b). To ensure a consistent sign convention of phases, we define that *anti-clockwise phases on the surface of the octahedron are positive*. For legibility, we suppressed losses and only show the directionality for BS couplings. Notice, that without squeezing, only two decoupled triangles of either modes or adjoints remain, where both are the same up to time-reversal. The only prevailing phase is then Φ , and as mentioned above, it becomes

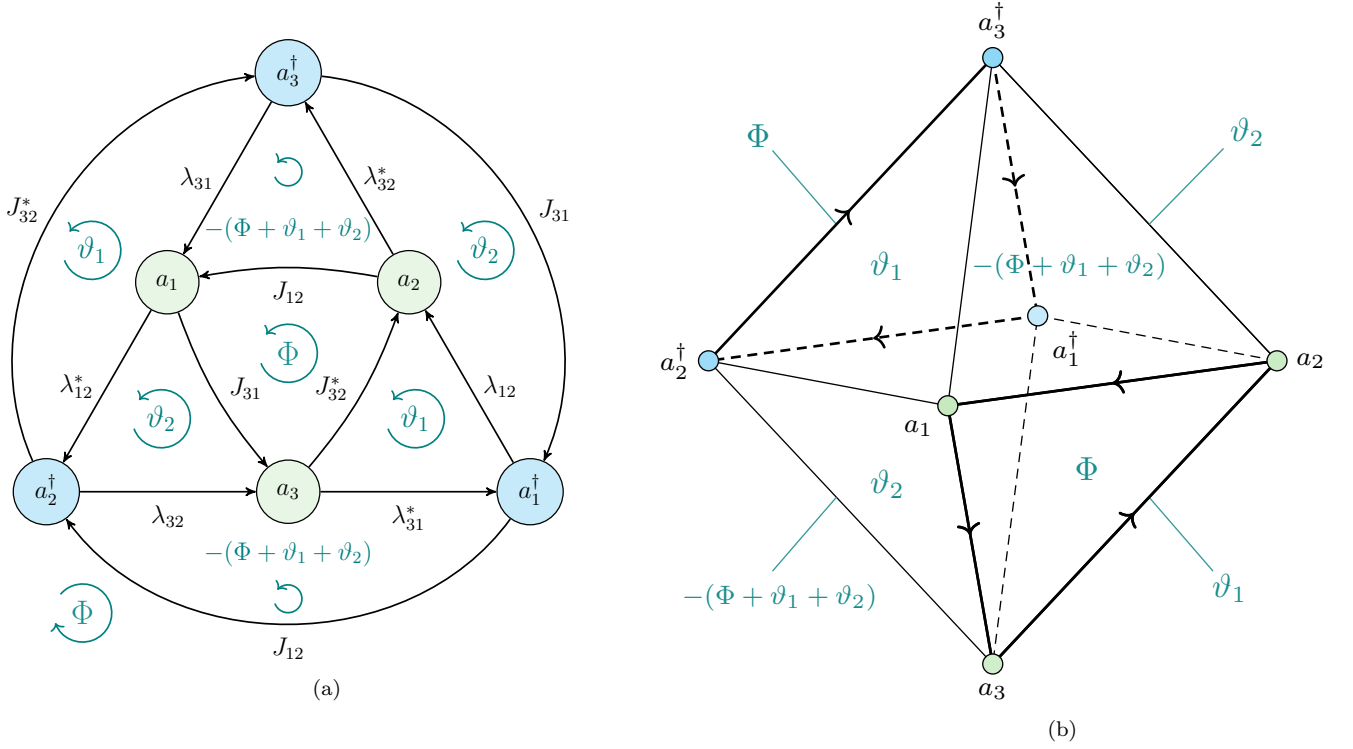


FIG. 6. Geometric representations of the three mode model and its couplings. Losses are not shown and implicitly assumed. (a) Coupling scheme sketching all gauge-invariant phases, where only a single direction is shown for each edge. The isolated phases are Φ , ϑ_1 and ϑ_2 . Anti-clockwise phases are positive. One plaquette-pair can be expressed by other phases enclosing it, as $-(\Phi + \vartheta_1 + \vartheta_2)$. Each phase of a plaquette is the negative sum of enclosing phases. (b) Abstract representation of couplings as an octahedron. Anti-clockwise phases on the outside are positive. The only directions shown are for BS interactions. Without squeezing, the system reduces to two disconnected triangles, where each is just the time-reversed version of the other. Edges on opposites show the same coupling.

completely sufficient to describe the system using only one triangle. Removing other couplings also yields decoupled triangles, but here modes and adjoints can still interact. This abstract representation substantially simplifies the identification of relevant phases, and can be (painfully) generalized for more extensive systems. For reduced models with fewer couplings, this representation is especially handy, since it becomes immediately clear which phases remain. This suggests an intriguing direction for future research, offering the possibility to uncover a clear correspondence between the physical properties of a given system and its geometric structure within this discrete “coupling space”, since the geometric representation can be understood as a complex directed graph (this is called a *digraph*, see Ref. [53]).

Now, we are fully equipped to express the equations of motion using these fluxes. First, consider a general gauge transformation with phases γ_j - yet to be determined, as

$$\langle a_j \rangle \rightarrow \langle a_j \rangle e^{i\gamma_j}. \quad (3.32)$$

The equations of motion (3.30) then become

$$\begin{aligned} \langle \dot{a}_1 \rangle &= -\frac{\kappa_1}{2} \langle a_1 \rangle - i \left(|J_{12}| e^{i(\alpha_{12} + \gamma_2 - \gamma_1)} \langle a_2 \rangle + |J_{31}| e^{-i(\alpha_{31} - \gamma_3 + \gamma_1)} \langle a_3 \rangle + |\lambda_{12}| e^{i(\beta_{12} - \gamma_2 - \gamma_1)} \langle a_2^\dagger \rangle + |\lambda_{31}| e^{i(\beta_{31} - \gamma_3 - \gamma_1)} \langle a_3^\dagger \rangle \right), \\ \langle \dot{a}_2 \rangle &= -\frac{\kappa_2}{2} \langle a_2 \rangle - i \left(|J_{12}| e^{-i(\alpha_{12} + \gamma_2 - \gamma_1)} \langle a_1 \rangle + |J_{32}| e^{-i(\alpha_{32} - \gamma_3 + \gamma_2)} \langle a_3 \rangle + |\lambda_{12}| e^{i(\beta_{12} - \gamma_2 - \gamma_1)} \langle a_1^\dagger \rangle + |\lambda_{32}| e^{i(\beta_{32} - \gamma_3 - \gamma_2)} \langle a_3^\dagger \rangle \right), \\ \langle \dot{a}_3 \rangle &= -\frac{\kappa_3}{2} \langle a_3 \rangle - i \left(|J_{31}| e^{i(\alpha_{31} - \gamma_3 + \gamma_1)} \langle a_1 \rangle + |J_{32}| e^{i(\alpha_{32} - \gamma_3 + \gamma_2)} \langle a_2 \rangle + |\lambda_{31}| e^{i(\beta_{31} - \gamma_3 - \gamma_1)} \langle a_1^\dagger \rangle + |\lambda_{32}| e^{i(\beta_{32} - \gamma_3 - \gamma_2)} \langle a_2^\dagger \rangle \right). \end{aligned} \quad (3.33)$$

Note, that six arguments inside the exponentials are just conjugates of others. Thus, an appropriate transformation can be found by only considering six arguments. However, we also have an additional constrain: There are only three gauge-invariant phases. And since they are the only physically relevant ones, three additional arguments can be set to zero. This gives us a set of closed and solvable algebraic equations. Note, that this choice is not unique. However, since an additional gauge-transformation is always applicable, the physics of the system remain invariant upon our choice (see Appendix B 1 for more). Hence, we choose to transform Eq. (3.33) using

$$\gamma_1 = \frac{\beta_{32} + \alpha_{32}}{2} - \alpha_{31}, \quad \gamma_2 = \frac{\beta_{32} - \alpha_{32}}{2}, \quad \gamma_3 = \frac{\beta_{32} + \alpha_{32}}{2}, \quad (3.34)$$

which eventually leads to

$$\begin{aligned} \langle \dot{a}_1 \rangle &= -\frac{\kappa_1}{2} \langle a_1 \rangle - i|J_{12}|e^{i\Phi} \langle a_2 \rangle - i|J_{31}| \langle a_3 \rangle - i|\lambda_{12}|e^{-i\vartheta_2} \langle a_2^\dagger \rangle - i|\lambda_{31}|e^{-i(\vartheta_1+\vartheta_2)} \langle a_3^\dagger \rangle, \\ \langle \dot{a}_2 \rangle &= -\frac{\kappa_2}{2} \langle a_2 \rangle - i|J_{12}|e^{-i\Phi} \langle a_1 \rangle - i|J_{32}| \langle a_3 \rangle - i|\lambda_{12}|e^{-i\vartheta_2} \langle a_1^\dagger \rangle - i|\lambda_{32}| \langle a_3^\dagger \rangle, \\ \langle \dot{a}_3 \rangle &= -\frac{\kappa_3}{2} \langle a_3 \rangle - i|J_{31}| \langle a_1 \rangle - i|J_{32}| \langle a_2 \rangle - i|\lambda_{31}|e^{-i(\vartheta_1+\vartheta_2)} \langle a_1^\dagger \rangle - i|\lambda_{32}| \langle a_2^\dagger \rangle, \end{aligned} \quad (3.35)$$

as the new equations of motion written in terms of circulator fluxes, with

$$\begin{aligned} J_{12} &= |J_{12}|e^{i\Phi}, & J_{31} &= |J_{31}|, & J_{32} &= |J_{32}|, \\ \lambda_{12} &= |\lambda_{12}|e^{-i\vartheta_2}, & \lambda_{31} &= |\lambda_{31}|e^{-i(\vartheta_1+\vartheta_2)}, & \lambda_{32} &= |\lambda_{32}|. \end{aligned} \quad (3.36)$$

For $\lambda_{ij} = 0$, it is immediately clear how the asymmetric coupling between the resonators $\langle a_1 \rangle$ and $\langle a_2 \rangle$ is expressed by the sign of the flux Φ . Thus, a non-symmetric coupling between mode 1 and 2 can only occur iff

$$J_{12} \neq J_{12}^*, \quad (3.37)$$

is fulfilled, which is analogous to

$$\Im(J_{12}) = |J_{12}| \Im(e^{i\Phi}) \neq 0 \implies \Phi \notin \{0, \pm\pi\} \pmod{2\pi}. \quad (3.38)$$

Thus, any non-symmetric transport between 1 and 2 needs a non-zero imaginary part for the BS interaction J_{12} . Even though this is a good first step, it is not at all sufficient for understanding nonreciprocity in our system. For this, we will consider a reduced two-port effective model, where both modes are coupled to the same effective reservoir, based on Ref. [1]. The reduced model can be seen as a limiting case of the three-mode system and clearly demonstrates how a resonator can be (partially or fully) decoupled from the dynamics of another, yielding the desired nonreciprocity.

As a small remark, it should be possible to find the exact number of gauge-invariant phases for a general bilinear system with N - modes. However, this seems like a challenging task. At least, the number of couplings can be fully determined, see Appendix B 2. This could give a hint at the exact number of non-trivial phases for any system.

Before jumping into the reduced model, we will make a small detour and introduce the Bogoliubov-de-Gennes (BdG) formalism for bosonic systems. This will not only make subsequent calculations more general but also more concise. However, this treatment needs a more careful and nuanced approach. Thus, the following can be seen as a technical toolkit for whats coming.

3. Properties of quadratic Bogoliubov-de-Gennes Hamiltonians

The *Bogoliubov-de-Gennes formalism* is a powerful tool for describing systems in which the dynamics of creation and annihilation operators are not completely decoupled but can influence each other. Historically, this formalism emerged to solve the many-body equation of motion in superconducting systems, see Refs. [54, 55], to appropriately diagonalize the Hamiltonian. However, this formalism has since been generalized to a wide range of systems - most famously with the introduction of quadrature operators in quantum optics. In this section, we will focus on some general, yet useful aspects of bosonic BdG Hamiltonians (which are often simply called “quadratic Hamiltonians” [55]).

To express the equations of motion for the whole system at once, we introduce a vector with annihilation/creation operators (for a general number of cavity modes N)

$$\mathbf{a} \equiv (\hat{a}_1, \dots, \hat{a}_N, \hat{a}_1^\dagger, \dots, \hat{a}_N^\dagger)^T, \quad (3.39)$$

where we use the convention that the adjoint vector

$$\mathbf{a}^\dagger \equiv (\hat{a}_1^\dagger, \dots, \hat{a}_N^\dagger, \hat{a}_1, \dots, \hat{a}_N), \quad (3.40)$$

is a row vector, whose entries are the adjoints of original entries.

a. The bosonic BdG Hamiltonian.

Before we can introduce the BdG Hamiltonian, we need to devise an expression for the commutator of non-Hermitian vectors $[\mathbf{a}_i, \mathbf{a}_j^\dagger]$. However, since the adjoint vector is defined as a row vector, this convention introduces an important nuance: How do we calculate expressions of the form $\mathbf{a}^\dagger \mathbf{a}$, where the desired result should be a matrix and not a scalar? For technical details regarding this question, consider Appendix B3, where consistent algebraic rules are introduced. However, we reveal the main result here, as this will be used heavily in subsequent chapters. For this, we define a column vector of adjoint elements

$$\mathbf{a}^\ddagger \equiv \mathbf{\Lambda}_x \mathbf{a} = (\hat{a}_1^\dagger, \dots, \hat{a}_N^\dagger, \hat{a}_1, \dots, \hat{a}_N)^T, \quad (3.41)$$

where $\mathbf{\Lambda}_x = \sigma_x \otimes \mathbf{1}_N$ is an extended Pauli-matrix, permuting elements inside the vector \mathbf{a} . Note, that we also introduced the new symbol \ddagger for readability, which acts only at the level of elements and does not transpose the original vector. Using this, we find

$$\mathbf{a}^\dagger \mathbf{a} = (\mathbf{a}^\ddagger \mathbf{a}^T)^T, \quad (3.42)$$

with the commutation relations

$$[\mathbf{a}_i, \mathbf{a}_j^\ddagger] = (\mathbf{\Lambda}_z)_{ij}, \quad \mathbf{\Lambda}_z = \begin{pmatrix} \mathbf{1}_N & 0 \\ 0 & -\mathbf{1}_N \end{pmatrix} = \sigma_z \otimes \mathbf{1}_N, \quad (3.43)$$

and

$$[\mathbf{a}_i, \mathbf{a}_j] = i(\mathbf{\Lambda}_y)_{ij}, \quad i\mathbf{\Lambda}_y = \begin{pmatrix} 0 & \mathbf{1}_N \\ -\mathbf{1}_N & 0 \end{pmatrix} = i\sigma_y \otimes \mathbf{1}_N, \quad (3.44)$$

where Λ_z is also an extended Pauli matrix. The matrix $i\Lambda_y \in \text{Sp}(2N, \mathbb{R})$ is a symplectic form $\Omega = i\Lambda_y$ and also an element of the symplectic group [40], which is defined as the set $\text{Sp}(2N, \mathbb{R}) = \{\mathbf{A} \in \mathbf{A}_{2N \times 2N}(\mathbb{R}) : \mathbf{A}^T \Omega \mathbf{A} = \Omega\}$. Consequently, we can express the (second quantized) system Hamiltonian in the BdG-form

$$H_{\text{sys}} = \sum_{i,j} \mathbf{a}_i^\dagger \mathbf{H}_{ij} \mathbf{a}_j, \quad (3.45)$$

with the *Hamiltonian matrix*

$$\mathbf{H}(\Phi, \vartheta_1, \vartheta_2) = \begin{pmatrix} \mathbf{h}_1(\Phi) & \mathbf{h}_2(\vartheta_1, \vartheta_2) \\ \mathbf{h}_2^*(\vartheta_1, \vartheta_2) & \mathbf{h}_1^*(\Phi) \end{pmatrix} \equiv \mathbf{H} = \begin{pmatrix} \mathbf{h}_1 & \mathbf{h}_2 \\ \mathbf{h}_2^* & \mathbf{h}_1^* \end{pmatrix}, \quad (3.46)$$

where $\mathbf{h}_1^\dagger = \mathbf{h}_1$ is hermitian and $\mathbf{h}_2^T = \mathbf{h}_2$ is symmetric. The submatrices for our system with $N = 3$ modes are given by

$$H_{\text{hop}} = \mathbf{a}^\dagger \begin{pmatrix} \mathbf{h}_1 & 0 \\ 0 & \mathbf{h}_1^* \end{pmatrix} \mathbf{a}, \quad \text{with} \quad \mathbf{h}_1 = \begin{pmatrix} 0 & J_{12} & J_{31}^* \\ J_{12}^* & 0 & J_{32}^* \\ J_{31} & J_{32} & 0 \end{pmatrix}, \quad (3.47)$$

$$H_{\text{sq}} = \mathbf{a}^\dagger \begin{pmatrix} 0 & \mathbf{h}_2 \\ \mathbf{h}_2^* & 0 \end{pmatrix} \mathbf{a}, \quad \text{with} \quad \mathbf{h}_2 = \begin{pmatrix} 0 & \lambda_{12} & \lambda_{31} \\ \lambda_{12} & 0 & \lambda_{32} \\ \lambda_{31} & \lambda_{32} & 0 \end{pmatrix}, \quad (3.48)$$

which encode the coherent beam-splitter and squeezing interactions, respectively. To understand the properties of this representation of the system, let us first consider a closed system. In this case, we need to find an expression for the commutator in the Heisenberg equation of motion, which is given by

$$i[\mathbf{H}, \mathbf{a}] = i \begin{pmatrix} -\mathbf{h}_1 & -\mathbf{h}_2 \\ \mathbf{h}_2^* & \mathbf{h}_1^* \end{pmatrix} \mathbf{a} = -i\Lambda_z \mathbf{H} \mathbf{a}. \quad (3.49)$$

Here we call

$$\mathbf{A} \equiv -i\Lambda_z \mathbf{H}, \quad (3.50)$$

the *dynamical matrix of the closed system*, which is *pseudo-Hermitian* for bosonic systems [40, 56]

$$1. \quad \mathbf{A} = \Lambda_x \mathbf{A}^* \Lambda_x \iff \mathbf{A}^T = \Lambda_x \mathbf{A}^\dagger \Lambda_x, \quad (3.51a)$$

$$2. \quad \mathbf{A} = -\Lambda_z \mathbf{A}^\dagger \Lambda_z, \quad (3.51b)$$

where both relations can be seen as the pseudo-Hermiticity of our dynamical matrix \mathbf{A} . The first relation basically states that \mathbf{A} and its complex conjugate are the same up to a permutation of blocks inside \mathbf{A} . This is the most important relationship for us and will give us intuition for the observed scattering behaviour of the system. The second condition directly relates the dynamical matrix to its adjoint via Λ_z , yet flips the sign, this can be roughly understood as a condition which stems from the commutator relation in Eq. (3.43). Nonetheless, we can relate \mathbf{A} to its adjoint \mathbf{A}^\dagger via the anti-commutator of \mathbf{H} and Λ_z in a slightly different way

$$\mathbf{A} = \mathbf{A}^\dagger - i\{\mathbf{H}, \Lambda_z\} = \mathbf{A}^\dagger - i2\Lambda_z(\mathbf{h}_1 \oplus \mathbf{h}_1^*). \quad (3.52)$$

It follows, for the commutator

$$\mathbf{A} = -\mathbf{A}^\dagger + i[\mathbf{H}, \mathbf{\Lambda}_z] = -\mathbf{A}^\dagger + 2\mathbf{\Lambda}_y(\mathbf{h}_2^* \oplus \mathbf{h}_2), \quad (3.53)$$

where the prior equation implies that the dynamical matrix for the closed system becomes Hermitian when no beam-splitter interaction is present, and the latter is a bit more abstract but will become important for the three-mode system without TMS. Here, we used the direct sum defined as $\mathbf{h}_i \oplus \mathbf{h}_i^* \equiv \text{diag}(\mathbf{h}_i, \mathbf{h}_i^*)$, and $\mathbf{\Lambda}_y = -i\mathbf{\Lambda}_z\mathbf{\Lambda}_x$. For completeness, both statements can also be summed up as

$$\mathbf{A} = \frac{i}{2}([\mathbf{H}, \mathbf{\Lambda}_z] - \{\mathbf{H}, \mathbf{\Lambda}_z\}), \quad (3.54)$$

For now, this concludes our considerations of the closed system. Formally speaking, this system can be solved in several ways, however, we will only do this for the case without squeezing, see Sec III G 1. We now move on to open system dynamics.

b. Extension of the BdG formalism to open systems.

The quantum Langevin equation of expectation values can be written as

$$\frac{d}{dt} \langle \mathbf{a}(t) \rangle = i \langle [\mathbf{H}, \mathbf{a}(t)] \rangle - \frac{1}{2} \tilde{\mathbf{K}} \langle \mathbf{a}(t) \rangle, \quad (3.55)$$

where $\tilde{\mathbf{K}} = \mathbb{1}_2 \otimes \text{diag}(\kappa_1, \dots, \kappa_N)$ is a matrix of dissipative couplings κ_i . In a more concise manner we can write

$$\frac{d}{dt} \langle \mathbf{a}(t) \rangle = \mathbf{D} \langle \mathbf{a}(t) \rangle, \quad (3.56)$$

where

$$\mathbf{D} \equiv \mathbf{A} - \frac{1}{2} \tilde{\mathbf{K}} = -i\mathbf{\Lambda}_z\mathbf{H} - \frac{1}{2} \tilde{\mathbf{K}}, \quad (3.57)$$

is the new *dynamical matrix of the open system*. Note that the dynamical matrix can become time-dependent, which will be important for the effective model when we introduce an explicitly time-dependent effective damping rate. This matrix still fulfills some of the features introduced above, yet behaves differently in others. For brevity, we state only the most useful properties. Consider the adjoint

$$\mathbf{D}^\dagger = \mathbf{A}^\dagger - \frac{1}{2} \tilde{\mathbf{K}}, \quad (3.58)$$

where we try to express the same pseudo-Hermiticity relations as before

$$1. \quad \mathbf{D} = \mathbf{\Lambda}_x \mathbf{D}^* \mathbf{\Lambda}_x \iff \mathbf{D}^T = \mathbf{\Lambda}_x \mathbf{D}^\dagger \mathbf{\Lambda}_x, \quad (3.59a)$$

$$2. \quad \mathbf{D} = -\mathbf{\Lambda}_z \mathbf{D}^\dagger \mathbf{\Lambda}_z - \tilde{\mathbf{K}}, \quad (3.59b)$$

yet we find that the dynamical matrix with dissipation is not even pseudo-Hermitian in general, which coincides nicely with Ref. [55]. However, we can also find an expression similar to Eq. (3.52) with $\mathbf{D}^\dagger - \mathbf{D} = \mathbf{A}^\dagger - \mathbf{A}$. From that, it follows

$$\mathbf{D} = \mathbf{D}^\dagger - i\{\mathbf{H}, \Lambda_z\} = \mathbf{D}^\dagger - i2\Lambda_z(\mathbf{h}_1 \oplus \mathbf{h}_1^*), \quad (3.60)$$

where we observe the same consequences as for the closed system: Without a beam-splitter interaction, the dynamical matrix becomes Hermitian, regardless of any dissipation. This is different for the commutator

$$\mathbf{D} + \mathbf{D}^\dagger = i[\mathbf{H}, \Lambda_z] - \tilde{\mathbf{K}} \quad (3.61)$$

compared to Eq. (3.53), where we used Eq. (3.58). This implies that the damping adds up after reversal, and we get the useful result

$$\mathbf{D} = -\mathbf{D}^\dagger - \tilde{\mathbf{K}} + i[\mathbf{H}, \Lambda_z] = -\mathbf{D}^\dagger - \tilde{\mathbf{K}} + 2\Lambda_y(\mathbf{h}_2^* \oplus \mathbf{h}_2), \quad (3.62)$$

see Appendix C3 for how this expression can be used. All this can again be summed up as

$$\mathbf{D} = \frac{i}{2}([\mathbf{H}, \Lambda_z] - \{\mathbf{H}, \Lambda_z\} + i\tilde{\mathbf{K}}), \quad (3.63)$$

C. Quadrature representation

In this part, we will introduce the quadrature basis of the optical phase space, since a cavity i driven by two-mode squeezing couples $\langle a_i \rangle$ with $\langle a_j^\dagger \rangle$ as evident by the dynamical matrix of Eq. (3.50). In presence of squeezing, the system can be described either in terms of mode or quadrature operators. Depending on the case at hand, one representation can become more useful than the other. Without squeezing, the matrix becomes block-diagonal and it is enough to just consider one block for the full dynamics of the system. However, the quadrature also accounts for non-zero off-diagonal blocks.

Here, we introduce position and momentum *quadratures*

$$\hat{x}_i(t) = \frac{1}{\sqrt{2}} \left(\hat{a}_i^\dagger(t) + \hat{a}_i(t) \right), \quad \hat{p}_i(t) = \frac{i}{\sqrt{2}} \left(\hat{a}_i^\dagger(t) - \hat{a}_i(t) \right), \quad (3.64)$$

and note that we can also re-express the creation/annihilation operators by their quadratures as

$$\hat{a}_i(t) = \frac{1}{\sqrt{2}} \left(\hat{x}_i(t) + i\hat{p}_i(t) \right), \quad \hat{a}_i^\dagger(t) = \frac{1}{\sqrt{2}} \left(\hat{x}_i(t) - i\hat{p}_i(t) \right). \quad (3.65)$$

These new operators fulfill the following equal-time commutation relations

$$\forall t : \quad [\hat{x}_i(t), \hat{p}_j(t)] = i\delta_{ij}, \quad [\hat{x}_i(t), \hat{x}_j(t)] = [\hat{p}_i(t), \hat{p}_j(t)] = 0, \quad (3.66)$$

which are the canonical commutation relation of momentum and position quantum operators. As a next step, we transform the vector from Eq. (3.39) into the quadrature basis using the convention

$$\mathbf{v}(t) = (x_1(t), p_1(t), \dots, x_N(t), p_N(t))^T, \quad (3.67)$$

fulfilling the commutation relation

$$[\mathbf{v}_i, \mathbf{v}_j] = i \boldsymbol{\Omega}_{ij}, \quad \text{with} \quad \boldsymbol{\Omega} = \bigoplus_{k=1}^N \begin{pmatrix} 0 & 1 \\ -1 & 0 \end{pmatrix} = \mathbf{1}_N \otimes i\sigma_y, \quad (3.68)$$

where $\boldsymbol{\Omega} \in \text{Sp}(2N, \mathbb{R})$ is a symplectic form (in a different basis compared to the form introduced earlier), see Ref. [40]. To change from mode to quadrature operators, we can find an unitary *transformation matrix* \mathbf{T} between the bases (for $N = 3$ in our case)

$$\mathbf{v}(t) = \begin{pmatrix} x_1(t) \\ p_1(t) \\ x_2(t) \\ p_2(t) \\ x_3(t) \\ p_3(t) \end{pmatrix} = \frac{1}{\sqrt{2}} \begin{pmatrix} 1 & 0 & 0 & 1 & 0 & 0 \\ -i & 0 & 0 & i & 0 & 0 \\ 0 & 1 & 0 & 0 & 1 & 0 \\ 0 & -i & 0 & 0 & i & 0 \\ 0 & 0 & 1 & 0 & 0 & 1 \\ 0 & 0 & -i & 0 & 0 & i \end{pmatrix} \begin{pmatrix} a_1(t) \\ a_2(t) \\ a_3(t) \\ a_1^\dagger(t) \\ a_2^\dagger(t) \\ a_3^\dagger(t) \end{pmatrix} \equiv \mathbf{T} \mathbf{a}(t), \quad (3.69)$$

which is composed of a rotation and a permutation. Note, the permutation aspect for N modes is not straightforward, consider Appendix B4 for more. By using \mathbf{T} , we can transform the dynamical matrix \mathbf{D} of Eq. (3.57) to the quadrature-representation and get

$$\mathbf{M} \equiv \mathbf{T} \mathbf{D} \mathbf{T}^\dagger. \quad (3.70)$$

The dynamical matrix \mathbf{M} describes the open system in the quadrature basis. Here we make an important remark about the convention used for distinguishing the bases: Every variable with a $\tilde{\cdot}$ -symbol will be in the mode-representation (except for distinct names like \mathbf{D} and \mathbf{M} etc.), i.e. the matrix encoding dissipation simply becomes $\mathbf{K} = \mathbf{T} \tilde{\mathbf{K}} \mathbf{T}^\dagger$ in the quadrature representation.

The Langevin equation in the quadrature basis is then

$$\frac{d}{dt} \langle \mathbf{v}(t) \rangle = \mathbf{M} \langle \mathbf{v}(t) \rangle. \quad (3.71)$$

Here, the dynamical matrix is always real and time-independent for the full model (all possibly complex couplings are now real). This is important to mention, as the dynamical matrix is not always real or time-independent for an effective model. The explicit representation of \mathbf{M} of our three-mode system can be found in Appendix B5.

D. Heisenberg-Langevin equation in frequency space

To understand the reason why we permute and not just simply dagger the elements of the mode vectors above, take the Fourier-transform of time-dependent operators: Remember, that equal-time commutation relations of (system) creation/annihilation operators are unit-less quantities

$$[a_i(t), a_j^\dagger(t)] = \delta_{ij} \implies [\mathbf{a}_i(t), \mathbf{a}_j^\dagger(t)] = (\boldsymbol{\Lambda}_z)_{ij},$$

By simply Fourier-transforming, it follows

$$a_i(t) \xrightarrow{\mathcal{F}} a_i[\omega], \quad a_i^\dagger(t) \xrightarrow{\mathcal{F}} a_i^\dagger[\omega], \quad (3.72)$$

where the latter is the Fourier-transform of the daggered mode. However, since we defined the Fourier-transform s.t. $(f[\omega])^\dagger = f^\dagger[-\omega]$ holds, we cannot simply transform and then dagger the elements, as this would flip the sign of ω . In short this implies

$$(\mathbf{a}[\omega])^\ddagger = ((\mathbf{a}[\omega])^\dagger)^T = (\mathbf{a}^\dagger[-\omega])^T = \mathbf{a}^\ddagger[-\omega]. \quad (3.73)$$

Thus, \ddagger transforms just like \dagger in frequency space with

$$\mathbf{a}^\dagger[\omega] = (\mathbf{a}[-\omega])^\dagger, \quad \mathbf{a}^\ddagger[\omega] = (\mathbf{a}[-\omega])^\ddagger. \quad (3.74)$$

By using Eq. (2.45) we get the EOMs in frequency space via

$$\mathcal{F}\{\dot{a}_i(t)\}[\omega] = i\omega a_i[\omega] \quad \text{and} \quad \mathcal{F}\{\dot{a}_i^\dagger(t)\}[\omega] = i\omega a_i^\dagger[\omega] \implies i\omega \mathbf{a}[\omega] = \mathbf{D} \mathbf{a}[\omega], \quad (3.75a)$$

$$\mathcal{F}\{\dot{x}_i(t)\}[\omega] = i\omega x_i[\omega] \quad \text{and} \quad \mathcal{F}\{\dot{p}_i(t)\}[\omega] = i\omega p_i[\omega] \implies i\omega \mathbf{v}[\omega] = \mathbf{M} \mathbf{v}[\omega]. \quad (3.75b)$$

This concludes our considerations regarding the BdG-formalism, which gives us a toolkit for understanding when the system will become nonreciprocal, and how to find expressions for the S-matrix or the output-noise spectral density.

E. Reservoir engineering and the nonreciprocal two-mode model

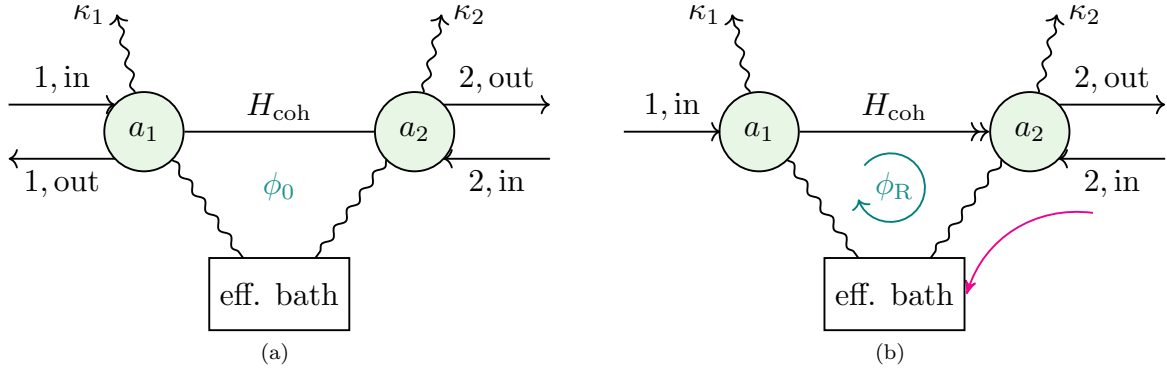


FIG. 7. Schematic illustrating (non)reciprocity in the effective model. Each resonator has a single input and output wave guide. Both are coherently coupled by H_{coh} . However resonators 1 and 2 are also dissipatively coupled through the effective reservoir “eff bath”. Nonreciprocity appears by balancing out coherent with dissipative interactions. (a) Reciprocal limit. Here, the flux is trivially set to $\Phi = \phi_0 = 0$ (see Eq. (3.103)). (b) Nonreciprocal case. For any other value of $\Phi \neq \phi_0$, there is unequal and nonreciprocal transport. For $\Phi = \phi_R = \pi/2$ (exactly a quarter flux quantum, see Eq. (3.102)), the system reaches the unidirectional limit. In that limit, input from 1 is fully transmitted to output 2, but input from port 2 is completely dissipated by the effective reservoir and never reaches 1.

The whole idea behind the paper of Metelmann and Clerk [1] was to construct a nonreciprocal two-mode model, without relying on a pre-engineered nonreciprocal reservoir. In their own words, the approach uses *reservoir engineering*,

“where a structured dissipative environment generates useful quantum behaviour” (taken from Ref. [1]). For this, a strongly damped auxiliary resonator is coupled to two other resonators and causes an effective dissipative interaction between them. The two resonators are coherently coupled (via a BS or TMS interaction), but also dissipatively to the effective reservoir. The recipe is then simple: By balancing out the coherent and dissipative interactions, destructive interference in one direction breaks reciprocity, see Fig. 7. This allows for nonreciprocal transport, since one cavity decouples from the other in a single direction, i.e. cavity 1 can drive 2, but not vice versa. In principle, this model can be assumed *ab initio* by choosing a corresponding jump operator of the shared reservoir using the Lindblad master equation. We approach this by eliminating the third resonator from the three-mode system, which acts as the auxiliary mode. To accomplish this, the auxiliary’s dynamical timescales must be significantly different from those of the rest of the system. A strongly damped auxiliary $\kappa_3 \gg \kappa_{1,2}$ will have a decreased relaxation time $\tau_3 = 1/\kappa_3$. And in this timescale, excitations entering the auxiliary will dissipate faster than they can re-enter other resonators - and the auxiliary reaches steady state. If any transport from port 1 to 2 behaves differently from reversed reciprocal process, namely from 2 to 1, the system becomes nonreciprocal. This in-turn violates the unitarity of the scattering matrix in this minimal (effective) model.

1. Markovian effective model via adiabatic elimination - the brute force way

The auxiliary mode can be eliminated in multiple ways. We compare two different approaches, 1. *Adiabatically eliminating the auxiliary*, and 2. *Fourier transforming the equations of motion and eliminating the auxiliary thereafter*. The first approach is simpler, but any additional knowledge of the auxiliary is lost, since it reaches steady-state. Thus, we call this the “brute force way”. Even though the second approach is harder to compute, it retains the frequency-information of the auxiliary. Implying, that not only does this approach give us a glimpse at the dynamical properties of the auxiliary, it is also treated equal to other modes. We will call this the “gentle way” of eliminating. As it will turn out at the end of both derivations, the first procedure leads to a *Markovian effective reservoir*, where the second procedure leads to a *non-Markovian reservoir*. Subsequently, we start with the adiabatic elimination.

As mentioned earlier, the decay rate of the auxiliary is assumed to be the dominant parameter $\kappa_3 \gg \kappa_{1,2}, J_{ij}, \lambda_{ij}$. Thus, the correlation time $\tau \equiv 1/\kappa_1 \approx 1/\kappa_2$, is significantly longer compared to the correlation time of the auxiliary $\tau_3 \ll \tau$. Thus, the auxiliary becomes quasi-static from the rest of the system and reaches steady state $\langle \dot{a}_3 \rangle = 0$ at long times. Using this, we can insert the steady state solution of the third cavity

$$\langle a_3 \rangle = \frac{2}{\kappa_3} (-iJ_{31} \langle a_1 \rangle - iJ_{32} \langle a_2 \rangle - i\lambda_{31} \langle a_1^\dagger \rangle - i\lambda_{23} \langle a_2^\dagger \rangle), \quad (3.76)$$

into the equations of motion for the remaining two resonators, giving us

$$\begin{aligned} \langle \dot{a}_1 \rangle &= \left[-\frac{2(|J_{31}|^2 - |\lambda_{31}|^2)}{\kappa_3} - \frac{\kappa_1}{2} \right] \langle a_1 \rangle - i \left[J_{12} + i \left(\frac{2(\lambda_{31}\lambda_{32}^* - J_{32}J_{31}^*)}{\kappa_3} \right) \right] \langle a_2 \rangle - i \left[\lambda_{12} + i \left(\frac{2(\lambda_{31}J_{32}^* - \lambda_{32}J_{31}^*)}{\kappa_3} \right) \right] \langle a_2^\dagger \rangle, \\ \langle \dot{a}_2 \rangle &= \left[-\frac{2(|J_{32}|^2 - |\lambda_{32}|^2)}{\kappa_3} - \frac{\kappa_2}{2} \right] \langle a_2 \rangle - i \left[J_{12}^* + i \left(\frac{2(\lambda_{31}^*\lambda_{32} - J_{32}^*J_{31})}{\kappa_3} \right) \right] \langle a_1 \rangle - i \left[\lambda_{12} - i \left(\frac{2(\lambda_{31}J_{32}^* - \lambda_{32}J_{31}^*)}{\kappa_3} \right) \right] \langle a_1^\dagger \rangle. \end{aligned} \quad (3.77)$$

By introducing some useful abbreviations

$$J := J_{12}, \quad \lambda := \lambda_{12}, \quad \Gamma_0 := \frac{4}{\kappa_3} |J|^2, \quad \Gamma_j := \Gamma_0 (|u_j|^2 - |v_j|^2), \quad (3.78)$$

$$u_j := \frac{J_{3j}}{J}, \quad v_j := \frac{\lambda_{3j}}{J}, \quad \mu := v_1 v_2^* - u_2 u_1^*, \quad \nu := v_1 u_2^* - v_2 u_1^*,$$

Eq. (3.77) precisely resembles the same result given by Metelmann and Clerk [1]

$$\langle \dot{a}_1 \rangle = -\frac{\Gamma_1 + \kappa_1}{2} \langle a_1 \rangle - i \left[J + i\mu \frac{\Gamma_0}{2} \right] \langle a_2 \rangle - i \left[\lambda + i\nu \frac{\Gamma_0}{2} \right] \langle a_2^\dagger \rangle, \quad (3.79a)$$

$$\langle \dot{a}_2 \rangle = -\frac{\Gamma_2 + \kappa_2}{2} \langle a_2 \rangle - i \left[J^* + i\mu^* \frac{\Gamma_0}{2} \right] \langle a_1 \rangle - i \left[\lambda - i\nu \frac{\Gamma_0}{2} \right] \langle a_1^\dagger \rangle. \quad (3.79b)$$

These equations tell us already a lot about the dynamics of the system. The first term in both equations is a modified damping rate: Each resonator i is coupled to its own local reservoir κ_i , and additionally to the shared reservoir with Γ_0 , scaled by the probability difference $|u_j|^2 - |v_j|^2$. This encodes how probable a decay to the effective reservoir is. The second and third terms describe how each mode is driven by the other mode. This can happen in multiple ways, either coherently (J or λ), or dissipatively with the non-local reservoir ($\mu\Gamma_0/2$ or $\nu\Gamma_0/2$). Balancing these distinct interaction pathways alters the symmetry in the way modes drive each other. To understand this, we dismiss the third term, and focus only on the second term: By setting $J = -i\mu\Gamma_0/2$, the second term of the first equation vanishes, where the same term of the second equation attains a higher value. In this case, $\langle \dot{a}_1 \rangle$ is not influenced by $\langle a_2 \rangle$ anymore, but $\langle \dot{a}_2 \rangle$ is driven by $\langle a_1 \rangle$. This is a fully unidirectional limit and immediately shows how nonreciprocity is attainable. So what is the reason we observe this behaviour? If we compare the second and third term of $\langle \dot{a}_1 \rangle$ to the respective terms of $\langle \dot{a}_2 \rangle$, we see something surprising: The terms are *almost* complex conjugates of each other - the only difference being the sign of the imaginary unit i in-front of dissipative interactions. Thus, coherent interactions becoming imaginary yield an asymmetry. This coincides perfectly with our considerations about the gauge-invariant phases before, as non-trivial values of the phases imply imaginary interactions. A trivial value will always lead to fully real interactions parameters and can thus not enforce nonreciprocity in this model. A more in-depth discussion about different limits can be found in Section III F.

2. Non-Markovian effective model via elimination by Fourier transforming - the gentle way

Contrary to the first elimination procedure, the auxiliary will be treated the same way as other modes. This will give us non-Markovian corrections to the adiabatically eliminated two-mode model. Consider the way we defined the Fourier transform in Sec. IID. By using Eq. (2.45) (and (2.42) for adjoint modes), we can transform the equations of motion (3.30) to frequency space. Solving the third mode gives us

$$\langle a_3[\omega] \rangle = \frac{1}{i\omega + \kappa_3/2} \left(-iJ_{31} \langle a_1[\omega] \rangle - iJ_{32} \langle a_2[\omega] \rangle - i\lambda_{31} \langle a_1^\dagger[\omega] \rangle - i\lambda_{32} \langle a_2^\dagger[\omega] \rangle \right). \quad (3.80)$$

Analogously to the adiabatic elimination, this solution is inserted into the remaining equations. This gives us a set of algebraic equations in frequency space. The equation for the first mode is then

$$\begin{aligned} i\omega \langle a_1[\omega] \rangle = & - \left[\frac{|J_{31}|^2 - |\lambda_{31}|^2}{i\omega + \kappa_3/2} + \frac{\kappa_1}{2} \right] \langle a_1[\omega] \rangle \\ & - i \left[J_{12} + i \left(\frac{\lambda_{31}\lambda_{32}^* - J_{32}J_{31}^*}{i\omega + \kappa_3/2} \right) \right] \langle a_2[\omega] \rangle - i \left[\lambda_{12} + i \left(\frac{\lambda_{31}J_{32}^* - \lambda_{32}J_{31}^*}{i\omega + \kappa_3/2} \right) \right] \langle a_2^\dagger[\omega] \rangle. \end{aligned} \quad (3.81)$$

And analogously for the second mode

$$\begin{aligned} i\omega \langle a_2[\omega] \rangle = & - \left[\frac{|J_{32}|^2 - |\lambda_{32}|^2}{i\omega + \kappa_3/2} + \frac{\kappa_2}{2} \right] \langle a_2[\omega] \rangle \\ & - i \left[J_{12}^* + i \left(\frac{\lambda_{31}^*\lambda_{32} - J_{32}^*J_{31}}{i\omega + \kappa_3/2} \right) \right] \langle a_1[\omega] \rangle - i \left[\lambda_{12} - i \left(\frac{\lambda_{31}J_{32}^* - \lambda_{32}J_{31}^*}{i\omega + \kappa_3/2} \right) \right] \langle a_1^\dagger[\omega] \rangle. \end{aligned} \quad (3.82)$$

By introducing similar abbreviations to the adiabatic procedure

$$J := J_{12}, \quad \lambda := \lambda_{12}, \quad \Gamma[\omega] := \frac{2}{i\omega + \kappa_3/2} |J|^2, \quad \Gamma_j[\omega] := \Gamma[\omega] (|u_j|^2 - |v_j|^2), \quad (3.83)$$

$$u_j := \frac{J_{3j}}{J}, \quad v_j := \frac{\lambda_{3j}}{J}, \quad \mu := v_1 v_2^* - u_2 u_1^*, \quad \nu := v_1 u_2^* - v_2 u_1^*,$$

we see how the effective damping rate $\Gamma[\omega]$ is now an ω - dependent, generalized exchange rate between each resonator and the effective reservoir. On resonance, the exchange rate simply reduces to the Markovian damping rate

$$\lim_{\omega \rightarrow 0} \Gamma[\omega] = \Gamma_0. \quad (3.84)$$

The introduced abbreviations are especially useful, since they yield a set of equations with a similar structure as for the elimination before:

$$i\omega \langle a_1[\omega] \rangle = - \left[\frac{\Gamma_1[\omega] + \kappa_1}{2} \right] \langle a_1[\omega] \rangle - i \left[J + i\mu \frac{\Gamma[\omega]}{2} \right] \langle a_2[\omega] \rangle - i \left[\lambda + i\nu \frac{\Gamma[\omega]}{2} \right] \langle a_2^\dagger[\omega] \rangle, \quad (3.85a)$$

$$i\omega \langle a_2[\omega] \rangle = - \left[\frac{\Gamma_2[\omega] + \kappa_2}{2} \right] \langle a_2[\omega] \rangle - i \left[J^* + i\mu^* \frac{\Gamma[\omega]}{2} \right] \langle a_1[\omega] \rangle - i \left[\lambda - i\nu \frac{\Gamma[\omega]}{2} \right] \langle a_1^\dagger[\omega] \rangle. \quad (3.85b)$$

Note, these equations can also be expressed in the BdG-form

$$i\omega \langle \mathbf{a}_{\text{eff}}[\omega] \rangle = \mathbf{D}_{\text{eff}}[\omega] \langle \mathbf{a}_{\text{eff}}[\omega] \rangle, \quad (3.86)$$

with the basis

$$\mathbf{a}_{\text{eff}} = (a_1, a_2, a_1^\dagger, a_2^\dagger)^T. \quad (3.87)$$

Here, the dynamical matrix $\mathbf{D}_{\text{eff}}[\omega]$ is explicitly frequency dependent and thus possibly complex (see Appendix B 6 for the expression), which is strikingly different to the behaviour of the full model. This can also be decomposed into a dynamical matrix of the isolated system and a damping matrix with $\mathbf{D}_{\text{eff}}[\omega] = \mathbf{A}_{\text{eff}}[\omega] - \tilde{\mathbf{K}}_{\text{eff}}[\omega]/2$. The damping matrix now encodes local and global reservoirs $\tilde{\mathbf{K}}_{\text{eff}}[\omega] = \text{diag}(\Gamma_1[\omega] + \kappa_1, \Gamma_2[\omega] + \kappa_2, \Gamma_1^*[\omega] + \kappa_1, \Gamma_2^*[\omega] + \kappa_2)$. In the quadrature representation, the dynamical matrix has now possible complex entries due to the ω dependency, which is also different compared to the full model. To transform $\mathbf{D}_{\text{eff}}[\omega]$ to the quadrature basis, we apply $\mathbf{v}_{\text{eff}}[\omega] = \mathbf{T}_{\text{eff}} \mathbf{a}_{\text{eff}}[\omega]$ with the truncated transformation matrix

$$\mathbf{T}_{\text{eff}} = \frac{1}{\sqrt{2}} \begin{pmatrix} 1 & 0 & 1 & 0 \\ -i & 0 & i & 0 \\ 0 & 1 & 0 & 1 \\ 0 & -i & 0 & i \end{pmatrix}. \quad (3.88)$$

This gives us

$$\mathbf{M}_{\text{eff}}[\omega] \equiv \mathbf{T}_{\text{eff}} \mathbf{D}_{\text{eff}}[\omega] \mathbf{T}_{\text{eff}}^\dagger, \quad (3.89)$$

as the sought out Langevin matrix (the explicit form can be found in Appendix B 7) with the EOM for the quadrature basis

$$i\omega \langle \mathbf{v}_{\text{eff}}[\omega] \rangle = \mathbf{M}_{\text{eff}}[\omega] \langle \mathbf{v}_{\text{eff}}[\omega] \rangle. \quad (3.90)$$

Although the equations of motion are similar to the adiabatic limit, there is a stark difference: The effective damping rate is now frequency dependent. To illustrate this, we can understand $i\Gamma[\omega]$ as a susceptibility in analogy to a *complex refractive index* n_Γ . For this, we make this expression unit-less by normalizing it with $\sqrt{\kappa_3\kappa}/4|J|^2$ (Note that it is closely related to the the impedance matching condition, see Sec. IV C). It follows,

$$n_\Gamma[\omega] \equiv \frac{\sqrt{\kappa_3\kappa}}{4|J|^2} (i\Gamma[\omega]) = \frac{i\sqrt{\kappa_3/\kappa}}{i2\omega/\kappa + \kappa_3/\kappa} = \underbrace{\frac{(2\omega/\kappa)\sqrt{\kappa_3/\kappa}}{(2\omega/\kappa)^2 + (\kappa_3/\kappa)^2}}_{\Re n_\Gamma} + i \underbrace{\frac{(\kappa_3/\kappa)\sqrt{\kappa_3/\kappa}}{(2\omega/\kappa)^2 + (\kappa_3/\kappa)^2}}_{\Im n_\Gamma}, \quad (3.91)$$

where the dispersion of waves upon entering the reservoir is proportional to the real part of the refractive index, while the absorption is proportional to the imaginary part. In this analogy, the probability of an excitation to couple to the eff. reservoir is a *Lorentzian shaped distribution*

$$|n_\Gamma[\omega]|^2 = \frac{\kappa_3/\kappa}{(2\omega/\kappa)^2 + (\kappa_3/\kappa)^2}, \quad (3.92)$$

with a HWHM = κ_3/κ , see Fig. 8. For the Markovian case, the distribution would just be a flat band in frequency

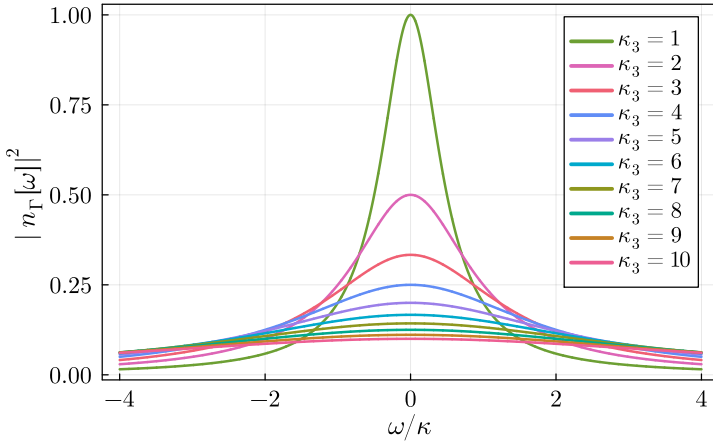


FIG. 8. Lorentzian shaped coupling probability $|n_\Gamma[\omega]|^2$ (normalized for $\kappa_3/\kappa = 1$) for the non-Markovian reservoir depending on ω . The distribution is shown for varying rates κ_3 . It has a HWHM = κ_3/κ , and becomes maximal at resonance ($\omega = 0$). The Markovian limit with $\lim_{\omega \rightarrow 0} \Gamma[\omega] = \Gamma_0 = 4|J|^2/\kappa_3$ leads to flat bands and an frequency-independent response of the reservoir to incident light, with the maximal value of the distribution. Moreover, it converges to the Markovian result for high κ_3 and becomes constant. The opposite happens for low κ_3 , where the auxiliary almost always correlates with the rest of the system. Thus, for low κ_3 , the auxiliary becomes an integral part of the coherent dynamics, which cannot be simply treated as a reservoir.

space, since it is independent of frequency. This changes however in the non-Markovian case, because the effective reservoir has now a narrow frequency band where it can respond to incoming excitations. Here, ω is the response frequency of the reservoir and κ_3 can be seen as the linewidth of this non-Markovian reservoir. As shown in Fig. 9, non-Markovian corrections with finite ω , imply a reduced response of the auxiliary to incident light. The support of the distribution vanishes for high frequencies, effectively acting as a band-pass filter. Furthermore, there is a clear phase dependence in the dispersion of $n_\Gamma[\omega]$, which is negative for $\omega < 0$ and positive for $\omega > 0$. The absorption broadens for growing values of κ_3 , implying that it converges to the Markovian case for high κ_3 , resembling the adiabatic limit. However, for low κ_3 this situation changes: The auxiliary correlates with the rest of the system only in a narrow band and becomes dynamically active. It is then part of the coherent dynamics and cannot be viewed as a simple reservoir anymore.

Next, we can check if the Markovian limit can be recovered for the equations of motion. For this we take the inverse Fourier transform, which is a bit more tricky. First, consider

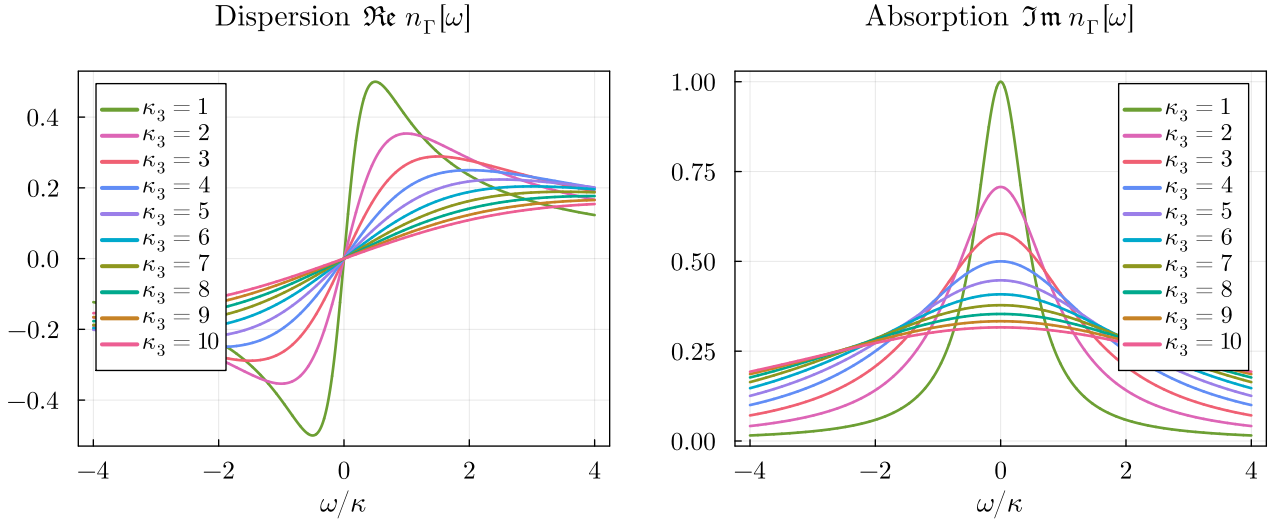


FIG. 9. Dispersion and absorption of $n_\Gamma[\omega]$ for different damping rates κ_3 . Here the real part of $n_\Gamma[\omega]$ describes the dispersion (left) and the imaginary part the absorption (right) behaviour of the auxiliary. Finite ω changes the response of the auxiliary to incoming waves, where the absorption drops for finite frequencies. The dispersion behaves like a typical dispersion of light-matter interactions, where there is a sign change for small ω , with a minimum for $\omega < 0$ and similar a maximum for $\omega > 0$ both close to the origin. If we move to the Markovian regime, namely, $\lim_{\omega \rightarrow 0} \Gamma[\omega] = \Gamma_0 = 4|J|^2/\kappa_3$, the dispersion vanishes and the absorption becomes maximal.

$$\mathcal{F}^{-1}\left\{\frac{\Gamma[\omega]}{2}\right\}(t) = \mathcal{F}^{-1}\left\{\frac{|J|^2}{i\omega + \kappa_3/2}\right\}(t) = 2\kappa_3^2\sqrt{2\pi}\Theta(t)\exp\left(-\frac{\kappa_3}{2}t\right) \equiv \frac{\Gamma(t)}{2}, \quad (3.93)$$

Then we use the convolution theorem: Consider two functions in frequency space, $f[\omega]$ and $g[\omega]$, then the reverse Fourier transform to the time domain can be computed using the convolution

$$\mathcal{F}^{-1}\{g[\omega] \cdot f[\omega]\}(t) = \frac{1}{\sqrt{2\pi}}(g * f)(t) = \frac{1}{\sqrt{2\pi}} \int_{-\infty}^{\infty} g(\tau)f(t - \tau) d\tau, \quad (3.94)$$

where $*$ is the convolution operator (the convolution theorem can be proven using Fubini's theorem, see Appendix B 9). Note, that $*$ is an associative and commutative operation. To recover the Markovian limit, consider following terms

$$\begin{aligned} \mathcal{F}^{-1}\left\{\frac{\Gamma[\omega]}{2} \cdot \langle a_i[\omega] \rangle\right\}(t) &= \frac{1}{\sqrt{2\pi}} \left(\frac{\Gamma}{2} * \langle a_i \rangle\right)(t) = 2\kappa_3^2 \int_0^\infty \exp\left(-\frac{\kappa_3}{2}\tau\right) \langle a_i(t - \tau) \rangle d\tau \\ &\approx 2\kappa_3^2 \left(\int_0^\infty \exp\left(-\frac{\kappa_3}{2}\tau\right) d\tau\right) \langle a_i(t) \rangle = 4\kappa_3 \langle a_i(t) \rangle = \frac{\Gamma_0}{2} \langle a_i(t) \rangle, \end{aligned} \quad (3.95)$$

appearing in Eq. (3.85). Here, κ_3 is assumed to be sufficiently large, which led us to approximate the second line in the equation with

$$\langle a_i(t - \tau) \rangle \approx \langle a_i(t) \rangle, \quad (3.96)$$

because we assumed that the bath becomes Markovian and any memory effects due to past values of $\langle a_i(t) \rangle$ dissipate accordingly. We can also express this differently: Since the exponential function decays faster than $\langle a_i(t) \rangle$ oscillates (for high κ_3), it will render $\langle a_i(t) \rangle$ to be local in time. By using this preliminary step, we are fully equipped to reverse Fourier transform all of Eq. (3.85), where we recover the above set of equations from Sec. III E 1, which can be found in Appendix B 9. This is the reason why the adiabatic elimination was called the Markovian limit and the Fourier-transform elimination the non-Markovian limit.

Thus, we have shown that both elimination procedures are mostly equivalent but the latter approach leads to an additional correction for the effective damping rate $\Gamma[\omega]$. This does not only change the response of the effective reservoir to incoming modes, but also means that the third mode does not lose its frequency dependence. Thus it is not inherently treated differently in comparison to the remaining modes. For example, if one considers a perfect circulator regime, where the system should be invariant to any labeling convention, namely, where every resonator is indistinguishable from the other, we could not simply just treat the auxiliary to be dynamically different to the rest of the system. For example, when interactions have the same value $|J_{ij}| \equiv |J|$ ($|\lambda_{ij}| \equiv |\lambda|$) as well as the local damping rates ($\kappa_i \equiv \kappa$), adiabatically eliminating the third resonator would not result in a perfect circulator. Only by additionally including the frequency response of the auxiliary resonator by Fourier transforming the equation of motion would result in a circulator.

At this point of the thesis we have only hinted at the occurrence of nonreciprocity, but there was still no formal discussion of this. So the logical question to ask is: ‘‘When does the system host nonreciprocal transport?’’, or rather ‘‘What is the condition for reciprocity in general?’’. These kind of questions will be touched upon in the subsequent section and will conclude the theoretical considerations needed to fully grasp the remaining parts of this thesis.

F. When is the system nonreciprocal?

As mentioned in Sections III B 2 and III E 1, only coherent interactions with an imaginary part can enforce nonreciprocity in this model. This can be illustrated by expressing the equations of motion (3.85) for this effective model in terms of gauge-invariant phases from Eq. (3.31). Using the same gauge transformations as before, it follows

$$i\omega \langle a_1[\omega] \rangle = - \left[\frac{\Gamma_1[\omega] + \kappa_1}{2} \right] \langle a_1[\omega] \rangle - i \left[|J|e^{i\Phi} + i \left(|\mu_1|e^{-i(\vartheta_1+\vartheta_2)} - |\mu_2| \right) \frac{\Gamma[\omega]}{2} \right] \langle a_2[\omega] \rangle - i \left[|\lambda|e^{-i\vartheta_2} + i \left(|\nu_1|e^{-i(\vartheta_1+\vartheta_2)} - |\nu_2| \right) \frac{\Gamma[\omega]}{2} \right] \langle a_2^\dagger[\omega] \rangle, \quad (3.97a)$$

$$i\omega \langle a_2[\omega] \rangle = - \left[\frac{\Gamma_2[\omega] + \kappa_2}{2} \right] \langle a_2[\omega] \rangle - i \left[|J|e^{-i\Phi} + i \left(|\mu_1|e^{i(\vartheta_1+\vartheta_2)} - |\mu_2| \right) \frac{\Gamma[\omega]}{2} \right] \langle a_1[\omega] \rangle - i \left[|\lambda|e^{-i\vartheta_2} - i \left(|\nu_1|e^{-i(\vartheta_1+\vartheta_2)} - |\nu_2| \right) \frac{\Gamma[\omega]}{2} \right] \langle a_1^\dagger[\omega] \rangle, \quad (3.97b)$$

where we introduced

$$\mu = \frac{1}{|J|^2} \left(|\lambda_{31}\lambda_{32}|e^{-i(\vartheta_1+\vartheta_2)} - |J_{32}J_{31}| \right) \equiv |\mu_1|e^{-i(\vartheta_1+\vartheta_2)} - |\mu_2|, \quad (3.98a)$$

$$\nu = \frac{1}{|J|^2} \left(|\lambda_{31}J_{32}|e^{-i(\vartheta_1+\vartheta_2)} - |\lambda_{32}J_{31}| \right) \equiv |\nu_1|e^{-i(\vartheta_1+\vartheta_2)} - |\nu_2|, \quad (3.98b)$$

for readability. As mentioned before, a mode $\langle a_i \rangle$ is driven either by $\langle a_j \rangle$ or the adjoint $\langle a_j^\dagger \rangle$. The system is reciprocal when $i \rightarrow j$ and $j \rightarrow i$ are equal, and nonreciprocal if there is an asymmetry. Thus, we need to (at least partially) decouple one mode from the other in one direction. How? If we only tune the coherent interactions J and λ at the same time and set them to

$$\begin{aligned}
J \stackrel{!}{=} \mp i \mu \frac{\Gamma_0}{2} &\implies |J| e^{i\Phi} \stackrel{!}{=} \mp i \left(|\mu_1| e^{-i(\vartheta_1 + \vartheta_2)} - |\mu_2| \right) \frac{\Gamma_0}{2}, \\
\lambda \stackrel{!}{=} \mp i \nu \frac{\Gamma_0}{2} &\implies |\lambda| e^{-i\vartheta_2} \stackrel{!}{=} \mp i \left(|\nu_1| e^{-i(\vartheta_1 + \vartheta_2)} - |\nu_2| \right) \frac{\Gamma_0}{2},
\end{aligned} \tag{3.99}$$

we can fully decouple one cavity from the other, where the upper sign decouples cavity 2 from the dynamics of cavity 1, and the lower sign does the opposite. For this choice, the system becomes maximally nonreciprocal which we call the unidirectional regime. Since our interaction amplitudes are time-independent, we cannot decouple the system for all frequencies in the non-Markovian regime, as this would imply time-dependent interactions. Thus, we need to make a choice. We have chosen the Markovian limit Γ_0 , as seen in Eq. (3.99). For $\omega = 0$, the system will then enter unidirectional transport from $1 \rightarrow 2$ if we set both $J = -i\mu\Gamma_0/2$ and $\lambda = -i\nu\Gamma_0/2$. However, the nonreciprocal transport will vanish for finite frequencies.

1. Optical isolator - effective model without squeezing

Here we focus on a specific instance of the two-mode model - the *optical isolator*. An isolator is defined as a two-port device with a non-symmetric scattering matrix $\mathbf{S} \neq \mathbf{S}^T$. Usually this is used for microwave or radio transmission to shield a given port from signals from the other port, see Ref. [57]. To achieve nonreciprocity, an isolator must incorporate a nonreciprocal element, which is typically a ferrite based material in microwave based isolators, see Ref. [58]. In the strongest (unidirectional) limit, it transmits all power from port i to j , while absorbing all power coming from port j . This means, that there will be no reflections at port i and j . Ideally, a scattering matrix of an isolator could look like this:

$$\mathbf{S} = \begin{pmatrix} 0 & 0 \\ 1 & 0 \end{pmatrix}. \tag{3.100}$$

The optical isolator effectively describes the same working principle. For this, we focus only on linear interactions and set TMS to zero $\lambda_{ij} = 0 \implies \mu = -|\mu_2|$. Here, we want to understand for which phase Φ nonreciprocity starts to occur. For clarity, we set the modulus of J to $|J| = |\mu_2|\Gamma_0/2$. Inserting it into Eq. (3.99) gives

$$|J| e^{i\Phi} \stackrel{!}{=} \pm i |\mu_2| \frac{\Gamma_0}{2} \implies e^{i\Phi} \stackrel{!}{=} \pm i. \tag{3.101}$$

By then taking the argument, it follows

$$\phi_{\text{R,L}} \equiv \pm \frac{\pi}{2} \pmod{2\pi}, \tag{3.102}$$

for the unidirectional circulator flux, where R (L) represents transport from $1 \rightarrow 2$ ($1 \leftarrow 2$). Additionally, $\phi_{\text{R}} \equiv \phi_{\text{L}} + \pi \mathbb{Z} \pmod{2\pi}$. Some authors call these *exceptional points* of the open dynamical matrix \mathbf{D} , which are spectral singularities of non-Hermitian systems, see Refs. [59–63]. This result resembles the discussion about J having at least a nonzero imaginary part from Eq. (3.37). The only points of reciprocity are the ones with a vanishing imaginary part

$$\phi_0 \in \{0, \pm\pi\} \pmod{2\pi}. \tag{3.103}$$

Thus, we can list all possible regimes of this model: 1. *Reciprocal limits* for $\Phi = \phi_0$, 2. *Nonreciprocal regime* for $\Im(\Phi) \neq 0$, and 3. *Unidirectional limit* for $\Phi = \phi_{\text{R,L}}$, which are already discussed in Refs. [1], [14]. Here, we used the imaginary part of Φ . Real and imaginary parts of a complex number $z \in \mathbb{C}$ are defined as

$$\Re(z) = \frac{z^* + z}{2}, \quad \text{and} \quad \Im(z) = \frac{i(z^* - z)}{2}. \quad (3.104)$$

Even though the limits of Φ are clear by now, one thing is still not ensured for the optical isolator to resemble a microwave isolator: The lack of reflections. The phase only enforces the directionality, however, reflections are still possible. To ensure for maximal transmittance without power-loss, further constrains on system-parameters are needed. This will be done in Section IV C.

Note, that the optical isolator is frequently used in this thesis as a minimal example to better understand nonreciprocal physics.

2. Parametrically driven directional amplifier

In general, TMS complicates the analysis from above, since there are multiple phases and couplings to keep track off. Here, we want demonstrate a simple model with only a single gauge-invariant phase using TMS. Recall, that setting $\lambda = \mp i\nu\Gamma_0/2$ fully decouples $\langle a_j^\dagger \rangle$ from $\langle a_i \rangle$, see Eq. (3.99). Additionally, we remove several interactions $J_{12} = J_{31} = \lambda_{32} = 0$, which means we need to re-express our abbreviations in terms of λ :

$$u_j := \frac{J_{3j}}{\lambda}, \quad v_j := \frac{\lambda_{3j}}{\lambda}, \quad \text{and} \quad \Gamma[\omega] := \frac{2}{i\omega + \kappa_3/2} |\lambda|^2. \quad (3.105)$$

This gives us

$$\mu = 0 \quad \text{and} \quad \nu = |\nu_1| e^{-i(\vartheta_1 + \vartheta_2)}.$$

But, this seems a bit misleading as ϑ_2 has now become a redundant phase, compare Fig. 6 (a). Therefore, the phase ϑ_2 is not protected against the violent act of *just gauging it away*, and can be safely removed by performing the following gauge transformation

$$\langle a_1 \rangle \rightarrow \langle a_1 \rangle e^{i\vartheta_2} \implies \langle a_1^\dagger \rangle \rightarrow \langle a_1^\dagger \rangle e^{-i\vartheta_2}.$$

This collapses the differential equations to

$$i\omega \langle a_1[\omega] \rangle = - \left[\frac{\Gamma_1[\omega] + \kappa_1}{2} \right] \langle a_1[\omega] \rangle - i \left[|\lambda| + i|\nu_1| e^{-i\vartheta_1} \frac{\Gamma[\omega]}{2} \right] \langle a_2^\dagger[\omega] \rangle, \quad (3.106a)$$

$$i\omega \langle a_2[\omega] \rangle = - \left[\frac{\Gamma_2[\omega] + \kappa_2}{2} \right] \langle a_2[\omega] \rangle - i \left[|\lambda| - i|\nu_1| e^{-i\vartheta_1} \frac{\Gamma[\omega]}{2} \right] \langle a_1^\dagger[\omega] \rangle. \quad (3.106b)$$

Each mode $\langle a_i \rangle$ is now only driven by the adjoint $\langle a_i^\dagger \rangle$ and depends on a single phase ϑ_1 . These sets of equations nicely resemble the optical isolator, just with parametric interactions. Next, we need to find out the limits of ϑ_1 . For clarity, we again set the modulus of λ to $|\lambda| = |\nu_1|\Gamma_0/2$, where it follows

$$|\lambda| e^{i\vartheta_1} \stackrel{!}{=} \mp i|\nu_1| \frac{\Gamma_0}{2} \implies e^{i\vartheta_1} \stackrel{!}{=} \mp i. \quad (3.107)$$

Taking the argument results in

$$\vartheta_{1,\mp} \equiv \mp \frac{\pi}{2} \pmod{2\pi}, \quad (3.108)$$

for the nonreciprocal case - which leads to an *amplification* of the signal. There is a seemingly weak analogue to the reciprocal case of the optical isolator by setting

$$\vartheta_{1,0} \in \{0, \pm\pi\} \pmod{2\pi}. \quad (3.109)$$

However, $\vartheta_1 = \vartheta_{1,0}$ gives us opposite signs for the imaginary part inside the brackets of Eq. 3.106. Thus, this limit will redistribute the phases of modes and is just a quasi-reciprocal limit, flipping quadratures after an exchange of source and detector.

At this point we have established a well rounded understanding of the reduced model regarding its reciprocity conditions. Before we understand how this system scatters incoming fields, we will take a look at the energy-spectrum of the three-mode and two-mode model.

G. Energy spectrum of the system

In this Section we set TMS to zero ($\lambda_{ij} = 0 \implies \mathbf{h}_2 = 0$), and only focus on the dissipative three-mode ring and the two-mode optical isolator.

1. Energy spectrum of the dissipative ring

If each interaction amplitude of the dissipative ring has the same magnitude $|J|$ and phase $\Phi/3$, it will become *translationally invariant*. Thus, we can use the *Bloch theorem* and diagonalize the Hamiltonian using plane-wave solutions, see Appendix B 8. The diagonal Hamiltonian in momentum space can then be written as

$$H_k \equiv \sum_{m=0,\pm 1} \bar{\omega}_m b_m^\dagger b_m, \quad \text{with plane-waves} \quad b_m^\dagger = \frac{1}{\sqrt{N}} \sum_j e^{i\frac{2\pi m}{3}j} a_j^\dagger, \quad (3.110)$$

and energies

$$\bar{\omega}_m \equiv \sum_m 2 \Re(J e^{-i(2\pi m/3)}) = \sum_m 2|J| \cos((\Phi - 2\pi m)/3). \quad (3.111)$$

The quantum number m can be interpreted as units of *quasi-momentum* of the plane-waves, see Ref. [14]. The energy spectrum in Fig. 10 (a) tells us a lot about the gauge-invariant phase Φ : If the system is in the reciprocal setting, two eigenstates become degenerate, i.e. for $\Phi = 0$ we observe $\bar{\omega}_{-1} = \bar{\omega}_1 = -1J$. The remaining eigenstate has a bigger distance from 0 with $\omega_0 = 2J$. Eigenvalues are not equidistant from 0, and non-symmetrically distributed over the energy scale for reciprocal limits. Moving away from this limit into the regions of nonreciprocity opens up the degeneracy. The distance becomes maximal for unidirectional limits, where one eigenstate always has zero energy, and the remaining become equidistant from 0 with a value of $\pm\sqrt{2|J|}$. Also, after the phase completes one cycle of 2π , each eigenvalue m loses one unit of angular quasi-momentum $m \rightarrow m - 1$, implying that the states are remapped $b_m \rightarrow b_{m'} = b_{m-1}$, where the state with the lowest angular momentum gets mapped to the state with the highest value of m . Therefore, after 3 cycles, namely $\Phi = 6\pi$, the states are mapped to their original value of m .

In the matrix notation, we introduce the vector $\mathbf{b} = (b_{-1}, b_0, b_1, b_{-1}^\dagger, b_0^\dagger, b_1^\dagger)^T$ and write

$$H_k \equiv \sum_{n,m} \mathbf{b}_n^\dagger(\mathbf{H}_k)_{nm} \mathbf{b}_m, \quad (3.112)$$

with $\mathbf{H}_k = \text{diag}(\bar{\omega}_{-1}, \bar{\omega}_0, \bar{\omega}_1, \bar{\omega}_{-1}, \bar{\omega}_0, \bar{\omega}_1)$, and $\bar{\omega}_m \in \mathbb{R}$. Energies come in pairs, but due to the hermeticity of H_k , have the same value. This changes for the (isolated) dynamical matrix

$$\mathbf{A}_k \equiv -i\boldsymbol{\Lambda}_z \mathbf{H}_k = -i \text{diag}(\bar{\omega}_{-1}, \bar{\omega}_0, \bar{\omega}_1, -\bar{\omega}_{-1}, -\bar{\omega}_0, -\bar{\omega}_1), \quad \text{with } \bar{\omega}_m \in \mathbb{R}, \quad (3.113)$$

see Fig. 10 (b). The imaginary part of the eigenvalues adheres to the same behaviour with respect to m , but eigenvalues are now fully imaginary with opposite signs for modes b_m and their adjoints. Therefore, we have two pairs of degenerate eigenstates for each reciprocal point, where the remaining states remain non-degenerate. Spectra of modes and adjoints remain decoupled for most values of Φ , but overlap for unidirectional values $\Phi = \pm\pi/2$. For example, for $\Phi = \pi/2$ we observe $\pm\bar{\omega}_0 = \mp\bar{\omega}_{-1}$, and $\bar{\omega}_1 = -\bar{\omega}_1$. This is different for $\Phi = -\pi/2$, where $\pm\bar{\omega}_m = \mp\bar{\omega}_{m+1(\text{mod } 3)}$. To find the spectrum of the open dynamical matrix \mathbf{D} , we make a small simplification by

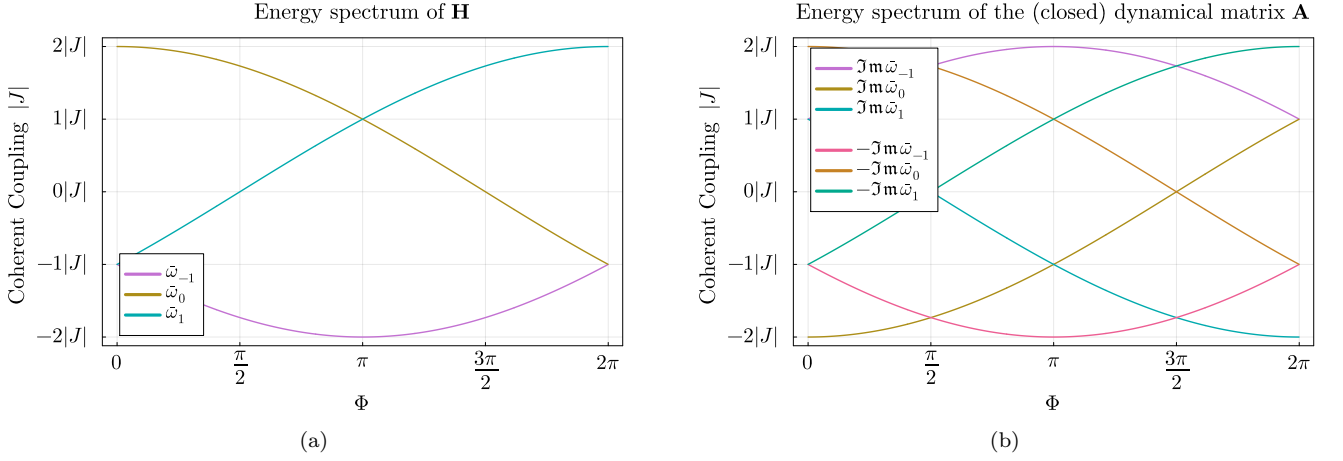


FIG. 10. Energy spectrum of the dissipative ring for a translationally invariant setting $J = |J|e^{i\Phi/3} \equiv J_{12} = J_{31} = J_{32}^*$. (a) Spectrum of the Hamiltonian \mathbf{H}_k . For reciprocal values, two eigenstates are degenerate with $\mp|J|$, and the remaining mode has magnitude $\pm 2|J|$. Therefore, energies are non-symmetrically centered around zero, always being 3 units of $|J|$ apart. The degeneracy is lifted for any other value of Φ , and reach maximal distance for the unidirectional limit. In this limit, one eigenstate has zero-energy, where the others have magnitude $\pm\sqrt{2}|J|$. After one complete cycle of 2π , each eigenvalue loses one unit of angular quasi-momentum. After three cycles, states regain their initial values of m . (b) Spectrum of the dynamical matrix \mathbf{A} of the closed system. Here, eigenvalues become fully imaginary, with opposite signs between modes b_m and adjoints b_m^\dagger . Even though eigenvalues for modes and adjoints are mostly decoupled, modes b_m cross adjoints b_m^\dagger with the same quasi-momentum at unidirectional limits and become degenerate.

assuming $\kappa \equiv \kappa_i$ (keeping the translational invariance intact), implying $\tilde{\mathbf{K}} = \kappa \mathbb{1}$. In this case, we need to only diagonalize \mathbf{A} , since the damping matrix is proportional to an identity. The damping matrix simply shifts imaginary eigenvalues on the real axis. The open dynamical matrix in momentum space is then

$$\mathbf{D}_k = \mathbf{A}_k - \frac{1}{2}\tilde{\mathbf{K}} = -\frac{1}{2}\text{diag}(\kappa + i2\bar{\omega}_{-1}, \kappa + i2\bar{\omega}_0, \kappa + i2\bar{\omega}_1, \kappa - i2\bar{\omega}_{-1}, \kappa - i2\bar{\omega}_0, \kappa - i2\bar{\omega}_1). \quad (3.114)$$

This implies, that real parts of the energies encode the dissipation and the imaginary parts encode oscillations. To see this more clearly, we solve the EOM via

$$\langle \mathbf{a}(t) \rangle = e^{\mathbf{D}t} \langle \mathbf{a}(0) \rangle \implies \langle \mathbf{b}(t) \rangle = e^{\mathbf{D}_k t} \langle \mathbf{b}(0) \rangle, \quad (3.115)$$

which implies – as expected – for the first mode

$$\langle b_{-1}(t) \rangle = e^{-\kappa t/2} e^{-i2\bar{\omega}_{-1}t} \langle b_{-1}(0) \rangle. \quad (3.116)$$

2. Energy spectrum of the optical isolator

The dynamical matrix of the optical isolator can be diagonalized in a straightforward way, and the spectrum of $\mathbf{D}_{\text{eff}}[\omega]$ reads

$$\bar{\omega}_{1,2} = -\frac{\kappa_1 + \kappa_2 + \Gamma_1[\omega] + \Gamma_2[\omega]}{4} \pm i\sqrt{\left(J + i\mu\frac{\Gamma[\omega]}{2}\right)\left(J^* + i\mu^*\frac{\Gamma[\omega]}{2}\right) - \frac{(\kappa_1 - \kappa_2 + \Gamma_1[\omega] - \Gamma_2[\omega])^2}{4}}. \quad (3.117)$$

For simplicity, we set $\omega = 0$, $|J_{ij}| = \kappa \implies \Gamma_0 = \Gamma_1 = \Gamma_2$, and $\kappa \equiv \kappa_1/2 = \kappa_2/2 = \kappa_3/2$ (where the latter choice is not by accident and will become clear in Sec. IV C). This implies that $\mu = -|\mu_2| = -1$. The Markovian (complex) energy spectrum in units of $|J|$ is given by

$$\bar{\omega}_{1,2} = -2|J| \pm i\sqrt{|J|^2 (e^{i\Phi} - i)(e^{-i\Phi} - i)} = |J|(-2 \mp \sqrt{2i \cos \Phi}), \quad \text{and} \quad \bar{\omega}_{3,4} = \bar{\omega}_{1,2}^*, \quad (3.118)$$

where $\bar{\omega}_{3,4}$ are complex-energies for adjoint modes, see Fig. 11. Different to before, imaginary parts vanish and

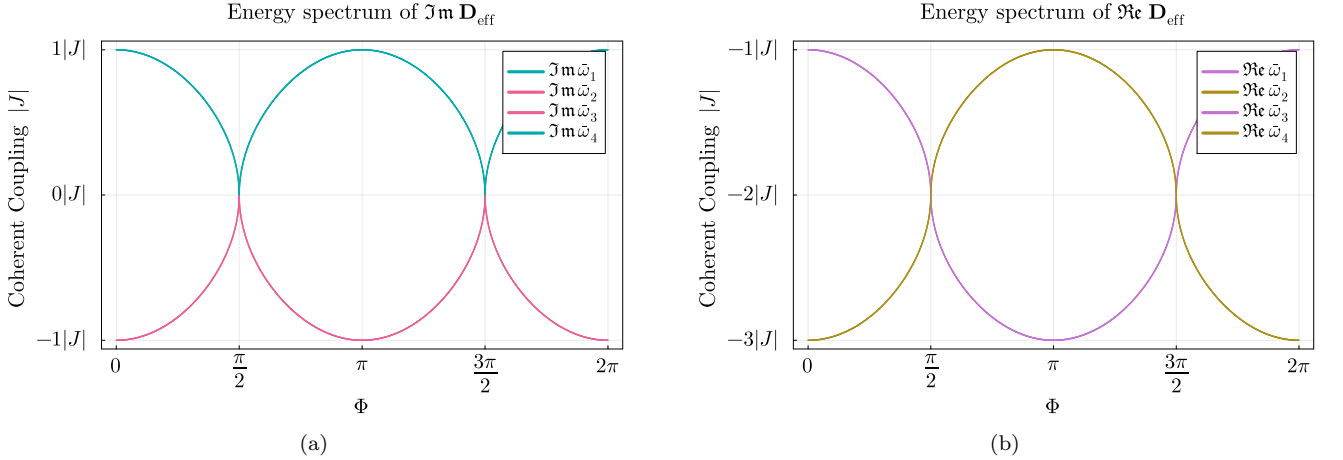


FIG. 11. Energy spectrum of the dynamical matrix \mathbf{D}_{eff} of the (Markovian) optical isolator for $|J_{ij}| = \kappa$, $\Gamma_0 = \Gamma_1 = \Gamma_2$, $\kappa \equiv \kappa_i/2$ and $\Gamma_0 = 2\kappa$, for $i, j = 1, 2, 3$. (a) Imaginary part of \mathbf{D}_{eff} representing the energies of the Hamiltonian. Energies vanish and eigenstates become degenerate for the unidirectional limit. In the reciprocal limit, they reach maximal distance with the same magnitude but opposite signs. (b) Real part of \mathbf{D}_{eff} representing dissipation. Dissipation always remains finite, regardless of Φ . However, damping rates become symmetric for unidirectional points with the same magnitude. This changes for other values of Φ , where damping rates get redistributed and reach full asymmetry for reciprocal points.

become degenerate for the unidirectional limit, but never cross. Damping on the other hand (the real part) does not vanish. This also holds true in the reciprocal limit

$$\bar{\omega}_{1,2} = |J|(-2 \mp \sqrt{2i}), \quad (3.119)$$

implying that damping always remains for every value of Φ . Damping rates meet at the unidirectional limits and have the same magnitude for both modes. However, the magnitude of damping is redistributed between modes for values of Φ different from unidirectional limits. This distance reaches its maximum at the reciprocal points.

IV. Scattering Matrix

To understand the transmission/reflection behaviour of the system, we will derive the *S-matrix* using I/O theory. An incident field entering the system will interact and get *scattered* before leaving the system as an output-field. The S-matrix exactly encodes how the scattering will occur and what the transmission/reflection probabilities are.

A. Derivation of the S-Matrix using I/O theory

This part of the thesis will be performed in the quadrature representation as the derivations are more illustrative that way. It should be noted that the derivation could be done from the mode representation directly. However, as we will demonstrate, we can simply transform the scattering matrix between bases using \mathbf{T} .

We start at the Heisenberg-Langevin equation in frequency space and equip it with reservoir fields, which are incident to the resonators

$$i\omega \mathbf{v}[\omega] = \mathbf{M} \mathbf{v}[\omega] - \sqrt{\mathbf{K}} \mathbf{v}_{\text{in}}[\omega], \quad (4.1)$$

and are compactly written in the vector $\mathbf{v}_{\text{in}}[\omega]$. Here, the dynamical matrix \mathbf{M} is not explicitly dependent on ω , but remember that this is not the case for the effective model. We also introduced the square root of the dissipation matrix \mathbf{K} as

$$\sqrt{\mathbf{K}} = \text{diag}(\sqrt{\kappa_1}, \sqrt{\kappa_2}, \sqrt{\kappa_3}) \otimes \mathbf{1}_2. \quad (4.2)$$

Combined with input-fields, the expression $\sqrt{\mathbf{K}} \mathbf{v}_{\text{in}}[\omega]$ can be interpreted as our operator-valued Langevin force. Since I/O theory holds at the level of operators, we do not need to take the expectation value for this derivation. By solving the Heisenberg equation in terms of input-fields, we find

$$\mathbf{v}[\omega] = -(i\omega \mathbf{1} - \mathbf{M})^{-1} \sqrt{\mathbf{K}} \mathbf{v}_{\text{in}}[\omega] \equiv -\chi[\omega] \sqrt{\mathbf{K}} \mathbf{v}_{\text{in}}[\omega], \quad (4.3)$$

where $\chi[\omega]$ is the response function of our system and will be denoted as our *susceptibility matrix*, see Wanjura *et al.* [64]. As mentioned earlier, this relates system modes $\mathbf{v}[\omega]$ to input-fields $\mathbf{v}_{\text{in}}[\omega]$. Output-fields are then related to input-fields using the I/O relation (see Eq. (2.68)), implying

$$\mathbf{v}_{\text{out}}[\omega] = \mathbf{v}_{\text{in}}[\omega] + \sqrt{\mathbf{K}} \mathbf{v}[\omega] = \left[\mathbf{1} - \sqrt{\mathbf{K}} \chi[\omega] \sqrt{\mathbf{K}} \right] \mathbf{v}_{\text{in}}[\omega] \equiv \mathbf{S}[\omega] \mathbf{v}_{\text{in}}[\omega], \quad (4.4)$$

where

$$\mathbf{S}[\omega] = \mathbf{1} - \sqrt{\mathbf{K}} \chi[\omega] \sqrt{\mathbf{K}} = \mathbf{1} - \sqrt{\mathbf{K}} (i\omega \mathbf{1} - \mathbf{M})^{-1} \sqrt{\mathbf{K}}, \quad (4.5)$$

is the S-matrix in the quadrature representation. Note that this expression is unitary for the full three-mode system, but unitarity can be broken for an effective model. Naturally, the S-matrix in the mode-representation $\tilde{\mathbf{S}}[\omega]$ can be recovered by applying the transformation matrix

$$\tilde{\mathbf{S}}[\omega] = \mathbf{T}^\dagger \mathbf{S}[\omega] \mathbf{T}, \quad (4.6)$$

where the rigorous proof can be found in Appendix C 1. Since there are notable differences in the S-matrix properties between the bases, we intend to take a closer look at them.

1. Differences of the S-matrix between the bases

Given that the dynamical matrix in the quadrature representation is real $\mathbf{M} = \mathbf{M}^*$, the complex conjugate of the susceptibility matrix

$$\chi^*[\omega] = (-i\omega\mathbb{1} - \mathbf{M})^{-1} = \chi[-\omega], \quad (4.7)$$

only changes the sign of ω , which implies for the S-matrix

$$\mathbf{S}^*[\omega] = \mathbf{S}[-\omega]. \quad (4.8)$$

This relation greatly simplifies many calculations and will become relevant in the analysis of the S-matrix and the noise later. However, this relationship does not hold in the mode basis, since the dynamical matrix is complex in general $\mathbf{D} \in \text{Mat}_{2N}(\mathbb{C})$. But as we learned in Section III B 3, the complex conjugate \mathbf{D}^* can be expressed as $\mathbf{D}^* = \mathbf{\Lambda}_x \mathbf{D} \mathbf{\Lambda}_x$ simply by permuting blocks. This implies for the susceptibility matrix

$$\tilde{\chi}^*[\omega] = (-i\omega\mathbb{1} - \mathbf{D}^*)^{-1} = (i(-\omega)\mathbb{1} - \mathbf{\Lambda}_x \mathbf{D} \mathbf{\Lambda}_x)^{-1} = \mathbf{\Lambda}_x \tilde{\chi}[-\omega] \mathbf{\Lambda}_x, \quad (4.9)$$

where we used the fact that $\mathbf{\Lambda}_x = \mathbf{\Lambda}_x^{-1}$, $(\mathbf{B}^{-1})^* = (\mathbf{B}^*)^{-1}$, and $(\mathbf{BCE})^{-1} = \mathbf{E}^{-1} \mathbf{C}^{-1} \mathbf{B}^{-1}$ for generic matrices $\mathbf{B}, \mathbf{C}, \mathbf{E}$. This property also holds for the S-matrix

$$\tilde{\mathbf{S}}^*[\omega] = \mathbf{\Lambda}_x \tilde{\mathbf{S}}[-\omega] \mathbf{\Lambda}_x, \quad (4.10)$$

since the damping matrix remains invariant under an exchange of blocks $\sqrt{\tilde{\mathbf{K}}} = \mathbf{\Lambda}_x \sqrt{\tilde{\mathbf{K}}} \mathbf{\Lambda}_x$ in the mode-basis. Thus, the relations are similar for both bases up to an exchange of blocks. However, this property in the mode basis has stark consequences, as the S-matrix flips the sign of ω for adjoint modes. To see this, consider $\mathbf{a}_{\text{out}}[\omega] = \tilde{\mathbf{S}}[\omega] \mathbf{a}_{\text{in}}[\omega]$, where it follows from $\mathbf{a}^\ddagger = \mathbf{\Lambda}_x \mathbf{a}$ and Eq. (4.10)

$$\mathbf{a}_{\text{out}}^\ddagger[\omega] = (\mathbf{a}_{\text{out}}^\ddagger[\omega])^T = \left(\mathbf{\Lambda}_x \left[\tilde{\mathbf{S}}[\omega] \mathbf{a}_{\text{in}}[\omega] \right] \right)^T = \left(\left[\mathbf{\Lambda}_x \tilde{\mathbf{S}}[\omega] \mathbf{\Lambda}_x \right] \left[\mathbf{\Lambda}_x \mathbf{a}_{\text{in}}[\omega] \right] \right)^T = \left(\tilde{\mathbf{S}}^*[-\omega] \mathbf{a}_{\text{in}}^\ddagger[\omega] \right)^T. \quad (4.11)$$

Thus, relating adjoint input- to output-fields changes the sign of the frequency inside the S-matrix

$$\mathbf{a}_{\text{out}}^\ddagger[\omega] = \tilde{\mathbf{S}}^*[-\omega] \mathbf{a}_{\text{in}}^\ddagger[\omega], \quad (4.12a)$$

$$\mathbf{a}_{\text{out}}^\ddagger[\omega] = \mathbf{a}_{\text{in}}^\ddagger[\omega] \tilde{\mathbf{S}}^\dagger[-\omega]. \quad (4.12b)$$

Additionally, we can define the action of \ddagger for the ω - dependent S-matrix

$$\tilde{\mathbf{S}}^\ddagger[\omega] \equiv \mathbf{\Lambda}_x \tilde{\mathbf{S}}[\omega] \mathbf{\Lambda}_x = \tilde{\mathbf{S}}^*[-\omega]. \quad (4.13)$$

At a first glance this is a surprising result, since Eq. (4.12a) can also be understood as the time-reversed process, where output-fields are incident, get scattered with an opposite ω -dependence, and leave the system as input-fields. Consider a unitary system $\tilde{\mathbf{S}}^\dagger \tilde{\mathbf{S}} = \mathbf{1} \iff \tilde{\mathbf{S}}^T \tilde{\mathbf{S}}^* = \mathbf{1}$, then Eq. (4.12a) can be formally written as

$$\mathbf{a}_{\text{in}}^\dagger[\omega] = \tilde{\mathbf{S}}^T[-\omega] \mathbf{a}_{\text{out}}^\dagger[\omega]. \quad (4.14)$$

The last equation has far-reaching consequences, which will become important shortly.

By rewriting the susceptibility matrix, we see why that sign flip happens for $\mathbf{a}_{\text{in}}^\dagger[\omega]$. For this, the dynamical matrix $\mathbf{D} = -i\mathbf{\Lambda}_z \mathbf{H} - \tilde{\mathbf{K}}/2$ lets us re-write the susceptibility as

$$\chi[\omega] = (i\omega \mathbf{1} - \mathbf{D})^{-1} = \left(i(\omega \mathbf{1} + \mathbf{\Lambda}_z \mathbf{H}) + \frac{1}{2} \tilde{\mathbf{K}} \right)^{-1} = \left(i\mathbf{\Lambda}_z (\omega \mathbf{\Lambda}_z + \mathbf{H}) + \frac{1}{2} \tilde{\mathbf{K}} \right)^{-1}, \quad (4.15)$$

which is then inserted into

$$\mathbf{a}^\dagger[\omega] = (\mathbf{\Lambda}_x \chi[\omega] \mathbf{\Lambda}_x) \sqrt{\tilde{\mathbf{K}}} \mathbf{a}_{\text{in}}^\dagger[\omega]. \quad (4.16)$$

The resulting system fields are then

$$\mathbf{a}^\dagger[\omega] = \left(-i\mathbf{\Lambda}_z ((-\omega) \mathbf{\Lambda}_z + \mathbf{H}^*) + \frac{1}{2} \tilde{\mathbf{K}} \right)^{-1} \sqrt{\tilde{\mathbf{K}}} \mathbf{a}_{\text{in}}^\dagger[\omega] = \chi^*[-\omega] \mathbf{a}_{\text{in}}^\dagger[\omega], \quad (4.17)$$

with $\mathbf{\Lambda}_x \mathbf{H} \mathbf{\Lambda}_x = \mathbf{H}^*$. Acting with $\mathbf{\Lambda}_x$ on ω -dependent matrices thus necessarily leads to a sign-change of ω , compare Eq. (4.13). However, the overall sign of the damping matrix remains untouched, thus it always acts as a dissipation, where energy always flows *out of the system*.

Ultimately, the properties of the S-matrix in the quadrature basis are different for the non-Markovian effective model. Similarly to the three-mode model in the mode basis, the dynamical matrix $\mathbf{M}_{\text{eff}}[\omega] \in \text{Mat}_{2N}(\mathbb{C})$ lives in the complex domain. This will lead to an observable effect of the scattering probabilities of the effective model in the quadrature basis.

B. Properties of the S-matrix and non-unitarity

To fully appreciate how non-unitary S-matrices can occur in effective models (i.e. the optical isolator), we will take a look at the general properties of the S-matrix. This Section roughly follows Moskalets [65].

As we know, the S-matrix for complete descriptions of a model, is always unitary and fulfills $\mathbf{S}^\dagger \mathbf{S} = \mathbf{1}$. Thus, we consider the case where no degrees of freedom are left out for this description. The unitarity is a direct consequence of *micro-reversibility*, and the *conservation of probability currents*, see Chapter 1 of Ref. [65]. For a simple system with two ports, we get the following S-matrix

$$\mathbf{S} = \begin{pmatrix} \mathbf{S}_{11} & \mathbf{S}_{12} \\ \mathbf{S}_{21} & \mathbf{S}_{22} \end{pmatrix}, \quad (4.18)$$

with complex transition amplitudes $\mathbf{S}_{ij} \equiv (\mathbf{S})_{ij} \in \mathbb{C}$, for $i, j = 1, 2$. By convention, we have chosen the left (right) port to be labeled 1 (2). The modulus squared of transition amplitudes $|\mathbf{S}_{ij}|^2$, gives the scattering probability from port $j \rightarrow i$. Diagonal elements $R_{11} = |\mathbf{S}_{11}|^2$ and $R_{22} = |\mathbf{S}_{22}|^2$ are the *reflection coefficients*. All remaining ones are the *transmission coefficients*, with $T_{21} = |\mathbf{S}_{21}|^2$ representing the probability of scattering from left to right ($1 \leftarrow 2$),

and $T_{12} = |\mathbf{S}_{12}|^2$ for the opposite direction ($1 \leftarrow 2$). Since probability currents have to be conserved (anything not reflected has to be transmitted, see Ref. [65]), we get the following properties for this two port system

$$|\mathbf{S}_{11}|^2 + |\mathbf{S}_{21}|^2 = 1, \quad |\mathbf{S}_{22}|^2 + |\mathbf{S}_{12}|^2 = 1. \quad (4.19)$$

The S-matrix used in Eq. (4.18) can be easily extended to systems with N channels. Simply summing up scattering probabilities for each column generalizes the property above

$$\sum_j^N |\mathbf{S}_{ji}|^2 = 1, \quad \forall i \in N, \quad (4.20)$$

see Ref. [65] for a more in-depth derivation of formula above using current-conservation. However, there is an even stricter condition for time-reversal symmetric systems (without magnetic fields): If ψ is a solution to the Schroedinger equation, there also exists a solution ψ^* . As in the Section before, we can relate incoming waves ψ_{in} to outgoing waves ψ_{out} via the S-matrix

$$\psi_{\text{out}} = \mathbf{S} \psi_{\text{in}}. \quad (4.21)$$

However, since the system is time-reversal symmetric, we can get a similar statement for time-reversed fields $\psi_{\text{in}} \rightarrow \psi_{\text{in}}^*$, and $\psi_{\text{out}} \rightarrow \psi_{\text{out}}^*$. After reversal, input-fields are expressed by ψ_{out}^* , and output-fields by ψ_{in}^* . As it turns out, the scattering process for reversed fields still need to be described by the same S-matrix (see Refs. [22, 65]), which implies

$$\psi_{\text{in}}^* = \mathbf{S} \psi_{\text{out}}^*. \quad (4.22)$$

The first equation can be written as

$$\psi_{\text{out}} = \mathbf{S} \psi_{\text{in}} \iff \psi_{\text{out}}^* = \mathbf{S}^* \psi_{\text{in}}^*, \quad (4.23)$$

implying for the S-matrix

$$\mathbf{S}^{-1} = \mathbf{S}^* \implies \mathbf{S}\mathbf{S}^* = \mathbb{1}. \quad (4.24)$$

With the unitarity $\mathbf{S}^{-1} = \mathbf{S}^\dagger$, we get a very strict condition for the S-matrix of time-reversal symmetric systems

$$\mathbf{S}^* = \mathbf{S}^\dagger \iff \mathbf{S} = \mathbf{S}^T. \quad (4.25)$$

Thus, the S-matrix becomes symmetric for a reciprocal system, and has equal reflection $|\mathbf{S}_{ii}|^2 = |\mathbf{S}_{jj}|^2$ and transmission $|\mathbf{S}_{ij}|^2 = |\mathbf{S}_{ji}|^2$ probabilities $\forall i, j$. This result can be inserted into Eq. (4.14), where a reciprocal system with the (unitary and symmetric) S-matrix $\tilde{\mathbf{S}}^T[\omega] = \tilde{\mathbf{S}}[\omega]$ implies

$$\mathbf{a}_{\text{in}}^\dagger[\omega] = \tilde{\mathbf{S}}[-\omega] \mathbf{a}_{\text{out}}^\dagger[\omega]. \quad (4.26)$$

By comparing this to the original expression $\mathbf{a}_{\text{out}}[\omega] = \tilde{\mathbf{S}}[\omega] \mathbf{a}_{\text{in}}[\omega]$, it becomes clear that adjoint modes (analogous to time-reversed modes) are scattered by the same S-matrix, but have a flipped sign of ω .

Nevertheless, this is different for a nonreciprocal system: The S-matrix for an idealized optical isolator (i.e. only allowing transport from $1 \rightarrow 2$) has only one non-zero element, e.g., $|\mathbf{S}_{21}|^2 = 1$. Consequently, the S-matrix is not symmetric, nor even unitary. The only way to achieve such a behaviour is to construct a reduced model, where missing elements of the full description protect the unitarity of the S-matrix. The non-unitary S-matrix is therefore a consequence of an effective description. However, this also implies, that such a S-matrix can be constructed in general.

C. Scattering behaviour of the optical isolator and maximizing power transfer

In this Section, we examine the scattering behaviour of the optical isolator and find a condition for maximizing power-transfer of the optical isolator and the dissipative ring. As discussed in Section III F 1, even in the extreme unidirectional limit, excitations do not necessarily traverse the system with maximized transmittance. Thus, reflection coefficients need to be minimized. If these vanish, the S-matrix in the unidirectional limit will resemble an idealized isolator. This is called *impedance-matching* and ensures maximum power-transfer and minimal reflections. To understand impedance-matching, we make an analogy with electrical impedance. For an electronic device (load) with an incident electromagnetic signal (source), the impedance $Z = R + iX$ represents the loads opposition to energy flow of (AC) signals, where R is the resistance and X the reactance. In DC currents, reactance vanishes, making impedance purely resistive. Power-loss occurs when the impedance of a load mismatches the phase of the source, causing reflections. Consequently, signals cannot properly enter the load. According to the *maximum power transfer theorem* [66], maximum power transfer occurs when the load impedance equals the conjugate of the source impedance, $Z_{\text{load}} = Z_{\text{source}}^*$. This implies, that resistances must be equal and the phase-difference between reactances must vanish.

After understanding the necessity of impedance-matching for unidirectional transport, we can refocus on the S-matrix. Although Eq. (4.5) provides an expression for the S-matrix, it does not offer sufficient insights into its underlying components. Therefore, we aim to derive an analytical expression for the S-matrix of the optical isolator. This will be beneficial for understanding nonreciprocity and determining an impedance-matching condition. Note, that the following derivation is done in the mode-representation.

We start by inserting the equations of motion, see Eq. (3.85), into the Heisenberg-Langevin equation (4.1). This gives us the subsequent solutions

$$\langle a_1[\omega] \rangle = -i \left[J + i\mu \frac{\Gamma[\omega]}{2} \right] \bar{\chi}_1[\omega] \langle a_2[\omega] \rangle - \sqrt{\kappa_1} \bar{\chi}_1[\omega] \langle a_{1,\text{in}}[\omega] \rangle, \quad (4.27\text{a})$$

$$\langle a_2[\omega] \rangle = -i \left[J^* + i\mu^* \frac{\Gamma[\omega]}{2} \right] \bar{\chi}_2[\omega] \langle a_1[\omega] \rangle - \sqrt{\kappa_2} \bar{\chi}_2[\omega] \langle a_{2,\text{in}}[\omega] \rangle, \quad (4.27\text{b})$$

with $\mu = -u_2 u_1^*$, and where we introduced the effective susceptibility

$$\bar{\chi}_i[\omega] \equiv \frac{2}{i2\omega + \kappa_i + \Gamma_i[\omega]} = \frac{2(\kappa_i + \Gamma_i[\omega])}{4\omega^2 + (\kappa_i + \Gamma_i[\omega])^2} - i \frac{4\omega}{4\omega^2 + (\kappa_i + \Gamma_i[\omega])^2}, \quad (4.28)$$

encoding the response of a mode $\langle a_i \rangle$ to any incoming excitation - either due to an input-field, or another mode $\langle a_j \rangle$. Note, that we additionally introduce a combined susceptibility for conciseness

$$\bar{\chi}[\omega] \equiv \bar{\chi}_1[\omega] \bar{\chi}_2[\omega]. \quad (4.29)$$

However, since the aim is to find a useful expression of the S-matrix, additional abbreviations for (coherent and dissipative) couplings are introduced

$$l_1[\omega] \equiv \left(J + i\mu \frac{\Gamma[\omega]}{2} \right), \quad l_2[\omega] \equiv \left(J^* + i\mu^* \frac{\Gamma[\omega]}{2} \right), \quad (4.30)$$

which can be reformulated as

$$l_{1,2}[\omega] = \left(|J| e^{\pm i\Phi} + i|\mu_2| \frac{\Gamma[\omega]}{2} \right). \quad (4.31)$$

Conclusively, the I/O relation from Eq. (4.4) and Eq. (4.27) written in terms of input-fields

$$\langle a_1[\omega] \rangle = \frac{1}{1 + \bar{\chi}[\omega] l_1[\omega] l_2[\omega]} \left(-\sqrt{\kappa_1} \bar{\chi}_1[\omega] \langle a_{1,\text{in}}[\omega] \rangle + i\sqrt{\kappa_2} \bar{\chi}[\omega] l_1[\omega] \langle a_{2,\text{in}}[\omega] \rangle \right), \quad (4.32a)$$

$$\langle a_2[\omega] \rangle = \frac{1}{1 + \bar{\chi}[\omega] l_1[\omega] l_2[\omega]} \left(-\sqrt{\kappa_2} \bar{\chi}_2[\omega] \langle a_{2,\text{in}}[\omega] \rangle + i\sqrt{\kappa_1} \bar{\chi}[\omega] l_2[\omega] \langle a_{1,\text{in}}[\omega] \rangle \right), \quad (4.32b)$$

give us the desired analytical expression of the S-matrix

$$\tilde{\mathbf{S}}_{\text{eff}}[\omega] = \frac{1}{1 + \bar{\chi}[\omega] l_1[\omega] l_2[\omega]} \begin{pmatrix} 1 + \bar{\chi}[\omega] l_1[\omega] l_2[\omega] - \kappa_1 \bar{\chi}_1[\omega] & i\sqrt{\kappa_1 \kappa_2} \bar{\chi}[\omega] l_1[\omega] \\ i\sqrt{\kappa_1 \kappa_2} \bar{\chi}[\omega] l_2[\omega] & 1 + \bar{\chi}[\omega] l_1[\omega] l_2[\omega] - \kappa_2 \bar{\chi}_2[\omega] \end{pmatrix}. \quad (4.33)$$

If the system is in the unidirectional regime, at least one of the l_i -terms must vanish at resonance. For convenience, the modulus (with $|\mu_2| = |J_{32} J_{31}|/|J|^2$, and $\Gamma_0 = 4|J|^2/\kappa_3$) is set to

$$\text{optical isolator:} \quad |J| \stackrel{!}{=} |\mu_2| \frac{\Gamma_0}{2}, \quad (4.34a)$$

$$\text{dissipative ring:} \quad |J_{12}| \stackrel{!}{=} |J_{31} J_{32}| \frac{4}{\kappa_3}, \quad (4.34b)$$

(where the result for the dissipative ring is analogously derived), which implies for the coupling

$$l_{1,2}[\omega] = \frac{|\mu_2|}{2} \left(e^{\pm i\Phi} \Gamma_0 - i\Gamma[\omega] \right). \quad (4.35)$$

By choosing an unidirectional limit of the phase, e.g. $\Phi = \phi_R$ ($1 \rightarrow 2$), the term $l_1[0] = 0$ becomes zero, implying that the transmission coefficient $|(\tilde{\mathbf{S}}_{\text{eff}})_{12}|^2 = 0$, vanishes as well. This clearly resembles the behavior of Eq. (4.32a), where the second mode cannot drive the first mode. However, reflections inside the S-matrix also change $(\tilde{\mathbf{S}}_{\text{eff}}[\omega])_{ii} = 1 - \kappa_i \bar{\chi}_i[\omega]$. And since these coefficients should vanish, impedance-matching can be formulated as follows:

$$\kappa_i \bar{\chi}_i[0] \stackrel{!}{=} 1 \implies \kappa_i \stackrel{!}{=} \Gamma_i[0], \quad (4.36)$$

for our choice of $|J|$ from Eq. (4.34b). Deviating from this condition will result in power-loss, so we call

$$\mathcal{C}_i \equiv \frac{\Gamma_i}{\Gamma} 0] \kappa_i, \quad (4.37)$$

the *cooperativity* of the damping parameters, which is maximized for the impedance-matching condition $\kappa_i = \Gamma_i \iff \mathcal{C} = 1$. The impedance-matching condition for the three-mode dissipative ring can be easily derived by inserting the explicit definition of Γ

$$\Gamma_i = \kappa_i \implies 4|J_{3i}|^2 = \kappa_i \kappa_3, \quad (4.38)$$

where the same condition can also be found by setting reflection coefficients of the dissipative ring to zero. Naturally, since both reflection coefficients of the optical isolator have to vanish, both cooperativities have to be maximized $\mathcal{C} \equiv \mathcal{C}_1 = \mathcal{C}_2 = 1$. Rearranging Eq. (4.38)

$$|J_{3i}| = \frac{\sqrt{\kappa_i \kappa_3}}{2}, \quad (4.39)$$

gives us for the impedance-matching condition of the optical isolator

$$|J| = \frac{\sqrt{\kappa_1 \kappa_2}}{2}. \quad (4.40)$$

In the subsequent, system-parameters are expressed as unit-less quantities. Of course, this choice is not unique. However, we focus on two impedance-matched regimes: *1. Symmetrically damped (or circulator) setting*, with $\kappa \equiv \kappa_1/2 = \kappa_2/2 = \kappa_3/2$ (for the optical isolator $\kappa \equiv \kappa_1/2 = \kappa_2/2 = 2|J|^2/\Gamma_0$), and *1. Asymmetrically damped (or ring) setting*, with $\kappa \equiv \kappa_1 = \kappa_2 = \kappa_3/4$ (for the optical isolator $\kappa \equiv \kappa_1 = \kappa_2 = |J|^2/\Gamma_0$). Thus, every other parameter in both models will be expressed in units of κ , e.g. for $\mathcal{C} = 1$, a valid choice becomes $|J|/\kappa = 1$ and $|J_{3i}|/\kappa = 1$. Recall, that impedance-matching is met for any parameter-choice respective to conditions mentioned earlier. And even though all reflection coefficients vanish in both settings, transmission will change depending on our specific choice of damping rates. Why is that? Consider the symmetric setting $\kappa = \kappa_i/2$. Here, the auxiliary behaves noticeably different between the Markovian and the non-Markovian regime, as κ_3 is not much bigger than other system-parameters. However, the auxiliary is damped much stronger $\kappa_3 > \kappa_{1,2}$ in the asymmetric setting, which implies that the non-Markovian correction closer resembles the Markovian regime, as shown in Fig. 8.

To see how impedance-matching effects the S-matrix, we assume the unidirectional limit $\Phi = \phi_R = \pi/2$, set $|J| = |\mu_2|\Gamma_0/2$, and choose symmetric damping rates $\kappa_{1,2}/2 \equiv \kappa$. Without impedance-matching $\Gamma_0 \neq 2\kappa$, the Markovian S-matrix (for $\omega = 0$) reduces to

$$\tilde{\mathbf{S}}_{\text{eff}}[0] = \begin{pmatrix} \frac{\Gamma_0/2 - \kappa}{\Gamma_0/2 + \kappa} & 0 \\ \frac{4\kappa\Gamma_0/2}{(\Gamma_0/2 + \kappa)^2} & \frac{\Gamma_0/2 - \kappa}{\Gamma_0/2 + \kappa} \end{pmatrix}. \quad (4.41)$$

By impedance matching, the reflections vanish $|(\tilde{\mathbf{S}}_{\text{eff}})_{ii}|^2 = 0$, and the only remaining transmission is $|(\tilde{\mathbf{S}}_{\text{eff}})_{21}|^2 = 1$ ($1 \rightarrow 2$), which perfectly resembles the S-matrix of an idealized isolator, compare Section III F 1. For $\Phi = \phi_L$ the only remaining element is the other transmission coefficient $|(\tilde{\mathbf{S}}_{\text{eff}})_{12}|^2 = 1$.

Figure 12 compares frequency dependent scattering probabilities $|\tilde{\mathbf{S}}_{a_i a_j}|^2 \equiv |(\tilde{\mathbf{S}}_{\text{eff}})_{ij}|^2$ of the optical isolator for varying transport limits, where solid (dashed) lines represent a Markovian (non-Markovian) effective reservoir. We assume a maximized cooperativity $\mathcal{C} = 1$ and $|J|/\kappa = 1$, where the first two pictures in each row show the symmetric $\kappa_i = 2\kappa$ and the last picture in each the asymmetric regime $\kappa_{1,2} = \kappa_3/4 = \kappa$. The first Fig. 12 (a) shows nonreciprocal transport for $\Phi = \phi_R$ and symmetric damping rates, where all reflections $|\tilde{\mathbf{S}}_{a_i a_i}|^2 = 0$ vanish, and transmission from

$a_1 \rightarrow a_2$ becomes unidirectional on resonance with $|\tilde{\mathbf{S}}_{a_2 a_1}|^2 = 1$ and $|\tilde{\mathbf{S}}_{a_1 a_2}|^2 = 0$. For a non-Markovian reservoir, clear dips/peaks around $|\omega|\kappa = \sqrt{2}$ are visible due to the additional oscillations of the auxiliary. Far off-resonance, reflections are maximized and transmission from $1 \rightarrow 2$ also vanishes. The second Fig. 12 (b) shows the same as before, only with $\Phi = \phi_L$, leading to $|\tilde{\mathbf{S}}_{a_1 a_2}|^2 = 1$, $|\tilde{\mathbf{S}}_{a_2 a_1}|^2 = 0$ and no reflections $|\tilde{\mathbf{S}}_{a_i a_i}|^2 = 0$ for $\omega = 0$. The third Figure 12 (c) in the first row shows (b) for asymmetric damping rates $\kappa \equiv \kappa_{1,2} = \kappa_3/4$. We see, how the non-Markovian curve converges to the Markovian limit, since the auxiliary is damped stronger. The dips/peaks compared to (b) are significantly weaker, and the frequency dependency of the non-Markovian auxiliary on the dynamics are barely noticeable. Figure 12 (d) shows the first reciprocal case with $\Phi = 0$ in the symmetric regime. Here, reflections and transmissions are the same for both modes. We see a symmetric line-shape for non-Markovian curves, which are not centered at $\omega = 0$. The oscillations of the auxiliary have a more noticeable effect on the probabilities, especially for negative ω as the difference between the Markovian and non-Markovian case is the strongest here. Thus, there is a clear sign dependence, since the non-Markovian case only slightly deviates from the Markovian limit for positive frequencies. The next Fig. 12 (e) for $\Phi = \pi$ shows the same behaviour, only flipped around the y -axis. However, the difference between (d) and this case vanishes at resonance. Thus, any asymmetry in scattering probabilities is only relevant for finite ω . Section VIA, attempts to further illuminate this behaviour. Note, that this result was already observed for similar systems, see Chen *et al.* [63]. The last Fig. 12 (f) shows $\Phi = 0$ in the asymmetrically damped setting, where the non-Markovian case again converges to the Markovian limit. The quadrature case can be found in Appendix C 5, see Fig. 30.

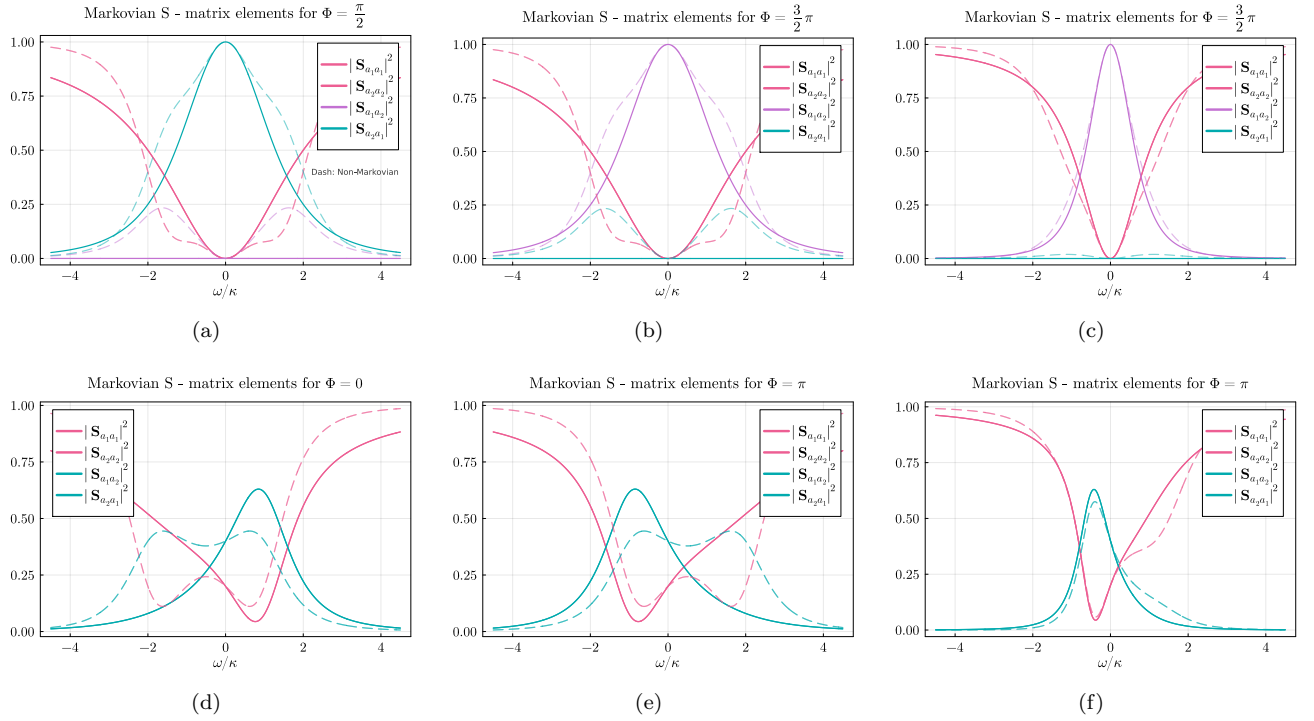


FIG. 12. Markovian (solid) and non-Markovian (dashed) scattering probabilities of the optical isolator, plotted against frequency for different limits of Φ . We assume the parameters $\mathcal{C} = 1$ and $|J|/\kappa = 1$. The first two pictures in each row show symmetric damping rates $\kappa = \kappa_i/2$, and the last picture asymmetric rates $\kappa_{1,2} = \kappa_3/4 = \kappa$. (a) Nonreciprocal case for $\Phi = \phi_R$ in the symmetric regime. On resonance, reflections $|\tilde{\mathbf{S}}_{a_i a_i}|^2 = 0$ vanish, and transmissions become $|\tilde{\mathbf{S}}_{a_2 a_1}|^2 = 1$, $|\tilde{\mathbf{S}}_{a_1 a_2}|^2 = 0$. Clear dips/peaks around $\omega/\kappa = \pm\sqrt{2}$ are visible due to the frequency dependence of the auxiliary, and correspond to the eigenvalues, see Sec. III G. (b) Nonreciprocal case with opposite phase $\Phi = \phi_L$, leading to $|\tilde{\mathbf{S}}_{a_1 a_2}|^2 = 1$, and $|\tilde{\mathbf{S}}_{a_2 a_1}|^2 = 0$. (c) The same as (a) with $\Phi = \phi_R$ but in the asymmetric regime. The non-Markovian case converges to the Markovian limit since the auxiliary is damped stronger. The dips/peaks are significantly weaker, and the effect of the auxiliary on the dynamics is barely noticeable. (d) Reciprocal case for $\Phi = 0$ in the symmetric regime. Reflections and transmissions are the same for both modes. Non-Markovian curves are symmetric, yet not centered at $\omega = 0$. The auxiliary has a noticeable effect on probabilities. The Markovian and non-Markovian curves differ considerably for negative frequencies. (e) Reciprocal case for $\Phi = \pi$, with the same behaviour as (d) only flipped around the y -axis. On resonance, the difference between (d) and this case vanishes. Thus, the behaviour of asymmetrically tilted curves is only relevant for finite ω . (f) Reciprocal case for $\Phi = 0$ for asymmetric damping rates. Again, the non-Markovian curve converges to the Markovian limit.

V. Noise and diffusion

A. Derivation of the output-noise

Up to now, we were only concerned with limiting cases and transport properties within the system. However, we still lack an understanding of how inputs are modified by traversing the system. Thus, the goal of this Section is to find an expression for the output-noise. This opens up a deeper analysis into the modulating effect of the system to incoming reservoir modes beyond the signal itself, i.e. by also including *thermal fluctuations/noise* into the picture. Here, we are only concerned with the noise at output-ports. Our system affects incident noise in two ways: 1. *The system acts as a filter, modulating and filtering the frequencies of incident noise* (see Sec. VB), and 2. *Noise entering a given port will be redistributed over (possibly multiple) output-ports of the system*. Where the S-matrix only tells us how resonantly the system responds to certain frequencies of incoming modes, *frequency* does mean something different for the output-noise spectrum: Incoming modes are scattered by the system (however the system may respond) and leave the system again as transformed modes, where some frequencies are cut-off and others modulated. So, *frequency* for the output-noise refers to frequencies of (in- or outgoing) waves themselves. Before jumping right into the derivation, we first explain our approach: The output-noise spectrum can be found by calculating the the covariances of output-modes, using their second statistical moments. Since quadrature operators are hermitian, they closely resemble classical (yet non-commuting) random variables, which can be used to simplify the derivation of the covariance matrix. Naturally, this is not the case for non-Hermitian operators like the standard mode operators, where one has to be more careful. Thus, we will first focus on an expression in the quadrature representation before moving on to the mode basis.

1. Output-noise in the quadrature basis

The (non-symmetrized) *covariance matrix* is given by subtracting the expectation values of quadratures $\langle \mathbf{v} \rangle \langle \mathbf{v}^T \rangle$ from their *second moments* $\langle \mathbf{v} \mathbf{v}^T \rangle$ (see Jacobs [67]):

$$\mathbf{C}_{\text{non-sym}} \stackrel{\text{def}}{=} \langle \langle \mathbf{v} \mathbf{v}^T \rangle \rangle \equiv \langle \mathbf{v} \mathbf{v}^T \rangle - \langle \mathbf{v} \rangle \langle \mathbf{v}^T \rangle. \quad (5.1)$$

Thus, the covariance matrix is a measure of how correlated quadratures are - the first term simply vanishes for uncorrelated quadratures. However, stochastic operators can be decomposed as

$$\mathbf{v} = \langle \mathbf{v} \rangle + \boldsymbol{\xi}_{\mathbf{v}}, \quad (5.2)$$

where $\boldsymbol{\xi}_{\mathbf{v}}$ is the operator-valued noise vector with zero-mean $\langle \boldsymbol{\xi}_{\mathbf{v}} \rangle = 0$. This way, thermal noise acts as the deviation from the expected value, analogous to (classical) force fluctuations in Brownian motion [33, 34]. Using this decomposition, it follows for the second moments

$$\langle \langle v_1 v_2 \rangle \rangle = \langle \langle (v_1 + \xi_{v_1})(v_2 + \xi_{v_2}) \rangle \rangle - \langle v_1 \rangle \langle v_2 \rangle = \langle \xi_{v_1} \xi_{v_2} \rangle + \langle v_1 \rangle \langle v_2 \rangle - \langle v_1 \rangle \langle v_2 \rangle = \langle \xi_{v_1} \xi_{v_2} \rangle, \quad (5.3)$$

implying that the covariance between quadratures v_1, v_2 actually gives us the covariance of their *fluctuations* (regardless of $\langle v_i \rangle$). Since we deal with non-commuting operators, we can symmetrize the former expression

$$\mathbf{C}_{\text{sym}} = \frac{1}{2} (\mathbf{C}_{\text{non-sym}} + \mathbf{C}_{\text{non-sym}}^T) = \frac{1}{2} (\langle \langle \mathbf{v} \mathbf{v}^T \rangle \rangle + \langle \langle \mathbf{v} \mathbf{v}^T \rangle \rangle^T) = \frac{1}{2} (\langle \mathbf{v} \mathbf{v}^T \rangle + \langle \mathbf{v} \mathbf{v}^T \rangle^T) - \langle \mathbf{v} \rangle \langle \mathbf{v}^T \rangle, \quad (5.4)$$

which is now independent on the order of operators, see Ref. [67]. This symmetrization procedure can be further extended if \mathbf{v} explicitly depends on additional arguments. For example, if quadratures in frequency space $\mathbf{v}[\omega]$ depend on a dynamical parameter ω , the fully symmetrized covariance matrix can be written as

$$\mathbf{C}[\omega, \omega'] = \frac{\mathbf{C}_{\text{sym}}[\omega, \omega'] + \mathbf{C}_{\text{sym}}[\omega', \omega]}{2} = \frac{1}{4} \left(\langle\langle \mathbf{v}[\omega] \mathbf{v}^T[\omega'] \rangle\rangle + \langle\langle \mathbf{v}[\omega] \mathbf{v}^T[\omega'] \rangle\rangle^T + \langle\langle \mathbf{v}[\omega'] \mathbf{v}^T[\omega] \rangle\rangle + \langle\langle \mathbf{v}[\omega'] \mathbf{v}^T[\omega] \rangle\rangle^T \right). \quad (5.5)$$

Therefore, we recover an expression for $\mathbf{C}[\omega, \omega']$ which is symmetric in ω and ω' . Naturally, the ω – dependency is exactly the reason why non-Hermitian operators need a more careful treatment. Since our aim is to find the output-noise, we can analogously write the covariance matrix for output-fields

$$\mathbf{C}_{\text{out}}[\omega, \omega'] = \frac{1}{4} \left(\langle\langle \mathbf{v}_{\text{out}}[\omega] \mathbf{v}_{\text{out}}^T[\omega'] \rangle\rangle + \langle\langle \mathbf{v}_{\text{out}}[\omega] \mathbf{v}_{\text{out}}^T[\omega'] \rangle\rangle^T + \langle\langle \mathbf{v}_{\text{out}}[\omega'] \mathbf{v}_{\text{out}}^T[\omega] \rangle\rangle + \langle\langle \mathbf{v}_{\text{out}}[\omega'] \mathbf{v}_{\text{out}}^T[\omega] \rangle\rangle^T \right), \quad (5.6)$$

and by using the S-matrix from Eq. (4.4)

$$\mathbf{v}_{\text{out}}[\omega] = \mathbf{S}[\omega] \mathbf{v}_{\text{in}}[\omega], \quad (5.7)$$

we find that output-field correlators can be expressed in terms of input-field correlators

$$\langle\langle \mathbf{v}_{\text{out}}[\omega] \mathbf{v}_{\text{out}}^T[\omega'] \rangle\rangle = \mathbf{S}[\omega] \langle\langle \mathbf{v}_{\text{in}}[\omega] \mathbf{v}_{\text{in}}^T[\omega'] \rangle\rangle \mathbf{S}^T[\omega']. \quad (5.8)$$

This implies for $\mathbf{C}_{\text{out}}[\omega, \omega']$

$$\begin{aligned} \mathbf{C}_{\text{out}}[\omega, \omega'] = & \frac{1}{4} \left(\mathbf{S}[\omega] \left[\langle\langle \mathbf{v}_{\text{in}}[\omega] \mathbf{v}_{\text{in}}^T[\omega'] \rangle\rangle + \langle\langle \mathbf{v}_{\text{in}}[\omega'] \mathbf{v}_{\text{in}}^T[\omega] \rangle\rangle^T \right] \mathbf{S}^T[\omega'] \right. \\ & \left. + \mathbf{S}[\omega'] \left[\langle\langle \mathbf{v}_{\text{in}}[\omega'] \mathbf{v}_{\text{in}}^T[\omega] \rangle\rangle + \langle\langle \mathbf{v}_{\text{in}}[\omega] \mathbf{v}_{\text{in}}^T[\omega'] \rangle\rangle^T \right] \mathbf{S}^T[\omega] \right). \end{aligned} \quad (5.9)$$

To progress further, we need to identify the input-correlators. Using the commutation relations of input-fields (see Ref. [34]), it follows

$$\langle\langle a_{i,\text{in}}[\omega] a_{j,\text{in}}^\dagger[\omega'] \rangle\rangle = \delta_{ij} (\bar{n}_j + 1) \delta(\omega + \omega'), \quad \langle\langle x_{i,\text{in}}[\omega] x_{j,\text{in}}[\omega'] \rangle\rangle = \delta_{ij} \left(\bar{n}_j + \frac{1}{2} \right) \delta(\omega + \omega'), \quad (5.10a)$$

$$\langle\langle a_{i,\text{in}}^\dagger[\omega] a_{j,\text{in}}[\omega'] \rangle\rangle = \delta_{ij} \bar{n}_j \delta(\omega + \omega'), \quad \langle\langle p_{i,\text{in}}[\omega] p_{j,\text{in}}[\omega'] \rangle\rangle = \delta_{ij} \left(\bar{n}_j + \frac{1}{2} \right) \delta(\omega + \omega'), \quad (5.10b)$$

$$\langle\langle a_{i,\text{in}}^\dagger[\omega] a_{j,\text{in}}^\dagger[\omega'] \rangle\rangle = \langle\langle a_{i,\text{in}}[\omega] a_{j,\text{in}}[\omega'] \rangle\rangle = 0, \quad \langle\langle x_{i,\text{in}}[\omega] p_{j,\text{in}}[\omega'] \rangle\rangle = \delta_{ij} \frac{i}{2} \delta(\omega + \omega'), \quad (5.10c)$$

where $\bar{n}_j \equiv n_j^{\text{th}} = n_{\text{B}}(T_j)$ are temperature dependent Bose-Einstein occupations of incident modes with index $j = 1, \dots, N$. As mentioned in Section II E 1, since this expression is a constant over the whole frequency-bandwidth of the reservoir, it describes *white noise*. Note, this is just an assumption we make and one could perfectly assume a different distribution for the input-noise. Recall, that reservoir modes for different frequencies are different modes altogether. Thus, we assume that each incoming mode looks exactly the same from the point of view of the system. Additionally, as the avid reader might see, modes i, j are assumed to be uncorrelated. Quadrature correlators result in the following non-symmetrized input covariance

$$\begin{aligned}
\mathbf{C}_{\text{in}}^{\text{non-sym}}[\omega, \omega'] &= \langle\langle \mathbf{v}_{\text{in}}[\omega] \mathbf{v}_{\text{in}}^T[\omega'] \rangle\rangle \equiv \delta(\omega + \omega') \mathcal{S}_{\text{in}}^{\text{non-sym}} = \delta(\omega + \omega') \bigoplus_{j=1}^N \left[\left(\bar{n}_j + \frac{1}{2} \right) \mathbb{1}_2 - \frac{1}{2} \sigma_y \right] \\
&= \delta(\omega + \omega') \left(\mathbb{1}_N \otimes \left[\left(\bar{n}_j + \frac{1}{2} \right) \mathbb{1}_2 - \frac{1}{2} \sigma_y \right]_j \right). \tag{5.11}
\end{aligned}$$

Here, $\mathcal{S}_{\text{in}}^{\text{non-sym}}$ is the frequency-independent input-noise spectral density. For an explicit form of the input correlation matrix, consider Appendix D5. Inserting the non-symmetrized input covariance matrix into Eq. (5.9), leads to

$$\mathbf{C}_{\text{out}}[\omega, \omega'] = \delta(\omega + \omega') \frac{1}{2} \left(\mathbf{S}[\omega] \left[\frac{\mathcal{S}_{\text{in}}^{\text{non-sym}} + (\mathcal{S}_{\text{in}}^{\text{non-sym}})^T}{2} \right] \mathbf{S}^T[\omega'] + \mathbf{S}[\omega'] \left[\frac{\mathcal{S}_{\text{in}}^{\text{non-sym}} + (\mathcal{S}_{\text{in}}^{\text{non-sym}})^T}{2} \right] \mathbf{S}^T[\omega] \right). \tag{5.12}$$

This can be further simplified by introducing a vector of thermal occupations $\mathbf{n}_{\text{th}} \equiv (\bar{n}_1, \bar{n}_1, \dots, \bar{n}_N)^T$, and calculating the symmetrized input-noise

$$\mathcal{S}_{\text{in}}(\mathbf{n}_{\text{th}}) \equiv \frac{\mathcal{S}_{\text{in}}^{\text{non-sym}} + (\mathcal{S}_{\text{in}}^{\text{non-sym}})^T}{2} = \mathbb{1}_N \otimes \frac{1}{2} \left[2 \left(\bar{n}_j + \frac{1}{2} \right) \mathbb{1}_2 - \frac{1}{2} (\sigma_y + \sigma_y^T) \right]_j = \mathbb{1}_N \otimes \left[\left(\bar{n}_j + \frac{1}{2} \right) \mathbb{1}_2 \right]_j, \tag{5.13}$$

where

$$\mathbf{C}_{\text{in}}[\omega, \omega'] = \delta(\omega + \omega') \mathcal{S}_{\text{in}}(\mathbf{n}_{\text{th}}), \tag{5.14}$$

is the symmetrized input-covariance. Here, we used the fact that the transpose of a Kronecker product distributes $(\mathbf{A} \otimes \mathbf{B})^T = \mathbf{A}^T \otimes \mathbf{B}^T$, and $\sigma_y^T = \sigma_y^* = -\sigma_y$ for the third equality in Eq. (5.13). The resulting expression

$$\mathcal{S}_{\text{in}}(\mathbf{n}_{\text{th}}) = \mathbb{1}_N \otimes \left[\left(\bar{n}_j + \frac{1}{2} \right) \mathbb{1}_2 \right]_j, \tag{5.15}$$

is the fully symmetrized, frequency-independent and diagonal *input-noise spectral density*. For completeness, it is also useful to note that the input-noise is trivially symmetric $\mathcal{S}_{\text{in}} = \mathcal{S}_{\text{in}}^T$. Finally, by inserting Eq. (5.15) into Eq. (5.12), we obtain the output covariance matrix (for $\omega' = -\omega$)

$$\mathbf{C}_{\text{out}}[\omega, \omega'] = \delta(\omega + \omega') \left[\frac{\mathbf{S}[\omega] \mathcal{S}_{\text{in}} \mathbf{S}^T[-\omega] + \mathbf{S}[-\omega] \mathcal{S}_{\text{in}} \mathbf{S}^T[\omega]}{2} \right], \tag{5.16}$$

where

$$\mathcal{S}_{\text{out}}[\omega] = \frac{\mathbf{S}[\omega] \mathcal{S}_{\text{in}} \mathbf{S}^T[-\omega] + \mathbf{S}[-\omega] \mathcal{S}_{\text{in}} \mathbf{S}^T[\omega]}{2}, \tag{5.17}$$

is the *spectral matrix of the output-noise operators* and describes the spectrum of output-currents. The output-noise spectral density then relates symmetrized correlations of the noise sources to their spectra (compare Eq. (5.14))

$$\mathbf{C}_{\text{out}}[\omega, \omega'] = \delta(\omega + \omega') \mathcal{S}_{\text{out}}[\omega]. \quad (5.18)$$

Since the S-matrix in the quadrature basis fulfills $\mathbf{S}[-\omega] = \mathbf{S}^*[\omega]$, the expression for the noise spectral density from Eq. (5.17) reduces to

$$\mathcal{S}_{\text{out}}[\omega] = \frac{\mathbf{S}[\omega] \mathcal{S}_{\text{in}} \mathbf{S}^\dagger[\omega] + (\mathbf{S}[\omega] \mathcal{S}_{\text{in}} \mathbf{S}^\dagger[\omega])^*}{2} = \Re \mathbf{e} (\mathbf{S}[\omega] \mathcal{S}_{\text{in}} \mathbf{S}^\dagger[\omega]). \quad (5.19)$$

This ensures that all elements of the output-noise spectrum are always real in the quadrature representation. Next, we find an expression of the output noise in the mode representation and highlight differences between both representations in the subsequent.

2. Output-noise in the mode basis

Before, the unitary \mathbf{T} from Eq. (3.69) was used to transform between bases. However, as it is not clear at this point if \mathbf{T} gives us the correct expression for the covariance in the mode basis, we need to approach this differently: Assume an operator-order and frequency-symmetrized expression for the output-covariance in the mode representation, which will be introduced here but justified later, expressed by the output-correlators

$$\tilde{\mathbf{C}}_{\text{out}}[\omega, \omega'] = \frac{1}{2} \left(\frac{1}{2} \left\langle\left\langle \left\{ \mathbf{a}_{\text{out}}[\omega], \mathbf{a}_{\text{out}}^\dagger[\omega'] \right\} \right\rangle\right\rangle + \frac{1}{2} \left\langle\left\langle \left\{ \mathbf{a}_{\text{out}}[\omega'], \mathbf{a}_{\text{out}}^\dagger[\omega] \right\} \right\rangle\right\rangle \right). \quad (5.20)$$

Here, $\{\hat{A}, \hat{B}\} = \hat{A}\hat{B} + \hat{B}\hat{A}$ is the anti-commutator for some generic operators \hat{A}, \hat{B} , which implies using Eq. (3.42) that $\{\mathbf{a}, \mathbf{a}^\dagger\} = \mathbf{a}\mathbf{a}^\dagger + (\mathbf{a}^\dagger \mathbf{a}^T)^T$. This expression is reminiscent of the expression given by Eq. (54) in Ref. [40]. Since (time-dependent) I/O operators have units of $1/\sqrt{s}$, the expression $\langle\langle a_{i,\text{in}}^\dagger(t) a_{i,\text{in}}(t) \rangle\rangle$ can be viewed as the *noise of the input particle flux*. As an illustrative example, we take the expectation value of the commutator for input-fields

$$\left\langle\left\langle \left[\mathbf{a}_{\text{in}}[\omega], \mathbf{a}_{\text{in}}^\dagger[\omega'] \right] \right\rangle\right\rangle = \left\langle\left\langle \mathbf{a}_{\text{in}}[\omega] \mathbf{a}_{\text{in}}^\dagger[\omega'] \right\rangle\right\rangle - \left\langle\left\langle \mathbf{a}_{\text{in}}^\dagger[\omega'] \mathbf{a}_{\text{in}}[\omega] \right\rangle\right\rangle^T = \delta(\omega + \omega') \delta_{ij} (\sigma_z \otimes \mathbf{1}_3), \quad (5.21)$$

and get an element of the symplectic group $\text{Sp}(2N, \mathbb{R})$, where we used Eq. (5.10) for the last equality. In turn, the expectation value of the anti-commutator results in a familiar expression

$$\frac{1}{2} \left\langle\left\langle \left\{ \mathbf{a}_{\text{in}}[\omega], \mathbf{a}_{\text{in}}^\dagger[\omega'] \right\} \right\rangle\right\rangle = \delta(\omega + \omega') \left[\bigoplus_{j=1}^N \left(\bar{n}_j + \frac{1}{2} \right) \right] \otimes \mathbf{1}_2 = \delta(\omega + \omega') (\mathbf{T}^\dagger \mathcal{S}_{\text{in}} \mathbf{T}) \equiv \delta(\omega + \omega') \tilde{\mathcal{S}}_{\text{in}}, \quad (5.22)$$

which is just the transformed input-covariance matrix

$$\tilde{\mathbf{C}}_{\text{in}}[\omega, \omega'] = \mathbf{T}^\dagger \mathbf{C}_{\text{in}}[\omega, \omega'] \mathbf{T}, \quad (5.23)$$

with

$$\tilde{\mathbf{C}}_{\text{in}}[\omega, \omega'] = \frac{1}{2} \left\langle\left\langle \left\{ \mathbf{a}_{\text{in}}[\omega], \mathbf{a}_{\text{in}}^\dagger[\omega'] \right\} \right\rangle\right\rangle, \quad (5.24)$$

and the input-noise

$$\tilde{\mathcal{S}}_{\text{in}} = \left[\bigoplus_{j=1}^N \left(\bar{n}_j + \frac{1}{2} \right) \right] \otimes \mathbf{1}_2. \quad (5.25)$$

To answer the question posed at the beginning of this derivation: Indeed, one can transform expression (5.20) back to the quadrature representation using \mathbf{T} . However, we need to understand *how to adequately* transform between the bases. We restate the transformation formula from Eq. (3.69)

$$\mathbf{a}[\omega] = \mathbf{T}^\dagger \mathbf{v}[\omega], \quad (5.26)$$

and multiply both sides by $\mathbf{\Lambda}_x$. This gives us $\mathbf{\Lambda}_x \mathbf{a}[\omega] = \mathbf{a}^\dagger[\omega]$ for the LHS, and by using

$$\mathbf{T} = \mathbf{T}^* \mathbf{\Lambda}_x, \quad (5.27)$$

we get

$$\mathbf{a}^\dagger[\omega] = \mathbf{\Lambda}_x \mathbf{T}^\dagger \mathbf{v}[\omega] = (\mathbf{T}^* \mathbf{\Lambda}_x)^T \mathbf{v}[\omega] = \mathbf{T}^T \mathbf{v}[\omega]. \quad (5.28)$$

Thus, $\mathbf{v}[\omega]$ can also be expressed as

$$\mathbf{v}[\omega] = \mathbf{T}^* \mathbf{a}^\dagger[\omega], \quad (5.29)$$

implying

$$\mathbf{v}^T[\omega] = \mathbf{a}^\dagger[\omega] \mathbf{T}^\dagger. \quad (5.30)$$

This expression is completely reasonable even from a physical perspective, as quadratures are hermitian and daggered elements should remain invariant compared to non-daggered ones with $\mathbf{v}^\dagger[\omega] = \mathbf{v}^T[\omega]$. With all these rather technical considerations, we are equipped to tackle the problem of transforming the covariance matrix between the bases. Naturally, we can perform the transformation starting from either basis, however, for didactic reasons we transform from the quadrature to the mode basis. As before, we start at Eq. (5.6), insert Eq. (5.7), arrive at Eq. (5.8) and then transform $\mathbf{T}^\dagger \mathbf{C}_{\text{out}}[\omega, \omega'] \mathbf{T}$. Due to brevity, we do that term-wise. By using Eq. (5.26), Eq. (4.12b), and $\mathbf{S}[\omega] = \mathbf{S}^*[-\omega]$ we get

$$\begin{aligned} & \mathbf{T}^\dagger \langle\langle \mathbf{v}_{\text{out}}[\omega] \mathbf{v}_{\text{out}}^T[\omega'] \rangle\rangle \mathbf{T} \\ &= \left\langle\left\langle \mathbf{T}^\dagger \mathbf{S}[\omega] \mathbf{v}_{\text{in}}[\omega] \mathbf{v}_{\text{in}}^T[\omega'] \underbrace{\mathbf{S}^T[\omega']}_{\mathbf{S}^\dagger[-\omega']} \mathbf{T} \right\rangle\right\rangle = \left\langle\left\langle \underbrace{(\mathbf{T}^\dagger \mathbf{S}[\omega] \mathbf{T})}_{\tilde{\mathbf{S}}[\omega]} \mathbf{a}_{\text{in}}[\omega] \mathbf{a}_{\text{in}}^\dagger[\omega'] \underbrace{(\mathbf{T}^\dagger \mathbf{S}^\dagger[-\omega'] \mathbf{T})}_{\tilde{\mathbf{S}}^\dagger[-\omega']} \right\rangle\right\rangle = \langle\langle \mathbf{a}_{\text{out}}[\omega] \mathbf{a}_{\text{out}}^\dagger[\omega'] \rangle\rangle. \end{aligned} \quad (5.31)$$

Transposed terms are a bit more tricky to transform, so we need to make a few remarks: First, we notice that complex conjugating the basis transform of the S-matrix results in

$$(\mathbf{T}^\dagger \mathbf{S}[-\omega] \mathbf{T})^* = \tilde{\mathbf{S}}^*[-\omega] \iff \mathbf{T}^T \underbrace{\mathbf{S}^*[-\omega]}_{\mathbf{S}[\omega]} \mathbf{T}^* = \tilde{\mathbf{S}}^*[-\omega]. \quad (5.32)$$

Next, Eq. (3.41) implies, that we can write $\mathbf{a}^\dagger \mathbf{\Lambda}_x = (\mathbf{\Lambda}_x \mathbf{a}^\dagger)^T = \mathbf{a}^T$. With Eq. (5.27), transposed terms can be calculated as

$$\begin{aligned} & \mathbf{T}^\dagger \langle\langle \mathbf{v}_{\text{out}}[\omega] \mathbf{v}_{\text{out}}^T[\omega'] \rangle\rangle^T \mathbf{T} \\ &= \langle\langle \mathbf{T}^T \mathbf{S}[\omega] \mathbf{v}_{\text{in}}[\omega] \mathbf{v}_{\text{in}}^T[\omega'] \underbrace{\mathbf{S}^T[\omega']}_{\mathbf{S}^\dagger[-\omega']} \mathbf{T}^* \rangle\rangle^T = \langle\langle \mathbf{T}^T \mathbf{S}[\omega] \underbrace{\mathbf{T}}_{\mathbf{T}^* \mathbf{\Lambda}_x} \mathbf{a}_{\text{in}}[\omega] \mathbf{a}_{\text{in}}^\dagger[\omega'] \underbrace{\mathbf{T}^\dagger}_{\mathbf{\Lambda}_x \mathbf{T}^T} \mathbf{S}^\dagger[-\omega'] \mathbf{T}^* \rangle\rangle^T \\ &= \langle\langle \underbrace{\mathbf{T}^T \mathbf{S}[\omega] \mathbf{T}^*}_{\tilde{\mathbf{S}}^*[-\omega]} \underbrace{\mathbf{\Lambda}_x \mathbf{a}_{\text{in}}[\omega]}_{\mathbf{a}_{\text{in}}^\dagger[\omega]} \mathbf{a}_{\text{in}}^T[\omega'] \underbrace{\mathbf{T}^T \mathbf{S}^\dagger[-\omega'] \mathbf{T}^*}_{\mathbf{S}^T[\omega']} \rangle\rangle^T = \langle\langle \tilde{\mathbf{S}}^*[-\omega] \mathbf{a}_{\text{in}}^\dagger[\omega] \mathbf{a}_{\text{in}}^T[\omega'] \mathbf{S}^T[\omega'] \rangle\rangle^T = \langle\langle \mathbf{a}_{\text{out}}^\dagger[\omega] \mathbf{a}_{\text{out}}^T[\omega'] \rangle\rangle^T, \end{aligned} \quad (5.33)$$

where remaining terms transform the same way for flipped ω, ω' . Indeed, the form of Eq. (5.20) for the output-covariance is justified, and we can change representations by simply applying the transformation

$$\tilde{\mathbf{C}}_{\text{out}}[\omega, \omega'] = \mathbf{T}^\dagger \mathbf{C}_{\text{out}}[\omega, \omega'] \mathbf{T}. \quad (5.34)$$

The output-covariance from Eq. (5.20) can also be expressed in terms of input-covariances (which is derived in Appendix D 2) as

$$\tilde{\mathbf{C}}_{\text{out}}[\omega, \omega'] = \frac{\tilde{\mathbf{S}}[\omega] \tilde{\mathbf{C}}_{\text{in}}[\omega, \omega'] \tilde{\mathbf{S}}^\dagger[-\omega'] + \tilde{\mathbf{S}}[\omega'] \tilde{\mathbf{C}}_{\text{in}}[\omega, \omega'] \tilde{\mathbf{S}}^\dagger[-\omega]}{2} = \delta(\omega + \omega') \left[\frac{\tilde{\mathbf{S}}[\omega] \tilde{\mathcal{S}}_{\text{in}} \tilde{\mathbf{S}}^\dagger[\omega] + \tilde{\mathbf{S}}[-\omega] \tilde{\mathcal{S}}_{\text{in}} \tilde{\mathbf{S}}^\dagger[-\omega]}{2} \right], \quad (5.35)$$

with the output-noise spectrum

$$\tilde{\mathcal{S}}_{\text{out}}[\omega] = \frac{\tilde{\mathbf{S}}[\omega] \tilde{\mathcal{S}}_{\text{in}} \tilde{\mathbf{S}}^\dagger[\omega] + \tilde{\mathbf{S}}[-\omega] \tilde{\mathcal{S}}_{\text{in}} \tilde{\mathbf{S}}^\dagger[-\omega]}{2}. \quad (5.36)$$

Recall, that $\tilde{\mathbf{S}}[-\omega] \neq \tilde{\mathbf{S}}^*[\omega]$, which implies that the last expression cannot be reduced any further. Thus, the output-noise is not protected to be real for all cases. However, since diagonal elements of the output-noise encode the *noise of the output-particle flux*, they are always positive real numbers with the same magnitude in both bases. This is a consequence of the vanishing commutator for off-diagonal elements

$$\langle\langle [x_{i,\text{out}}[\omega], p_{j,\text{out}}[\omega']] \rangle\rangle = i \delta_{ij} \delta(\omega + \omega'), \quad (5.37)$$

which implies that diagonal correlators

$$\langle\langle a_{i,\text{out}}[\omega] a_{i,\text{out}}^\dagger[\omega'] \rangle\rangle = \frac{\langle\langle x_{i,\text{out}}[\omega] x_{i,\text{out}}[\omega'] \rangle\rangle + \langle\langle p_{i,\text{out}}[\omega] p_{i,\text{out}}[\omega'] \rangle\rangle}{2}. \quad (5.38)$$

indeed have the same magnitude in both bases. Since it will become handy shortly, we can correspond each element of the noise-matrix by their respective operators with the notation $\mathcal{S}_{a_i a_j^\dagger} \equiv (\tilde{\mathcal{S}}_{\text{out}})_{ij}$ for the mode basis. In the quadrature basis, we introduce $\mathcal{S}_{v_i w_j} \equiv (\mathcal{S}_{\text{out}})_{ij}$, with indices $(i', j') = (\lceil i/2 \rceil, \lceil j/2 \rceil)$, and $v, w \in \{x, p\}$, where $\lceil \cdot \rceil$ is the ceiling function. Note, that $v = x$ ($w = x$), if the index i (j) is odd, and $v = p$ ($w = p$), for an even index i (j), i.e. $(\mathcal{S}_{\text{out}})_{36} = \mathcal{S}_{x_2 p_3}$.

B. Analytical properties of the output-noise spectrum

In this Section, we stay in the quadrature picture. The output-noise spectrum can be intuitively understood by the concept of a *filter*, see Ref. [67]. A *filter* is an object, which takes the noise spectrum of an input $\mathcal{S}_{\text{in}}[\omega]$, and gives us the output-noise spectrum $\mathcal{S}_{\text{out}}[\omega]$. Thus, the output-noise is just the input-noise modified by some frequency-dependent function. Naturally, the filter is our system - where the latter is called the *transfer function*. In our case, this can be written in a more formal way

$$\mathcal{S}_{\text{out}}[\omega] = \mathcal{G}[\omega] \mathcal{S}_{\text{in}}, \quad (5.39)$$

where $\mathcal{G}[\omega]$ is the transfer function defined by the action (compare with Eq. (5.17))

$$\mathcal{G}[\omega] \mathcal{S}_{\text{in}} \equiv \frac{\mathbf{S}[\omega] \mathcal{S}_{\text{in}} \mathbf{S}^T[-\omega] + \mathbf{S}[-\omega] \mathcal{S}_{\text{in}} \mathbf{S}^T[\omega]}{2}. \quad (5.40)$$

Since this transfer is just composed of the S-matrix, we can look at the individual constituents of the noise spectral density to better understand its behaviour and get a correspondence between the noise spectrum and the S-matrix. For zero-temperature, only vacua are entering and the occupation-vector vanishes $\mathbf{n}_{\text{th}} = 0$. Thus, the input-noise of Eq. (5.13) becomes

$$\mathcal{S}_{\text{in}}(0) = \bigoplus_{j=1}^N \left(0 + \frac{1}{2} \right) \mathbb{1}_2 = \frac{1}{2} \mathbb{1}_{2N}, \quad (5.41)$$

where the vacuum-input is denoted as $\mathcal{S}_0 \equiv \mathcal{S}_{\text{in}}(0)$. This input leads to a frequency-independent, and diagonal output-noise matrix:

$$\mathcal{S}_{\text{vac}} = \frac{1}{2} \Re \left(\mathbb{1}_{2N} \underbrace{\mathbf{S}[\omega] \mathbf{S}^\dagger[\omega]}_{\mathbb{1}_{2N}} \right) = \mathcal{S}_0, \quad (5.42)$$

which we will call the vacuum-output \mathcal{S}_{vac} . Thus, for a passive device without parametric interactions (which could squeeze the vacuum), the system does not filter incident modes and becomes unresponsive, where output-noise is equal to input-noise for all frequencies. However, this situation changes for some finite temperature of the reservoir, where small thermal fluctuations are entering (at least) one of the three ports. Since \mathcal{S}_{in} is diagonal, it follows

$$(\mathcal{S}_{\text{in}})_{kk} = \left(\left[\bar{n}_{\lceil k/2 \rceil} + \frac{1}{2} \right] \mathbb{1}_{2N} \right)_{kk}, \quad (5.43)$$

where $\lceil \cdot \rceil$ is the ceiling function - ensuring we end up with correct indices for thermal occupations. By using Eq. (5.19), the output-noise (in terms of its entries $1 \leq i, j, k, l \leq 2N$) simply becomes

$$(\mathcal{S}_{\text{out}}[\omega])_{ij} = \sum_{k,l=1}^{2N} \Re \left\{ (\mathbf{S}[\omega])_{ik} (\mathcal{S}_{\text{in}})_{kl} (\mathbf{S}[\omega])_{lj}^\dagger \right\} = \sum_k \left(\bar{n}_{\lceil k/2 \rceil} + \frac{1}{2} \right) (\mathbf{1}_{2N})_{kk} \Re \left\{ (\mathbf{S}[\omega])_{ik} (\mathbf{S}^\dagger[\omega])_{kj} \right\}. \quad (5.44)$$

This gives us a full analytical expression for the output-noise

$$(\mathcal{S}_{\text{out}}[\omega])_{ij} = \sum_k \left(\bar{n}_{\lceil k/2 \rceil} + \frac{1}{2} \right) \Re \left\{ (\mathbf{S}[\omega])_{ik} (\mathbf{S}^\dagger[\omega])_{kj} \right\}. \quad (5.45)$$

This expression shows how the output-noise is nothing more than the frequency-response of the system, which is scaled by the input-contribution entering the ports. Thus, the system redistributes and modulates input-noise via scattering probabilities, thus, the frequency bandwidth for the output-noise is directly dependent on how responsive the system acts to frequencies of inputs. Note, that Eq. (5.45) in the mode basis becomes

$$(\tilde{\mathcal{S}}_{\text{out}}[\omega])_{ij} = \frac{1}{2} \sum_k \left(\bar{n}_{k \pmod{N}} + \frac{1}{2} \right) \left((\tilde{\mathbf{S}}[\omega])_{ik} (\tilde{\mathbf{S}}^\dagger[\omega])_{kj} + (\tilde{\mathbf{S}}[-\omega])_{ik} (\tilde{\mathbf{S}}^\dagger[-\omega])_{kj} \right). \quad (5.46)$$

For convenience, we can decompose Eq. (5.45) into two parts

$$\mathcal{S}_{\text{out}}[\omega] = \mathcal{S}_{\text{vac}} + \mathcal{S}_{\text{th}}[\omega], \quad (5.47)$$

where

$$(\mathcal{S}_{\text{vac}})_{ij} = \frac{1}{2} \delta_{ij}, \quad (5.48)$$

is only the contribution of vacua - acting as a *noise floor*, and

$$(\mathcal{S}_{\text{th}}[\omega])_{ij} = \sum_k \bar{n}_{\lceil k/2 \rceil} \Re \left\{ (\mathbf{S}[\omega])_{ik} (\mathbf{S}^\dagger[\omega])_{kj} \right\} \quad (5.49)$$

is the contribution of thermal noise. Since the S-matrix is unitary for the full model and thus preserves probability currents, see Eq. (4.20), the trace of the noise-input

$$\text{Tr}\{\mathcal{S}_{\text{in}}\} = 2(\bar{n}_1 + \dots + \bar{n}_N) + N, \quad (5.50)$$

has to be equal to the trace of the output-noise. Thus, Eq. (5.45) implies

$$\text{Tr}\{\mathcal{S}_{\text{out}}\} = \sum_i (\mathcal{S}_{\text{out}})_{ii} = \sum_{i,k} \left(\bar{n}_{\lceil k/2 \rceil} + \frac{1}{2} \right) |\mathbf{S}_{ik}|^2 = \sum_k \left(\bar{n}_{\lceil k/2 \rceil} + \frac{1}{2} \right) \underbrace{\left(|\mathbf{S}_{kk}|^2 + \sum_{j \neq k} |\mathbf{S}_{jk}|^2 \right)}_{=(\mathbf{1}_{2N})_{kk}, \text{ see Eq. (4.20)}} = \text{Tr}\{\mathcal{S}_{\text{in}}\}. \quad (5.51)$$

Naturally, this is not true for the effective model, since the S-matrix does not conserve probability currents.

Similarly to Eq. (5.42), if all reservoir-temperatures are the same, i.e. $\bar{n}_j = \bar{n}$, where $\bar{n} > 0$ for all j . Then, the thermal contribution of the noise, and incidentally also the output-noise itself becomes frequency-independent and proportional to \mathcal{S}_0

$$\mathcal{S}_{\text{th}} = \bar{n} \Re(\mathbb{1}_{2N} \underbrace{\mathbf{S}[\omega] \mathbf{S}^\dagger[\omega]}_{\mathbb{1}_{2N}}) = 2\bar{n} \mathcal{S}_0 \implies \mathcal{S}_{\text{out}} = (2\bar{n} + 1) \mathcal{S}_0. \quad (5.52)$$

Thus, the system also becomes passive and unresponsive, where fluctuations entering is equal to fluctuations at the output. The state of the system is now independent of the fluctuations at I/O ports and no modulation or redistribution will occur. Thus, the system is highly dependent on the temperature bias of surrounding reservoirs.

Now, we are equipped to make the comparison between elements of the output-noise and scattering probabilities. Similar to previous Sections, the optical isolator will serve as a toy model, where we analyze its behaviour to incident noise. However, the effective model inherits artifacts from the elimination procedure, which will become apparent in the output-noise spectrum.

C. Noise spectral density of the optical isolator in the mode basis

As before, we assume $\lambda_{ij} = 0 \implies \nu = 0, \mu = -|\mu_2|$. By eliminating the auxiliary mode, we made an additional implicit assumption: Not only did we eliminate the auxiliary from the set of differential equations, we also assumed that any fluctuations of the third mode in the Langevin equation vanish, with $a_{3,\text{in}}[\omega] = 0 \implies \langle\langle a_{3,\text{in}}[\omega] a_{3,\text{in}}^\dagger[\omega'] \rangle\rangle = 0$. A full treatment, which ensures that the reduced model properly sees the fluctuations of the third mode, is only achieved when considering the three-mode dissipative ring, see Section VIA. Thus, we need to keep in mind that contributions of the noise from the auxiliary will be missing.

Consider Fig. 13 (a), showing the Markovian (solid) and non-Markovian (dashed) output-noise elements for $\Phi = \phi_R$ ($\Phi = \phi_L$) in the symmetric regime $\kappa = \kappa_i/2$. We assume thermal excitations entering only at port 1 (from the left side) with $\bar{n}_1 = 10$. First, we focus on the Markovian limit for the unidirectional phase $\Phi = \phi_R$. As clearly visible by scattering coefficients, see Fig. 12 (a), only the transmission $|\mathbf{S}_{a_2 a_1}[0]|^2 = 1$ does not vanish at resonance. This should be resembled in the output-noise: We observe, that all thermal fluctuations end up at output 2 with $\mathcal{S}_{a_2^\dagger a_2}[0] = 10.5$ (green line), and no fluctuations are seen at output 1 (no reflections) with $\mathcal{S}_{a_1^\dagger a_1}[0] = 0$ (red). So, the system indeed shows maximized transmittance for the unidirectional limit, where not even vacuum fluctuations can be found at port 1. Whenever this happens, we can say that the noise is fully *transferred* to a different port. The only reason $\mathcal{S}_{a_1^\dagger a_1}[0]$ ends up below the noise floor (grey dashed line) with $\mathcal{S}_{\text{vac}} = 0.5$, is because the disregard of $a_{3,\text{in}} = 0$. For the full model, this element is exactly $\mathcal{S}_{a_1^\dagger a_1}[0] = \mathcal{S}_{\text{vac}}$. The output-noise for the non-Markovian (dashed) regime is similar, yet has a narrower frequency-bandwidth, implying that fluctuations are filtered more strongly. Additionally, there is a build-up of anti-correlations $\Re \mathcal{S}_{a_1^\dagger a_2} = \Re \mathcal{S}_{a_2^\dagger a_1} < 0$ (purple) for finite ω/κ . These anti-correlations become maximal at exactly the point where curves of the diagonal elements $\mathcal{S}_{a_1^\dagger a_1}$ and $\mathcal{S}_{a_2^\dagger a_2}$ meet, at $\omega/\kappa = \pm\sqrt{2}$ for the non-Markovian regime, corresponding to eigenvalues, compare Sec. III G. This was verified numerically. After this inflection point, anti-correlations start to disappear and fluctuations of different modes become uncorrelated again. The accumulation of (anti-) correlations might be attributed to the growing superposition of states at both outputs for finite frequencies, making it unclear at which output the information is to be expected. Anti-correlations are thus interpreted as a lack of knowledge. The magnitude of these correlations is exactly the difference of the input, minus the outputs we see at each port

$$|\mathcal{S}_{a_1^\dagger a_2}| = |\mathcal{S}_{a_2^\dagger a_1}| = \left| \bar{n}_1 + 1/2 - (\mathcal{S}_{a_1^\dagger a_1} + \mathcal{S}_{a_2^\dagger a_2}) \right|. \quad (5.53)$$

The imaginary part of anti-correlations will be discussed for the three-mode model in Sec. VIA 3, but is shown for the optical isolator in Fig. 31 (b) inside App. D 4. In comparison, this situation significantly changes for $\Phi = \phi_L$: Since we still consider the same input, we would expect no information leaving the second port. If we focus on port 1, the noise reaches its minimum at zero-frequency and coincides with the noise-floor. This happens, since output 1

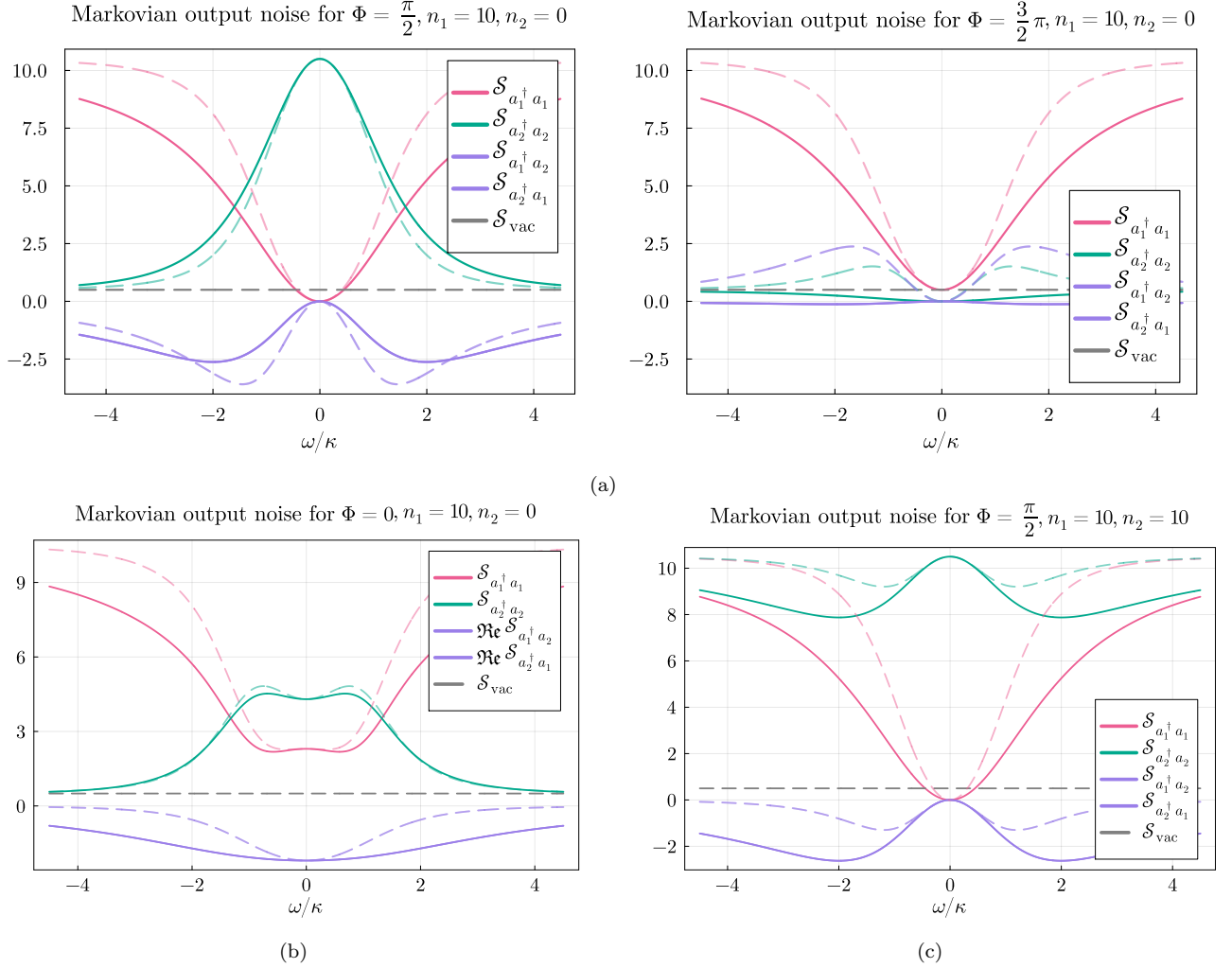


FIG. 13. Markovian (solid) and non-Markovian (dashed) elements of the output-noise matrix for the optical isolator with varying values of Φ and thermal-inputs, plotted against ω/κ . Parameters are $\mathcal{C} = 1$ with $\kappa = \kappa_i/2$, and $|J| = |\mu_2|\Gamma_0/2$. (a) Comparison between ϕ_R (Left) and ϕ_L (Right) for the input-occupations $\bar{n}_1 = 10, \bar{n}_2 = 0$. (Left) Here, fluctuations entering port 1 are fully transferred to output 2 with $\mathcal{S}_{a_2^\dagger a_2}[0] = 10.5$, and $\mathcal{S}_{a_1^\dagger a_1}[0] = 0$. Output 1 drops below the noise floor (grey dashed line), since inputs of the auxiliary mode are missing for the effective model. Anti-correlations (purple) build up and are maximal, where fluctuations of outputs 1 and 2 reach the same value. Non-Markovianity narrows the bandwidth of thermal-fluctuations. (Right) Here, $\mathcal{S}_{a_1^\dagger a_1}[0] = 0.5$, and $\mathcal{S}_{a_2^\dagger a_2}[0] = 0$, since output 1 sees vacuum from port 2, but output 2 gets no input from the auxiliary. Fluctuations entering port 1 just disappear, as the phase is unidirectional in the opposite direction. Positive correlations appear where some fluctuations reach output 2 for finite frequencies. (b) Reciprocal case for $\Phi = 0$ and $\bar{n}_1 = 10, \bar{n}_2 = 0$. Here, since there is only input at port 1, the outputs 1 and 2 do not have the exact same value, but balance out for low frequencies. However, more noise is found at output 2 for $\omega = 0$. Both outputs are always above the noise floor. Real parts of anti-correlations (purple) become maximal for $\omega = 0$. (c) Similar to (a, Left), but with inputs at both ports $\bar{n}_1 = \bar{n}_2 = 10$. The only difference is, that noise at output 2 does not vanish for finite frequencies, as there always is input at port 2 present. Imaginary parts of anti-correlations can be found in App. D 4.

sees the vacuum entering port 2. However, port 2 coincides with the noise-floor for finite frequencies, yet vanishes for $\omega = 0$, indicating that the reasoning above is sound: There is no (vacuum) contribution from the third mode which could end up in output 2. Cross-correlations only show a small peak for zero frequency for the Markovian limit. Non-Markovianity narrows the bandwidth for output 1, but also introduces correlations between output mode 1 and 2. This introduces two symmetric peaks for the output port 2 for finite frequencies, where the output at 2 and the correlations again vanish for zero frequency. However, these correlations are positive this time, also indicating a superposition, but not of the type *its either at port 1, or port 2* (as for ϕ_R), but of the type *its either at port 1*

and 2, or neither. This makes sense, since for finite frequencies, some fluctuations will reach output 2, while most fluctuations are still at output 1.

For the reciprocal case, see Fig. 13 (b), as expected from the S-matrix, the system equally responds to both directions of transport. Nevertheless, the noise output is not equal, since we do not have equal input. To understand this, we start at finite frequencies and work our way to zero-frequency: From the left, fluctuations from port 1 (red line) enter the system. As the noise at output 1 decreases, output 2 has increasing thermal fluctuations. However, closer to $\omega = 0$, fluctuations still want to enter the system but start to saturate at some point. Here, output 1 starts to reach a stable value, which no longer changes much. This is similar for output 2, as some fluctuations reach the output, but at some point the number of fluctuations does not increase anymore. This can be understood as some kind of “filling” effect: Since the system is in the reciprocal limit, both directions of transport have the same hierarchy and neither is specially protected. Thus, fluctuations at output 2 can not grow indefinitely, as they can enter the system again and just leave via output 1. So in a way, the system reaches something similar to a *detailed balance* of noise for $\omega = 0$. This also makes sense when looking at both peaks of the output-currents centered around $\omega = 0$: The system responds a little bit to the change in frequency, but is still stabilized. Only a big change in frequency can change the response again. At exactly $\omega = 0$, anti-correlations become maximal and are shared between both ports, where output 2 also shows vacuum contributions. Anti-correlations thus have magnitude

$$|\mathcal{S}_{a_1^\dagger a_2}| = |\mathcal{S}_{a_2^\dagger a_1}| = \frac{1}{2} \left| \bar{n}_1 + 1 - (\mathcal{S}_{a_1^\dagger a_1} + \mathcal{S}_{a_2^\dagger a_2}) \right|. \quad (5.54)$$

In the last panel, see Fig. 13 (c), shows unidirectional transport for $\Phi = \phi_R$, where both ports have inputs with $\bar{n}_1 = \bar{n}_2 = 10$. Surprisingly, the curve for output 2 has exactly the same shape as the curve showing cross-correlations. Here, similar to the first Figure, fluctuations at output 1 (red) vanish (with no vacuum contributions) for $\omega = 0$, and fluctuations become maximal at output 2 (green). Different to above, the green line does not vanish for finite ω , as there always will be an input present at port 2. This is reasonably not true for port 1, as fluctuations can enter the system at port 1, while there is no way for fluctuations entering port 2 to reach port 1. Thus, since no transmissions from input 2 to 1 can occur, the red curve has exactly the same shape as before (a). The same reasoning also applies to cross-correlations (purple). Similar to the S-matrix, choosing the asymmetric damping regime leads to sharper peaks and a closer correspondence between Markovian and non-Markovian behaviour, which can be found in App. D 6. Also notice, that these curves are always symmetric around $\omega = 0$, which is completely different to the behaviour we have seen for scattering probabilities. The output-noise in the quadrature basis looks exactly the same and can thus only be found in Appendix D 5.

VI. Analysis of thermal noise and transport for selected models

A. Dissipative three-mode ring

For the dissipative three-mode ring, see Fig. 5 (a), we consider the dynamical matrix \mathbf{D} in the mode representation without any squeezing ($\lambda_{ij} = 0 \implies \mathbf{h}_2 = 0$). Since it becomes block-diagonal, see Eq. (3.46), we only consider a single block, denoted by \mathbf{D}_3 . As mentioned in Sec. III G 1, when all damping rates and interactions are the same ($\Phi = \phi/3$ is equally shared over all interactions), the system becomes translationally invariant. In the unidirectional and non-Markovian regime, we could refer to this system as an *optical circulator*, see Ref. [68]. However, a true circulator has indistinguishable labels, where fluctuations are just permuted over ports. Thus, calling our model a circulator is a bit misleading, as modes can mutually differ in some limits. Thus, we refer to this model as the *dissipative ring*. Like before, we consider two impedance-matching conditions: 1. *Symmetric damping rates* with $\kappa \equiv \kappa_i/2$, and 2. *Asymmetric damping rates* with $\kappa \equiv \kappa_{1,2} = \kappa_3/4$. Recall, that the non-Markovian reservoir closer resembles the Markovian limit for the second condition. Similar to the optical isolator, Φ is the only relevant phase in this system. The system will become nonreciprocal by employing the same conditions on interactions as before.

1. S-matrix of the dissipative ring in the mode basis

Here, the goal is to obtain an analytical expression of the S-matrix in the mode basis. Also, we assume equal damping rates $\kappa \equiv \kappa_i/2$. All parameters are expressed in units of κ and read $|J_{3i}|/\kappa = 1$, implying $\mu = -|\mu_2| = -1$ and $|J_{12}|/\kappa = |\mu_2| = 1$. The dynamical matrix (in units of κ) is given by

$$\mathbf{D}_3 = - \begin{pmatrix} 1 & ie^{i\phi} & i \\ ie^{-i\phi} & 1 & i \\ i & i & 1 \end{pmatrix}, \quad (6.1)$$

and the phase-dependent S-matrix at resonance reads

$$\tilde{\mathbf{S}}_3[0] = \frac{1}{2i + \cos \Phi} \begin{pmatrix} \cos \Phi & i - e^{i\Phi} & i \cos \Phi - (1 + \sin \Phi) \\ i - e^{-i\Phi} & \cos \Phi & i \cos \Phi - (1 - \sin \Phi) \\ i \cos \Phi - (1 + \sin \Phi) & i \cos \Phi - (1 - \sin \Phi) & \cos \Phi \end{pmatrix}. \quad (6.2)$$

This expression already tells us a lot about scattering: For non-trivial phases, reflection coefficients always vanish, and transmission probabilities become maximal in only one direction for each pair of modes. Thus, the system becomes unidirectional with circular transport, i.e. for $\Phi = \phi_R = \pi/2$, the only non-zero transmissions are

$$|\tilde{\mathbf{S}}_{a_2 a_1}|^2 = |\tilde{\mathbf{S}}_{a_3 a_2}|^2 = |\tilde{\mathbf{S}}_{a_1 a_3}|^2 = 1, \quad (6.3)$$

meaning that we recover reflection-less circular transmission from $a_1 \rightarrow a_2 \rightarrow a_3 \rightarrow a_1$. As expected, for $\Phi \rightarrow \phi_L = -\pi/2$, we observe opposite transport

$$|\tilde{\mathbf{S}}_{a_3 a_1}|^2 = |\tilde{\mathbf{S}}_{a_2 a_3}|^2 = |\tilde{\mathbf{S}}_{a_1 a_2}|^2 = 1, \quad (6.4)$$

from $a_1 \leftarrow a_2 \leftarrow a_3 \leftarrow a_1$. This changes for the reciprocal limit, i.e. $\Phi = 0$, where we get

$$\forall i, j: \quad |\tilde{\mathbf{S}}_{a_i a_i}|^2 = \frac{1}{5}, \quad \text{and} \quad |\tilde{\mathbf{S}}_{a_i a_j}|^2 = \frac{2}{5}. \quad (6.5)$$

From this we can draw a few conclusions about the S-matrix: As noted before, a complete system conserves probability currents, see Eq. (4.20). For the dissipative ring, this law holds for all limiting cases: In the unidirectional limit, each column has exactly one element with a probability of 1, where all other elements vanish, thus summing up each column gives us exactly 1 each time, so the probability is conserved. In the reciprocal limit, this is also true for all columns. Also, the S-matrix of the reciprocal limit is symmetric $\tilde{\mathbf{S}}[\omega] = \tilde{\mathbf{S}}^T[\omega]$, a clear indication for dynamics preserving time-reversal symmetry, which is not the case in the nonreciprocal limit, see Sec. IV B. As already explained, probability conservation needs to hold for a complete picture, but can be broken for an effective model. We observed this for the optical isolator, where the S-matrix can resemble the one of an ideal isolator.

The S-matrix probabilities for different limits are shown in Fig. 14 for $\kappa \equiv \kappa_i/2$ and $\omega = 0$. Note, that we show modes and their adjoints. Even though this seems redundant, there is a reason to stress the full picture: Similar to the reciprocal limit of the optical isolator (see Fig. 12 (d)), S-matrix probabilities for the dissipative circulator also have an asymmetric line-shape, where modes and their adjoints are treated differently for finite frequencies. Consider the left panel, see Fig. 14 (a), which corresponds to clockwise transport with $\Phi = \phi_R$. We see how transmissions resemble a permutation matrix, transferring fluctuations in a circular manner between resonators. Note, that the 2×2 sub-block for modes 1 and 2 fully recaptures the behaviour of the optical isolator with its non-unitary S-matrix. In Fig. 14 (b), we show the reciprocal phase $\Phi = 0$. Here, reflection coefficients are finite and have the same magnitude $|\tilde{\mathbf{S}}_{a_i a_i}|^2 = 1/5$. Transmission coefficients are also finite and share the same magnitude $|\tilde{\mathbf{S}}_{a_i a_j}|^2 = 2/5$. The right Fig. 14 (c), with $\Phi = \phi_L$, shows the opposite behaviour compared to the first, behaving like an anti-clockwise permutation matrix. Other cases can be found in Appendix E 1 a.

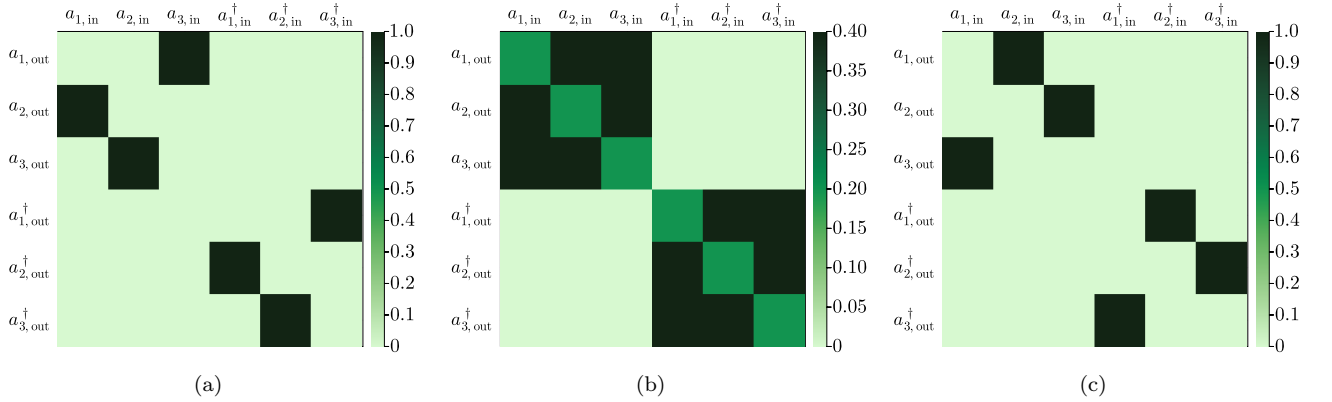


FIG. 14. S-matrix probabilities depending on the phase Φ , for the parameters $\omega = 0$ and $C = 1$ with rates $\kappa \equiv \kappa_i/2$. (a) Unidirectional limit for $\Phi = \phi_R$ (b) Reciprocal limit for $\Phi = \phi_0$ (c) Unidirectional for $\Phi = \phi_L$. For limits (a) and (c), reflection coefficients vanish and transport becomes unidirectional. In reciprocal limits, i.e. (b), reflection coefficients do not vanish and there is no preferred in transmission direction.

a. Unidirectional limit. To understand how scattering probabilities depend on frequency, consider Fig. 15. Here, Markovian (solid) and non-Markovian (dashed) scattering coefficients are shown in dependency of ω/κ , for $\Phi = \phi_R$ and symmetric damping rates $\kappa \equiv \kappa_i/2$. The first row, see Fig. 15 (a), shows the reflections. As expected, all reflections vanish on resonance in the unidirectional limit. In the non-Markovian regime, reflections all have the same curve with three distinct dips at $\omega/\kappa = 0, \pm\sqrt{2}$, as before, consider Sec. III G. For the Markovian regime, where the auxiliary becomes stationary, all curves are smoother, as the dips seem to meet at the origin. However, the reflection coefficient of the auxiliary starts to behave strikingly different compared to the others, where the curve becomes flatter, but vanishes over a wider bandwidth of ω . By moving away from resonance, reflections start to grow and become maximal $|\mathbf{S}_{a_i a_i}|^2 = 1$ far off-resonance, for all modes. Transmission coefficients are shown in the second and third row, see Fig. 15 (b). Here the lower row shows the opposite transport direction compared to the middle row. The transmission coefficients can be gathered into groups of three, where one group becomes maximal (purple, teal and green curve) and the other minimal (yellow, red, brown), on resonance. Thus, we observe unidirectional transport from $1 \rightarrow 2 \rightarrow 3 \rightarrow 1$, with vanishing transmissions for the opposite direction. In the non-Markovian regime and off-resonance, we again see distinct peaks at the same positions as before $\omega/\kappa = \pm\sqrt{2}$. Similar to reflections, curves of one group have the same line-shape in the non-Markovian limit. However, far off-resonance, all coefficients vanish. The transmission behaviour changes in the Markovian limit, as the third mode becomes stationary and all transmission coefficients from- or to the auxiliary become wider and dips start to overlap more. Thus, the first column (elements between mode 1 and 2, which fully describe the transmissions of the optical isolator) acts differently from the other coefficients in their respective group. The element $|\mathbf{S}_{a_1 a_2}|^2 = 0$ vanishes for all frequencies in the Markovian limit, where the remaining

elements of the same group are non-zero for finite frequencies. Far off-resonance, all transmissions vanish.

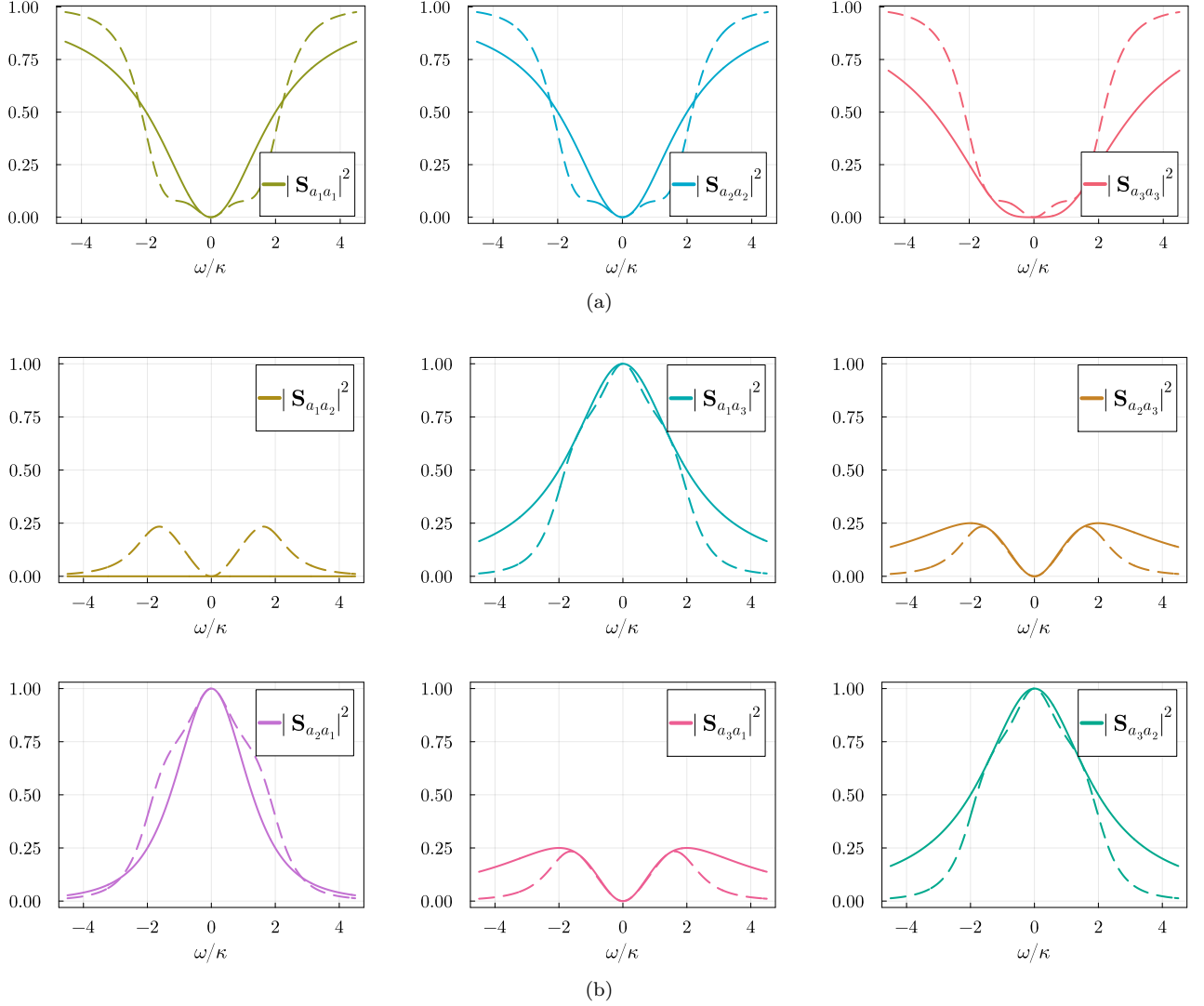


FIG. 15. Markovian (solid) and non-Markovian (dashed) scattering probabilities for $\Phi = \phi_R$ and symmetric damping rates $\kappa_i/2 = \kappa$, plotted against ω/κ . (a) Reflection coefficients. On resonance, all reflections vanish. Off-resonance, reflections for all modes increases and become maximal $|S_{a_i a_i}|^2 = 1$ far off-resonance. (b) Transmission coefficients, where the lower row shows the opposite transport direction compared to the first row. Transmissions can be gathered into groups of three, where one becomes maximal (purple, teal, green) and the other minimal (yellow, red, brown) on resonance. Thus, we observe unidirectional and clockwise transport from $1 \rightarrow 2 \rightarrow 3 \rightarrow 1$, where transmission in the opposite direction vanishes. On resonance, the Markovian and non-Markovian limits always have the same value. Far off-resonance, all transmissions vanish. In the non-Markovian case, transmissions of the same type show the same behaviour. However, in the Markovian case, the auxiliary becomes stationary and allows for some reciprocal transport at finite frequencies between itself and other modes, as these transmission coefficients start to increase for a wide range of ω/κ .

b. Reciprocal limit. We have yet merely glossed over the dips inside scattering coefficients, but before understanding how they arise, we take a look at scattering in the reciprocal limit. Figure 16 shows heatmaps of the non-Markovian scattering probabilities with $\Phi = 0$ and $\kappa \equiv \kappa_i/2$, for varying values of $\omega/\kappa = 0, \pm 2$. The heatmaps clearly show that scattering for modes and adjoints behaves exactly the same at resonance. For finite frequencies, modes and adjoints are treated the opposite way. In Fig. 16 (a) with $\omega/\kappa = -2$, modes are transmitted with a higher probability, where adjoints are more strongly reflected. The opposite behaviour happens in Fig. 16 (c) with $\omega/\kappa = 2$. Thus, scattering probabilities behave similar to the ones of the optical isolator: If Φ moves away from the unidirectional limit, scattering probabilities become asymmetric and start to either *tilt* or *move* (or both) in a preferred direction when sweeping across frequency. This effect is most profound if the phase reaches a trivial limit with $\Phi = 0, \pm\pi$. As an example, consider Fig. 17, with damping rates $\kappa \equiv \kappa_i/2$ and a phase $\Phi = 0$. The first row shows reflections,

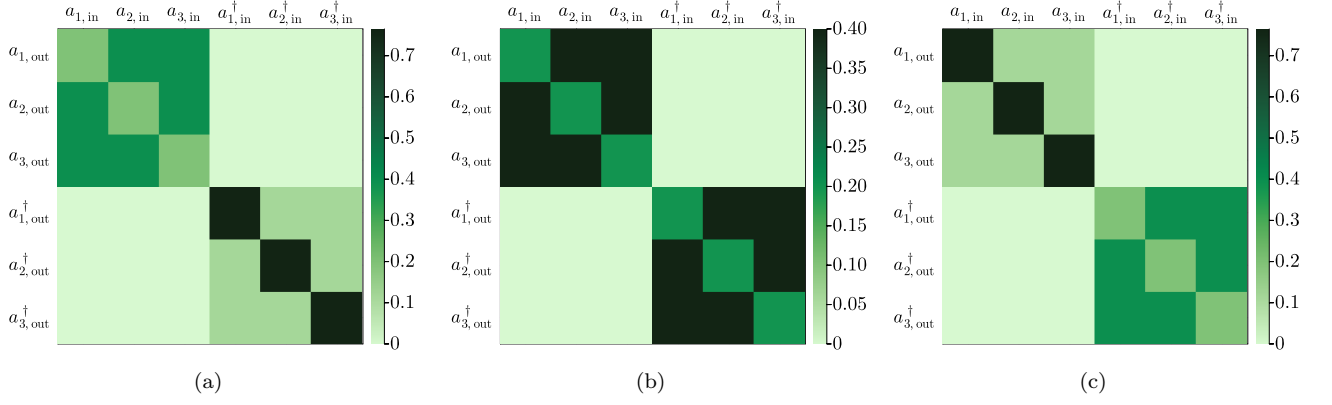


FIG. 16. Scattering probabilities for $\kappa \equiv \kappa_i/2$ in the reciprocal limit $\Phi = \phi_0$ for different values of ω (a) Off-resonant case for $\omega/\kappa = -2$ (b) Resonant case for $\omega/\kappa = 0$ (c) Off-resonant case for $\omega/\kappa = 2$. We see how modes and adjoints are treated the opposite way when moving away from the resonant case.

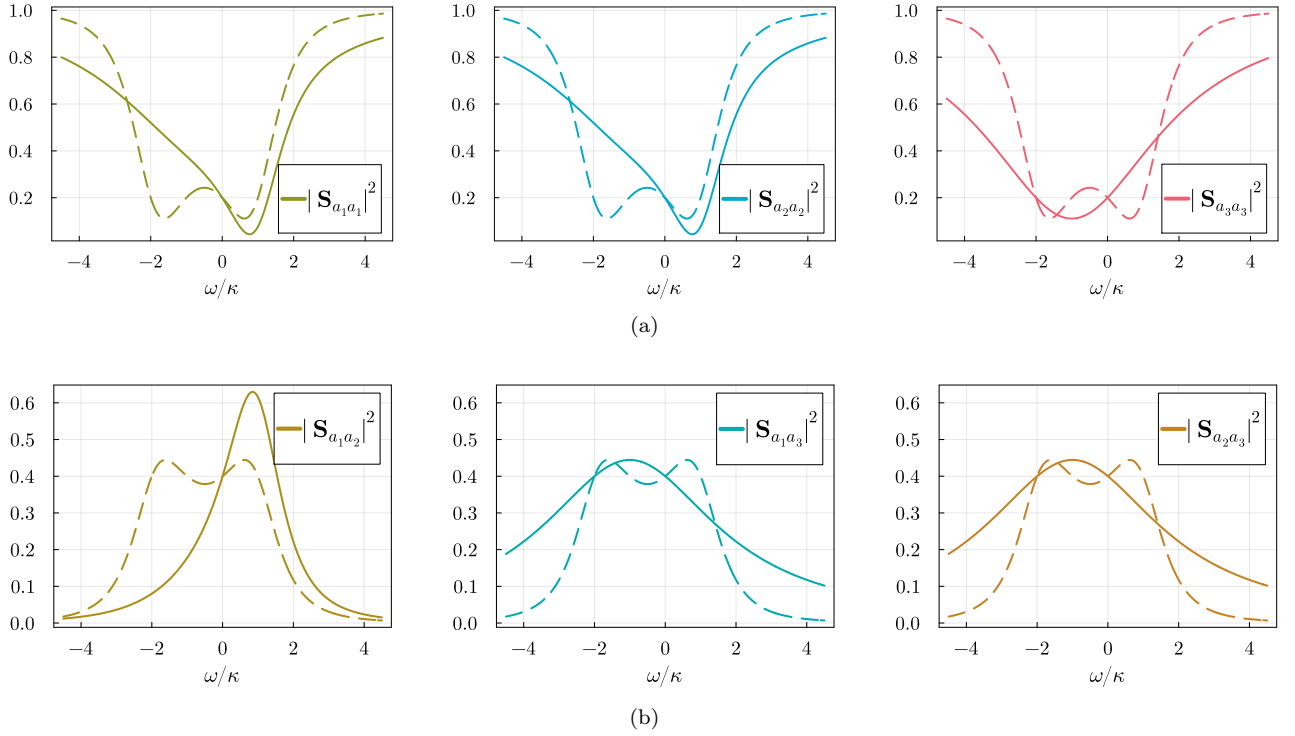


FIG. 17. Markovian (solid) and non-Markovian (dashed) scattering probabilities for $\Phi = 0$ and $\kappa \equiv \kappa_i/2$. Note, the same probabilities for adjoint modes are just flipped around the x -axis. (a) Reflections with a characteristic offset/tilt due to degenerate quasi-momenta eigenstates, see Sec. III G. (b) Transmissions with a characteristic offset/tilt coinciding with the peaks/dips of reflections.

where the remaining rows show transmissions. In Fig. 17 (a), we first focus on the non-Markovian regime (dashed). Reflection coefficients are the same in all cases, but have pronounced dips with a non-zero peak between them. However, this peak is not centered at $\omega = 0$, but slightly to the left for $\omega < 0$. Thus, the curves are not symmetric around the origin, which is a surprising feature at this point. The situation becomes more apparent for the Markovian regime (solid), where the curves for modes 1 and 2 become tilted, have a lower (however non-zero) minima at $\omega > 0$, and have a missing dip for negative frequencies. The auxiliary behaves (almost) opposite to that, with a flipped (but shallower) curve around the x -axis, with a minima for $\omega < 0$, and a missing dip for positive frequencies. All reflection coefficients maximize far off-resonance, as expected, but never vanish for any values of ω . At resonance, there is no difference between the non-Markovian and Markovian regime, just as suggested by the global damping rate

$\Gamma[0] = \Gamma_0$ of the optical isolator in the effective picture. Transmissions, see Fig. 17 (b), behave as expected: Transport is reversible for each pair of resonators, since all transmission probabilities between a given pair of resonators are completely alike. Also, each dip (peak) for reflections coincide perfectly with a peak (dip) for transmission, which is exactly what one would expect. In the non-Markovian limit (dashed), every transmission coefficients has exactly the same shape and all are centered to the left. This again changes for the Markovian regime (solid), where the curves for modes 1 and 2 are tilted and centered to the right, again coinciding with the reflection coefficients. Just as observed several times, the third mode behaves opposite to that, where all transmissions to or from the auxiliary have the same shape, are all centered to the left, and are in general more shallow compared to the aforementioned ones of modes 1 and 2. Note, that all these descriptions of the reciprocal case for $\Phi = 0$ are flipped at the y-axis for $\Phi = \pm\pi$.

c. Understanding the dips/peaks inside scattering probabilities. Since we have now talked about the general behaviour, we can understand the dips of the scattering probabilities. Understanding how and why they appear will give us a lot of insight into the scattering behaviour. For this, we restate the analytical expression of the S-matrix from Eq. (4.5), and the susceptibility matrix from Eq. (4.3), with

$$\tilde{\mathbf{S}}[\omega] = \mathbb{1} - \sqrt{\tilde{\mathbf{K}}}\tilde{\chi}[\omega]\sqrt{\tilde{\mathbf{K}}}, \quad \tilde{\chi}[\omega] = (i\omega\mathbb{1} - \mathbf{D})^{-1}.$$

The S-matrix mainly depends on the susceptibility, which itself only depends on the (inverse) sum of two things: The frequency $i\omega$, and the dynamical matrix \mathbf{D} . Thus, we can safely say that the dynamical matrix just modulates the frequency $i\omega$ (in analogy to simple response functions seen in physics). By diagonalizing the dynamical matrix, we can clearly see the modulating effect of the system: The imaginary part of the eigenvalues, which are multiplied by i , just offset $i\omega$ (in analogy to a detuning). Thus, they encode the frequency response of the system and in turn the positions of the peaks. The real parts however, are not multiplied by i and thus not oscillatory in nature. Therefore, since the susceptibility matrix is proportional to the inverse of \mathbf{D} , increasing the real part of the dynamical matrix will lead to a broadening of the susceptibility. This can be achieved by increasing damping rates κ_i . In Sec. III G 1,

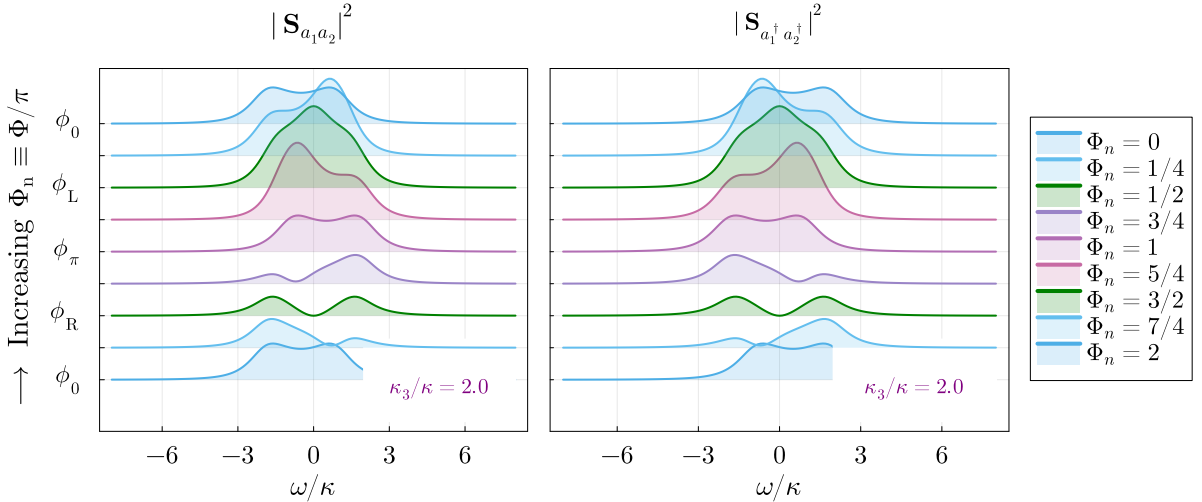


FIG. 18. Frequency (ω/κ) and phase ($\Phi_n \equiv \Phi/\pi$) dependence of transmission probabilities between a given pair of modes and their respective adjoints, for damping rates $\kappa \equiv \kappa_i/2$.

especially in Fig. 10, it was shown how the system can be diagonalized with quasi-momenta states. The energies of the diagonal dynamical matrix \mathbf{D}_k are symmetric around 0 only for the nonreciprocal limit with $\bar{\omega}_m = 0, \pm\sqrt{2|J|}$ (for $J = |J|e^{\Phi/3} \equiv J_{12} = J_{31} = J_{32}^*$), which is exactly the position of the peaks/dips in Fig. 15. By moving away from that, two out of three quasi-momenta states start to move closer till they become degenerate at the reciprocal limit, explaining the position of the peaks/dips in Fig. 17. The energies at that limit are not equidistant from 0, and there is now a bigger weight either for negative or positive ω/κ . This explains the asymmetric look of scattering probabilities in the reciprocal limit, see the heatmap in Fig. 16, where we see that depending on the sign of ω , modes and adjoints have the opposite scattering behaviour. All this can be seen as a consequence of the formula $\tilde{\mathbf{S}}^*[\omega] = \mathbf{\Lambda}_x \tilde{\mathbf{S}}[-\omega] \mathbf{\Lambda}_x$, where modes and adjoints have an opposite frequency dependence of the S-matrix in the mode representation. In Fig. 18 we see that more strikingly, where a single (non-Markovian) transmission probability between modes a_1 and a_2

is compared to the same probability between adjoints a_1^\dagger and a_2^\dagger , depending on the value of the phase Φ . The green curves show that the unidirectional limit symmetrizes the scattering. If we change the phase, curves start to tilt and become maximally asymmetric in the reciprocal limit. Note, that for all Φ we can relate the following in absence of squeezing

$$|\tilde{\mathbf{S}}_{a_i^\dagger a_i^\dagger}[\omega]|^2 = |\tilde{\mathbf{S}}_{a_i a_i}[-\omega]|^2. \quad (6.6)$$

2. S-matrix of the dissipative ring in the quadrature basis

As established several times already, the dynamical matrix in the quadrature basis is real $\mathbf{M} = \mathbf{M}^*$, and the S-matrix fulfills $\mathbf{S}^*[\omega] = \mathbf{S}[-\omega]$. Since quadrature operators are superpositions of modes and their adjoints, this has implications for scattering probabilities. Without squeezing, we can express probabilities in the quadrature basis by transforming $|\tilde{\mathbf{S}}_{a_i, a_j}|^2$ with \mathbf{T} . By using Eq. (6.6), it follows

$$|\mathbf{S}_{x_i x_j}[\omega]|^2 = |\mathbf{S}_{p_i p_j}[\omega]|^2 = \frac{1}{4} \left(|\tilde{\mathbf{S}}_{a_i a_j}[\omega]|^2 + |\tilde{\mathbf{S}}_{a_i a_j}[-\omega]|^2 + 2\Re\{\tilde{\mathbf{S}}_{a_i a_j}[\omega]\tilde{\mathbf{S}}_{a_i a_j}[-\omega]\} \right), \quad (6.7a)$$

$$|\mathbf{S}_{x_i p_i}[\omega]|^2 = |\mathbf{S}_{p_i x_i}[\omega]|^2 = \frac{1}{4} \left(|\tilde{\mathbf{S}}_{a_i a_i}[\omega]|^2 + |\tilde{\mathbf{S}}_{a_i a_i}[-\omega]|^2 - 2\Re\{\tilde{\mathbf{S}}_{a_i a_i}[\omega]\tilde{\mathbf{S}}_{a_i a_i}[-\omega]\} \right), \quad (6.7b)$$

$$|\mathbf{S}_{x_i p_j}[\omega]|^2 = |\mathbf{S}_{p_i x_j}[\omega]|^2 = 0. \quad (6.7c)$$

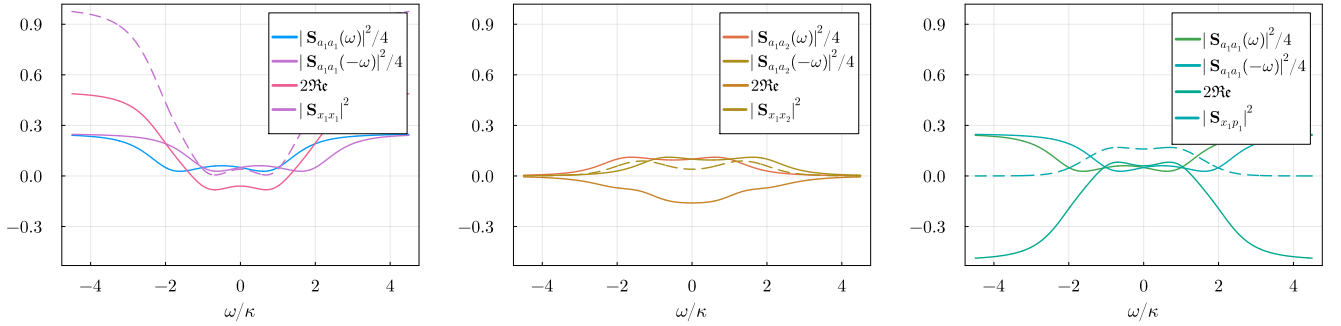


FIG. 19. Selection of non-Markovian scattering probabilities in the quadrature basis as a sum of S-matrix elements in the mode basis for $\Phi = 0$ and $\kappa \equiv \kappa_i/2$. Probabilities between other quadratures are either zero or the same and are thus not shown here. (Left) Reflection between the same type of quadratures $|\mathbf{S}_{x_1 x_1}[\omega]|^2 = |\mathbf{S}_{p_1 p_1}[\omega]|^2$. Here, the third label is $2\Re\{\tilde{\mathbf{S}}_{a_1 a_1}[\omega]\tilde{\mathbf{S}}_{a_1 a_1}[-\omega]\}$. (Middle) Transmission coefficients between the same type of quadratures $|\mathbf{S}_{x_1 x_2}[\omega]|^2 = |\mathbf{S}_{p_1 p_2}[\omega]|^2$. Here, the third label is $2\Re\{\tilde{\mathbf{S}}_{a_1 a_2}[\omega]\tilde{\mathbf{S}}_{a_1 a_2}[-\omega]\}$. (Right) Transmission coefficient between different quadratures of the same port 1 with $|\mathbf{S}_{x_1 p_1}[\omega]|^2 = |\mathbf{S}_{p_1 x_1}[\omega]|^2$. Note, that $\mathbf{S}_{p_i x_i}[\omega] = -\mathbf{S}_{x_i p_i}[\omega] \quad \forall i$. As these elements are non-vanishing, this indicates that there is a phase-shift in the quadrature space for a reciprocal system. Here, the third label is $-2\Re\{\tilde{\mathbf{S}}_{a_1 a_1}[\omega]\tilde{\mathbf{S}}_{a_1 a_1}[-\omega]\}$.

This implies that scattering probabilities in the quadrature picture are always symmetric in frequency, regardless of the phase Φ . For this, see Fig. 19, with parameters $\kappa \equiv \kappa_i/2$, in the reciprocal limit $\Phi = 0$. Here, we have shown examples of how summing up specific probabilities in the mode picture (solid lines) yield the always symmetric probabilities in the quadrature picture (dashed lines). We can write the matrix of scattering probabilities $(\mathbf{P}[\omega])_{ij} \equiv |(\mathbf{S}[\omega])_{ij}|^2$ as a block-matrix containing sub-matrices $\mathbf{P}_{ij}[\omega]$ of scattering coefficients. The resonant case is simply

$$\mathbf{P}[0] = \left(\begin{array}{c|c|c} 0 & 0 & \mathbf{P}_{13}[0] \\ \hline \mathbf{P}_{21}[0] & 0 & 0 \\ \hline 0 & \mathbf{P}_{32}[0] & 0 \end{array} \right), \quad \text{with} \quad \mathbf{P}_{ij}[\omega] \equiv \begin{pmatrix} |\mathbf{S}_{x_i, x_j}[\omega]|^2 & |\mathbf{S}_{x_i, p_j}[\omega]|^2 \\ \hline |\mathbf{S}_{p_i, x_j}[\omega]|^2 & |\mathbf{S}_{p_i, p_j}[\omega]|^2 \end{pmatrix}. \quad (6.8)$$

For the unidirectional limit $\Phi = \phi_R$, the blocks have the same position as elements in the mode basis. This ensures

unidirectional scattering with perfect transmission between blocks, but which quadratures inside the blocks retain this information can change depending on the value for the local phases α_{ij} . Consider, $\Phi = \alpha_{12} = \pi/2$, and $\alpha_{31} = \alpha_{32} = \pm\pi/2$, where blocks at resonance become diagonal $\mathbf{P}_{13} = \mathbf{P}_{21} = \mathbf{P}_{32} = \mathbb{1}_2$. This changes for $\Phi = \alpha_{12} = \pi/2$, and $\alpha_{31} = \alpha_{32} = 0, \pm\pi$, since quadratures get flipped with $\mathbf{P}_{21} = \mathbb{1}_2$, and $\mathbf{P}_{13} = \mathbf{P}_{32} = \sigma_x$. However, what happens if α_{3j} is between π and $\pi/2$? For $\alpha_{31} = \alpha_{32} = \pm\pi/4$, probabilities inside each respective block are evenly distributed, resulting in $\mathbf{P}_{21} = \mathbb{1}_2$, and $\mathbf{P}_{13} = \mathbf{P}_{32} = (\mathbb{1}_2 + \sigma_x)/2$. Thus, *which* α_{ij} we set to $\alpha_{ij} = \Phi$, decides which the block becomes diagonal, where $\mathbf{P}_{ij} = \mathbb{1}_2$, and remaining blocks $\mathbf{P}_{i'j'}$ depend on the specific value of $\alpha_{i'j'}$. Formally, this becomes

$$\mathbf{P}_{ij} = \cos^2(\alpha_{ij})\sigma_x + \sin^2(\alpha_{ij})\mathbb{1}_2. \quad (6.9)$$

Consider equally distributed phases $\Phi/3 = \alpha_{12} = \alpha_{31} = -\alpha_{32}$, with $J_{12} = J_{31} = J_{32}^*$. Then, all sub-matrices for any unidirectional limit $\Phi \in \{\phi_R, \phi_L\}$ has the same form $\mathbf{P}_{ij} = (3\sigma_x + \mathbb{1}_2)/4$.

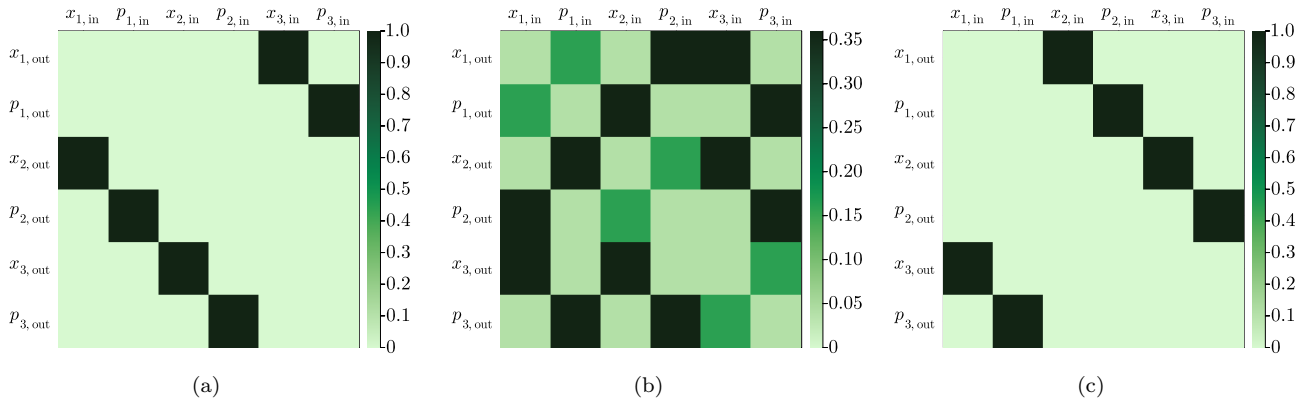


FIG. 20. Scattering probabilities for quadratures $|(\mathbf{S}[0])_{ij}|^2$, with $\kappa \equiv \kappa_i/2$, $\alpha_{31} = \alpha_{32} = \pi/2$ and varying phases Φ . (a) Unidirectional limit $\Phi = \phi_R$, showing nonreciprocal transport between quadrature blocks, where quadratures always drive the same quadrature of another mode. (b) Reciprocal limit $\Phi = 0$. Here, reflections always flip quadratures, with reciprocal transmission between different quadratures for $1 \leftrightarrow 2$, and same quadratures for $1 \leftrightarrow 3$, and $2 \leftrightarrow 3$. This flip for $1 \leftrightarrow 2$ is a consequence of setting $\alpha_{12} = \Phi = 0 \neq \alpha_{3i}$. (c) Unidirectional limit $\Phi = \phi_L$, having the same behaviour as (a) only in the opposite direction.

Now, we look at limiting cases of the transport. As shown in Fig. 20, heatplots for quadrature scattering coefficients are compared for unidirectional and reciprocal limits. The parameters are $\omega = 0$, $\kappa \equiv \kappa_i/2$, and $\alpha_{31} = \alpha_{32} = \pi/2$. The left Fig. 20 (a) shows the unidirectional limit $\Phi = \alpha_{12} = \phi_R$, with distinct nonreciprocal blocks, which enforce transport from $1 \rightarrow 2 \rightarrow 3 \rightarrow 1$ for the same quadrature. The middle plot, see Fig. 20 (b), shows the reciprocal limit with non-vanishing reflection coefficients. Here, the scattering probabilities are always symmetric in frequency. The last plot, see Fig. 20 (c), shows the opposite transport direction compared to (a). If we now focus on the frequency dependence of scattering probabilities, we find that the unidirectional limit behaves exactly the same in both bases, if considering the corresponding quadratures, see Appendix E 1 c. For the reciprocal limit, the situation changes and all elements are always symmetric in frequency, consider Fig. 21. In the non-Markovian regime (dashed curves), reflections are all the same, which also holds for transmissions. All probabilities are symmetric in frequency. As before, in the Markovian limit (solid curves), the auxiliary becomes static and probabilities broaden and become flatter. This coincides with a stronger transmission probability from 1 to 2, and vice versa.

To conclude this Section, we compare the scattering probabilities between the bases in the reciprocal limit with $\Phi = 0$ and $\kappa \equiv \kappa_{1,2}/2$. As Fig. 22 shows, increasing the auxiliary damping rate κ_3/κ , also increases the overlap of peaks inside transmission coefficients $|\tilde{\mathbf{S}}_{a_1 a_2}[\omega]|^2$ and $|\mathbf{S}_{x_1 x_2}[\omega]|^2$. The biggest effect happens for values below the impedance-matching condition $\kappa_3 < 2\kappa$. For the impedance-matched case $\kappa_3 = 2\kappa$ (green line), the coefficient $|\tilde{\mathbf{S}}_{a_1 a_2}[\omega]|^2$ is not centered at $\omega = 0$. This is different for quadratures, as peaks already start at symmetric positions and begin to overlap, yet remain equidistant from $\omega = 0$. Our result closely resembles Fig. 3 of Chen *et al.* [63], where the same *tilting* of scattering probabilities outside exceptional points was observed for a similar optomechanical setup.

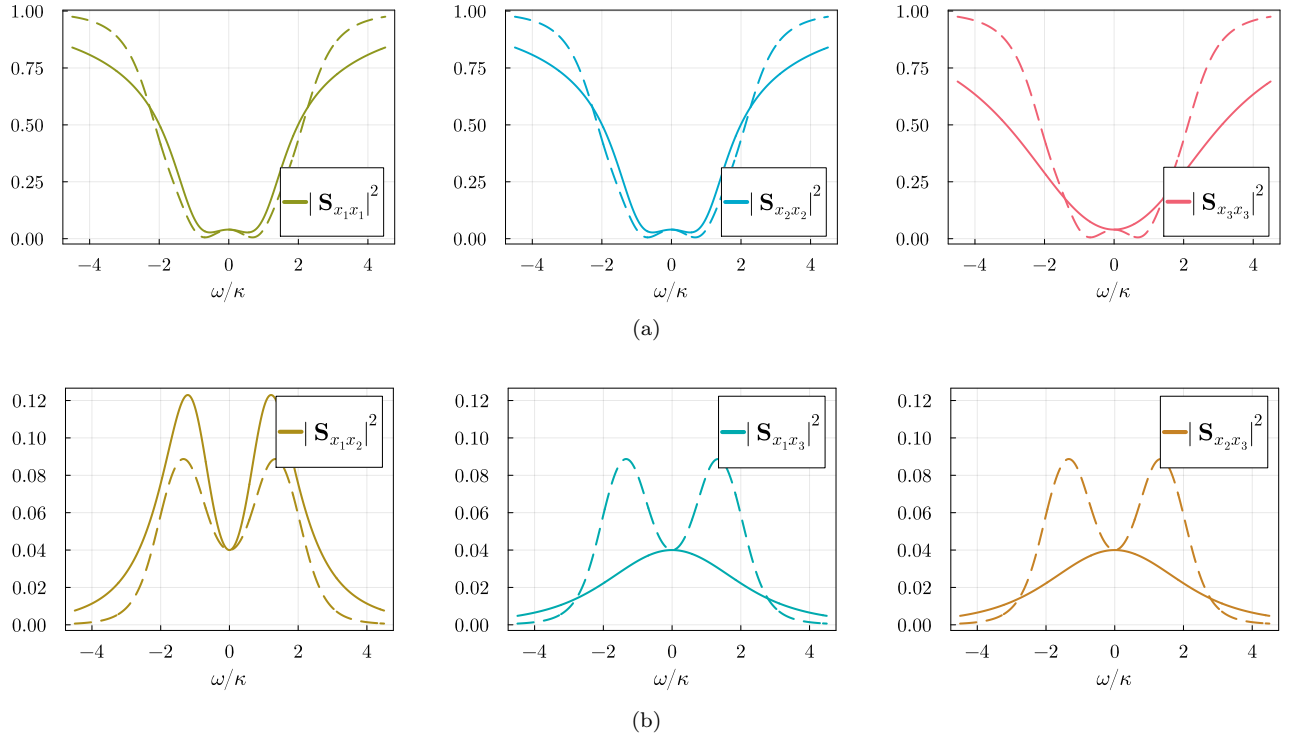


FIG. 21. Markovian (solid) and non-Markovian (dashed) scattering probabilities $|\mathbf{S}_{x_i x_j}|^2$ for quadratures with $\Phi = 0$ and $\kappa \equiv \kappa_i/2$. Note, that all coefficients are the same for x and p quadratures. Not shown coefficients are zero. (a) Reflection coefficients for x -quadratures, which are the same in the non-Markovian regime, but quadratures of the auxiliary behave differently for the Markovian limit, as already observed. (b) Transmissions for x -quadratures, which again are the same in the non-Markovian regime, and scattering with the auxiliary behaves differently for the Markovian limit.

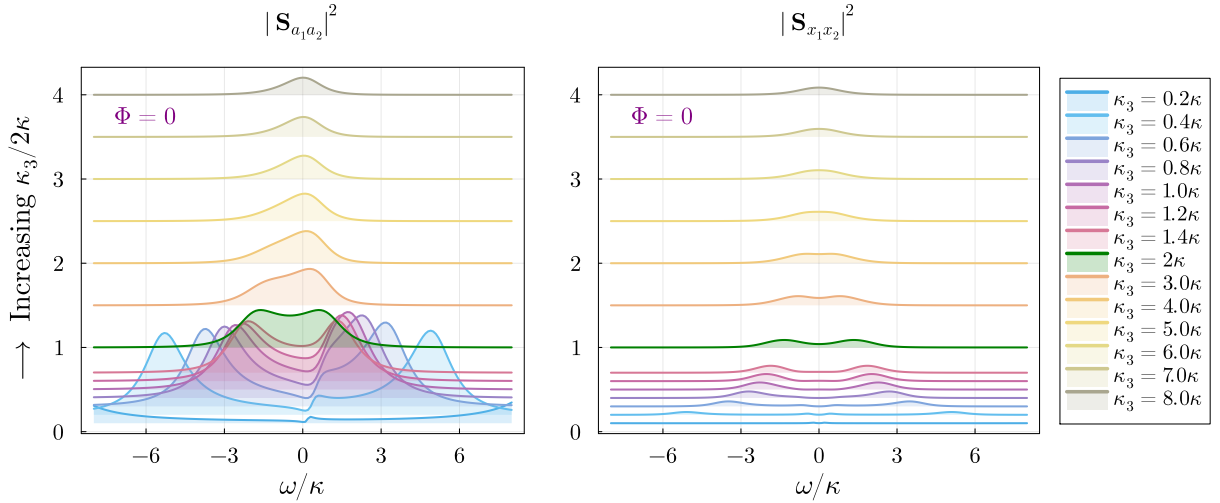


FIG. 22. Change of the non-Markovian transmission probability from $2 \rightarrow 1$ by increasing κ_3 , in the mode (left) and x -quadratures (right) for $\kappa \equiv \kappa_{1,2}/2$, plotted against ω/κ . By increasing κ_3 , curves overlap more and the relative distance of peaks from the origin starts to move to the origin in both bases. In the mode basis, they are not equidistant from $\omega = 0$ and are asymmetric for the impedance-matched case (green line) with $\kappa_3 = 2\kappa$, whereas transmissions remain symmetric for quadratures for all values of κ_3 . If the auxiliary becomes increasingly lossy, distinct peaks merge and move to a single maximum centered around $\omega = 0$, for both bases.

3. Output-noise spectrum of the dissipative ring

Before we bluntly jump into the output-noise spectrum of the dissipative ring, we make a small remark: Since the covariance matrix is composed of the input-noise and the S-matrix, we can take a deeper look into the composition of the output-noise matrix. Knowing how these elements come about will be useful for our understanding. For this, we stay in the quadrature representation as it offers a simple way of applying an approximation to the output-noise. Note, that the following can be analogously done in the mode basis. For this, consider an extreme case for the input, where incident thermal noise at port 1 is assumed to be much larger than vacuum fluctuations entering the system, with no thermal noise entering remaining ports. Also, we impedance-match by setting damping rates to $\kappa \equiv \kappa_i/2$ with a cooperativity of $\mathcal{C} = 1$. This regime can be formally written as

$$\bar{n}_1 \gg \frac{1}{2} \gg \bar{n}_2 = \bar{n}_3 \approx 0. \quad (6.10)$$

Hence, we can outright dismiss the vacuum contribution to the input-noise

$$\mathcal{S}_{\text{in}} \approx \bar{n}_1 \mathbf{1}_2 \oplus 0 \cdot \mathbf{1}_4, \quad (6.11)$$

where the input vector $\mathbf{n}_{\text{th}} = (\bar{n}_1, \bar{n}_1, 0, \dots, 0)^T$, has non-zero entries only for x_1 and p_1 . By dismissing the vacua and using Eq. (5.45), it follows for the output-noise matrix

$$(\mathcal{S}_{\text{out}}[\omega])_{ij} \approx \bar{n}_1 \left(\Re \left\{ (\mathbf{S}[\omega])_{i1} (\mathbf{S}^\dagger[\omega])_{1j} \right\} + \Re \left\{ (\mathbf{S}[\omega])_{i2} (\mathbf{S}^\dagger[\omega])_{2j} \right\} \right), \quad (6.12)$$

where the diagonal elements (thermal noise at a given output-port) are just

$$(\mathcal{S}_{\text{out}}[\omega])_{ii} \approx \bar{n}_1 (|(\mathbf{S}[\omega])_{i1}|^2 + |(\mathbf{S}[\omega])_{i2}|^2), \quad (6.13)$$

By using this approximation, we can compare the output-noise of the first port $\mathcal{S}_{x_1 x_1}$ ($\mathcal{S}_{p_1 p_1}$) with scattering probabilities $|\mathbf{S}_{x_1, x_1}|^2$ ($|\mathbf{S}_{p_1, x_1}|^2$) and $|\mathbf{S}_{x_1, p_1}|^2$ ($|\mathbf{S}_{p_1, p_1}|^2$), and do the the same for the remaining ports $\mathcal{S}_{x_2 x_2}$ ($\mathcal{S}_{p_2 p_2}$) and $\mathcal{S}_{x_3 x_3}$ ($\mathcal{S}_{p_3 p_3}$). Since equation above implies, that quadratures of the same mode are equal $\mathcal{S}_{x_i x_i} = \mathcal{S}_{p_i p_i}$, it is sufficient to only consider the x -quadratures for the moment. More precisely, we get

$$\begin{aligned} (\mathcal{S}_{\text{out}}[\omega])_{11} &\equiv \mathcal{S}_{x_1 x_1}[\omega] = \bar{n}_1 (|\mathbf{S}_{x_1 x_1}[\omega]|^2 + |\mathbf{S}_{x_1 p_1}[\omega]|^2), \\ (\mathcal{S}_{\text{out}}[\omega])_{33} &\equiv \mathcal{S}_{x_2 x_2}[\omega] = \bar{n}_1 (|\mathbf{S}_{x_2 x_1}[\omega]|^2 + |\mathbf{S}_{x_2 p_1}[\omega]|^2), \\ (\mathcal{S}_{\text{out}}[\omega])_{55} &\equiv \mathcal{S}_{x_3 x_3}[\omega] = \bar{n}_1 (|\mathbf{S}_{x_3 x_1}[\omega]|^2 + |\mathbf{S}_{x_3 p_1}[\omega]|^2), \end{aligned} \quad (6.14)$$

which means that the output-noise for port i is just the sum of transmission probabilities of both quadratures coming from port 1, re-scaled by the thermal noise entering port 1. However, remember that we do not consider any single-mode squeezing, thus, terms like $|\mathbf{S}_{x_i p_i}|^2 = |\mathbf{S}_{p_i x_i}|^2 = 0 \quad \forall i$ always vanish, even though they contribute to the noise in general, see Eq. (5.45). In Fig. 23, this is shown for $\mathcal{S}_{x_2 x_2}$ in the unidirectional limit $\Phi = \phi_{\text{R}}$, where other diagonal elements can be found in Appendix E1d. As already explained for the optical isolator, the output-noise can never drop below the noise floor for a full description.

a. Understanding limits in the mode-basis. Since we have seen the composition of diagonal noise-elements for the unidirectional limit, we can try to understand these limiting cases better. For this, consider the output-noise matrix of Fig. 24 in the mode basis, with $\omega = 0$, $\kappa \equiv \kappa_i/2$, and a thermal-input $\bar{n}_1 = 10$, $\bar{n}_2 = \bar{n}_3 = 0$. The first heatmap, see Fig. 24 (a), shows the unidirectional limit $\Phi = \phi_{\text{R}}$. Here, all elements except the diagonal ones vanish. Input noise fully ends up at output 2 with $\mathcal{S}_{a_2 a_2^\dagger} = \mathcal{S}_{a_2^\dagger a_2} = 10.5$, where remaining diagonal elements only show the contribution of vacuum noise coming from other ports. However, the noise matrix becomes complex for any value of Φ outside

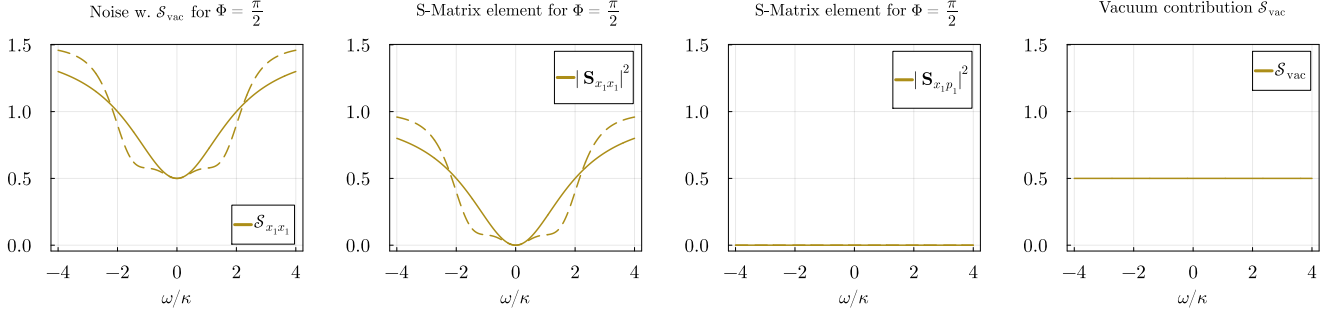


FIG. 23. Markovian (solid) and non-Markovian (dashed) output-noise $\mathcal{S}_{x_2x_2}$, for the unidirectional limit $\Phi = \phi_R$, damping rates $\kappa \equiv \kappa_i/2$, with little noise entering port 1: $n_1 = 1, n_2 = n_3 = 0$, plotted against frequency. In general, the output-noise does not only consist of (scaled) scattering probabilities but also on incident vacuum, where the latter is kept to show the effect of the noise floor on the output-noise. Also, even though the approximation above only applies to high thermal-inputs, the effect is most visible for low noise. Thus, n_1 is kept small compared to other parameters. (1st Fig.) Output-noise $\mathcal{S}_{x_2x_2}$ of port 2 with the vacuum contribution. (2nd Fig.) Transmission coefficient $|\mathcal{S}_{x_2x_1}|^2$, for $x_1 \rightarrow x_2$. (3rd Fig.) Transmission coefficient $|\mathcal{S}_{x_2p_1}|^2 = 0$ between different quadratures $p_1 \rightarrow x_2$. Note, that this element is zero, since we consider no single-mode squeezed input. (4th Fig.) Incident vacuum noise contribution \mathcal{S}_{vac} acting as a noise floor. Thus, output-noise should never drop below this lower bound.

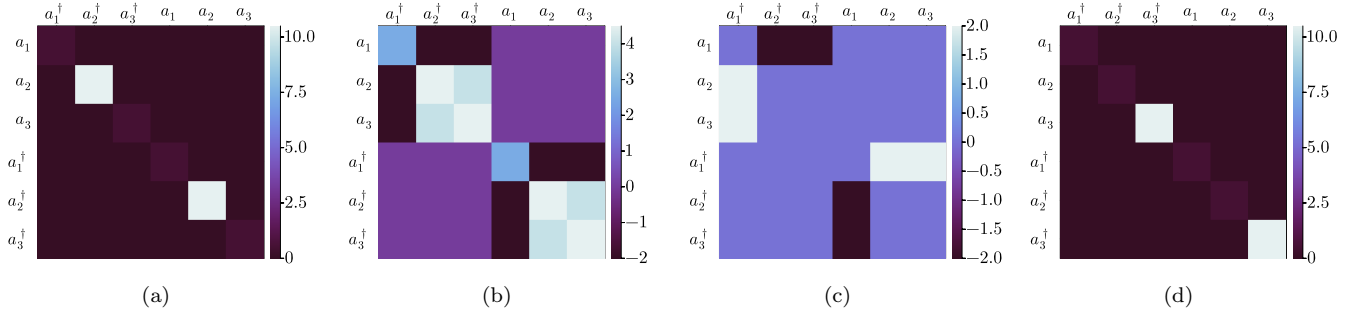


FIG. 24. Output-noise matrix in the mode basis for zero-frequency $\omega = 0$, damping rates $\kappa \equiv \kappa_i/2$, thermal-input $\bar{n}_1 = 10$, and $\bar{n}_2 = \bar{n}_3 = 0$, for different limiting cases of Φ . (a) Nonreciprocal limit $\Phi = \phi_R$. Where all elements except the diagonal ones vanish. The input signal fully ends up at $\mathcal{S}_{a_2a_2^\dagger} = 10.5$, where the remaining diagonal elements only show the contribution of the noise floor. (b) Real part of the noise matrix in the reciprocal limit $\Phi = 0$. Cross-correlations between the port receiving an input and possible output ports are anti-correlated. Remaining cross-correlations are positively correlated. The noise of output 1 shows back-reflections, and other outputs show equal noise. (c) Imaginary part of the noise matrix in the reciprocal limit $\Phi = 0$. Since elements of the noise-spectrum become complex for any values of Φ outside the nonreciprocal limit, we see that the imaginary part for cross-correlations of the noise between modes and adjoints has opposite sign, with $\Im \mathcal{S}_{a_i a_j^\dagger} = \Im \mathcal{S}_{a_j^\dagger a_i} = -\Im \mathcal{S}_{a_j a_i^\dagger} = -\Im \mathcal{S}_{a_i^\dagger a_j}$, see Fig. 26 for more details. (d) Nonreciprocal limit $\Phi = \phi_L$, with the opposite behaviour compared to (a), showing only output at $\mathcal{S}_{a_3 a_3^\dagger}$.

the unidirectional limit, thus, for $\Phi = 0$, we consider the real and imaginary part of the noise matrix. We start at the real part, see Fig. 24 (b). Here, cross-correlations between the port receiving an input (here port 1) and possible output-ports are anti-correlated. The reason why these elements become anti-correlated was already discussed in Sec. V C, compare Fig. 13. Remaining cross-correlations are positively correlated. The output-noise of port 1 shows back-reflections, and other output-ports show equal noise. The imaginary part in the reciprocal limit, is shown in Fig. 24 (c). Since elements of the output-noise spectrum become complex, we see phase shifts for cross-correlations of the noise, with $\Im \mathcal{S}_{a_i a_j^\dagger} = \Im \mathcal{S}_{a_j^\dagger a_i} = -\Im \mathcal{S}_{a_j a_i^\dagger} = -\Im \mathcal{S}_{a_i^\dagger a_j}$, where cross-correlations between a pair of modes behave the opposite way compared to cross-correlations of their respective adjoints. The last heatmap shows the nonreciprocal limit in the opposite direction with $\Phi = \phi_L$, showing only an output at $\mathcal{S}_{a_3 a_3^\dagger} = \mathcal{S}_{a_3^\dagger a_3} = 10.5$.

As before, the unidirectional limit is compared to the reciprocal limit for frequency-dependent elements of the noise matrix. Noise-correlations for quadratures can be directly related to noise-correlations for modes, see Appendix E 1 e. Thus, we consider the output-noise in both bases at the same time. First, recall that diagonal elements of the noise matrix can be seen as the *noise of the output particle flux*, implying that diagonal elements are always real and lower

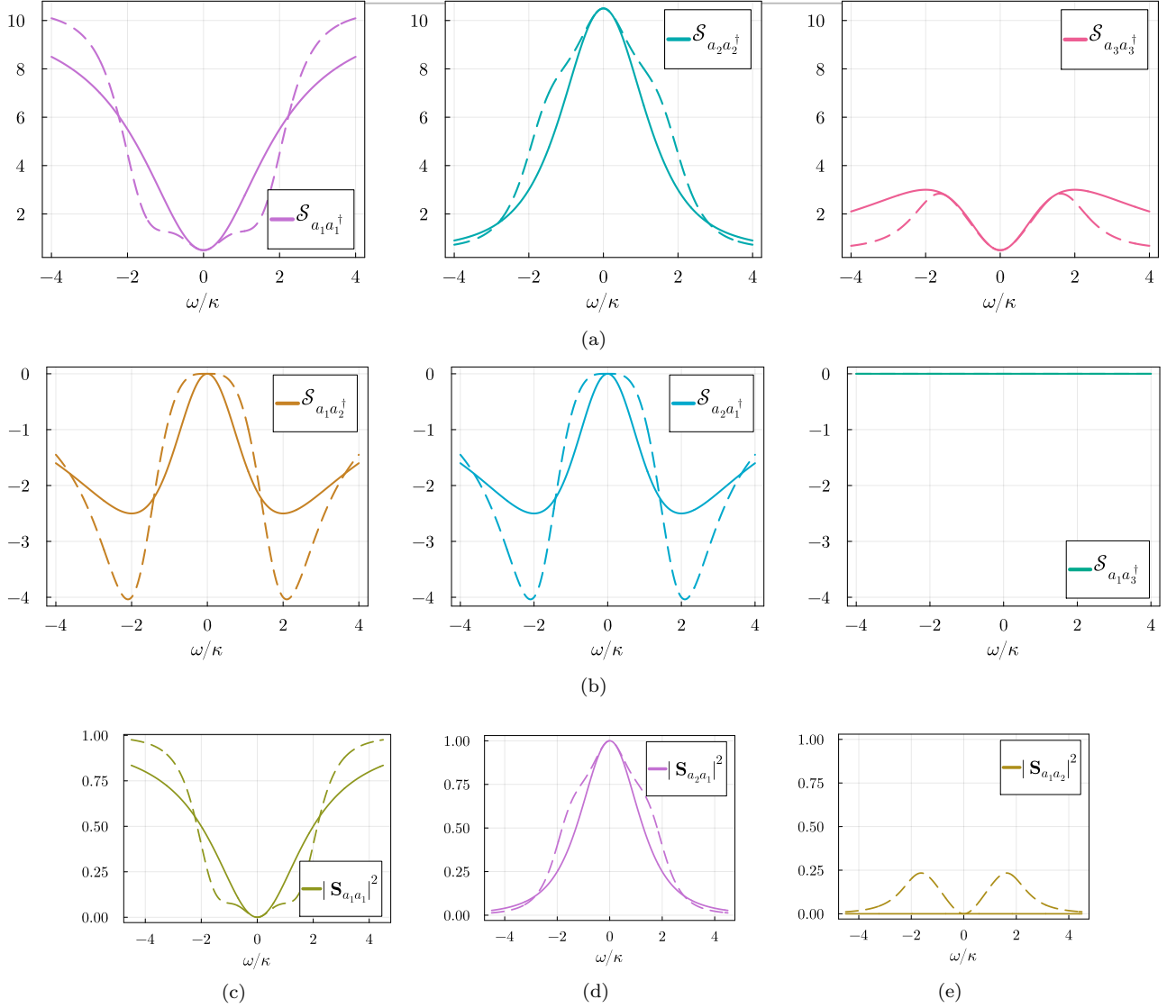


FIG. 25. Comparison of Markovian (solid) and non-Markovian (dashed) output-noise elements (first and second row) and scattering probabilities (last row) for $\Phi = \phi_R$, $\kappa \equiv \kappa_i/2$, and $\bar{n}_1 = 10$, $\bar{n}_2 = \bar{n}_3 = 0$. (a) Here, fluctuations at outputs are shown, where noise incident to 1 is fully transferred to output 2, with $\mathcal{S}_{a_2 a_2^\dagger}[0] = 10.5$. The remaining outputs only show vacuum fluctuations $\mathcal{S}_{a_1 a_1^\dagger}[0] = \mathcal{S}_{a_3 a_3^\dagger}[0] = 0.5$ from other ports. Non-Markovian elements show characteristic peaks/dips. Fluctuations at port 2 vanish for finite frequencies, where they remain at output 1. (b) Cross-correlations showing the same behaviour as the optical isolator (Sec. VC), where noise is anti-correlated, since noise is superposed and appears either at output 1 or 2. Correlations vanish for $\omega = 0$. (c), (d), and (e) Show scattering probabilities, compare with Fig. 15.

bounded by the noise floor. Additionally, since the noise matrix is symmetric in operator-ordering, the element (i, j) is always the same as the element (j, i) . However, changing labels $i \leftrightarrow j$, produces different effects depending on the basis, where elements are complex conjugated for modes, but undergo a sign change for quadratures. These general properties can be summed up as (for all i, j)

$$\mathcal{S}_{a_i a_j} = \mathcal{S}_{a_j^\dagger a_i^\dagger} = 0, \quad \mathcal{S}_{x_i p_i} = 0, \quad \forall i, j, \quad (6.15a)$$

$$\mathcal{S}_{a_i a_j^\dagger} = \mathcal{S}_{a_j^\dagger a_i}, \quad \mathcal{S}_{v_i w_j} = \mathcal{S}_{w_j v_i}, \quad \forall i, j, \quad \text{where } v, w \in \{x, p\}, \quad (6.15b)$$

$$\mathcal{S}_{a_i a_j^\dagger} = \mathcal{S}_{a_j^\dagger a_i}^*, \quad \mathcal{S}_{v_i w_j} = -\mathcal{S}_{v_j w_i}, \quad i \neq j, \quad \text{where } v \neq w \in \{x, p\}. \quad (6.15c)$$

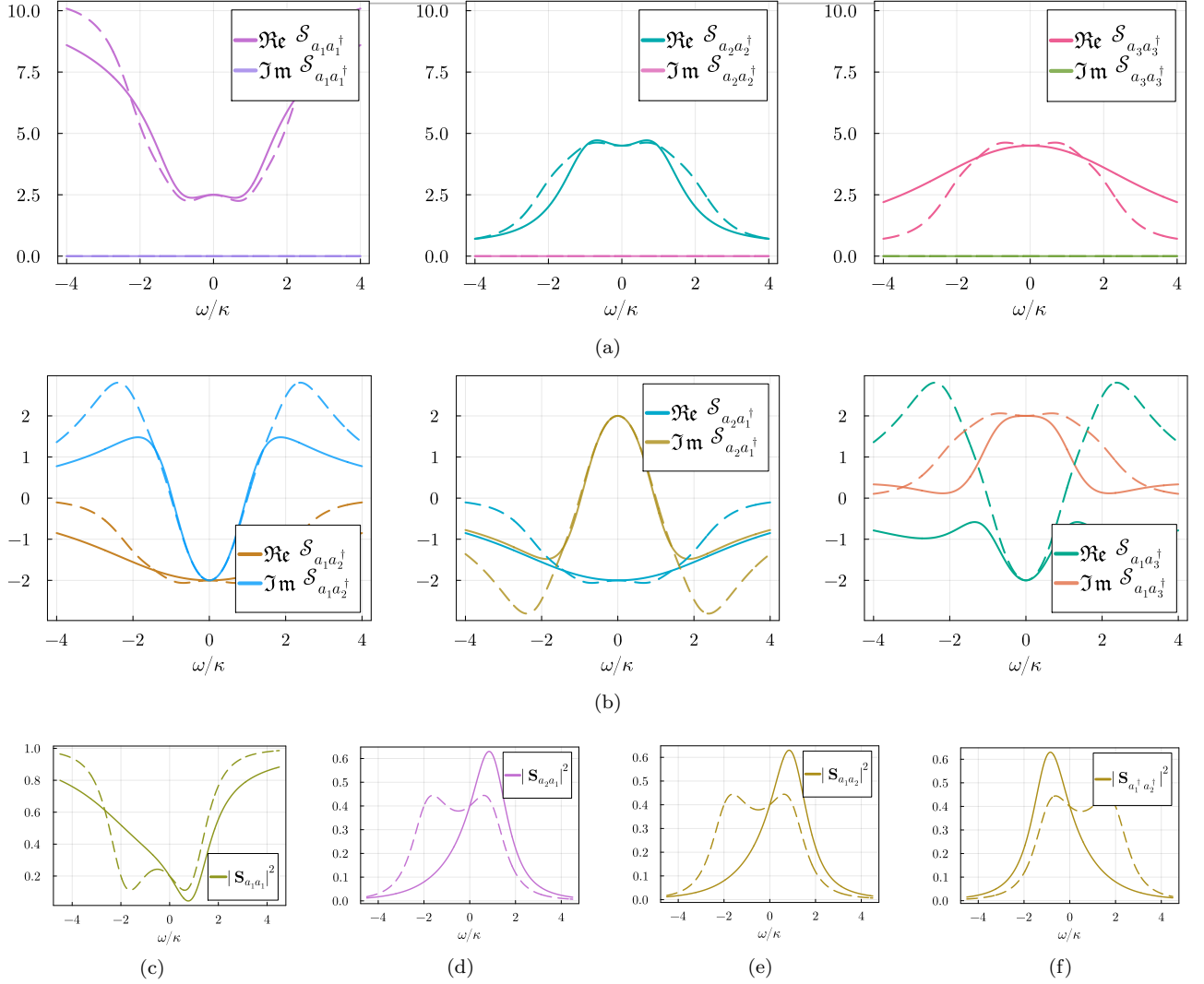


FIG. 26. Comparison between Markovian (solid) and non-Markovian (dashed) output-noise matrix elements (first and second row) and scattering probabilities (last row) for $\Phi = 0$, $\kappa \equiv \kappa_i/2$, and $\bar{n}_1 = 10$, $\bar{n}_2 = \bar{n}_3 = 0$. (a) Here, fluctuations at outputs are shown, with the same behaviour as in Fig. 13, with the difference that the third mode has a broader curve than the other modes. (b) Cross-correlations where the real part behaves similar to Fig. 13. However, this time, there are additional imaginary parts, which are maximized for the reciprocal limit and vanish for the unidirectional limit. In a sense, they track the phase-difference between mode i and adjoint mode j , which seems to disappear when modes and adjoints have symmetrically treated scattering probabilities. (c) Reflection at output 1. (d) Transmission from $1 \rightarrow 2$. (e) Transmission from $2 \rightarrow 1$. (f) Transmission from $2 \rightarrow 1$ for adjoint modes.

Note, that the noise for different quadrature types is the same $\mathcal{S}_{x_i x_j} = \mathcal{S}_{p_i p_j} \forall i, j$. Thus, we need to only show a limited amount of output-noise elements. Consider Fig. 25 in the mode basis, in the unidirectional limit $\Phi = \phi_R$, with damping rates $\kappa \equiv \kappa_i/2$. Again, Markovian (solid) and non-Markovian (dashed) elements of the noise-matrix are shown. The first row, see Fig. 25 (a), illustrates thermal fluctuations $\mathcal{S}_{a_i a_i^\dagger}[\omega]$ at outputs. As expected for an incident input at 1, only output 2 shows thermal noise with $\mathcal{S}_{a_2 a_2^\dagger}[0] = 10.5$, where other outputs show vacuum fluctuations $\mathcal{S}_{a_1 a_1^\dagger}[0] = \mathcal{S}_{a_3 a_3^\dagger}[0] = 0.5$. Thus, thermal fluctuations are fully transferred to output 2, without any leakage to other outputs. This fully coincides with the expected scattering behaviour, see Figs. 25 (c), (d), and (e), where the only allowed transmission is $1 \rightarrow 2$. As before, non-Markovian effects introduce more distinct dips/peaks due to eigenvalues of the dynamical matrix. Cross-correlations behave the same way as for the optical isolator, see the discussion for Fig. 13 in Section V C.

However, off-diagonal elements can become complex for any value of Φ outside the unidirectional limit. Consider Fig. 26, showing Markovian (solid) and non-Markovian (dashed) elements of the output-noise matrix for $\Phi = 0$ and $\kappa \equiv \kappa_i/2$. Each element is decomposed into real and imaginary parts, which can be related to quadrature elements (see Appendix E 1 e), by using Eqs. (6.15) and Eq. (3.65), resulting in (for $v, w \in \{x, p\}$)

$$\Re \mathcal{S}_{a_i a_j^\dagger}[\omega] = \mathcal{S}_{v_i v_j}[\omega], \quad \text{and} \quad \Im \mathcal{S}_{a_i a_j^\dagger}[\omega] = -\mathcal{S}_{x_i p_j}[\omega]. \quad (6.16)$$

Here, diagonal elements behave the same way in both bases, as seen in the noise of the optical isolator, compare Fig. 13 with Fig. 32. Only noise at output 3 differs from the rest by having a broader curve. As mentioned, off-diagonal elements are complex for the reciprocal limit, see Fig. 26 (b). Why are they real in the unidirectional limit? We propose the following explanation: Since the imaginary part of cross-correlations between the noise of mode i and noise of the adjoint j , is composed of cross-correlations between *different quadrature types* x_i, p_j , this can be related to the difference of S-matrix amplitudes between modes or adjoints. Suppose we have a S-matrix amplitude for a process between two modes $a_i \rightarrow a_j$, then, this will be compared to the amplitude for $a_i^\dagger \rightarrow a_j^\dagger$. This was shown in Appendix E 1 e. Formally speaking, we can say $\mathcal{S}_{a_i a_j^\dagger} = \mathcal{S}_{x_i x_j} - i\mathcal{S}_{x_i p_j}$, see Eq. (E3), where

$$\mathcal{S}_{x_i p_j} = -\frac{\bar{n}_i}{2} \Im \left\{ \tilde{\mathbf{S}}_{a_i a_i}[\omega] \tilde{\mathbf{S}}_{a_j a_i}^*[\omega] + \tilde{\mathbf{S}}_{a_i a_i}[-\omega] \tilde{\mathbf{S}}_{a_j a_i}^*[-\omega] \right\}, \quad (6.17)$$

is the imaginary part for an input $\bar{n}_i > \bar{n}_j = 0$, see Eq. (E3). These elements only exist if the scattering between modes and between adjoints differ. This can also be seen for transmission coefficients in Fig. 26 (e) and Fig. 26 (f), where the scattering probabilities are flipped along the x - axis. As we know, this tilt disappears for the unidirectional limit, as well as any imaginary parts in the correlations. Since the reciprocal limit is maximally asymmetric for scattering probabilities, it also has the highest imaginary parts. Both features disappear at the same time for the nonreciprocal limit.

As a concluding remark, note that a deeper analysis into the disappearance of imaginary parts for correlations could hint at the exact relationship between output-operators and exceptional points in general.

B. Dissipative directional transistor

In this Section we will introduce a novel, four-mode model which enables us to not only observe directional transport but also the cancellation of any transport in some direction of a chosen pair of ports. For this, consider Fig 27, where four modes are coherently coupled by beam-splitter interactions and where each mode is again damped by a coupling to their own local reservoir. This model can be understood as an extension of the three-mode model, where the additional 4th mode acts as some kind of *phase-splitter* of the original gauge-phase Φ , which can now be written as the sum of the individual phases $\Phi = \tau_1 + \tau_2 + \tau_3$. This lets us control the phases individually and as it turns out, leads to highly interesting regimes. We start with the interaction picture Hamiltonian which can be written as

$$H_T = J_{12}a_1^\dagger a_2 + J_{31}a_3^\dagger a_1 + J_{32}a_3^\dagger a_2 + J_{41}a_4^\dagger a_1 + J_{42}a_4^\dagger a_2 + J_{43}a_4^\dagger a_3 + \text{H.c.}, \quad (6.18)$$

where the subscript of H_T stands for *transistor*, and whenever we will use the strong set of tools defined above and introduce some new quantity, we will use this subscript for this model. Similar to above we get the following equations

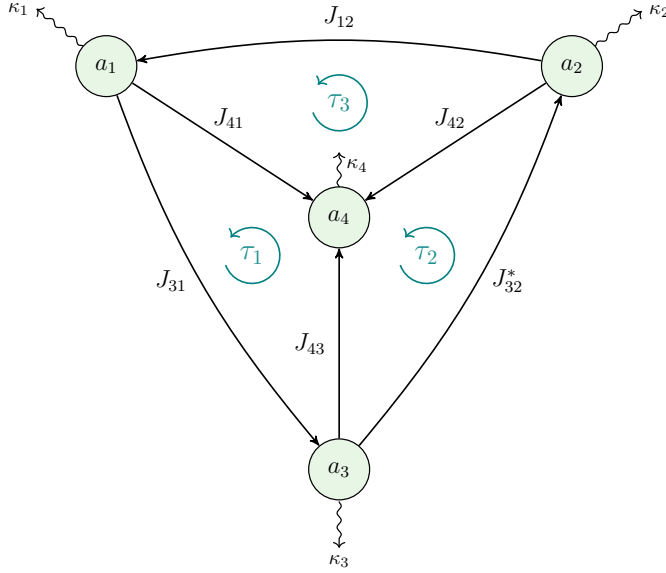


FIG. 27. Directional transistor model with four modes, where each mode a_j is coherently coupled to another mode a_i via a beam-splitter interaction J_{ij} and is locally damped with strength κ_j . In an intuitive manner, due to the addition of mode a_4 , the phase Φ is “split up”, giving us more control over the transport behaviour of the system, as more limiting cases are possible. Thus, the model has three distinct gauge-invariant phases τ_i , which can be individually tuned to achieve aforementioned different regimes. Alongside the known reciprocal and (usual) unidirectional regimes (like the three mode model), there are also novel *off*-regimes, where any transport between a pair of given modes fully vanishes. These regimes are always highly dependent on the pair of modes considered, as an *off*-regime for a given pair of modes implies a nonreciprocal regime for a different pair. Suppose, that transport between a_1 and a_2 vanishes, then there also will be no transport between a_3 and a_4 . However, there is unidirectional transport $1 \rightarrow 4 \rightarrow 2 \rightarrow 3 \rightarrow 1$.

of motion via the Langevin equation

$$\langle \dot{a}_1 \rangle = -\frac{\kappa_1}{2} \langle a_1 \rangle - iJ_{12} \langle a_2 \rangle - iJ_{31}^* \langle a_3 \rangle - iJ_{41}^* \langle a_4 \rangle, \quad (6.19a)$$

$$\langle \dot{a}_2 \rangle = -\frac{\kappa_2}{2} \langle a_2 \rangle - iJ_{12}^* \langle a_1 \rangle - iJ_{32}^* \langle a_3 \rangle - iJ_{42}^* \langle a_4 \rangle, \quad (6.19b)$$

$$\langle \dot{a}_3 \rangle = -\frac{\kappa_3}{2} \langle a_3 \rangle - iJ_{31} \langle a_1 \rangle - iJ_{32} \langle a_2 \rangle - iJ_{43}^* \langle a_4 \rangle, \quad (6.19c)$$

$$\langle \dot{a}_4 \rangle = -\frac{\kappa_4}{2} \langle a_4 \rangle - iJ_{41} \langle a_1 \rangle - iJ_{42} \langle a_2 \rangle - iJ_{43} \langle a_3 \rangle, \quad (6.19d)$$

which we will also write in a concise manner by introducing a new vector $\mathbf{a}_T := (a_1, \dots, a_4, a_1^\dagger, \dots, a_4^\dagger)^T$ (where we keep the daggered modes just for generality, even though it is a redundancy for this explicit model). Then with $\tilde{\mathbf{K}}_T = \mathbb{1}_2 \otimes \text{diag}(\kappa_1, \kappa_2, \kappa_3, \kappa_4)$, we can again write it in the compact form

$$\langle \dot{\mathbf{a}}_T(t) \rangle = \left(-i\mathbf{\Lambda}_z \mathbf{H}_T - \frac{1}{2} \tilde{\mathbf{K}}_T \right) \langle \mathbf{a}_T(t) \rangle \equiv \left(\mathbf{A}_T - \frac{1}{2} \tilde{\mathbf{K}}_T \right) \langle \mathbf{a}_T(t) \rangle \equiv \mathbf{D}_T \langle \mathbf{a}_T(t) \rangle. \quad (6.20)$$

Similar to above, by transforming the modes via $\langle a_j \rangle \rightarrow \langle a_j \rangle e^{i\tau_j}$, see Appendix E 2 a, we can isolate the Aharonov-Bohm phases and get the following interaction parameters

$$J_{12} = |J_{12}|e^{i\tau_3}, \quad J_{31} = |J_{31}|e^{i(\tau_1+\tau_2)}, \quad J_{32} = |J_{32}|, \quad (6.21)$$

$$J_{41} = |J_{41}|, \quad J_{42} = |J_{42}|, \quad J_{43} = |J_{43}|e^{-i\tau_2}, \quad (6.22)$$

with the phases

$$\tau_1 \equiv \arg(J_{31}J_{41}^*J_{43}) = \alpha_{31} - \alpha_{41} + \alpha_{43} \pmod{2\pi}, \quad (6.23)$$

$$\tau_2 \equiv \arg(J_{32}^*J_{42}J_{43}^*) = -\alpha_{32} + \alpha_{42} - \alpha_{43} \pmod{2\pi}, \quad (6.24)$$

$$\tau_3 \equiv \arg(J_{12}J_{41}J_{42}^*) = \alpha_{12} + \alpha_{41} - \alpha_{42} \pmod{2\pi}. \quad (6.25)$$

As mentioned already, summing up these phases gives us the Aharonov-Bohm phase from the three-mode model. Again, by finding an adequate effective model, we get an understanding of the possible transport regimes of this system. Choosing which modes one needs to eliminate to obtain the highest number of distinct limits, is not unique. Therefore, these choices can have better or worse implications on the difficulty of actually tuning the system to all limits. As a general rule of thumb, the more phases we need to control at the same time to switch regimes, the less achievable this becomes in an experimental setting. However, after we have constructed *any* effective model, the key insights help us to then look at the full model and consider the behaviour for all modes at once. Thus, we just eliminate mode 3 and 4 by Fourier-transforming the system, see Appendix E 2, and introduce

$$\begin{aligned} |\delta| &:= |J_{12}|, & \chi_i[\omega] &:= \frac{1}{i\omega + \kappa_i/2}, & \bar{\chi}[\omega] &:= \chi_3[\omega]\chi_4[\omega], & \bar{d}[\omega] &:= \frac{1}{1 + \bar{\chi}[\omega]|J_{43}|^2}, \\ \lambda_1[\omega] &:= \chi_3[\omega]\bar{d}[\omega]|J_{31}J_{32}|, & \lambda_2[\omega] &:= \chi_4[\omega]\bar{d}[\omega]|J_{41}J_{42}|, & \mu_1[\omega] &:= \bar{d}[\omega]|J_{31}J_{42}J_{43}|, & \mu_2[\omega] &:= \bar{d}[\omega]|J_{41}J_{32}J_{43}|, \end{aligned} \quad (6.26)$$

where $\bar{d}[\omega]$ is a unit-less quantity acting as a scaling factor, and

$$\bar{\sigma}_i[\omega] := 2\bar{\chi}[\omega]\bar{d}[\omega]|J_{3i}J_{4i}J_{43}|, \quad \frac{\bar{\gamma}_i[\omega]}{2} := \frac{\kappa_i + 2\chi_3[\omega]\bar{d}[\omega]|J_{3i}|^2 + 2\chi_4[\omega]\bar{d}[\omega]|J_{4i}|^2}{2}, \quad (6.27)$$

are damping rates of the shared reservoir. With these definitions, the EOMs for the effective model can be written in a concise manner and read

$$\begin{aligned} i\omega \langle a_1[\omega] \rangle &= \left(-\frac{\bar{\gamma}_1[\omega]}{2} + i\bar{\sigma}_1[\omega] \cos \tau_1 \right) \langle a_1[\omega] \rangle \\ &\quad - \left(\lambda_1[\omega]e^{-i(\tau_1+\tau_2)} + \lambda_2[\omega] - i(\mu_1[\omega]\bar{\chi}[\omega]e^{-i\tau_1} + \mu_2[\omega]\bar{\chi}[\omega]e^{-i\tau_2} - |\delta|e^{i\tau_3}) \right) \langle a_2[\omega] \rangle, \end{aligned} \quad (6.28)$$

$$\begin{aligned} i\omega \langle a_2[\omega] \rangle &= \left(-\frac{\bar{\gamma}_2[\omega]}{2} + i\bar{\sigma}_2[\omega] \cos \tau_2 \right) \langle a_2[\omega] \rangle \\ &\quad - \left(\lambda_1[\omega]e^{i(\tau_1+\tau_2)} + \lambda_2[\omega] - i(\mu_1[\omega]\bar{\chi}[\omega]e^{i\tau_1} + \mu_2[\omega]\bar{\chi}[\omega]e^{i\tau_2} - |\delta|e^{-i\tau_3}) \right) \langle a_1[\omega] \rangle. \end{aligned} \quad (6.29)$$

Before analyzing these terms, we make a few notes about the Markovian regime. For the Markovian regime, we get $\chi_i[\omega = 0] \in \mathbb{R}_{>0}$. Thus, parameters $\lambda_i \equiv \lambda_i[0]$, $\mu_i \equiv \mu_i[0]$, $\bar{d} \equiv \bar{d}[0]$, $\bar{\sigma}_i \equiv \bar{\sigma}_i[0]$, $\bar{\gamma}_i \equiv \bar{\gamma}_i[0] \in \mathbb{R}_{>0}$, are all positive real numbers. This gives us

$$i\omega \langle a_1[\omega] \rangle = \left(-\frac{\bar{\gamma}_1}{2} + i\bar{\sigma}_1 \cos \tau_1 \right) \langle a_1[\omega] \rangle - \left(|\lambda_1| e^{-i(\tau_1+\tau_2)} + |\lambda_2| - i \left(|\mu_1| \bar{\chi} e^{-i\tau_1} + |\mu_2| \bar{\chi} e^{-i\tau_2} - |\delta| e^{i\tau_3} \right) \right) \langle a_2[\omega] \rangle, \quad (6.30)$$

$$i\omega \langle a_2[\omega] \rangle = \left(-\frac{\bar{\gamma}_2}{2} + i\bar{\sigma}_2 \cos \tau_2 \right) \langle a_2[\omega] \rangle - \left(|\lambda_1| e^{i(\tau_1+\tau_2)} + |\lambda_2| - i \left(|\mu_1| \bar{\chi} e^{i\tau_1} + |\mu_2| \bar{\chi} e^{i\tau_2} - |\delta| e^{-i\tau_3} \right) \right) \langle a_1[\omega] \rangle, \quad (6.31)$$

which are highly simplified EOMs for the effective model. We will hereby call this effective model the *effective transistor*. Immediately, one sees that the model can host unidirectional transport (similar to the three-mode model) by choosing one of either conditions for the interaction parameters

$$\text{case 1: } |\lambda_1| e^{-i(\tau_1+\tau_2)} + |\lambda_2| \stackrel{!}{=} +i \left(|\mu_1| \bar{\chi} e^{-i\tau_1} + |\mu_2| \bar{\chi} e^{-i\tau_2} - |\delta| e^{i\tau_3} \right), \quad (6.32)$$

$$\text{case 2: } |\lambda_1| e^{i(\tau_1+\tau_2)} + |\lambda_2| \stackrel{!}{=} +i \left(|\mu_1| \bar{\chi} e^{i\tau_1} + |\mu_2| \bar{\chi} e^{i\tau_2} - |\delta| e^{-i\tau_3} \right), \quad (6.33)$$

which balances out different dynamics, just as before. However, as already discussed in the literature, see Ref. [1, 14], nonreciprocal dynamics seem to always appear when *coherent* and *dissipative* interactions are balanced out. Naturally, one question arises: ‘‘Can we observe the same behaviour when balancing out two dissipative (or coherent) interactions?’’ Our effective transistor model strains this rule a bit: Compared to the optical isolator from Metelmann and Clerk [1], the balancing-out procedure here is a bit more nuanced: Instead of having a clear distinction between *coherent* and *dissipative* dynamics, the interactions μ_i and λ_i of our effective transistor depend on the susceptibilities $\bar{\chi}[\omega]$. First we note that $|\delta| = |J_{12}|$ has the same effect as for the aforementioned J of the optical isolator, so it definitely constitutes as the coherent part of this system. Secondly, we note that $\lambda_i[\omega]$ has a similar structure to $\Gamma[\omega]$ of the optical isolator. Thus, $\lambda_i[\omega]$ can surely be interpreted as the dissipative interaction for our effective model. But, making the case for $\mu_i[\omega]$ is not so straightforward. Even though this quantity depends on the shared reservoir and the damping rates $\kappa_{3,4}$ due to $\bar{d}[\omega]$, it only indirectly does so, as the *coherent* interactions inside $\mu_i[\omega]$ are re-scaled by a unit-less factor $\bar{d}[\omega]$. In a way, it still acts like a *coherent* interaction, but energies are renormalized by the shared reservoir. However, there undoubtedly is still a clear effect of auxiliary modes on μ_i , so it could also be seen as an *effective dissipative* interaction. The concluding remark is then: This rule of always having to balance out coherent with dissipative interactions may not be so strict, and could be a matter of definition. One consistent way would be to simply call μ_i renormalized but still consider it as *coherent*, meaning the rule above still seems to hold.

Coming back to the transport behaviour, we set $\kappa \equiv \kappa_i/2$, $|J_{ij}|/\kappa = 1$ (this choice will become clearer shortly), and it follows, $|\lambda_i|/\kappa = |\mu_i|/\kappa = 1/2$, which gives us two possibilities for (partially) decoupling mode 1 from 2, and vice versa,

$$\text{case 1: } e^{-i(\tau_1+\tau_2)} + 1 - i \left(e^{-i\tau_1} + e^{-i\tau_2} - 2e^{i\tau_3} \right) \stackrel{!}{=} 0, \quad (6.34)$$

$$\text{case 2: } e^{i(\tau_1+\tau_2)} + 1 - i \left(e^{i\tau_1} + e^{i\tau_2} - 2e^{-i\tau_3} \right) \stackrel{!}{=} 0. \quad (6.35)$$

At first this system seems inhibit the same dynamics as before, where we choose one of either case and in-turn enforce nonreciprocity. However, since we now have a bigger parameter-space in this model, we can find an additional limit, where both cases above are true at the same time. Note, that this limit can be achieved for finite (and thus non-trivial) interaction parameters. Here, the system acts like a *dark state*, see Ref. [69], where both modes fully decouple from each other in both directions and any transport fully vanishes. For example, consider $\tau_1 = \tau_2 = -\tau_3 = \pi/2$, which implies

$$\text{case 1: } e^{-i(\pi/2+\pi/2)} + 1 - i \left(e^{-i\pi/2} + e^{-i\pi/2} - 2e^{i(-\pi/2)} \right) = -1 + 1 - i(-i - i + 2i) = 0, \quad (6.36)$$

$$\text{case 2: } e^{i(\pi/2+\pi/2)} + 1 - i \left(e^{i\pi/2} + e^{i\pi/2} - 2e^{-i(-\pi/2)} \right) = -1 + 1 - i(i + i - 2i) = 0. \quad (6.37)$$

Therefore, both cases hold and we see full cancellation in both directions at the same time! This limit will be generally denoted as the *off*-regime between given mode-pairs (since there are several possible limiting regions for different pairs,

Class	Transport	τ_1	τ_2	τ_3
R	$1 \leftrightarrow 2$	0	0	0
NR	$1 \rightarrow 2$	$\pi/2$	0	0
NR	$1 \leftarrow 2$	$-\pi/2$	0	0
R	$1 \leftrightarrow 2$	$\pi/2$	$\pi/2$	$\pi/2$
NR	$1 \rightarrow 2$	$\pi/2$	$-\pi/2$	$\pi/2$
NR	$1 \leftarrow 2$	$\pi/2$	$-\pi/2$	$-\pi/2$
<i>off</i>	$1 \leftrightarrow 2$	$\pi/2$	$\pi/2$	$-\pi/2$
<i>off</i>	$1 \leftrightarrow 2$	$-\pi/2$	$-\pi/2$	$\pi/2$

TABLE II. Interesting limit cases of the directional transistor with $\kappa \equiv \kappa_i/2$, $|J_{ij}|/\kappa = 1$, for different values of the Aharonov-Bohm phases τ_i . Here, “R” denotes reciprocal and “NR” unidirectional transport. The class “*off*” represents the regime where no transport between mode a_1 and a_2 is possible. Note, that this situation is different for each possible pairs of modes a_i and a_j . Also note, that “Class” is loosely defined here, as it only holds on the level of (partially) decoupling a pair of modes in each possible effective model (we could eliminate different modes) and does not mean regimes in the same class are the same. In fact, the classes of the 2nd and 3th row are distinctively different from the 5th and 6th row. We will touch on that briefly in the coming Section.

more on that later). Lets focus on the effective damping rates for a second: Apart from the term $-\bar{\gamma}_i[\omega]/2$, which acts the same way as the global reservoir of the optical isolator, we also have an additional term $i\bar{\sigma}_i[\omega] \cos \tau_i$, which acts as a detuning and encodes additional oscillations of the respective mode of interest. Thus, even if we only look at damping rates for each mode and consider the steady state, there would still be some dynamical activity happening, so instead of just observing an exponential decay, we would observe additional oscillations till the mode in the steady state relaxes to the lowest possible energy. By looking closer at our definition of $\bar{\sigma}_i$, oscillations happen because excitations can now traverse along a closed loop and end up at the mode they started at, i.e. for $\bar{\sigma}_1 \propto |J_{31}J_{41}J_{43}|$, an excitation can travel as such: $1 \rightarrow 4 \rightarrow 3 \rightarrow 1$. However, this is highly dependent on the phase τ_1 , where the cosine vanishes for non-trivial values, namely $\tau_1 = \pm\pi/2$. Thus, these oscillations become maximal for trivial values of the phases, $\tau_{1,\text{triv}} = 0, \pm\pi \implies \cos(\tau_{1,\text{triv}}) = 1$.

Now we come back to the limit cases of the system regarding transport. Note, that there are several of these reciprocal (R)/unidirectional (NR)/*off* limits, which are highly dependent on the pair of modes considered, see Table VI B. How does that happen? To understand this, we look at the scattering probabilities after finding an appropriate impedance-matching condition.

1. Scattering and noise of the directional transistor

Here, we will focus again on the full, four-mode model. To impedance match the system, we need to ensure that the diagonal probabilities of the S-matrix all vanish. Similar to above (see Eq. (4.36)), the model is impedance-matched if for some κ , with $\kappa_{3,4} \propto \kappa$, we get $\kappa^2 \bar{\chi}[0] = 1$. This implies

$$\kappa^2 \bar{\chi}[0] \stackrel{!}{=} 1 \iff \kappa_3 \kappa_4 \stackrel{!}{=} 4\kappa^2, \quad (6.38)$$

Again, there are several options for the rates κ_i , which could be used for this condition to hold. Here, we will focus on the most symmetric choice, which was already used above, namely $\kappa \equiv \kappa_i/2$, where all four damping rates have the same value. As before, interaction parameters can then be expressed in units of κ , with $|J_{ij}|/\kappa = 1$. To show the effect of the phases on the transport, we will focus only on a specific number of limiting regimes in the Markovian approximation.

Consider Fig. 28, where we have shown different regimes for the Markovian S-matrix with $\omega = 0$. The first case, see Fig. 28 (a) with $\tau_1 = -\tau_2 = \tau_3 = \pi/2$, shows one possible NR limit, where there are no reflection coefficients (due to impedance matching) and the only transport allowed is from $1 \rightarrow 2 \rightarrow 4 \rightarrow 3 \rightarrow 1$. In this regime, we see how mode 2 and 3 fully decouple, so the NR transport in 1 and 2 happens at the same time as the *off*-limit for modes 2 and 3. This is an important feature of this model, as vanishing transport between a pair of modes coincides with NR transport between others. From the perspective of the effective transistor (the upper left 2×2 block of the S-matrix), where mode a_3 and a_4 are eliminated, it behaves like the optical isolator with $\Phi = \phi_R$. The opposite transport is seen in the third Fig. 28 (c) with $\tau_1 = -\tau_2 = -\tau_3 = \pi/2$, which tells us that the 4-mode model effectively reproduces the optical isolator for these limiting cases. However, this changes in Fig. 28 (b) with $\tau_1 = \tau_2 = -\tau_3 = \pi/2$, which one of several possible *off*-regimes of the effective transistor for modes 1 and 2. Here, neither reflection nor transmission happens in the upper left 2×2 sub-block. Effectively speaking, any information entering port 1 or 2 completely vanishes, as

their is destructive interference in both directions of propagation. In the effective picture, this limit behaves singular and information seems to get destroyed. Of course, in the full model this is not what is happening, and as mentioned in (a), if one interaction between a pair vanishes in this limit, another does also vanish - here mode 3 and 4 also fully decouple. There is unidirectional transport in a circle as $1 \rightarrow 4 \rightarrow 2 \rightarrow 3 \rightarrow 1$. In the last Fig. 28 (d) with $\tau_1 = -\tau_2 = \tau_3/2 = \pi/2$, one of several reciprocal regimes are shown, where the upper left sub-block behaves like the reciprocal optical isolator with $\Phi = \phi_0$. However, there is perfect transmission from mode 4 to mode 3, but not from any other mode. Nonetheless, mode 1 couples to mode 2 in a reciprocal manner and there is some transport from 1 (2) to 4 and also from 3 to 1 (2). This limit is an intermediate limit where changing τ_3 would lead to one of the NR regimes (a) and (c).

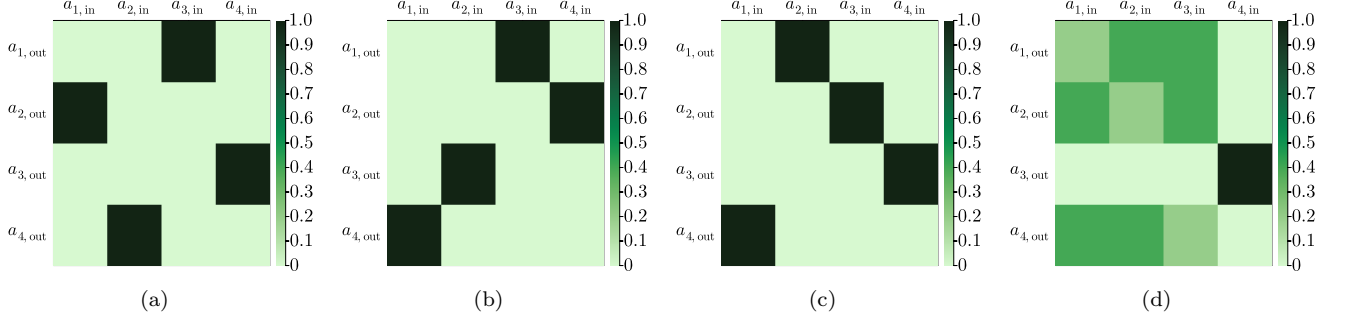


FIG. 28. Scattering probabilities of the directional transistor for the impedance-matched case $\kappa_i/2 \equiv 2\kappa$, $|J_{ij}|/\kappa = 1$, and different values of the Aharonov-Bohm phases τ_i . (a) NR limit for $\tau_1 = -\tau_2 = \tau_3 = \pi/2$, with transport from $1 \rightarrow 2 \rightarrow 4 \rightarrow 3 \rightarrow 1$ in the full model. In the effective model we have unidirectional transport from $1 \rightarrow 2$. (b) *off*-limit for $\tau_1 = \tau_2 = -\tau_3 = \pi/2$, with no transport between $1 \leftrightarrow 2$ and vanishing reflection in the effective picture. In the full model there is unidirectional transport from $1 \rightarrow 4 \rightarrow 2 \rightarrow 3 \rightarrow 1$ (c) NR limit for $\tau_1 = -\tau_2 = -\tau_3 = \pi/2$, with unidirectional transport from $2 \rightarrow 1$ in the effective picture, with unidirectional transport from $1 \rightarrow 4 \rightarrow 3 \rightarrow 2 \rightarrow 1$ for the full model. (d) R limit for $\tau_1 = -\tau_2 = \tau_3/2 = \pi/2$, with reciprocal transport between $1 \rightarrow 2$ in the effective picture.

After understanding Fig. 28, we are equipped to look at specific scattering and output-noise elements. For this, we will fix one of the three phases, in our case $\tau_1 = \pi/2$, and tune other phases to see when transport occurs. We investigate the resonant case for $\omega = 0$ in the Markovian regime for simplicity (which is justified, as the Markovian coincides with the non-Markovian regime for $\omega = 0$). For this, consider Fig. 29, where we compare different ports for $\omega = 0$, $\kappa \equiv \kappa_i/2$, a fixed phase $\tau_1 = \pi/2$, and plot it against $\tau_{2,3}$. In Fig. 29 (a), the transmission from $2 \rightarrow 1$ (left) and $1 \rightarrow 2$ (right) are shown. As we can see, there are distinct regions for limiting transport regimes, consider Table VI B. To understand the limit cases, we need to always look at the left and right plot at the same time: NR transport with full cancellation from $2 \rightarrow 1$ happens at $\tau_1 = -\tau_2 = -\tau_3 = \pi/2$, where the probability becomes maximal (minimal) in the left (right) picture. The reciprocal region is at $\tau_2 = \tau_3 = \pi/2$, where transmissions in both directions are the same. However, we see clear dark regions in both pictures (the diagonal region in the left plot from $(\tau_2, \tau_3) = (0, 2\pi)$ to $(\tau_2, \tau_3) = (2\pi, 0)$, and the horizontal region for $\tau_3 = -\pi/2$ on the right). If both dark regions meet on both sides, the transport in both directions vanishes fully. This *off*-limit happens with full cancellation at $\tau_2 = -\tau_3 = \pi/2$, resembling the theoretical result from earlier. We can tune the system to different limits by simply tuning the phases and leaving other parameters invariant. However, by only changing a single phase we cannot turn the transistor off between nonreciprocal regions, since the off-region on the left is on a diagonal region. To do that, we would need to change both phases at the same time. This can be experimentally challenging, thus we consider ports 2 and 4 in Fig. 29 (b), showing transmission from $4 \rightarrow 2$ (left) and $2 \rightarrow 4$ (right). We see how the limiting regions are now displaced compared to before. Interestingly, the NR regions are now on different corners to before, and both *off*-regions are not diagonally placed. Here, the NR regions are $\tau_2 = -\tau_3 = \pi/2$ (the *off*-region of (a), and $\tau_3 = -\tau_2 = \pi/2$ (the same NR region as in (a)). The reciprocal region sits between the NR regions at $\tau_2 = \tau_3 = \pi/2$. If we sit at one of the NR regions, we can change to the reciprocal region by simply tuning one of the phases. Since the *off*-regions are now on non-diagonal lines and intersect at $\tau_2 = \tau_3 = \pi/2$, the transistor can be turned off between the NR regions then change the direction of the “source” and “drain” of this transistor. This flips the *bias*. The “gate” always has to be controlled by two phases, to achieve all limits. In Fig. 29 (c) diagonal elements of the noise for output 1 and 2 and a noise-input vector $\mathbf{n}_{th} = (10, 10, 0, 0)$ are shown. We see – as expected from the scattering (a), that the transport is unidirectional at NR regions and reaches its *off*-limit at $\tau_2 = -\tau_3 = \pi/2$. In Fig. 29 (d), we have shown the diagonal output-noise elements for output 2 and 4 and an input of $\mathbf{n}_{th} = (0, 10, 0, 10)$. We see, that there is no thermal-noise at the output of either port in the *off*-limit, and there are no back-reflections and the system behaves like a dark state. Thus, this is a highly versatile system which can be looked at from varying angles and ports can be chosen to meet

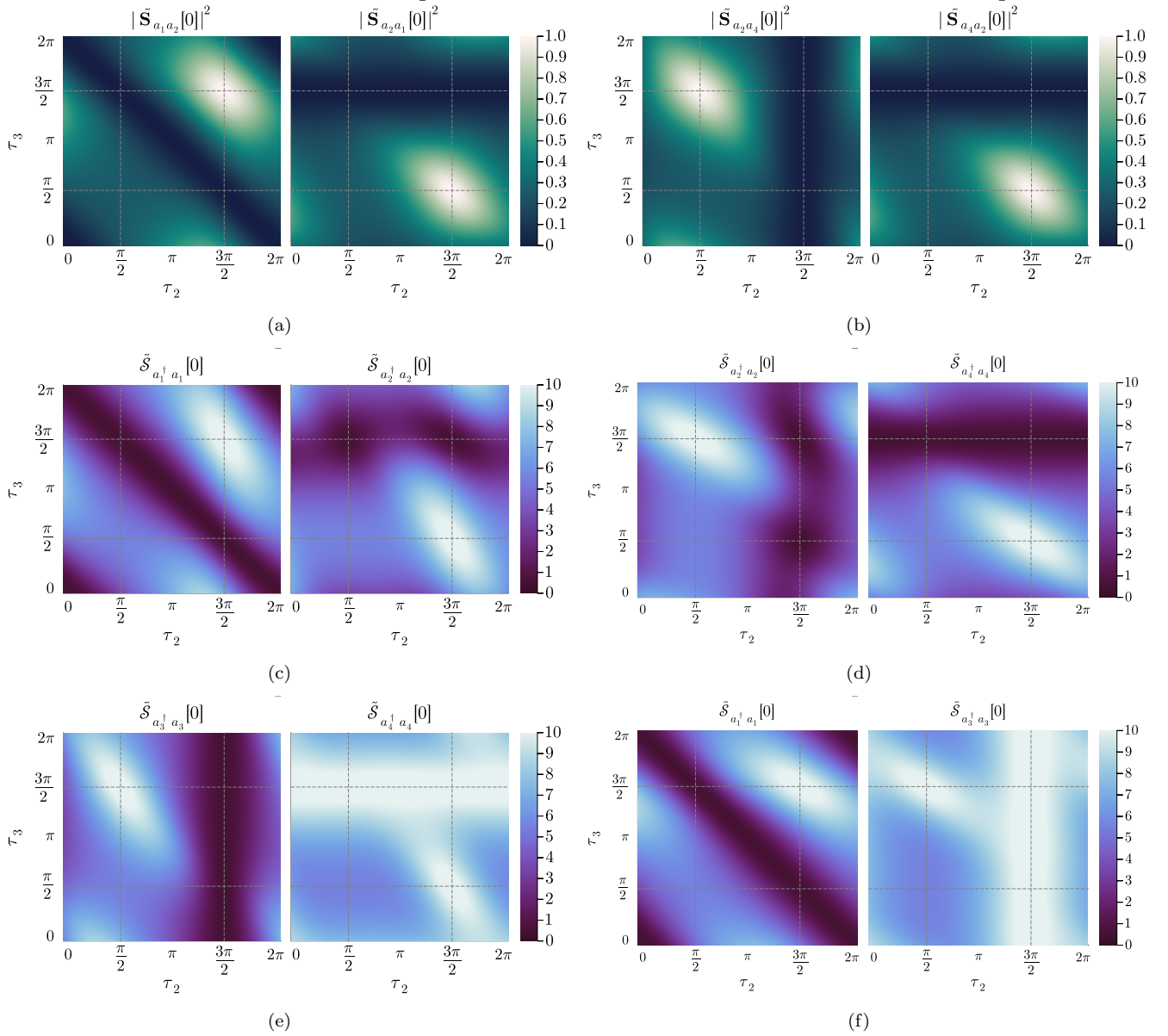


FIG. 29. Comparison between scattering probabilities and fluctuations at outputs for $\omega = 0$, $\kappa \equiv \kappa_i/2$, a fixed phase $\tau_1 = \pi/2$, plotted against $\tau_{2,3}$, with varying input-noise. (a) The transmissions from 2 \rightarrow 1 (left) and 1 \rightarrow 2 (right). There are distinct regions for limiting transport regimes. To understand the limits, we need to consider the left and right plot at the same time. If dark regions meet on both sides, the transport in both directions vanishes fully. The system reaches different limits if we simply tune the phases and leave all other parameters invariant. (b) The same as before, only for ports 2 and 4. We see how these regions are now displaced. Since the off-regions are now non-diagonal lines and intersect at $\tau_2 = \tau_3 = \pi/2$, we can turn the transistor off between NR regions and change the “source/drain” direction of the transistor. The “gate” is always controlled by two phases, but now it is sufficient to only tune a single phase at a time to change regions. (c) and (e) Diagonal elements of the output-noise and a noise-input vector $\mathbf{n} = (10, 10, 0, 0)$. For (c), transport is unidirectional at NR regions and reaches its *off*-limit at $\tau_2 = -\tau_3 = \pi/2$ on both sides for outputs 1 and 2. (d) and (f) Diagonal output-noise with an input of $\mathbf{n}_{\text{th}} = (0, 10, 0, 10)$.

certain demands of the system. We see in Fig. 29 (e) (and Fig. 29 (f)) that the noise missing at the off-regions for output 1 (2) and 2 (4) can be found at output 3 (1) and 4 (3). Comparing the left (c) and (e) and the right column (d) and (f), we notice that the left can be transformed to the right by mirroring all heatmaps at the $y = x$ axis with an angle of π . Thus, this model is predictable and can be further analyzed. To conclude this Section, we make a comment about $\omega \neq 0$: As expected, the system analogously behaves to the three-mode system, as the transport is highly dependent on the resonance. Additional details can be found in the App. E 2 c, and App. E 2 d.

VII. Discussion

In this thesis, we reviewed various appearances and aspects of nonreciprocity in several few-mode bosonic systems. In particular, we focused on transport limits and their relation to gauge-invariant phases, as well as the influence of (non)reciprocity on thermal noise. Additionally, we examined how these effects might differ between mode operators and quadratures. The underlying system we considered consists of a three-resonator design with dissipative and coherent couplings, arranged in an Aharonov-Bohm ring configuration. Each resonator is locally coupled to a thermal reservoir, and pairs of resonators interact through either linear (beam-splitter) or parametric (two-mode squeezing) interactions. Since this is an open bilinear system, it was modeled using the input-output formalism and the quantum Langevin equation (see Sec. II E and Sec. III B). By extending the bosonic Bogoliubov-de-Gennes (BdG) formalism to open systems (see Sec. III B 3), we were able to concisely describe system-environment interactions, including the scattering behaviour and the system's influence on thermal noise. The BdG formalism resulted in equations of motion for the resonators with the dynamical matrix \mathbf{D} (\mathbf{A}), encoding the complete dynamics of the open (closed) system. Since the arrangement of the three-mode system leads to the emergence of gauge-invariant phases (Φ for linear, and $\vartheta_{1,2}$ for parametric interactions), we devised a method to isolate all relevant phases and express our dynamical matrices in terms of these phases (see Sec. III B 2). By assuming that one resonator is highly damped, it becomes quasi-static compared to the rest of the system and effectively acts as a shared dissipative reservoir, reproducing the effective two-mode model of Metelmann and Clerk [1]. We showed that the auxiliary can be eliminated from the equations of motion in two ways: either by assuming that the auxiliary reaches a steady state and adiabatically eliminating it, or by transforming the equations of motion to the frequency domain and solving for the auxiliary. The former elimination yields the Markovian limit, while the latter results in the non-Markovian regime of the shared reservoir, as the frequency response of the auxiliary remains intact. To understand the difference between the Markovian and non-Markovian regimes, we drew an analogy comparing the dissipative coupling to a complex refractive index, where the non-Markovian case converges to the Markovian limit if the dissipation rate of the auxiliary is increased. By balancing coherent and dissipative interactions in the effective model, we identified conditions under which the gauge-invariant phases enforce nonreciprocal transport by (partially) decoupling one mode from another. To analyze the influence of nonreciprocity on transport and thermal noise, we compared several few-mode bosonic systems. The majority of the thesis focused on linearly coupled models, neglecting any parametric interactions. Specifically, we considered the effective *two-mode optical isolator* as proposed by Ref. [1], the general *dissipative three-mode ring*, and our four-mode extension, the *dissipative directional transistor*. Since the optical isolator is just an effective model of the dissipative ring, we first focus only on those two. We considered two extreme transport limits for both models, the *reciprocal limits* for $\Phi = \{0, \pi\}$ and the *unidirectional limits* for $\Phi = \pm\pi/2$ (see Sec. III F).

Consider the optical isolator, where we examined the complex spectrum of the dynamical matrix \mathbf{D}_{eff} (see Sec. III G 2). Imaginary parts of the spectrum represent the energies of the Hamiltonian, where we observed degenerate zero-energy eigenstates for unidirectional limits. By moving away from that limit, eigenstates begin to split up with finite energies with opposite signs, and reach their maximum at reciprocal limits. The real parts of the complex spectrum encode dissipation and remain finite for all values of Φ , but equalize for unidirectional limits. In this limit, eigenstates coalesce, implying that the non-Hermitian system reaches an exceptional point, see Refs. [59–62]. In Sec. IV A we derived a general expression for the S-matrix using I/O theory, and showed that modes and adjoints are treated differently by the S-matrix with respect to ω , where adjoints get scattered by a S-matrix with negative frequencies. This changes for quadratures, as the frequency dependence of the S-matrix does not depend on the quadratures. We could show that this is a feature of non-Hermitian operators and is thus only relevant for mode operators. Additionally, we suspect that this could also be explained with properties of complex Fourier transforms versus real Fourier transforms. We could reproduce the non-unitary S-matrix for the optical isolator in the unidirectional limit known from Metelmann and Clerk [1] (see. Sec. IV C), which resembles an idealized isolator for maximized power transfer due to impedance-matching. Additionally, we also considered the reciprocal limit, which was not shown in Ref. [1], where scattering probabilities for modes become asymmetric and tilt to a preferred direction in frequency (with opposite tilts for adjoints). However, this result is already known from Ref. [63] for a similar optomechanical setup, where scattering probabilities re-symmetrize by reaching exceptional points. Why this tilt appears for reciprocal points will become clear when we discuss the three-mode model. In the non-Markovian regime, scattering probabilities are symmetric in general but not centered at the origin, where the Markovian limit shows a more noticeable tilt with an asymmetric curve. Thus, the auxiliary has a big influence on the transport. To see this, we noticed that transport in the non-Markovian regime strongly differs from the Markovian limit if the system was impedance-matched with equal dissipation rates $\kappa \equiv \kappa_{1,2,3}/2$, but if the auxiliary damping increases compared to other rates, i.e. $\kappa \equiv \kappa_{1,2} = 4\kappa_3$, the non-Markovian regime converges to the Markovian limit. This behavior is analogous to our earlier discussion of the complex refractive index, reinforcing the consistency of our findings across different aspects of the system. Noticeably, scattering probabilities between quadratures always yield symmetric curves in all transport limits, as shown in App.

C5. In Sec. V, we derived the noise-spectral density $\tilde{\mathcal{S}}_{\text{out}}[\omega]$ for output-ports. This derivation involved expressing covariances of output fields in terms of input fields. Our derivation revealed that a combination of S-matrix elements act as a transfer function, effectively filtering and redistributing incident noise to respective output ports. In our analysis we assumed *white noise* entering the input-ports. This incident noise, after traversing the optical isolator, leaves the system with a finite support over a narrow frequency bandwidth, as detailed in Sec. VB and Sec. VC. The behavior is analogous to a band-pass filter, which eliminates high and low frequency components of an input signal. We compared the output-noise of the optical isolator for different transport limits and could show that noise incident at port i is fully *transferred* to port j in the unidirectional limit $\mathcal{S}_{a_j^\dagger a_j}[0] = \bar{n}_i$, as expected by the S-matrix (for the only non-zero element $|\tilde{\mathbf{S}}_{ji}|^2 = 1$). If both ports have the same thermal input ($\bar{n}_1 = \bar{n}_2 > 0$), the system in the unidirectional limit does not become unresponsive and still fully transfers the noise in one direction (i.e. $1 \rightarrow 2$), where noise incident to port 2 cannot be found at any output (since it will enter the auxiliary and leave output 3, which this model does not account for). In the reciprocal limit, noise entering port i can be found at both outputs, which starts to saturate for $\omega = 0$, and where more fluctuations exist at output j . Noticeably, the output-noise of the optical isolator can drop below the noise-floor, since eliminating the auxiliary also eliminates any inputs of the auxiliary to remaining modes. Correlations $\mathcal{S}_{a_i^\dagger a_j}$ between outputs can appear for finite frequencies, since noise at the output is superposed. These reach their maximal value for $\omega/\kappa = \pm\sqrt{2}$ in the non-Markovian regime. Anti-correlations $\mathcal{S}_{a_i^\dagger a_j} < 0$ starts to appear if it is unclear at which output the information is to be expected, i.e. the reciprocal limit $i \leftrightarrow j$, with $\bar{n}_i \gg \bar{n}_j = 0$. Outputs are positively correlated $\mathcal{S}_{a_i^\dagger a_j} > 0$ if noise exists either at both outputs at the same time or none at all, i.e. the unidirectional limit $2 \rightarrow 1$ with $\bar{n}_1 \gg \bar{n}_2 = 0$. Also, outside the unidirectional limits, cross-correlations can become complex.

Next, we discuss how the behaviour of three-mode ring differs compared to the effective optical isolator. The Hamiltonian of the dissipative ring was diagonalized with quasi-momenta eigenstates, where two of them are always degenerate in reciprocal limits, and maximally nondegenerate in unidirectional limits, see Sec. III G 1. We could show in Sec. VI A 1 that the three-mode model acts like a circulator with an unitary S-matrix for unidirectional limits, e.g. for $\Phi = \pi/2$ and $\omega = 0$, reflections vanish and only the transmissions $|\tilde{\mathbf{S}}_{a_2 a_1}|^2 = |\tilde{\mathbf{S}}_{a_3 a_2}|^2 = |\tilde{\mathbf{S}}_{a_1 a_3}|^2 = 1$ remain. In the reciprocal limit, transmissions have equal probability and reflections do not vanish. As before, scattering probabilities are tilted for the reciprocal limit in the mode basis. Additionally, we could relate the imaginary part of the eigenvalues of \mathbf{D} to the peaks and dips of scattering probabilities (which also holds true for the optical isolator). The real part of the eigenvalues correspond to dissipation and leads to an overlap of quasi-momenta eigenstates, explaining why scattering is not centered at $\omega = 0$ for the reciprocal limit, as two eigenstates always become degenerate. The output-noise of the three-mode ring, which behaves similarly to the optical isolator. However, the noise at outputs never drops below the noise floor, since all inputs/outputs are considered in this model. Different to the optical isolator, the system becomes unresponsive for equal inputs $\bar{n}_1 = \bar{n}_2 = \bar{n}_3 > 0$, since all outputs show white noise for all values of Φ for all frequencies. Next, we showed that relating correlations in the mode basis to correlations in the quadrature basis $\mathcal{S}_{a_i a_j^\dagger} = \mathcal{S}_{x_i x_j} - i\mathcal{S}_{x_i p_j}$ can become quite useful when the latter is expressed using S-matrix amplitudes in the mode basis. Using that, we found that the imaginary part of correlations only appear for the reciprocal limit since modes and adjoints are scattered differently with respect to ω . If scattering between modes behaves the same as between adjoints in ω , imaginary parts of correlations vanish, which is exactly the case in unidirectional limits. Thus, the imaginary component of cross-correlations and the asymmetry in scattering amplitudes serve as key indicators for determining the transport regime of the system.

Section VI B finishes this thesis with the last model we analyzed. For this, the three-mode ring was extended by an additional fourth dissipative resonator, coupling linearly to all other resonators. We could show that this arrangement results in three distinct gauge-invariant phases, which can be independently tuned to achieve multiple transport limits. This system not only reproduces known transport limits of the three-mode ring, but also offers novel transport regimes, which, if the phases are tuned accordingly, lead to a full cancellation of transport between a given pair of modes. This cancellation is most importantly non-trivial, as no interactions between the mode-pair are neglected from the beginning. On the contrary, they destructively interfere in both directions at the same time, where transport simply gets redirected to the other two modes. We have shown that this new *off-limit* can be understood as the off-state of a transistor (by considering a effective two-mode transistor). However, different to conventional transistors, the *gate* (our phases) does not only work as an on/off switch, but also controls the *bias* of the transistor in the on-state, as transport can still be tuned to be unidirectional or reciprocal. So this is not only an extension of the isolator design, but also an extension of a conventional transistor. Since signals just get redirected to other modes in the off-limit, considering the full four-mode model offers a very versatile configuration for controlling light flow.

VIII. Conclusion and further outlook

This thesis shows how expressing everything in terms of gauge-invariant phases can become quite useful for comparing full descriptions to effective models. Also, we showed how different regimes of the auxiliary reservoir influences transport and filtering properties of the system. Moreover, looking at modes and quadratures at the same time became a flexible tool for a greater insight into the constituents of the S-matrix and the output-noise, and helped us to find a clear distinction between reciprocal and unidirectional limits. Additionally, we showed how the dynamics of the auxiliary strongly influences transmissions, where a resonator with a bad quality factor (and strong dissipation) narrows down transmissions, moving the response closer to the resonant value. Furthermore, we hope this thesis emphasis on phases, transmissions and the output-noise provides a toolkit for constructing new, more versatile, yet minimal control systems. Especially the directional transistor we introduced, shows how a simple linearly coupled system yields novel regimes for the flow of light. The advantage of minimal systems is clear: Since the experimental realization of models is generally a challenging task, small few-boson systems are less prone to unwanted noise, and can be realized in a wide range of different platforms, such as photonic and optomechanical systems, or superconducting circuits. Thus, control systems which are easy to manufacture can become widely used components for complex control networks. For example, consider an application for controllable (unidirectional) transmission in quantum communication, more sophisticated fiber-optical distribution networks (remember that two circulators can be used to multiplex bidirectional transmission from two ports to a single optical-fiber [70]), or such systems could be used for high-fidelity state transfer in quantum computers.

This thesis offers many possible avenues to explore for future research. From a theorists perspective, an interesting next step is considering the signal to noise (S/N) ratio at output-ports. As the noise for a impedance-matched system in the unidirectional limit is quantum-limited, knowing the exact influence of signals on fluctuations could illuminate new ways of protecting signal-amplitudes while still maintaining a low amount of noise. Even though we considered parametric interactions in the beginning, most of this thesis focused only on linear interactions. As nonreciprocal systems with parametric interactions directionally amplify signals, see Ref. [1, 64, 71], understanding the exact impact of an amplification on the noise offers multiple promising applications, which is also true for other nonlinear effects. For example, by finding the S/N ratio, one could devise a way to find quantum-limited photonic analogs to low-noise amplifiers like silicon FET amplifiers. These components are frequently used in integrated solid state circuits and amplify low-power signals without considerably worsening its S/N ratio, see Ref. [72]. Since the optical isolator and the dissipative ring both work as narrow band-pass filters, another compelling direction is to directly engineer systems with a specific attenuation profile to filter out unwanted frequencies. Since the output-noise is dependent on a combination of S-matrix elements, finding a way to directly design S-matrix amplitudes themselves could offer a way to build filters with different profiles. Recall that the number of dips/peaks of scattering amplitudes depends on the number of eigenstates, so simply increasing the amount of modes (i.e. a nonreciprocal circulator with more than three modes) widens the frequency bandwidth of the filter, especially if dissipation rates are high. However, damping rates cannot be too high, as impedance-matching maximizes power-transfer, so there is an interplay between the signal-amplitude (maximized if impedance-matched) and the size of the passband of the filter (which can be increased by the number of modes). Additionally, when several two-port systems are connected in a lattice configuration, the S/N ratio could serve as an order parameter for topological phase transitions, by connecting the noise properties to topological invariants. In thermodynamics, a promising direction could be the investigation of thermodynamic uncertainty relation (TUR) violations. Especially defining quadrature currents and finding appropriate TURs remains an area that has not been explored yet.

Acknowledgements

I thank my supervisors Patrick Potts and Matteo Brunelli for their endless patience, guidance, time, and good ideas in the development of this thesis. The pursuit of this work has been a great opportunity to strengthen my understanding of physics, which I am very grateful for. I also thank the QTD Basel group for their hospitality and helpful conversations, namely Aaron Daniel, who always kept me motivated and loved stimulating discussions, Marcelo Janovitch, who tirelessly explained many concepts to me with an iron will, and Kacper Prech, who often provided his aid in technical manners. I also thank many physicists and fellow students for much needed help and support, namely Hans-Peter Weber, Jan Neuser, Joël Aschwanden, Brennan Hughes, Fabrizio Volante, Michael Sturzenegger, Livia Benedict, Roberto Scalera, Leon Behrens, Nadine Lenke, Kurt Meier, Alex Merstetter, Jannik Wyss, Luca Lichtenberger, Elias Oulaïd, Daniel Saenz, Gabriel Steiner and Jérôme Liviero. Lastly I thank my family and my friends, especially Clarissa and Gaetano Rago, and Joëlle Broch, calming my temper in stressful times.

You have all helped so much more than you thought.

-
- [1] A. Metelmann and A. A. Clerk, *Nonreciprocal Photon Transmission and Amplification via Reservoir Engineering*, Phys. Rev. X **5**, 021025 (2015).
- [2] J. F. Poyatos, J. I. Cirac, and P. Zoller, *Quantum Reservoir Engineering with Laser Cooled Trapped Ions*, Phys. Rev. Lett. **77**, 4728–4731 (1996).
- [3] D. Jalas, A. Petrov, M. Eich, W. Freude, S. Fan, Z. Yu, R. Baets, M. Popović, A. Melloni, J. D. Joannopoulos, M. Vanwolleghem, C. R. Doerr, and H. Renner, *What is - and what is not - an optical isolator*, Nat. Photonics **7**, 579–582 (2013).
- [4] N. Nagaosa and Y. Yanase, *Nonreciprocal Transport and Optical Phenomena in Quantum Materials*, Annu. Rev. Condens. Matter Phys. **15**, 63–83 (2023).
- [5] L. Deák and T. Fülöp, *Reciprocity in quantum, electromagnetic and other wave scattering*, Ann. Phys. (NY) **327**, 1050–1077 (2012).
- [6] F. Ruesink, M.-A. Miri, A. Alù, and E. Verhagen, *Nonreciprocity and magnetic-free isolation based on optomechanical interactions*, Nat. Commun. **7** (2016).
- [7] T.-T. Dong, N. Wang, Z.-X. Su, N. Yuan, S.-Y. Li, L. Yu, and A.-D. Zhu, *Enhancement and manipulation of nonreciprocity via dissipative coupling*, Opt. Express **32**, 25726–25739 (2024).
- [8] N. Reiskarimian, A. Nagulu, T. Dinc, and H. Krishnaswamy, *Nonreciprocal Electronic Devices: A Hypothesis Turned Into Reality*, IEEE Microw. Mag. **20**, 94–111 (2019).
- [9] A. Nagulu and H. Krishnaswamy, *Non-Magnetic Non-Reciprocal Microwave Components — State of the Art and Future Directions*, IEEE J. Microw. **1**, 447–456 (2021).
- [10] H.-L. Huang, D. Wu, D. Fan, and X. Zhu, *Superconducting quantum computing: a review*, Sci. China Inf. Sci. **63** (2020).
- [11] D. Malz, L. D. Tóth, N. R. Bernier, A. K. Feofanov, T. J. Kippenberg, and A. Nunnenkamp, *Quantum-Limited Directional Amplifiers with Optomechanics*, Phys. Rev. Lett. **120** (2018).
- [12] F. Lecocq, L. Ranzani, G. Peterson, K. Cicak, A. Metelmann, S. Kotler, R. Simmonds, J. Teufel, and J. Aumentado, *Microwave Measurement beyond the Quantum Limit with a Nonreciprocal Amplifier*, Phys. Rev. Appl. **13**, 044005 (2020).
- [13] K. Fang, J. Luo, A. Metelmann, M. H. Matheny, F. Marquardt, A. A. Clerk, and O. Painter, *Generalized non-reciprocity in an optomechanical circuit via synthetic magnetism and reservoir engineering*, Nat. Phys. **13**, 465–471 (2017).
- [14] A. A. Clerk, *Introduction to quantum non-reciprocal interactions: from non-Hermitian Hamiltonians to quantum master equations and quantum feedforward schemes*, SciPost Phys. Lect. Notes, 44 (2022).
- [15] Y. Aharonov and D. Bohm, *Significance of Electromagnetic Potentials in the Quantum Theory*, Phys. Rev. **115**, 485–491 (1959).
- [16] M. Peshkin and A. Tonomura, *The Aharonov-Bohm Effect*, Lect. Notes Phys. (Springer, Berlin, Heidelberg, 2014).
- [17] A. Metelmann and H. E. Türeci, *Nonreciprocal signal routing in an active quantum network*, Phys. Rev. A **97**, 043833 (2018).
- [18] C. Caloz, A. Alù, S. Tretyakov, D. Sounas, K. Achouri, and Z.-L. Deck-Léger, *Electromagnetic Nonreciprocity*, Phys. Rev. Appl. **10**, 047001 (2018).
- [19] R. Luo, G. Benenti, G. Casati, and J. Wang, *Onsager reciprocal relations with broken time-reversal symmetry*, Phys. Rev. Res. **2**, 022009 (2020).
- [20] R. Carminati, J. J. Sáenz, J.-J. Greffet, and M. Nieto-Vesperinas, *Reciprocity, unitarity, and time-reversal symmetry of the S matrix of fields containing evanescent components*, Phys. Rev. A **62**, 012712 (2000).
- [21] A. W. W. Ludwig, *Topological phases: classification of topological insulators and superconductors of non-interacting fermions, and beyond*, Phys. Scr. **2016**, 014001 (2015).
- [22] A. Maznev, A. Every, and O. Wright, *Reciprocity in reflection and transmission: What is a ‘phonon diode’?*, Wave Motion **50**, 776–784 (2013).
- [23] A. Invitado, *The Aharonov-Bohm effect, controversial features of a long-standing debate* (2018).
- [24] M. Peshkin, *Aharonov-Bohm effect in bound states: Theoretical and experimental status*, Phys. Rev. A **23**, 360–361 (1981).
- [25] M. Peshkin, *The Aharonov-Bohm effect: Why it cannot be eliminated from quantum mechanics*, Phys. Rep. **80**, 375–386 (1981).
- [26] C. Liu, *The Aharonov-Bohm Effect and the Reality of Wave Packets*, Br. J. Philos. Sci. **45**, 977–1000 (1994).
- [27] T. Lancaster and S. J. Blundell, *Quantum Field Theory for the Gifted Amateur* (Oxford University Press, 2014).
- [28] R. D. Parks, *Quantized Magnetic Flux in Superconductors*, Science **146**, 1429–1435 (1964).
- [29] R. B. Laughlin, *Anomalous Quantum Hall Effect: An Incompressible Quantum Fluid with Fractionally Charged Excitations*, Phys. Rev. Lett. **50**, 1395–1398 (1983).
- [30] F. D. M. Haldane, *Model for a Quantum Hall Effect without Landau Levels: Condensed-Matter Realization of the “Parity Anomaly”*, Phys. Rev. Lett. **61**, 2015–2018 (1988).
- [31] E. Cohen, H. Larocque, F. Bouchard, F. Nejdassattari, Y. Gefen, and E. Karimi, *Geometric phase from Aharonov–Bohm to Pancharatnam–Berry and beyond*, Nature Reviews Physics **1**, 437–449 (2019).
- [32] J. C. Solem and L. C. Biedenharn, *Understanding geometrical phases in quantum mechanics: An elementary example*, Found. Phys. **23**, 185–195 (1993).
- [33] D. F. Walls and G. J. Milburn, *Quantum optics* (Springer Berlin, 2008).
- [34] P. Meystre, *Quantum Optics: Taming the Quantum*, Graduate Texts in Physics (Springer International Publishing, 2021).
- [35] C. Weedbrook, S. Pirandola, R. García-Patrón, N. J. Cerf, T. C. Ralph, J. H. Shapiro, and S. Lloyd, *Gaussian quantum information*, Rev. Mod. Phys. **84**, 621–669 (2012).
- [36] M. Zhang, *Properties and Application of Gaussian Quantum Processes* (2021), arXiv:2107.01474.

- [37] R. Loudon, *The Quantum Theory of Light* (Oxford University Press, 2000).
- [38] U. Leonhardt and H. Paul, *Measuring the quantum state of light*, Prog. Quantum Electron. **19**, 89–130 (1995).
- [39] S. Olivares, *Quantum optics in the phase space: A tutorial on Gaussian states*, Eur. Phys. J.: Spec. Top. **203**, 3–24 (2012).
- [40] G. Adesso, S. Ragy, and A. R. Lee, *Continuous Variable Quantum Information: Gaussian States and Beyond*, Open Syst. Inf. Dyn. **21**, 1440001 (2014).
- [41] A. A. Clerk, M. H. Devoret, S. M. Girvin, F. Marquardt, and R. J. Schoelkopf, *Introduction to quantum noise, measurement, and amplification*, Rev. Mod. Phys. **82**, 1155–1208 (2010).
- [42] V. Weisskopf and E. Wigner, *Berechnung der natürlichen Linienbreite auf Grund der Diracschen Lichttheorie*, Z. Phys. **63**, 54–73 (1930).
- [43] W. Heisenberg, *A quantum-theoretical reinterpretation of kinematic and mechanical relations*, Z. Phys. **33**, 879–893 (1925).
- [44] I. J. R. Aitchison, D. A. MacManus, and T. M. Snyder, *Understanding Heisenberg’s “magical” paper of July 1925: A new look at the calculational details*, Am. J. Phys. **72**, 1370–1379 (2004).
- [45] P. A. M. Dirac, *The fundamental equations of quantum mechanics*, Proc. R. Soc. A: Math. Phys. Eng. Sci. **109**, 642–653 (1925).
- [46] C. Cohen-Tannoudji, B. Diu, and F. Laloë, *Quantum Mechanics* (Wiley, 1977).
- [47] D. S. Lemons and A. Gythiel, *Paul Langevin’s 1908 paper “On the Theory of Brownian Motion” [“Sur la théorie du mouvement brownien,” C. R. Acad. Sci. (Paris) 146, 530–533 (1908)]*, Am. J. Phys. **65**, 1079–1081 (1997).
- [48] A. Einstein, *Zur Theorie der Brownschen Bewegung*, Ann. Phys. (Berl.) **324**, 371–381 (1906).
- [49] C. W. Gardiner and M. J. Collett, *Input and output in damped quantum systems: Quantum stochastic differential equations and the master equation*, Phys. Rev. A **31**, 3761–3774 (1985).
- [50] R. Zwanzig, *Nonequilibrium Statistical Mechanics* (Oxford University Press, 2001).
- [51] K. Jacobs, *Topics in Quantum Measurement and Quantum Noise* (1998), arXiv:quant-ph/9810015.
- [52] K. Fujii, *Introduction to the Rotating Wave Approximation (RWA) : Two Coherent Oscillations* (2014), arXiv:1301.3585.
- [53] R. A. Brualdi and D. Cvetkovic, *A Combinatorial Approach to Matrix Theory and Its Applications* (Chapman and Hall/CRC, 2008).
- [54] J. Zhu, *Bogoliubov-de Gennes Method and Its Applications*, Lect. Notes Phys. (Springer, Berlin, Heidelberg, 2016).
- [55] M.-W. Xiao, *Theory of transformation for the diagonalization of quadratic Hamiltonians* (2009), arXiv:0908.0787.
- [56] A. Das, *Pseudo-Hermitian quantum mechanics*, J. Phys. Conf. Ser. **287**, 012002 (2011).
- [57] D. M. Pozar, *Microwave engineering; 3rd ed.* (Wiley, Hoboken, NJ, 2005).
- [58] A. G. Fox, S. E. Miller, and M. T. Weiss, *Behavior and applications of ferrites in the microwave region*, Bell Syst. Tech. J. **34**, 5–103 (1955).
- [59] T. He, Z. Zhang, J. Zhu, Y. Shi, Z. Li, H. Wei, Z. Wei, Y. Li, Z. Wang, C.-W. Qiu, and X. Cheng, *Scattering exceptional point in the visible*, Light Sci. Appl. **12** (2023).
- [60] M.-A. Miri and A. Alù, *Exceptional points in optics and photonics*, Science **363**, eaar7709 (2019).
- [61] W. D. Heiss, *The physics of exceptional points*, J. Phys. A: Math. Theor. **45**, 444016 (2012).
- [62] A. Li, H. Wei, M. Cotrufo, W. Chen, S. Mann, X. Ni, B. Xu, J. Chen, J. Wang, S. Fan, C.-W. Qiu, A. Alù, and L. Chen, *Exceptional points and non-Hermitian photonics at the nanoscale*, Nat. Nanotechnol. **18**, 10.1038/s41565-023-01408-0 (2023).
- [63] Z. Chen, Q. Liu, J. Zhou, P. Zhao, H. Yu, T. Li, and Y. Liu, *Parity-dependent unidirectional and chiral photon transfer in reversed-dissipation cavity optomechanics*, Fundamental Research **3**, 21–29 (2023).
- [64] C. C. Wanjura, M. Brunelli, and A. Nunnenkamp, *Topological framework for directional amplification in driven-dissipative cavity arrays*, Nat. Commun. **11** (2020).
- [65] M. V. Moskalets, *Scattering Matrix Approach to Non-Stationary Quantum Transport* (Imperial College Press, London, 2012).
- [66] C. S. Kong, *A general maximum power transfer theorem*, IEEE Trans. on Educ. **38**, 296–298 (1995).
- [67] K. Jacobs, *Quantum Measurement Theory and its Applications* (Cambridge University Press, 2014).
- [68] R. Hui and M. O’Sullivan, *Characterization of Optical Devices*, in *Fiber Optic Measurement Techniques* (Academic Press, Boston, 2009) pp. 259–363.
- [69] P. Lambropoulos and D. Petrosyan, *Fundamentals of Quantum Optics and Quantum Information* (Springer, Berlin, Heidelberg, 2006).
- [70] R. J. Cameron, C. M. Kudsia, and R. R. Mansour, *Multiplexer Theory and Design*, in *Microwave Filters for Communication Systems: Fundamentals, Design, and Applications* (Wiley Telecom, 2018) pp. 569–608.
- [71] M. Tian, F. Sun, K. Shi, H. Xu, Q. He, and W. Zhang, *Nonreciprocal amplification transition in a topological photonic network*, Photon. Res. **11**, 852–857 (2023).
- [72] A. Boornard, E. Herrmann, and S. Hsu, *Low-noise integrated silicon-gate FET amplifier*, IEEE J. Solid-State Circuits **10**, 542–544 (1975).
- [73] G. E. Uhlenbeck and L. S. Ornstein, *On the Theory of the Brownian Motion*, Phys. Rev. **36**, 823–841 (1930).
- [74] G. T. Landi, M. J. Kewming, M. T. Mitchison, and P. P. Potts, *Current Fluctuations in Open Quantum Systems: Bridging the Gap Between Quantum Continuous Measurements and Full Counting Statistics*, PRX Quantum **5**, 020201 (2024).
- [75] Y. He and C.-C. Chien, *Topological classifications of quadratic bosonic excitations in closed and open systems with examples*, J. Phys. Condens. Matter **34**, 175403 (2022).
- [76] M. Verschuren, *Coherent states in quantum mechanics (Bachelorthesis)* (2011).
- [77] A. Ullah, M. T. Naseem, and Özgür E. Müstecaplıoğlu, *Preparation of thermal coherent state and its role in quantum thermometry* (2023), arXiv:2306.04369.

APPENDIX

A. THEORETICAL BACKGROUND

To calculate the equations of motion of a dissipative system we need the toolbox of open quantum systems, usually via the *Lindblad master equation*

$$\frac{d}{dt}\hat{\rho} = \mathcal{L}\hat{\rho} \equiv \underbrace{-i[\hat{H}_{\text{sys}}, \hat{\rho}]}_{\text{von Neumann eq.}} + \underbrace{\sum_j \kappa_j [1 - \bar{n}_j(\omega_j)] \mathcal{D}[\hat{a}_j]\hat{\rho} + \kappa_j \bar{n}_j(\omega_j) \mathcal{D}[\hat{a}_j^\dagger]\hat{\rho}}_{\text{local dissipation}}, \quad (\text{A1})$$

for quantum systems coupled to Markovian reservoirs with strength κ_j , where \mathcal{L} is the *Liouvillian superoperator*, acting on an abstract operator-space and transforming our system operator $\hat{\rho}$ via an universal dynamical map to a new system state $\hat{\rho}'$ at a different time. The first term of the equation above is the (Hermitian) von Neumann equation and describes the coherent, energy-conserving dynamics, whereas the second and third term are the non-Hermitian part of the dynamics and encode the dissipation of particles/energy from the system to its environment and vice versa. Here, $\bar{n}_j(\omega_j)$ is the Bose-Einstein occupation of a reservoir with temperature T_j , chemical potential μ_j , and ω_j is the respective energy of a particle leaving/entering. The dissipation is described by the *dissipation superoperator*

$$\mathcal{D}[\hat{\sigma}]\hat{\rho} = \hat{\sigma}\hat{\rho}\hat{\sigma}^\dagger - \frac{1}{2}\{\hat{\sigma}^\dagger\hat{\sigma}, \hat{\rho}\}, \quad (\text{A2})$$

where $\hat{\sigma}$ is a system jump operator and

$$\{\hat{A}, \hat{B}\} = \hat{A}\hat{B} + \hat{B}\hat{A}, \quad (\text{A3})$$

is the anticommutator for any general operators \hat{A}, \hat{B} . At this point we will set the occupation-factor $\bar{n}_j(\omega_j) = 0$, only allowing for dissipation leaving our system. More precisely, the remaining dissipator in Eq. (A1) now describes how each cavity j is being coupled to a local Markovian reservoir with coupling strength κ_j and jump operator \hat{a}_j . In general, one could also include the third term of Eq. (A1), where the system gains energy/particles from the reservoir, but this is dismissed since we will mitigate for this later using the formalism of input-output theory. To calculate the dynamics of the cavity mode expectation value of a respective cavity \hat{a}_s , one could transform the Lindblad master equation into the Heisenberg picture. A way to do this is by using the adjoint Liouvillian, defined as

$$\mathcal{L}^\dagger \hat{a}_s \equiv +i[\hat{H}_{\text{sys}}, \hat{a}_s] + \sum_j \kappa_j \mathcal{D}^\dagger[\hat{a}_j]\hat{a}_s, \quad \text{with} \quad \mathcal{D}^\dagger[\hat{\sigma}]\hat{a}_s = \hat{\sigma}^\dagger \hat{a}_s \hat{\sigma} - \frac{1}{2}\{\hat{\sigma}^\dagger \hat{\sigma}, \hat{a}_s\}, \quad (\text{A4})$$

where $\mathcal{D}^\dagger[\hat{\sigma}]\hat{a}_s$ is the adjoint dissipator. Then, one can express the time dynamics of the operator expectation value with the Heisenberg equation of motion and simply calculate

$$\frac{d}{dt} \langle \hat{a}_s \rangle = \text{Tr} \left\{ \hat{a}_s \frac{d}{dt} \hat{\rho} \right\} = \text{Tr} \{ \hat{a}_s (\mathcal{L}\hat{\rho}) \} = \text{Tr} \{ (\mathcal{L}^\dagger \hat{a}_s) \hat{\rho} \} = \langle \mathcal{L}^\dagger \hat{a}_s \rangle. \quad (\text{A5})$$

This will give us the equations of motion for the cavity expectation values.

B. SYSTEM AND MODEL

1. Isolating the gauge-invariant phases

Since some phases are just the complex conjugates of others, it is sufficient to only consider six terms

$$\begin{aligned}
 1. \quad & \alpha_{12} + \gamma_2 - \gamma_1, & 4. \quad & \beta_{12} - \gamma_2 - \gamma_1, \\
 2. \quad & \alpha_{31} + \gamma_1 - \gamma_3, & 5. \quad & \beta_{31} - \gamma_1 - \gamma_3, \\
 3. \quad & \alpha_{32} + \gamma_2 - \gamma_3, & 6. \quad & \beta_{32} - \gamma_2 - \gamma_3,
 \end{aligned} \tag{B1}$$

for the gauge transformation. To find a useful transformation which rewrites eqs. (3.30) in terms of the before mentioned Aharonov-Bohm phases, we can safely set three of the terms above to zero, since the only relevant phases are Φ , ϑ_1 and ϑ_2 . This choice is not unique but we hereby choose to set the terms 2., 3. and 6. to zero, which gives us a closed set of equations with

$$2. \quad \alpha_{31} + \gamma_1 - \gamma_3 \stackrel{!}{=} 0 \implies \gamma_1 = \gamma_3 - \alpha_{31}, \tag{B2}$$

$$3. \quad \alpha_{32} + \gamma_2 - \gamma_3 \stackrel{!}{=} 0 \implies \gamma_2 = \gamma_3 - \alpha_{32}, \tag{B3}$$

$$6. \quad \beta_{32} - \gamma_2 - \gamma_3 \stackrel{!}{=} 0 \implies \gamma_3 = -\gamma_2 + \beta_{32}, \tag{B4}$$

with the following solutions

$$2. \quad \gamma_1 = \frac{\beta_{32} + \alpha_{32}}{2} - \alpha_{31}, \quad 3. \quad \gamma_2 = \frac{\beta_{32} - \alpha_{32}}{2}, \quad 6. \quad \gamma_3 = \frac{\beta_{32} + \alpha_{32}}{2}. \tag{B5}$$

Using these solutions, the remaining terms simply become

$$\begin{aligned}
 1. \quad & \alpha_{12} + \gamma_2 - \gamma_1 = \alpha_{12} + \alpha_{31} - \alpha_{32} = \Phi, \\
 4. \quad & \beta_{12} - \gamma_2 - \gamma_1 = \beta_{12} + \alpha_{31} - \beta_{32} = -\vartheta_2, \\
 5. \quad & \beta_{31} - \gamma_1 - \gamma_3 = \beta_{31} + \alpha_{31} - \beta_{32} - \alpha_{32} + (\beta_{12} - \beta_{12}) \\
 & = \beta_{12} + \alpha_{31} - \beta_{32} - \beta_{12} + \beta_{31} - \alpha_{32} \\
 & = -(\vartheta_1 + \vartheta_2).
 \end{aligned} \tag{B6}$$

Note, that if we want to reorder these phases, we can just perform a gauge-transformation of the type

$$\langle a_j \rangle \rightarrow \langle a'_j \rangle = e^{i\gamma_j} \langle a_j \rangle, \tag{B7}$$

where γ_j is any of the non-trivial Aharonov-Bohm phases considered. This has a neat implication: Suppose, we have a more complicated model and want to remove a certain interaction. Also suppose that the interaction is needed to have a non-trivial loop. If the interaction is now lacking, it would imply that some ϑ_j vanishes, but maybe this is not seen easily in the equations of motion. By performing the transformation above, the phase γ_j can be placed in a way where it will only appear at that interaction site - and by removing the interaction, one will faithfully lose the gauge-invariant phase.

2. Counting the number of interactions for a general bilinear system

Here, the number of interactions for a general bilinear system with N - modes is determined. This should give us a preliminary hint at the exact number of non-trivial phases for a general system. Each mode can couple to $N - 1$ other modes via BS interactions (excluding that a mode couples to itself). Nonetheless, since exactly $N - 1$ couplings

would be counted twice, this number needs to be divided by two. For N resonators, the number of BS interactions is exactly

$$\# \text{ BS int. for } N \text{ modes} = N(N-1)/2.$$

If we also include adjoint modes, this number becomes twice as large and coincides with the number of two-mode squeezing interactions. It simply reads

$$\# \text{ BS int. for } N \text{ modes (and adjoints)} = \# \text{ TMS int. for } N \text{ modes} = N(N-1),$$

which gives us the total number of all interactions of a bilinear system with N (and N adjoint) modes

$$\# \text{ Total int.} = 2N(N-1).$$

However, exactly finding the number of non-trivial phases is still not straightforward and can be seen as a challenging task for the future.

3. Understanding the outer-product of non-Hermitian vectors

Before we can write Eq. (3.28) as a system of differential equations which encode the coherent and dissipative dynamics of the complete system, we need to find the commutator $[\mathbf{a}, \mathbf{a}^\dagger]$ first. However, the definition of \mathbf{a}^\dagger introduces an important nuance when calculating the product of two vectors: If we consider the product $\mathbf{a}\mathbf{a}^\dagger$, the result is a matrix due to the way the outer-product acts, but if we consider $\mathbf{a}^\dagger\mathbf{a}$ from a naive standpoint, this would give us a scalar. The commutator would then be ill-defined and we need to find an adequate way to perform the outer-product. Thus, we need to make a few remarks: Take for an example two vectors $\mathbf{v}_1, \mathbf{v}_2$, with hermitian-operators defined as $\mathbf{v}_i = (\hat{x}_i, \hat{p}_i)^T$, then the commutator can be calculated as

$$[\mathbf{v}_1, \mathbf{v}_2] = \mathbf{v}_1\mathbf{v}_2^T - (\mathbf{v}_2\mathbf{v}_1^T)^T. \quad (\text{B8})$$

This gives us a matrix with the correct elements, which can be checked easily and is a known result for hermitian operators (see Ref. [67]). Luckily, the same logic can be applied to devise a way for dealing with non-Hermitian operators.

Consider a simple vector with only two elements $\mathbf{a} = (\hat{a}, \hat{a}^\dagger)^T$ for now, where the difference to the case above is clear: Acting with a dagger on the outside of a vector transposes the vector and daggers the elements

$$\mathbf{a}^\dagger = \left[\begin{pmatrix} \hat{a} \\ \hat{a}^\dagger \end{pmatrix} \right]^\dagger \equiv \left[\begin{pmatrix} (\hat{a})^\dagger \\ (\hat{a}^\dagger)^\dagger \end{pmatrix} \right]^T = (\hat{a}^\dagger, \hat{a}), \quad (\text{B9})$$

but we need to find an action which gives us a column vector of conjugate transposed elements (or more precisely just permutes the elements with their adjoint counterparts), but does not transpose the vector itself, such that we can find a way to define the outer-product of $\mathbf{a}^\dagger\mathbf{a}$. For this, we introduce a slight nuance for algebraic precision: The action of considering the daggered elements inside a vector will be denoted by a new symbol \ddagger , which permutes the elements inside the vector. Some authors use the $*$ symbol at the level of elements instead of the usual \dagger , nonetheless, we will use basically do the opposite and keep the \dagger for the adjoint elements inside the vector, but use \ddagger for the non-transposed adjoint vector itself. Consider

$$\mathbf{a}^\ddagger = \begin{pmatrix} \hat{a}^\dagger \\ \hat{a} \end{pmatrix}, \quad (\text{B10})$$

which is nothing more than the action of permuting the elements inside the vector by multiplying the extended Pauli matrix $\mathbf{\Lambda}_x = \sigma_x \otimes \mathbb{1}_N$ to it (where the number of modes is $N = 1$ for this simple case), namely

$$\mathbf{a}^\ddagger \equiv \mathbf{\Lambda}_x \mathbf{a} = \begin{pmatrix} \hat{a}^\ddagger \\ \hat{a} \end{pmatrix}. \quad (\text{B11})$$

Note, that $\mathbf{\Lambda}_x$ is orthogonal with $\mathbf{\Lambda}_x^T = \mathbf{\Lambda}_x^{-1} = \mathbf{\Lambda}_x$. All this translates to

$$\mathbf{a}^\ddagger = (\mathbf{a}^\ddagger)^T = (\mathbf{\Lambda}_x \mathbf{a})^T = \mathbf{a}^T \mathbf{\Lambda}_x, \quad (\text{B12})$$

or alternatively

$$\mathbf{a}^\ddagger = (\mathbf{a}^\ddagger)^T, \quad (\text{B13})$$

where the outer-product $\mathbf{a}\mathbf{a}^\ddagger$ is still defined as the expected action

$$\mathbf{a}\mathbf{a}^\ddagger = \mathbf{a}(\mathbf{a}^\ddagger)^T = \begin{pmatrix} \hat{a} \\ \hat{a}^\ddagger \end{pmatrix} \left[\mathbf{\Lambda}_x \begin{pmatrix} \hat{a} \\ \hat{a}^\ddagger \end{pmatrix} \right]^T = \begin{pmatrix} \hat{a} \\ \hat{a}^\ddagger \end{pmatrix} (\hat{a}^\ddagger, \hat{a}), \quad (\text{B14})$$

of a vector multiplied to a transposed vector from the left side - resulting in a matrix. However, if the daggered vector is on the left side of the multiplication, we can use the newly defined symbol and define the outer-product in a similar way to the hermitian example above

$$\mathbf{a}^\ddagger \mathbf{a} = (\mathbf{a}^\ddagger \mathbf{a}^T)^T, \quad (\text{B15})$$

which again gives us the desired, properly defined product of vectors resulting in a matrix, as \ddagger only acts at the level of elements and permutes them. This implies

$$\mathbf{a}^\ddagger \mathbf{a} = (\mathbf{a}^\ddagger \mathbf{a}^T)^T = ([\mathbf{\Lambda}_x \mathbf{a}] \mathbf{a}^T)^T = ([\mathbf{\Lambda}_x] [\mathbf{a}\mathbf{a}^T])^T = (\mathbf{a}\mathbf{a}^T)^T \mathbf{\Lambda}_x, \quad (\text{B16})$$

where we used $(\mathbf{A}\mathbf{B})^T = \mathbf{B}^T \mathbf{A}^T$ (for any matrices \mathbf{A}, \mathbf{B}), and $\mathbf{\Lambda}_x^T = \mathbf{\Lambda}_x$ for the last equality. We need to make an additional remark here: The way we applied the usual matrix-transpose only acts on the level of matrices, whereas the transpose *inside* the outer-product (acting on the level of vectors) does not. To ensure consistent algebra, applying the transpose of the last equality to the inside of the outer-product would give us a wrong equality, thus we need to be careful with it. To mitigate for that, we will only act with the transpose on matrices (or products of matrices and vectors, but never on vector-vector outer-products), where it acts in the usual manner. All this implies that

$$(\mathbf{a}\mathbf{a}^T)^T \mathbf{\Lambda}_x \neq \mathbf{a}\mathbf{a}^T \mathbf{\Lambda}_x, \quad (\text{B17})$$

does not hold. This concludes our remarks.

4. Generalizing the transformation matrix

For $N = 1$, we have $\mathbf{v} = (x, p)^T$ and $\mathbf{a} = (a, a^\ddagger)^T$, implying

$$\mathbf{v} = \mathbf{T}_1 \mathbf{a}, \quad \text{with} \quad \mathbf{T}_1 = \frac{1}{\sqrt{2}} \begin{pmatrix} 1 & 1 \\ -i & i \end{pmatrix}. \quad (\text{B18})$$

For $N = 2$, we have $\mathbf{v} = (x_1, p_1, x_2, p_2)^T$ and $\mathbf{a} = (a_1, a_2, a_1^\ddagger, a_2^\ddagger)^T$, implying

$$\mathbf{v} = \mathbf{T}_2 \mathbf{a}, \quad \text{with} \quad \mathbf{T}_{N=2} = \frac{1}{\sqrt{2}} \begin{pmatrix} 1 & 0 & 1 & 0 \\ -i & 0 & i & 0 \\ 0 & 1 & 0 & 0 \\ 0 & -i & 0 & i \end{pmatrix}. \quad (\text{B19})$$

We would like to find a way to write this for a general case. However, simply multiplying

$$\mathbf{T}_1 \otimes \mathbf{1}_{N=2} = \frac{1}{\sqrt{2}} \begin{pmatrix} 1 & 0 & 1 & 0 \\ 0 & 1 & 0 & 1 \\ -i & 0 & i & 0 \\ 0 & -i & 0 & i \end{pmatrix}, \quad (\text{B20})$$

does not give us the right expression (similarly for $\mathbf{1}_{N=2} \otimes \mathbf{T}_1$), there is still a permutation needed

$$\mathbf{P}_C = \begin{pmatrix} 1 & 0 & 0 & 0 \\ 0 & 0 & 1 & 0 \\ 0 & 1 & 0 & 0 \\ 0 & 0 & 0 & 1 \end{pmatrix}. \quad (\text{B21})$$

Applying this will give us the correct expression

$$\mathbf{T}_2 = \mathbf{P}_C (\mathbf{T}_1 \otimes \mathbf{1}_2). \quad (\text{B22})$$

However, this is only the formula for $N = 2$, can we find an expression for \mathbf{P}_C for greater N in a formal way? Yes, for a $l \times k$ matrix, the permutation leaves corner elements invariant $(1, 1) = (l, k) = 1$, and permutes just the insides. This can be achieved with a so-called *commutation matrix*, defined as

$$\mathbf{P}_C^{(l,k)} = \sum_{i=1}^l \sum_{j=1}^k (\mathbf{e}_i \otimes \mathbf{e}_j)(\mathbf{e}_j \otimes \mathbf{e}_i)^T, \quad (\text{B23})$$

where \mathbf{e}_i (\mathbf{e}_j) is a vector of dimension l (k) with zero entries except the i -th (j -th) entry. Since we only have two types of fields (modes and adjoints), it follows that $k = 2$, and $l = N$ represents the number of modes we have. This way, a general transformation matrix for N modes can be written as

$$\mathbf{T}_N = \mathbf{P}_C^{(N,2)} (\mathbf{T} \otimes \mathbf{1}_N). \quad (\text{B24})$$

5. Dynamical matrix of the dissipative ring in the quadrature representation

The dynamical matrix \mathbf{M} can be explicitly written as

$$\mathbf{M} = \mathbf{T} \mathbf{D} \mathbf{T}^\dagger = \begin{pmatrix} -\kappa_1/2 & 0 & \Im(J_{12} + \lambda_{12}) & \Re(J_{12} - \lambda_{12}) & -\Im(J_{31} - \lambda_{31}) & \Re(J_{31} - \lambda_{31}) \\ 0 & -\kappa_1/2 & -\Re(J_{12} + \lambda_{12}) & \Im(J_{12} - \lambda_{12}) & -\Re(J_{31} + \lambda_{31}) & -\Im(J_{31} + \lambda_{31}) \\ -\Im(J_{12} - \lambda_{12}) & \Re(J_{12} - \lambda_{12}) & -\kappa_2/2 & 0 & -\Im(J_{32} - \lambda_{32}) & \Re(J_{32} - \lambda_{32}) \\ -\Re(J_{12} + \lambda_{12}) & -\Im(J_{12} + \lambda_{12}) & 0 & -\kappa_2/2 & -\Re(J_{32} + \lambda_{32}) & -\Im(J_{32} + \lambda_{32}) \\ \Im(J_{31} + \lambda_{31}) & \Re(J_{31} - \lambda_{31}) & \Im(J_{32} + \lambda_{32}) & \Re(J_{32} - \lambda_{32}) & -\kappa_3/2 & 0 \\ -\Re(J_{31} + \lambda_{31}) & \Im(J_{31} - \lambda_{31}) & -\Re(J_{32} + \lambda_{32}) & \Im(J_{32} - \lambda_{32}) & 0 & -\kappa_3/2 \end{pmatrix}, \quad (\text{B25})$$

which is time-independent for the full model (since the hopping J_{ij} , squeezing λ_{ij} , and damping κ_i parameters are explicitly time-independent). In contrast to the mode representation, this matrix is completely real, which is an important feature in this representation for the full model.

6. Dynamical matrix of the optical isolator in the mode representation

The dynamical matrix of $i\omega \langle \mathbf{a}_{\text{eff}}[\omega] \rangle = \mathbf{D}_{\text{eff}}[\omega] \langle \mathbf{a}_{\text{eff}}[\omega] \rangle$ in the basis $\mathbf{a}_{\text{eff}} = (a_1, a_2, a_1^\dagger, a_2^\dagger)^T$ is

$$\mathbf{D}_{\text{eff}}[\omega] = \frac{1}{2} \begin{pmatrix} -\Gamma_1[\omega] - \kappa_1 & -i(2J + i\mu\Gamma[\omega]) & 0 & -i(2\lambda + i\nu\Gamma[\omega]) \\ -i(2J^* + i\mu^*\Gamma[\omega]) & -\Gamma_2[\omega] - \kappa_2 & -i(2\lambda - i\nu\Gamma[\omega]) & 0 \\ 0 & i(2\lambda^* - i\nu^*\Gamma^*[\omega]) & -\Gamma_1^*[\omega] - \kappa_1 & i(2J^* - i\mu^*\Gamma^*[\omega]) \\ i(2\lambda^* + i\nu^*\Gamma^*[\omega]) & 0 & i(2J - i\mu\Gamma[\omega]) & -\Gamma_2^*[\omega] - \kappa_2 \end{pmatrix}, \quad (\text{B26})$$

7. Dynamical matrix of the optical isolator in the quadrature representation

Using the same transformation as above, we can recover the following dynamical matrix for the effective model in the quadrature representation

$$\mathbf{M}_{\text{eff}}[\omega] = \frac{1}{2} \begin{pmatrix} -\kappa_1 - \Re(\Gamma_1[\omega]) & \Im(\Gamma_1[\omega]) & 2\Im(J + \lambda) + \Re((\mu + \nu)\Gamma[\omega]) & 2\Re(J - \lambda) - \Im((\mu - \nu)\Gamma[\omega]) \\ -\Im(\Gamma_1[\omega]) & -\kappa_1 - \Re(\Gamma_1[\omega]) & -2\Re(J + \lambda) + \Im((\mu + \nu)\Gamma[\omega]) & 2\Im(J - \lambda) + \Re((\mu - \nu)\Gamma[\omega]) \\ -2\Im(J - \lambda) + \Re((\mu^* - \nu)\Gamma[\omega]) & 2\Re(J - \lambda) - \Im((\mu^* + \nu)\Gamma[\omega]) & -\kappa_2 - \Re(\Gamma_2[\omega]) & \Im(\Gamma_2[\omega]) \\ -2\Re(J + \lambda) + \Im((\mu^* - \nu)\Gamma[\omega]) & -2\Im(J + \lambda) + \Re((\mu^* + \nu)\Gamma[\omega]) & -\Im(\Gamma_2[\omega]) & -\kappa_2 - \Re(\Gamma_2[\omega]) \end{pmatrix}, \quad (\text{B27})$$

which is frequency-dependent and complex for the non-Markovian correction.

8. Derivation of the energies by transforming the system to momentum space

Note, that this derivation closely resembles the calculations done in Clerk [14].

For ease of notation, we will use a different labeling convention for the beam-splitter interaction between mode 1 and 2, namely, $J_{21} = J_{12}^*$. More generally, we can write $J_{jj'} = J_{j'j}^*$. Also, note that even though we use the label a_3 for the auxilliary, mode 1 and mode 3 still only exhibit a distance of 1 from each other, thus we could also write $a_3 \rightarrow a_{2'}$. However, this would become a bit messy to read, and thus we stay at the usual notation but keep in mind that the distance is just 1 in the real-space lattice. With this, our Hamiltonian (for $N = 3$) is written as

$$H_{\text{sys}} = J_{21}a_2^\dagger a_1 + J_{31}a_3^\dagger a_1 + J_{32}a_3^\dagger a_2 + \text{H.c.} = \sum_{j>j'} J_{jj'} a_j^\dagger a_{j'} + J_{jj'}^* a_{j'}^\dagger a_j. \quad (\text{B28})$$

If all interactions are the same $J \equiv J_{21} = J_{31} = J_{32}$, which implies that the gauge-invariant phase is equally distributed over all interactions $\Phi/3$, the system becomes *translationally invariant*. Thus, can employ *Bloch's theorem* [46] and write the basis states as a sum of *plane-wave* solutions. For this, we introduce the single-particle position eigenstate $|j\rangle \equiv a_j^\dagger|0\rangle$ (where $|0\rangle$ is our vacuum state) and write the plane-waves as a linear combination of position states

$$|k_m\rangle = \frac{1}{\sqrt{N}} \sum_j e^{ik_m j} |j\rangle, \quad (\text{B29})$$

with the single particle wave-vector

$$k_m = \frac{2\pi}{N} m, \quad (\text{B30})$$

where $m = 0, \pm 1$ are different values for the *quasi-momentum*. Similarly, using the reverse transformation gives us

$$|j\rangle = \frac{1}{\sqrt{N}} \sum_m e^{-ik_m j} |k_m\rangle. \quad (\text{B31})$$

In the 1st quantized picture, the momentum space Hamiltonian is simply

$$H_k = \sum_m \underbrace{\langle k_m | H | k_m \rangle}_{H(k_m)} |k_m\rangle \langle k_m|, \quad (\text{B32})$$

where $H(k_m) = E(k_m)$, if $|k_m\rangle$ diagonalizes our system. However, by identifying $|k_m\rangle \equiv b_m^\dagger |0\rangle$, we can directly work in the second-quantized picture. We can employ the orthogonality condition for complex exponentials, namely

$$\sum_j e^{i(m'-m)j} = N\delta_{m,m'}, \quad (\text{B33})$$

which implies

$$\begin{aligned} H_k &= \sum_{j>j'} J \left(\frac{1}{N} \sum_{m,m'} e^{-ik_m j} e^{ik_{m'} j'} \right) b_m^\dagger b_{m'} + J^* \left(\frac{1}{N} \sum_{m,m'} e^{-ik_{m'} j'} e^{ik_m j} \right) b_{m'}^\dagger b_m \\ &= \sum_{m,m'} J \left(\frac{1}{N} \sum_{j'} e^{-ik_m(j'+1)} e^{ik_{m'} j'} \right) b_m^\dagger b_{m'} + J^* \left(\frac{1}{N} \sum_{j'} e^{-ik_{m'} j'} e^{ik_m(j'+1)} \right) b_{m'}^\dagger b_m \\ &= \sum_{m,m'} J \underbrace{\left(\frac{1}{N} \sum_{j'} e^{i(k_{m'}-k_m)j'} \right)}_{\delta_{m,m'}} e^{-ik_m} b_m^\dagger b_{m'} + J^* \underbrace{\left(\frac{1}{N} \sum_{j'} e^{i(k_m-k_{m'})j'} \right)}_{\delta_{m,m'}} e^{ik_m} b_{m'}^\dagger b_m \\ &= \sum_m 2\Re(J e^{-ik_m}) b_m^\dagger b_m = \sum_m 2|J| \cos((\Phi - 2\pi m)/3) b_m^\dagger b_m. \end{aligned}$$

This can be more compactly written as

$$H_k = \sum_{m=0,\pm 1} \bar{\omega}_m b_m^\dagger b_m, \quad (\text{B34})$$

where

$$\bar{\omega}_m \equiv \sum_n 2\Re(J e^{-ik_m}) = \sum_m 2|J| \cos((\Phi - 2\pi m)/3), \quad (\text{B35})$$

are eigenenergies of the Hamiltonian in the momentum-representation. To write H_k in the matrix notation, we introduce the momentum-space mode vector $\mathbf{b} = (b_{-1}, b_0, b_1, b_{-1}^\dagger, b_0^\dagger, b_1^\dagger)^T$, and get

$$H_k = \sum_{n,m} \mathbf{b}_n^\dagger (\mathbf{H}_k)_{nm} \mathbf{b}_m, \quad \text{with} \quad \mathbf{H}_k = \text{diag}(\bar{\omega}_{-1}, \bar{\omega}_0, \bar{\omega}_1, \bar{\omega}_{-1}, \bar{\omega}_0, \bar{\omega}_1). \quad (\text{B36})$$

Note, that the energies come in pairs, but since \mathbf{H}_k is Hermitian, they have the same value for the modes and their adjoint. However, this is different for the dynamical matrix \mathbf{A} ,

$$\mathbf{A}_k = -i\Lambda_z \mathbf{H}_k = -i \text{diag}(\bar{\omega}_{-1}, \bar{\omega}_0, \bar{\omega}_1, -\bar{\omega}_{-1}, -\bar{\omega}_0, -\bar{\omega}_1). \quad (\text{B37})$$

meaning that real eigenvalues of the isolated system are now fully imaginary and come in pairs with opposite signs.

9. Fourier-transform and convolution theorem

a. Proof of convolution theorem

Here we proof the convolution theorem using Fubini's theorem (in short lets us exchange the measure of the integrals). It is a quite standard procedure, but shows how memory effects (the past becoming relevant in the time-integral) can appear as a consequence from it:

$$\begin{aligned}
\mathcal{F}^{-1}\left\{\tilde{g}[\omega] \cdot \tilde{f}[\omega]\right\}(t) &= \frac{1}{\sqrt{2\pi}} \int_{-\infty}^{\infty} \left(\frac{1}{\sqrt{2\pi}} \int_{-\infty}^{\infty} g(\tau) e^{-i\omega\tau} d\tau \frac{1}{\sqrt{2\pi}} \int_{-\infty}^{\infty} f(\tau') e^{-i\omega\tau'} d\tau' \right) e^{i\omega t} d\omega \\
&= \frac{1}{\sqrt{2\pi}} \int_{-\infty}^{\infty} \int_{-\infty}^{\infty} g(\tau) f(\tau') \underbrace{\left(\frac{1}{2\pi} \int_{-\infty}^{\infty} e^{-i\omega(\tau+\tau'-t)} d\omega \right)}_{=\delta(\tau+\tau'-t)} d\tau d\tau' \\
&= \frac{1}{\sqrt{2\pi}} \int_{-\infty}^{\infty} \int_{-\infty}^{\infty} g(\tau) f(\tau') \delta(\tau+\tau'-t) d\tau d\tau' \\
&= \frac{1}{\sqrt{2\pi}} \int_{-\infty}^{\infty} g(\tau) f(t-\tau) d\tau \\
&= \frac{1}{\sqrt{2\pi}} (g * f)(t).
\end{aligned}
\tag{B38}$$

b. Fourier-transforming the equations of motion of the optical isolator from frequency to time

We use this the convolution theorem above, to apply the reverse Fourier-transform on $i\omega \langle a_{1,2}[\omega] \rangle$. This gives us

$$\begin{aligned}
\mathcal{F}^{-1}\left\{i\omega \langle a_1[\omega] \rangle\right\}(t) &= \partial_t \langle a_1(t) \rangle \\
&= -\frac{1}{2} \left[\frac{1}{\sqrt{2\pi}} \left(\Gamma_1 * \langle a_1 \rangle \right) (t) + \kappa_1 \langle a_1(t) \rangle \right] - i \left[J \langle a_2(t) \rangle + \frac{i\mu}{2} \frac{1}{\sqrt{2\pi}} \left(\Gamma * \langle a_2 \rangle \right) (t) \right] - i \left[\lambda \langle a_2^\dagger(t) \rangle + \frac{i\nu}{2} \frac{1}{\sqrt{2\pi}} \left(\Gamma * \langle a_2^\dagger \rangle \right) (t) \right] \\
&= -\left[\frac{\Gamma_1 + \kappa_1}{2} \right] \langle a_1(t) \rangle - i \left[J + i\mu \frac{\Gamma}{2} \right] \langle a_2(t) \rangle - i \left[\lambda + i\nu \frac{\Gamma}{2} \right] \langle a_2^\dagger(t) \rangle, \\
\mathcal{F}^{-1}\left\{i\omega \langle a_2[\omega] \rangle\right\}(t) &= \partial_t \langle a_2(t) \rangle \\
&= -\frac{1}{2} \left[\frac{1}{\sqrt{2\pi}} \left(\Gamma_2 * \langle a_2 \rangle \right) (t) + \kappa_2 \langle a_2(t) \rangle \right] - i \left[J^* \langle a_1(t) \rangle + \frac{i\mu^*}{2} \frac{1}{\sqrt{2\pi}} \left(\Gamma * \langle a_1 \rangle \right) (t) \right] - i \left[\lambda \langle a_1^\dagger(t) \rangle - \frac{i\nu}{2} \frac{1}{\sqrt{2\pi}} \left(\Gamma * \langle a_1^\dagger \rangle \right) (t) \right] \\
&= -\left[\frac{\Gamma_2 + \kappa_2}{2} \right] \langle a_2(t) \rangle - i \left[J^* + i\mu^* \frac{\Gamma}{2} \right] \langle a_1(t) \rangle - i \left[\lambda - i\nu \frac{\Gamma}{2} \right] \langle a_1^\dagger(t) \rangle,
\end{aligned}
\tag{B39}$$

where we used the approximation that the shared reservoir is highly damped and thus static from the point of view of $\langle a_i(t-\tau) \rangle$, implying $\tau \ll t$ and thus

$$\langle a_i(t-\tau) \rangle \approx \langle a_i(t) \rangle.
\tag{B40}$$

C. S-MATRIX

1. Proof of transformation formula

Here, we prove $\tilde{\mathbf{S}}[\omega] = \mathbf{T}^\dagger \mathbf{S}[\omega] \mathbf{T}$:

Since $\mathbf{M} = \mathbf{T} \mathbf{D} \mathbf{T}^\dagger$, and $\chi[\omega] = (i\omega \mathbf{1} - \mathbf{M})^{-1}$, it follows

$$\chi^{-1}[\omega] = (i\omega \mathbf{1} - \mathbf{T} \mathbf{D} \mathbf{T}^\dagger) = \mathbf{T} \mathbf{T}^\dagger (i\omega \mathbf{1} - \mathbf{T} \mathbf{D} \mathbf{T}^\dagger) \mathbf{T} \mathbf{T}^\dagger = \mathbf{T} (i\omega \underbrace{\mathbf{T}^\dagger \mathbf{1} \mathbf{T}}_{\mathbf{1}} - \underbrace{\mathbf{T}^\dagger \mathbf{T}}_{\mathbf{1}} \underbrace{\mathbf{D} \mathbf{T}^\dagger \mathbf{T}}_{\mathbf{1}}) \mathbf{T}^\dagger = \mathbf{T} (i\omega \mathbf{1} - \mathbf{D}) \mathbf{T}^\dagger, \quad (\text{C1})$$

taking the inverse of both expressions gives us with $(\mathbf{T}^\dagger) = \mathbf{T}^{-1}$ the following

$$\chi[\omega] = (i\omega \mathbf{1} - \mathbf{M})^{-1} = (\mathbf{T} (i\omega \mathbf{1} - \mathbf{D}) \mathbf{T}^\dagger)^{-1} \iff (i\omega \mathbf{1} - \mathbf{M})^{-1} = \mathbf{T} (i\omega \mathbf{1} - \mathbf{D})^{-1} \mathbf{T}^\dagger, \quad (\text{C2})$$

and by introducing the susceptibility in the mode-representation

$$\tilde{\chi}[\omega] \equiv (i\omega \mathbf{1} - \mathbf{D})^{-1}, \quad (\text{C3})$$

we can relate both via

$$\chi[\omega] = \mathbf{T} \tilde{\chi}[\omega] \mathbf{T}^\dagger. \quad (\text{C4})$$

Finally, this implies

$$\tilde{\mathbf{S}}[\omega] = \mathbf{T}^\dagger \mathbf{S}[\omega] \mathbf{T} = \mathbf{T}^\dagger \left(\mathbf{1} - \sqrt{\tilde{\mathbf{K}}} \chi[\omega] \sqrt{\tilde{\mathbf{K}}} \right) \mathbf{T} = \mathbf{1} - \underbrace{(\mathbf{T}^\dagger \sqrt{\tilde{\mathbf{K}}} \mathbf{T})}_{\sqrt{\tilde{\mathbf{K}}}} \underbrace{(\mathbf{T}^\dagger \chi[\omega] \mathbf{T})}_{\tilde{\chi}[\omega]} \underbrace{(\mathbf{T}^\dagger \sqrt{\tilde{\mathbf{K}}} \mathbf{T})}_{\sqrt{\tilde{\mathbf{K}}}} = \left[\mathbf{1} - \sqrt{\tilde{\mathbf{K}}} \tilde{\chi}[\omega] \sqrt{\tilde{\mathbf{K}}} \right], \quad (\text{C5})$$

where $\sqrt{\tilde{\mathbf{K}}}$ is the matrix with damping elements in the mode-basis. This concludes the proof - *qed*.

2. Alternative way of enforcing non-Markovianity to the susceptibility matrix and the S-matrix

Note that the only frequency dependence of the S-Matrix resides within the susceptibility $\chi[\omega]$. For the three-mode model with a frequency-independent Langevin matrix \mathbf{M} , the susceptibility becomes $\chi[\omega] = (i\omega \mathbf{1} - \mathbf{M})^{-1}$. As the identity matrix multiplied by the frequency is a relic of the time-derivative of the cavity mode differential equations (due to Fourier transforming), we can also find a way to treat the auxiliary mode as Markovian - without doing a formal (adiabatic) elimination of the differential equations. This is useful since we are still in the full three-mode picture from our point of view and can look at the complete system dynamics without referring to the reduced effective model. To be more precise, by transforming eqs. (3.30) into frequency space, the differential operator becomes $\partial_t \rightarrow i\omega$, and since the dynamics of a stationary system vanishes $\partial_t \langle a_i(t) \rangle = 0$, the same is true in frequency space with $i\omega \langle a_i[\omega] \rangle = 0$. This is similar to saying that we can tune the correlation times for each cavity of interest (meaning, coupling them stronger to the reservoir, for example by dropping the quality factor of the respective resonators resulting in a higher permeability between the system and the environment, effectively assuming that cavity i has a high κ_i). But similarly, one can also assume that the frequency response of the cavity i approaches zero, where cavity i then becomes stationary. This can be done more formally by introducing a new matrix Ξ_m by hand

$$i\omega \mathbf{1}_6 \rightarrow i\omega \Xi_m \equiv i\omega (\mathbf{1}_4 \oplus m \mathbf{1}_2) = i\omega \text{diag}(1, 1, 1, 1, m, m), \quad (\text{C6})$$

written in the quadrature basis. In our case, we want to have control over the frequency response of the auxiliary, thus we the system-specific parameter $m \in [0, 1]$ is related to the correlation times by

$$m = \begin{cases} 1, & \text{for } \tau_3 \approx \tau_{1,2} \\ 0, & \text{for } \tau_3 \ll \tau_{1,2} \end{cases}, \quad (\text{C7})$$

where $m = 1$ is the non-Markovian regime with vanishing correlation time and memory effects, and $m = 0$ is the Markovian regime with memoryless dissipation and is local in time. Next, it is easily shown that the limiting cases are

$$1. \text{ non-Markovian: } \lim_{m \rightarrow 1} i\omega \Xi_m = i\omega \Xi_1 = i\omega \mathbf{1}, \quad (\text{C8a})$$

$$2. \text{ Markovian: } \lim_{m \rightarrow 0} i\omega \Xi_m = i\omega \Xi_0 = i\omega \text{diag}(1, 1, 1, 1, 0, 0). \quad (\text{C8b})$$

Inserting this back into Eq. (4.5) results in the S-matrix

$$\mathbf{S}_m[\omega] \equiv \left[\mathbf{1} - \sqrt{\mathbf{K}} \chi_m[\omega] \sqrt{\mathbf{K}} \right] = \left[\mathbf{1} - \sqrt{\mathbf{K}} (i\omega \Xi_m - \mathbf{M})^{-1} \sqrt{\mathbf{K}} \right], \quad \text{with} \quad \chi_m[\omega] \equiv (i\Xi_m[\omega] - \mathbf{M})^{-1}, \quad (\text{C9})$$

which can be either in the non-Markovian or the Markovian limit for the three-mode model.

3. Expressing the S-matrix in terms of damping rates

Using Eq. (3.62), we can find a different way to express the S-matrix, which will end up in a novel, yet quite general statement. To understand what this representation entails, can be seen as a challenging, but probably insightful endeavour for future research. First we note, that the susceptibility matrix fulfills

$$\tilde{\chi}^\dagger[\omega] = \left((i\omega \mathbf{1} - \mathbf{D})^{-1} \right)^\dagger = (i(-\omega) \mathbf{1} - \mathbf{D}^\dagger)^{-1}, \quad (\text{C10})$$

where we used the fact that $(\mathbf{L}^{-1})^\dagger = (\mathbf{L}^\dagger)^{-1}$ for any invertible matrix \mathbf{L} . Next, we consider the dissipative ring with $\lambda_{ij} = 0 \implies \mathbf{h}_2 = 0$, where it follows for Eq. (3.62)

$$\mathbf{D} = -\mathbf{D}^\dagger - \tilde{\mathbf{K}}. \quad (\text{C11})$$

Now, we re-express $\tilde{\chi}[-\omega]$ as

$$\tilde{\chi}[-\omega] = (i(-\omega) \mathbf{1} - \mathbf{D})^{-1} = \left(i(-\omega) \mathbf{1} + \mathbf{D}^\dagger + \tilde{\mathbf{K}} \right)^{-1} = - \left(i\omega \mathbf{1} - \tilde{\mathbf{K}} - \mathbf{D}^\dagger \right)^{-1}. \quad (\text{C12})$$

Since $\tilde{\mathbf{K}}$ is a diagonal matrix, we can express it as $\tilde{\mathbf{K}} = \sum_j \kappa_j |j\rangle\langle j|$ and write it into the argument of the $\tilde{\chi}$ function, giving us

$$\begin{aligned} \tilde{\chi}[-\omega] &= - \left(i \sum_j^N (\omega + i\kappa_j) |j\rangle\langle j| - \mathbf{D}^\dagger \right)^{-1} = - \left(i \text{diag}(\omega + i\kappa_1, \dots, \omega + i\kappa_N) - \mathbf{D}^\dagger \right)^{-1} \\ &\equiv -\tilde{\chi}^\dagger[-\omega + i\kappa_1, \dots, -\omega + i\kappa_N]. \end{aligned} \quad (\text{C13})$$

Note, that the last equality can be made less ambiguous after impedance matching with $\kappa_i/2 \equiv \kappa$, resulting in

$$\tilde{\chi}[-\omega] = -\tilde{\chi}^\dagger[-\omega + i2\kappa, \dots, -\omega + i2\kappa] \equiv -\tilde{\chi}^\dagger[-\omega + i2\kappa]. \quad (\text{C14})$$

If we know calculate the adjoint

$$\tilde{\chi}^\dagger[-\omega] = (i\omega\mathbb{1} - \mathbf{D}^\dagger)^{-1} \implies \tilde{\chi}^\dagger[-\omega + i\kappa_1, \dots, -\omega + i\kappa_N] = (i \operatorname{diag}(\omega + i\kappa_1, \dots, \omega + i\kappa_N)^* - \mathbf{D}^\dagger)^{-1} \\ = (i \operatorname{diag}(\omega - i\kappa_1, \dots, \omega - i\kappa_N) - \mathbf{D}^\dagger)^{-1}, \quad (\text{C15})$$

it can be related to $\tilde{\chi}[-\omega]$ as

$$\tilde{\chi}[-\omega] = -\tilde{\chi}^\dagger[-\omega + i\kappa_1, \dots, -\omega + i\kappa_N], \quad \text{or conversely} \quad \tilde{\chi}[\omega] = -\tilde{\chi}^\dagger[\omega + i\kappa_1, \dots, \omega + i\kappa_N]. \quad (\text{C16})$$

This equality of the susceptibilities has implications for the S-matrix. Recall that the S-matrix is given by

$$\tilde{\mathbf{S}}[\omega] = \mathbb{1} - \sqrt{\tilde{\mathbf{K}}}\tilde{\chi}[\omega]\sqrt{\tilde{\mathbf{K}}}, \quad (\text{C17})$$

then it follows from the susceptibility matrix,

$$\tilde{\mathbf{S}}[-\omega] = \mathbb{1} + \sqrt{\tilde{\mathbf{K}}}\tilde{\chi}^\dagger[-\omega + i\kappa_1, \dots, -\omega + i\kappa_N]\sqrt{\tilde{\mathbf{K}}}, \quad (\text{C18})$$

which gives us

$$\tilde{\mathbf{S}}[-\omega] = 2\mathbb{1} - \tilde{\mathbf{S}}^\dagger[-\omega + i\kappa_1, \dots, -\omega + i\kappa_N]. \quad (\text{C19})$$

We can also rearrange this expression

$$\mathbb{1} = \frac{\tilde{\mathbf{S}}[-\omega] + \tilde{\mathbf{S}}^\dagger[-\omega + i\kappa_1, \dots, -\omega + i\kappa_N]}{2}. \quad (\text{C20})$$

The last expression tells us, how the S-matrix and its adjoint relate directly, which is different to the formula used in the main text,

$$\tilde{\mathbf{S}}[-\omega] = \mathbf{\Lambda}_x \tilde{\mathbf{S}}^*[\omega] \mathbf{\Lambda}_x, \quad (\text{C21})$$

which tells us that the action of flipping the sign in front of the frequencies is the same as taking the conjugate and flipping blocks. For the case derived here, the S-matrix for negative frequencies can be expressed as its adjoint with an additional phase shift in energy due to the damping rates $\tilde{\kappa}$. This shift extends the frequencies to the complex plane. Now, its visible how damping rates explicitly affect the scattering behaviour of the system. Since the only condition we assumed in the beginning was that all squeezing interactions vanish, this equation holds true for all systems which can be written as a bilinear BdG Hamiltonian of a similar form.

4. Non-Markovian S-matrix for the optical isolator

The non-Markovian S-matrix for symmetric damping rates $\kappa \equiv \kappa_i/2$ is

$$\tilde{\mathbf{S}}_{\text{eff}}[\omega] = \begin{pmatrix} 1 - \frac{2\kappa}{i2\omega + \kappa + \Gamma[\omega]} & \frac{2\kappa(e^{i(\Phi+i\pi/2)}\Gamma_0 + \Gamma[\omega])}{(i2\omega + \kappa + \Gamma[\omega])^2 - (e^{i(\Phi+i\pi/2)}\Gamma_0 + \Gamma[\omega])(e^{-i(\Phi-i\pi/2)}\Gamma_0 + \Gamma[\omega])} \\ \frac{2\kappa(e^{-i(\Phi-i\pi/2)}\Gamma_0 + \Gamma[\omega])}{(i2\omega + \kappa + \Gamma[\omega])^2 - (e^{i(\Phi+i\pi/2)}\Gamma_0 + \Gamma[\omega])(e^{-i(\Phi-i\pi/2)}\Gamma_0 + \Gamma[\omega])} & 1 - \frac{2\kappa}{i2\omega + \kappa + \Gamma[\omega]} \end{pmatrix}, \quad (\text{C22})$$

which becomes for the unidirectional limit (recovering the adiabatic result by assuming $\kappa_3 \gg \kappa \implies \Gamma[\omega] \rightarrow \Gamma_0$)

$$\tilde{\mathbf{S}}_{\text{eff}}[\omega] = \begin{pmatrix} 1 - \frac{2\kappa}{i2\omega + \kappa + \Gamma[\omega]} & \frac{2\kappa(\Gamma[\omega] \mp \Gamma_0)}{(i2\omega + \kappa + \Gamma[\omega])^2 + (\Gamma_0^2 - \Gamma^2[\omega])} \\ \frac{2\kappa(\Gamma[\omega] \pm \Gamma_0)}{(i2\omega + \kappa + \Gamma[\omega])^2 + (\Gamma_0^2 - \Gamma^2[\omega])} & 1 - \frac{2\kappa}{i2\omega + \kappa + \Gamma[\omega]} \end{pmatrix} \xrightarrow{\kappa_3 \gg \kappa} \begin{pmatrix} 1 - \frac{2\kappa}{i2\omega + \kappa + \Gamma_0} & \frac{2\kappa(\Gamma_0 \mp \Gamma_0)}{(i2\omega + \kappa + \Gamma_0)^2} \\ \frac{2\kappa(\Gamma_0 \pm \Gamma_0)}{(i2\omega + \kappa + \Gamma_0)^2} & 1 - \frac{2\kappa}{i2\omega + \kappa + \Gamma_0} \end{pmatrix}, \quad (\text{C23})$$

where the upper (lower) sign stands for $\Phi = \phi_R$ ($\Phi = \phi_L$). For a reciprocal setting $\Phi = \phi_0 = 0$, the diagonal elements are the same as for the above regime, where transmissions elements become equal

$$(\tilde{\mathbf{S}}_{\text{eff}}[\omega])_{12} = (\tilde{\mathbf{S}}_{\text{eff}}[\omega])_{21} = \frac{2\kappa(i\Gamma_0 + \Gamma[\omega])}{(i2\omega + \kappa + \Gamma[\omega])^2 - (i\Gamma_0 + \Gamma[\omega])^2}, \quad (\text{C24})$$

and the scattering probabilities for the resonant, impedance-matched case read

$$|(\tilde{\mathbf{S}}_{\text{eff}}[0])_{11}|^2 = |(\tilde{\mathbf{S}}_{\text{eff}}[0])_{22}|^2 = 0, \quad \text{and} \quad |(\tilde{\mathbf{S}}_{\text{eff}}[0])_{12}|^2 = |(\tilde{\mathbf{S}}_{\text{eff}}[0])_{21}|^2 = \frac{1}{5}. \quad (\text{C25})$$

5. Scattering behaviour of the optical isolator for quadratures

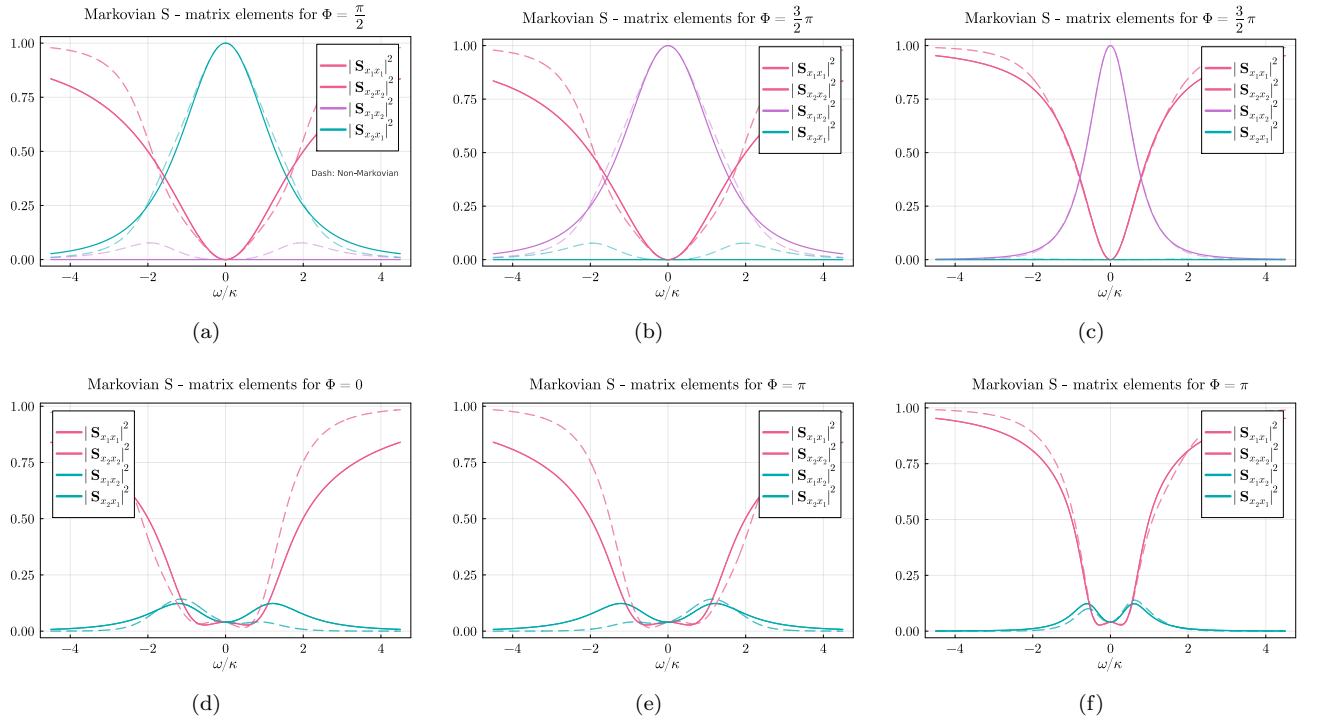


FIG. 30. Markovian (solid) and non-Markovian (dashed) scattering probabilities of the optical isolator for x -quadratures, plotted against frequency for different limits of Φ . We assume the parameters $\mathcal{C} = 1$ and $|J|/\kappa = 1$. The first two pictures in each row show $\kappa = \kappa_i/2$, and the last picture in each $\kappa_{1,2} = \kappa_3/4 = \kappa$. (a) Unidirectional case for $\Phi = \phi_R$ for symmetric dissipation. The behaviour is the same as in Fig. 12b, with $|S_{x_i x_i}|^2 = |S_{x_1 x_2}|^2 = 0$, and $|S_{x_2 x_1}|^2 = 1$. (b) Nonreciprocal case for $\Phi = \phi_L$, leading to $|S_{x_1 x_2}|^2 = 1$, and $|S_{x_2 x_1}|^2 = 0$. (c) The same as (a) with $\Phi = \phi_R$ but in the asymmetric regime. The non-Markovian case converges to the Markovian limit since the auxiliary is damped stronger. (d) Reciprocal case for $\Phi = 0$ in the symmetric regime. Different to the three-mode model, the dynamical matrix $\mathbf{M}_{\text{eff}}[\omega]$ is frequency dependent, and thus not real. Similar to modes in the full and effective model, quadrature curves also become asymmetric for finite ω . (e) Reciprocal case for $\Phi = \pi$, with the same behaviour as (d) only flipped around the x -axis. (f) Reciprocal case for $\Phi = 0$ for asymmetric damping rates. Again, the non-Markovian curve converges to the Markovian limit.

D. NOISE SPECTRAL DENSITY

1. Explicit form of the input-correlation matrix in the quadrature basis

We can explicitly write the input correlator-matrix as

$$\begin{aligned}
 \langle \mathbf{v}_{\text{in}}[\omega] \mathbf{v}_{\text{in}}^T[\omega'] \rangle &= \begin{pmatrix} \langle x_{1,\text{in}}[\omega] x_{1,\text{in}}[\omega'] \rangle & \langle x_{1,\text{in}}[\omega] p_{1,\text{in}}[\omega'] \rangle & \dots & \langle x_{1,\text{in}}[\omega] x_{n,\text{in}}[\omega'] \rangle & \langle x_{1,\text{in}}[\omega] p_{n,\text{in}}[\omega'] \rangle \\ \langle p_{1,\text{in}}[\omega] x_{1,\text{in}}[\omega'] \rangle & \langle p_{1,\text{in}}[\omega] p_{1,\text{in}}[\omega'] \rangle & \dots & \langle x_{1,\text{in}}[\omega] x_{n,\text{in}}[\omega'] \rangle & \langle x_{1,\text{in}}[\omega] p_{n,\text{in}}[\omega'] \rangle \\ \vdots & \vdots & \ddots & \vdots & \vdots \\ \langle x_{n,\text{in}}[\omega] x_{1,\text{in}}[\omega'] \rangle & \langle x_{n,\text{in}}[\omega] p_{1,\text{in}}[\omega'] \rangle & \dots & \langle x_{n,\text{in}}[\omega] x_{n,\text{in}}[\omega'] \rangle & \langle x_{n,\text{in}}[\omega] p_{n,\text{in}}[\omega'] \rangle \\ \langle p_{n,\text{in}}[\omega] x_{1,\text{in}}[\omega'] \rangle & \langle p_{n,\text{in}}[\omega] p_{1,\text{in}}[\omega'] \rangle & \dots & \langle p_{n,\text{in}}[\omega] x_{n,\text{in}}[\omega'] \rangle & \langle p_{n,\text{in}}[\omega] p_{n,\text{in}}[\omega'] \rangle \end{pmatrix} \\
 &= \delta(\omega + \omega') \begin{pmatrix} n_1^{\text{th}} + 1/2 & i/2 & & & \\ -i/2 & n_1^{\text{th}} + 1/2 & & & \\ & & \ddots & & \\ & & & n_n^{\text{th}} + 1/2 & i/2 \\ & & & -i/2 & n_n^{\text{th}} + 1/2 \end{pmatrix}.
 \end{aligned} \tag{D1}$$

2. Explicit form of the output-correlation matrix in the mode basis

We have shown how the transformation is still viable for the output-covariance and the form of Eq. (5.20) is justified, which can now be used to find an adequate expression for the output-noise,

$$\begin{aligned}
 \tilde{\mathbf{C}}_{\text{out}}[\omega, \omega'] &= \frac{1}{4} \left(\langle \mathbf{a}_{\text{out}}[\omega] \mathbf{a}_{\text{out}}^\dagger[\omega'] \rangle + \langle \mathbf{a}_{\text{out}}^\dagger[\omega'] \mathbf{a}_{\text{out}}^T[\omega] \rangle^T + \langle \mathbf{a}_{\text{out}}[\omega'] \mathbf{a}_{\text{out}}^\dagger[\omega] \rangle + \langle \mathbf{a}_{\text{out}}^\dagger[\omega] \mathbf{a}_{\text{out}}^T[\omega'] \rangle^T \right) \\
 &= \frac{1}{4} \left(\tilde{\mathbf{S}}[\omega] \langle \mathbf{a}_{\text{in}}[\omega] \mathbf{a}_{\text{in}}^\dagger[\omega'] \rangle \tilde{\mathbf{S}}^\dagger[-\omega'] + \left(\tilde{\mathbf{S}}^*[-\omega'] \langle \mathbf{a}_{\text{in}}^\dagger[\omega'] \mathbf{a}_{\text{in}}^T[\omega] \rangle^T \tilde{\mathbf{S}}^T[\omega] \right)^T \right. \\
 &\quad \left. + \tilde{\mathbf{S}}[\omega'] \langle \mathbf{a}_{\text{in}}[\omega'] \mathbf{a}_{\text{in}}^\dagger[\omega] \rangle \tilde{\mathbf{S}}^\dagger[-\omega] + \left(\tilde{\mathbf{S}}^*[-\omega] \langle \mathbf{a}_{\text{in}}^\dagger[\omega] \mathbf{a}_{\text{in}}^T[\omega'] \rangle^T \tilde{\mathbf{S}}^T[\omega'] \right)^T \right) \\
 &= \frac{1}{4} \left(\tilde{\mathbf{S}}[\omega] \left(\langle \mathbf{a}_{\text{in}}[\omega] \mathbf{a}_{\text{in}}^\dagger[\omega'] \rangle + \langle \mathbf{a}_{\text{in}}^\dagger[\omega'] \mathbf{a}_{\text{in}}^T[\omega] \rangle^T \right) \tilde{\mathbf{S}}^\dagger[-\omega'] + \tilde{\mathbf{S}}[\omega'] \left(\langle \mathbf{a}_{\text{in}}[\omega'] \mathbf{a}_{\text{in}}^\dagger[\omega] \rangle + \langle \mathbf{a}_{\text{in}}^\dagger[\omega] \mathbf{a}_{\text{in}}^T[\omega'] \rangle^T \right) \tilde{\mathbf{S}}^\dagger[-\omega] \right) \\
 &= \frac{1}{2} \left(\tilde{\mathbf{S}}[\omega] \tilde{\mathbf{C}}_{\text{in}}[\omega, \omega'] \tilde{\mathbf{S}}^\dagger[-\omega'] + \tilde{\mathbf{S}}[\omega'] \tilde{\mathbf{C}}_{\text{in}}[\omega, \omega'] \tilde{\mathbf{S}}^\dagger[-\omega] \right) = \delta(\omega, \omega') \left[\frac{\tilde{\mathbf{S}}[\omega] \tilde{\mathbf{S}}_{\text{in}} \tilde{\mathbf{S}}^\dagger[\omega] + \tilde{\mathbf{S}}[-\omega] \tilde{\mathbf{S}}_{\text{in}} \tilde{\mathbf{S}}^\dagger[-\omega]}{2} \right],
 \end{aligned} \tag{D2}$$

giving us

$$\tilde{\mathbf{S}}_{\text{out}}[\omega] = \frac{\tilde{\mathbf{S}}[\omega] \tilde{\mathbf{S}}_{\text{in}} \tilde{\mathbf{S}}^\dagger[\omega] + \tilde{\mathbf{S}}[-\omega] \tilde{\mathbf{S}}_{\text{in}} \tilde{\mathbf{S}}^\dagger[-\omega]}{2} \tag{D3}$$

3. Proof of transformation formula between the mode and the quadrature basis of the output-noise

Here we intend to prove that $\mathbf{C}_{\text{out}}[\omega, \omega'] = \mathbf{T} \tilde{\mathbf{C}}_{\text{out}}[\omega, \omega'] \mathbf{T}^\dagger$. First, we transform the right hand side to the quadrature basis with \mathbf{T} , from that it follows

$$\begin{aligned}
& \mathbf{T} \tilde{\mathbf{C}}_{\text{out}}[\omega, \omega'] \mathbf{T}^\dagger \\
&= \frac{1}{4} \mathbf{T} \left[\mathbf{T}^\dagger \langle \mathbf{v}_{\text{out}}[\omega] \mathbf{v}_{\text{out}}^\dagger[\omega'] \rangle \mathbf{T} + \langle \mathbf{T}^T \mathbf{v}_{\text{out}}[\omega'] \mathbf{v}_{\text{out}}^T[\omega] \mathbf{T}^* \rangle^T + \mathbf{T}^\dagger \langle \mathbf{v}_{\text{out}}[\omega'] \mathbf{v}_{\text{out}}^\dagger[\omega] \rangle \mathbf{T} + \langle \mathbf{T}^T \mathbf{v}_{\text{out}}[\omega] \mathbf{v}_{\text{out}}^T[\omega'] \mathbf{T}^* \rangle^T \right] \mathbf{T}^\dagger \\
&= \frac{1}{4} \left[\langle \mathbf{v}_{\text{out}}[\omega] \mathbf{v}_{\text{out}}^T[\omega'] \rangle + \langle \mathbf{v}_{\text{out}}[\omega] \mathbf{v}_{\text{out}}^T[\omega'] \rangle^T + \langle \mathbf{v}_{\text{out}}[\omega'] \mathbf{v}_{\text{out}}^T[\omega] \rangle + \langle \mathbf{v}_{\text{out}}[\omega'] \mathbf{v}_{\text{out}}^T[\omega] \rangle^T \right] = \mathbf{C}_{\text{out}}[\omega, \omega'],
\end{aligned} \tag{D4}$$

which is exactly the result for the output-covariance matrix in the quadrature basis, see Eq. (5.6).

As a last remark we note that the transformation in the opposite direction is only valid up to the point where we assume that $\mathbf{S}[-\omega] = \mathbf{S}^*[\omega]$, as this does not hold for mode-operators, namely, we need to transform Eq. (5.17) and not Eq. (5.19).

4. Output-noise in the reciprocal limit of the optical isolator

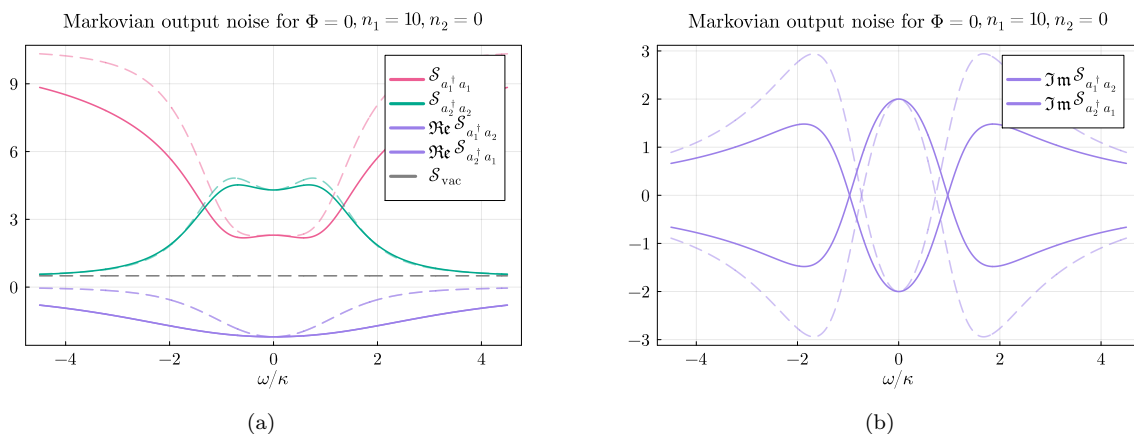


FIG. 31. Output-noise in the reciprocal limit for the optical isolator with $\mathcal{C} = 1$, and $\kappa \equiv \kappa_i/2$. In reciprocal limits, cross-correlations become complex. This behaviour was explained for the three-mode model, see discussion in Sec. VIA.

5. Output-noise spectrum of the optical isolator for quadratures

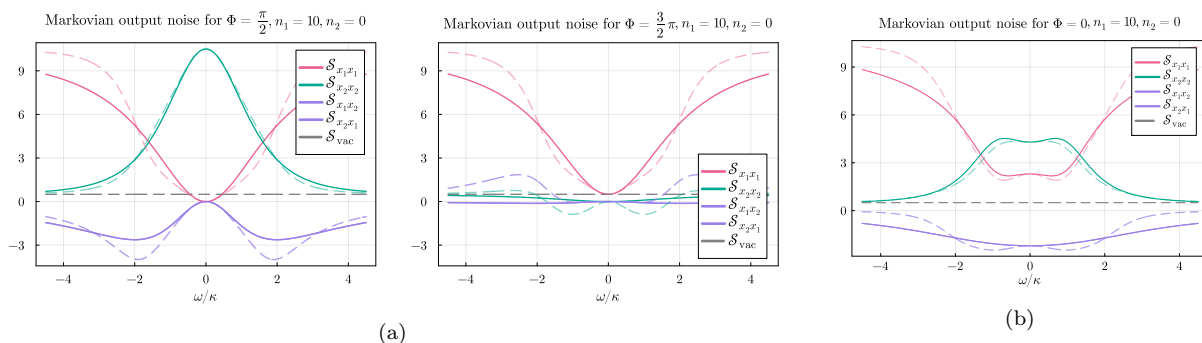


FIG. 32. Markovian (solid) and non-Markovian (dashed) quadrature elements of the output-noise matrix for the optical isolator with varying values of Φ and thermal-inputs, plotted against ω/κ . Parameters are $\mathcal{C} = 1$ and $|J| = |\mu_2|\Gamma_0/2$. (a) Comparison between ϕ_R (Left) and ϕ_L (Right) for the input-occupations $\bar{n}_1 = 10, \bar{n}_2 = 0$. The behaviour is the same as for Fig. 13a. (b) Also similar to Fig. 13b, with the only difference that cross-correlations are always real.

6. Output-noise spectrum of the optical isolator for asymmetric dissipation rates

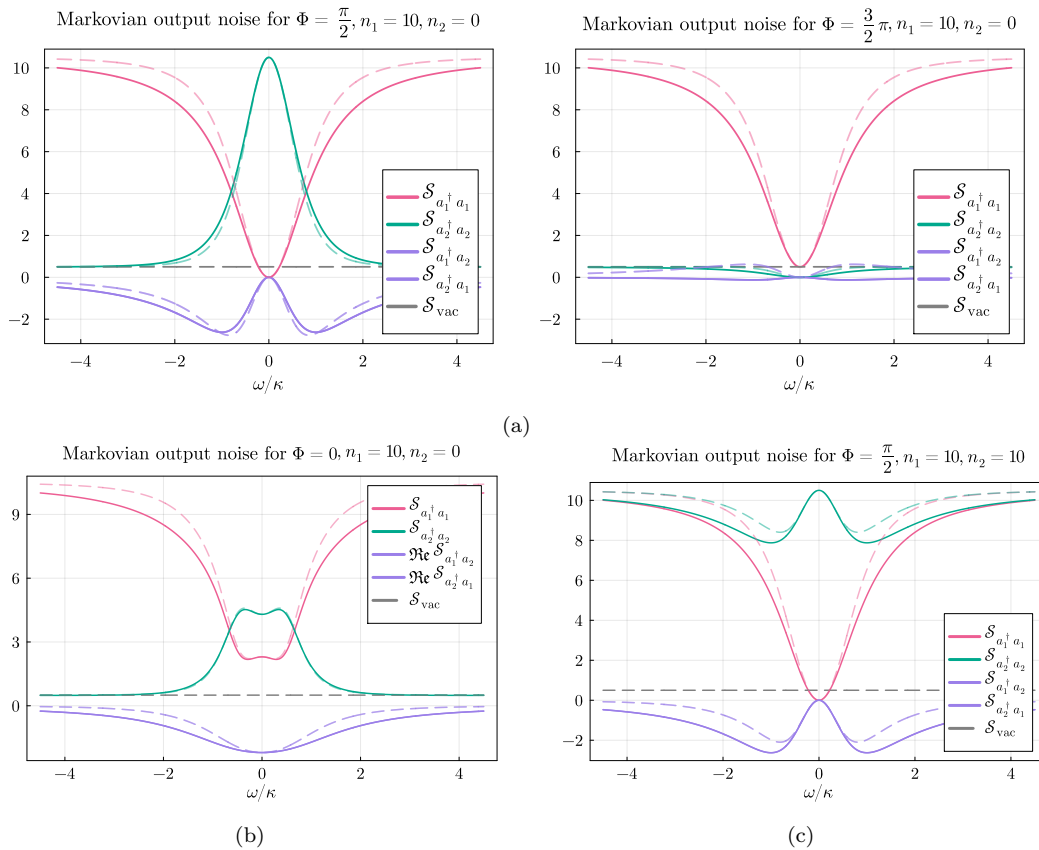


FIG. 33. Markovian (solid) and non-Markovian (dashed) elements of the output-noise matrix for the optical isolator with varying values of Φ and thermal-inputs, plotted against ω/κ . Parameters are $\mathcal{C} = 1$ with $\kappa = \kappa_{1,2} = \kappa_3/4$, and $|J| = |\mu_2|\Gamma_0/2$. (a) Comparison between ϕ_R (Left) and ϕ_L (Right) for the input-occupations $\bar{n}_1 = 10, \bar{n}_2 = 0$. (Left) Here, fluctuations entering port 1 are fully transferred to output 2 with $\mathcal{S}_{a_2^\dagger a_2}[0] = 10.5$, and $\mathcal{S}_{a_1^\dagger a_1}[0] = 0$. (Right) Here, $\mathcal{S}_{a_1^\dagger a_1}[0] = 0.5$, and $\mathcal{S}_{a_2^\dagger a_2}[0] = 0$, since output 1 sees vacuum from port 2, but output 2 gets no input from the auxiliary. (b) Reciprocal case for $\Phi = 0$ and $\bar{n}_1 = 10, \bar{n}_2 = 0$. (c) Similar to (a, Left), but with inputs at both ports $\bar{n}_1 = \bar{n}_2 = 10$.

E. DIFFUSION BEHAVIOUR OF SELECTED MODELS

1. Dissipative three-mode ring

a. Heatmaps of scattering probabilities for different cases

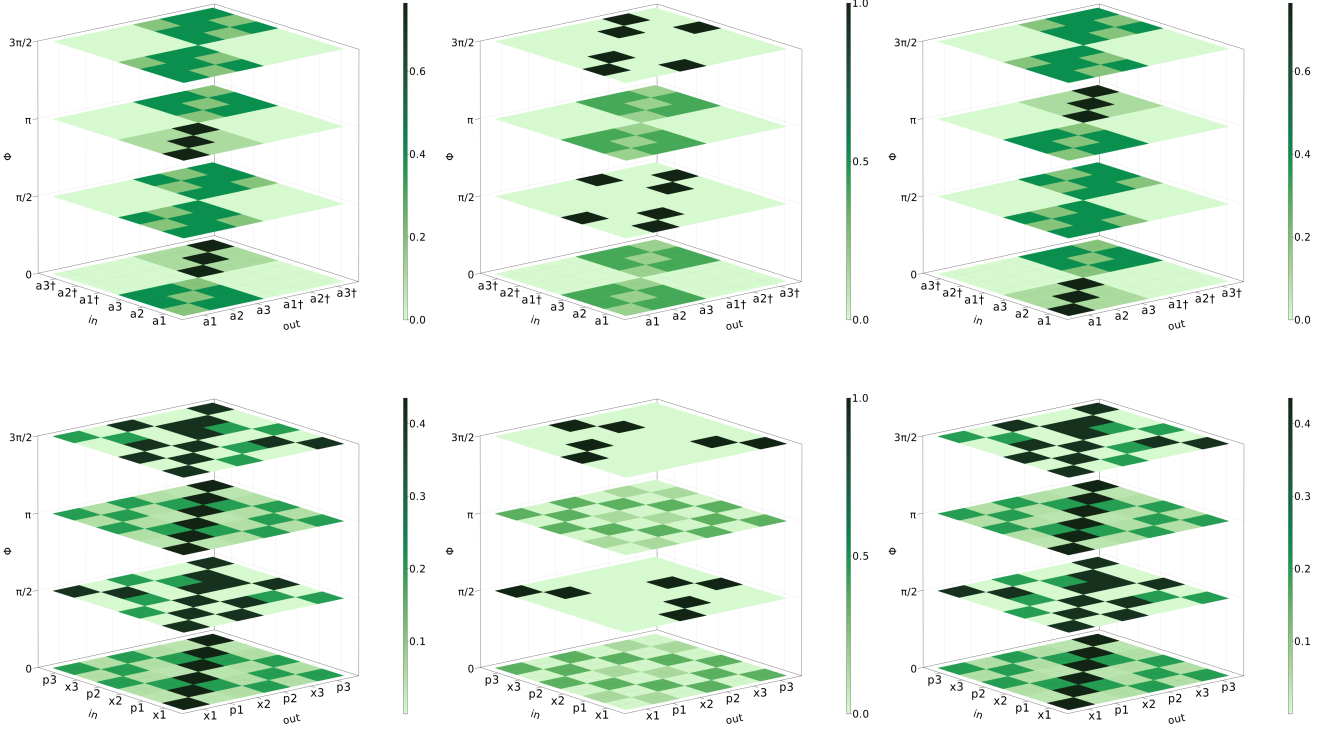


FIG. 34. Comparison of scattering probabilities plotted against Φ , for different values of ω . In the upper row, heatmaps in the mode basis are shown, and heatmaps for quadratures are in the lower row, respectively. The left column is the case $\omega/\kappa = -2$, the middle $\omega/\kappa = 0$, and the right $\omega/\kappa = 2$. If we focus on the upper row, we immediately see how scattering between modes and adjoints are treated the opposite way, having the same behaviour for positive and negative frequencies only for unidirectional limits. For any other value of the phase, transport is asymmetric in ω . This is different for quadratures, which are always symmetric in ω , for all values of Φ .

b. *S*-matrix coefficients for asymmetric damping rates

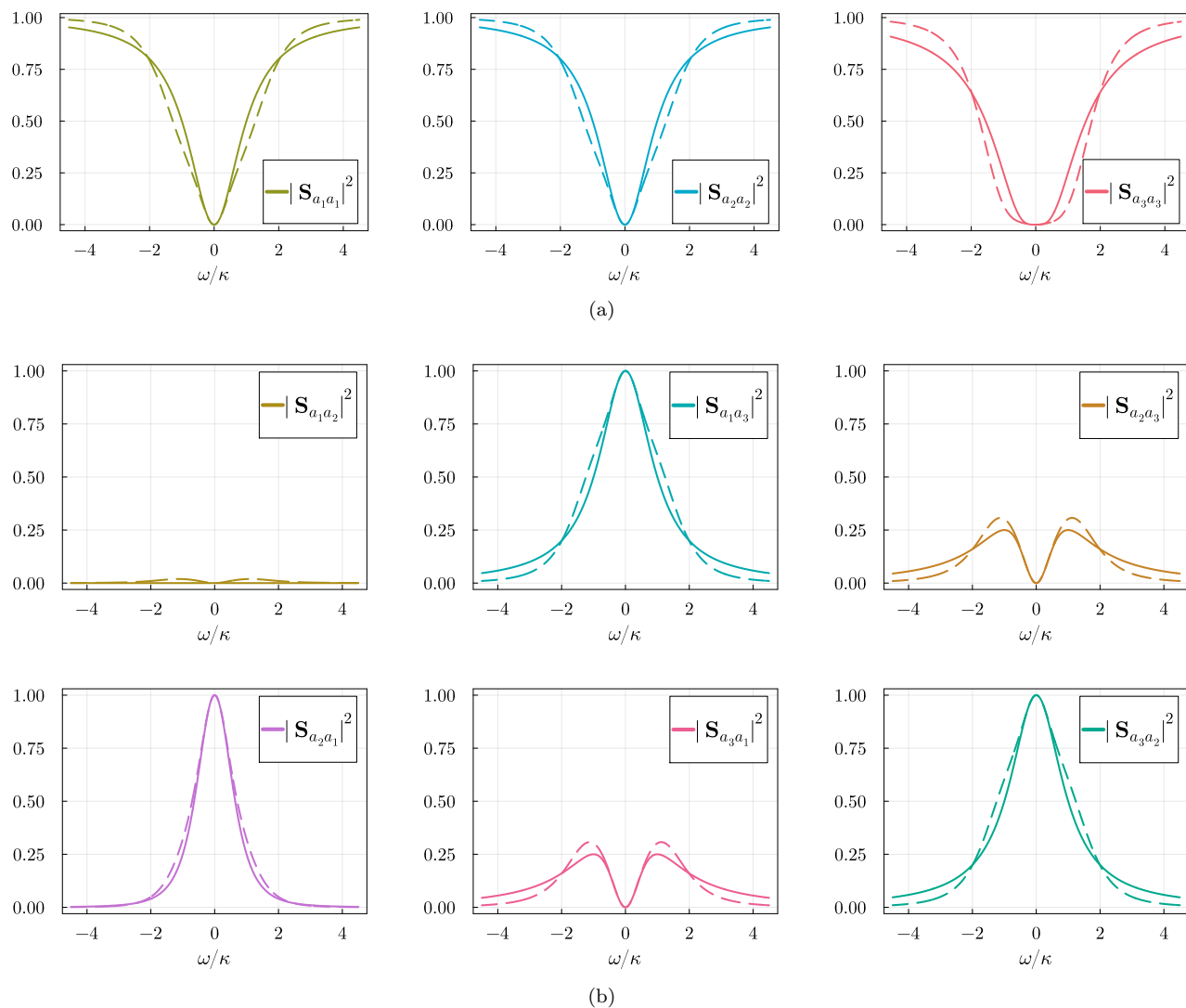


FIG. 35. Markovian (solid) and non-Markovian (dashed) scattering probabilities for $\Phi = \phi_R$ and asymmetric damping rates $\kappa \equiv \kappa_{1,2} = \kappa_3/4$, plotted against ω/κ . Here, the same behaviour is seen as in Fig. 15, only with narrower curves, since the auxiliary is closer to the Markovian limit. (a) Reflection coefficients. (b) Transmission coefficients.

c. *S*-matrix coefficients in the quadrature basis

Scattering probabilities for the unidirectional limit $\Phi = \alpha_{12} = \alpha_{31} = \alpha_{32} = \phi_R = \pi/2$ with $\kappa \equiv \kappa_i/2$, which behave similarly to the scattering probabilities in the mode basis.

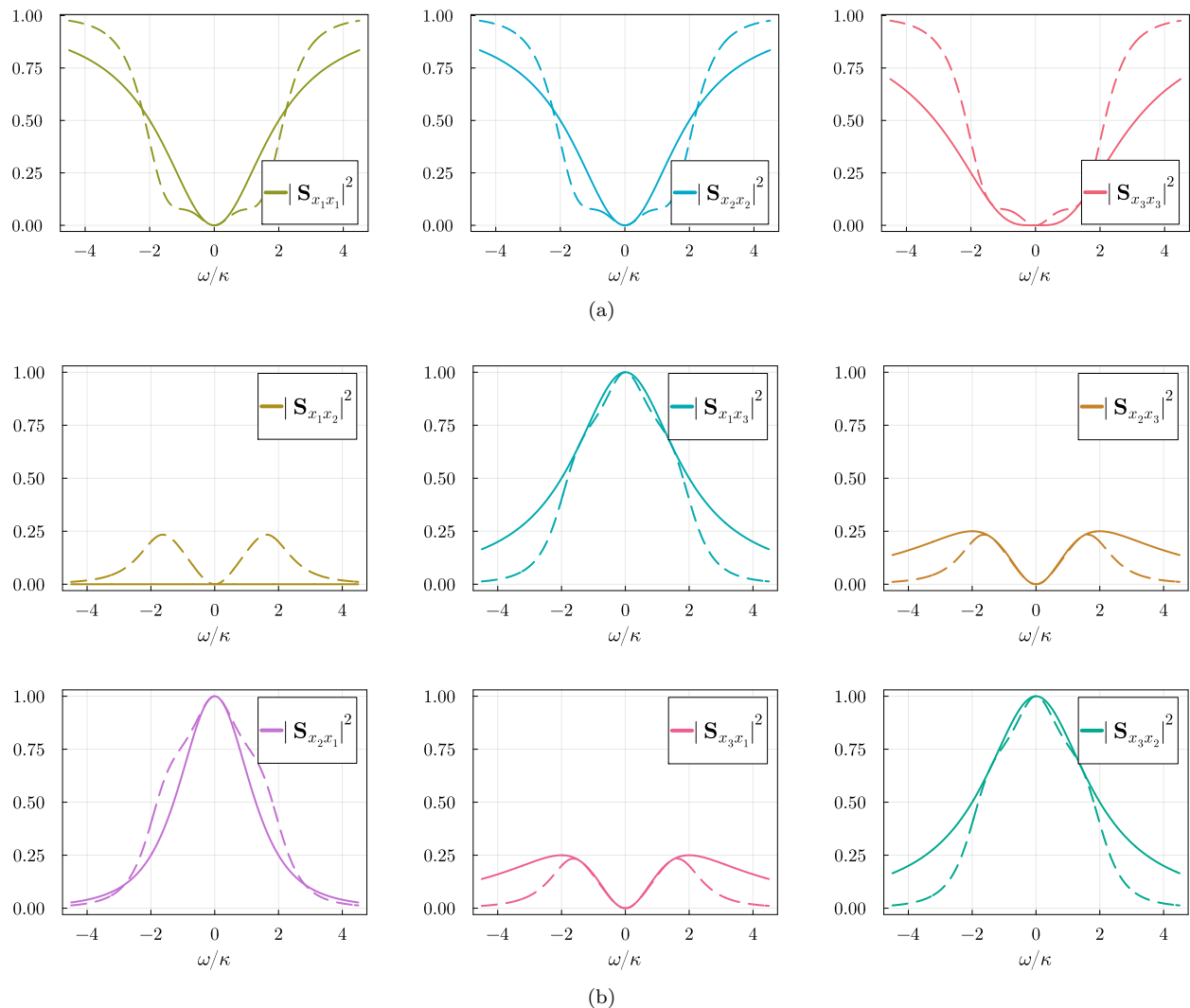


FIG. 36. Markovian (solid) and non-Markovian (dashed) scattering probabilities in the quadrature basis for $\Phi = \alpha_{12} = \alpha_{31} = \alpha_{32} = \phi_R = \pi/2$, and $\kappa \equiv \kappa_i/2$. Shown are the coefficients between x -quadratures, since p -quadratures vanish (this comes from our choice of α_{ij}), as do elements between different quadratures. (a) Reflections for x -quadratures. (b) Transmissions between x -quadratures. Compare with Fig. 15.

d. Composition of the output-noise in the quadrature representation by scattering probabilities

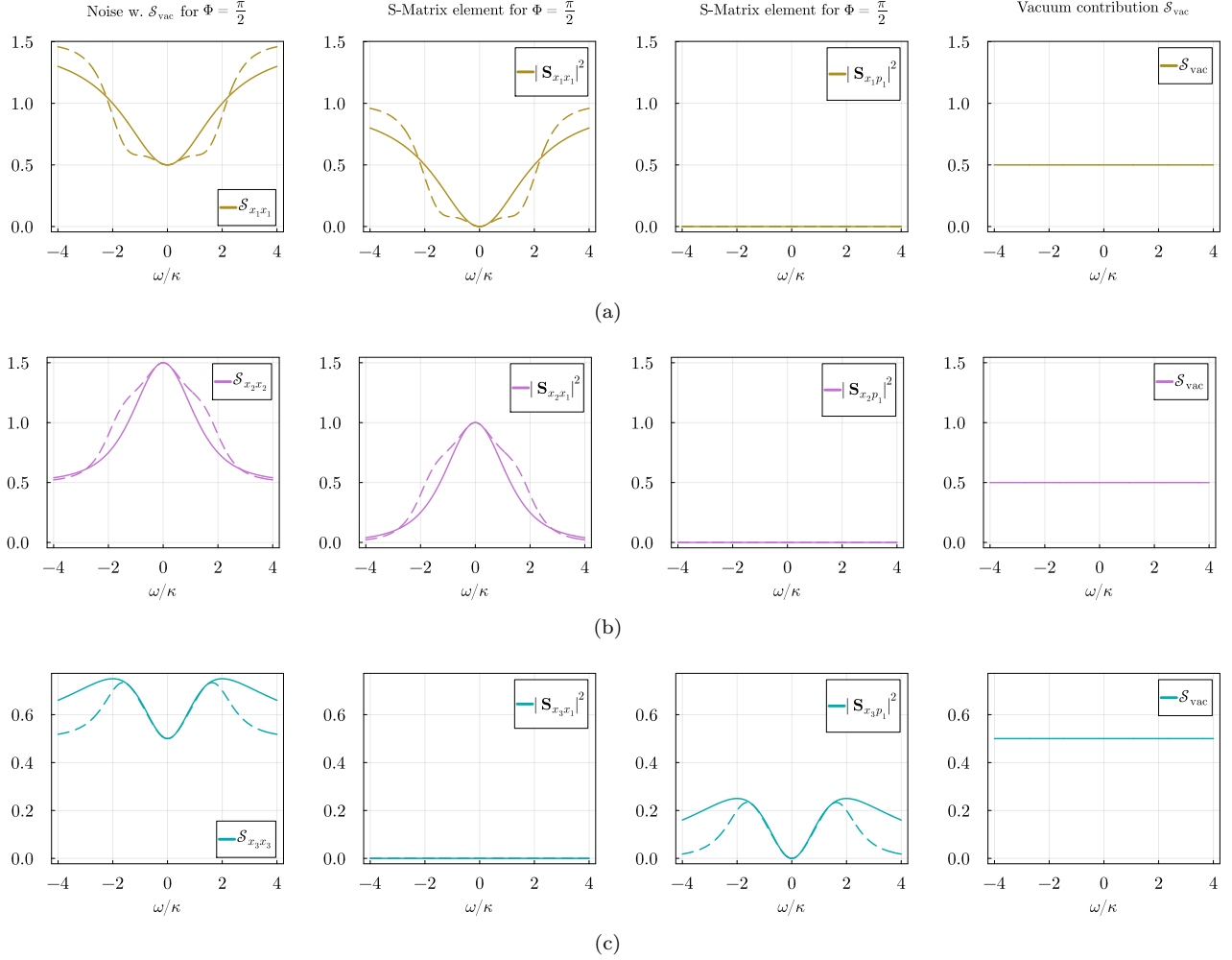


FIG. 37. Diagonal elements of the output-noise spectrum in the quadrature representation composed of S-matrix amplitudes and the incident vacua (acting as a noise floor) for $\Phi = \phi_R$ and $\kappa_1 = \kappa_2 = \kappa_3 = 2\kappa$ for small thermal fluctuations entering the first port: $n_1 = 1, n_2 = n_3 = 0$. On the left side of each row, there is the diagonal element of the noise spectrum showing the output fluctuations leaving the system. The second and third column is the respective non-zero S-matrix amplitude, where we chose to show the vacuum contribution to the noise for this figure. The S-matrix probability amplitudes get scaled by a factor and by adding them with the incident vacuum, we get the respective output noise spectrum element. Note, that any S-matrix amplitude of different quadratures with the same index are zero, namely $|\mathbf{S}_{x_i p_i}|^2 = |\mathbf{S}_{p_i x_i}|^2 = 0$, since we only consider linear driving and no single-mode squeezed input.

e. Expressing output-noise in the mode basis by elements of the quadrature representation

Since the noise-matrix is symmetric in operator-ordering, an element (i, j) is always the same as the element (j, i) . However, switching labels $i \leftrightarrow j$ (for $i \neq j$), produces different effects depending on the basis, where elements are complex conjugated for modes, but undergo a sign change for quadratures. Additionally, without squeezing, elements of the type $\mathcal{S}_{a_i a_j} = \mathcal{S}_{a_i^\dagger a_j^\dagger} = \mathcal{S}_{x_i p_i} = 0$ all vanish (where we suppressed the argument ω), for all i, j . Thus, we can sum this up as

modes:

quadratures:

$$\mathcal{S}_{a_i a_j} = \mathcal{S}_{a_i^\dagger a_j^\dagger} = 0, \quad \mathcal{S}_{x_i p_i} = 0, \quad \forall i, j, \quad (\text{E1a})$$

$$\mathcal{S}_{a_i a_j^\dagger} = \mathcal{S}_{a_j^\dagger a_i}, \quad \mathcal{S}_{v_i w_j} = \mathcal{S}_{w_j v_i}, \quad \forall i, j, \quad \text{where } v, w \in \{x, p\}, \quad (\text{E1b})$$

$$\mathcal{S}_{a_i a_j^\dagger} = \mathcal{S}_{a_j^\dagger a_i^*}, \quad \mathcal{S}_{v_i w_j} = -\mathcal{S}_{v_j w_i}, \quad i \neq j, \quad \text{where } v \neq w \in \{x, p\}. \quad (\text{E1c})$$

Note, that the noise for different quadrature types is the same

$$\mathcal{S}_{x_i x_j} = \mathcal{S}_{p_i p_j} \quad \forall i, j. \quad (\text{E2})$$

Using all rules from above, we can transform the output-noise from the quadrature to the mode basis via \mathbf{T} (see Eq. (3.69)), and express it in this simple form

$$\tilde{\mathcal{S}}_{\text{out}}[\omega] = \begin{pmatrix} \mathcal{S}_{x_1 x_1} & \mathcal{S}_{x_1 x_2} - i\mathcal{S}_{x_1 p_2} & \mathcal{S}_{x_1 x_3} - i\mathcal{S}_{x_1 p_3} \\ \mathcal{S}_{x_2 x_1} - i\mathcal{S}_{x_2 p_1} & \mathcal{S}_{x_2 x_2} & \mathcal{S}_{x_2 x_3} - i\mathcal{S}_{x_2 p_3} \\ \mathcal{S}_{x_3 x_1} - i\mathcal{S}_{x_3 p_1} & \mathcal{S}_{x_3 x_2} - i\mathcal{S}_{x_3 p_2} & \mathcal{S}_{x_2 x_2} \\ & & \mathcal{S}_{x_1 x_1} & \mathcal{S}_{x_1 x_2} + i\mathcal{S}_{x_1 p_2} & \mathcal{S}_{x_1 x_3} + i\mathcal{S}_{x_1 p_3} \\ & & \mathcal{S}_{x_2 x_1} + i\mathcal{S}_{x_2 p_1} & \mathcal{S}_{x_2 x_2} & \mathcal{S}_{x_2 x_3} + i\mathcal{S}_{x_2 p_3} \\ & & \mathcal{S}_{x_3 x_1} + i\mathcal{S}_{x_3 p_1} & \mathcal{S}_{x_3 x_2} + i\mathcal{S}_{x_3 p_2} & \mathcal{S}_{x_3 x_3} \end{pmatrix}, \quad (\text{E3})$$

which implies that diagonal elements are always real (quadrature noise is never complex), but correlations in the mode basis can become complex, due to terms of the form $\mathcal{S}_{x_i p_j}$. To understand whats going on, we will look at a single element $\mathcal{S}_{x_1 p_2}$ and try to find an expression in terms of S-matrix elements. For this, we consider

$$\mathcal{S}_{\text{out}}[\omega] = \mathbf{T} \tilde{\mathcal{S}}_{\text{out}}[\omega] \mathbf{T}^\dagger = \frac{1}{2} \mathbf{T} (\tilde{\mathbf{S}}[\omega] \tilde{\mathbf{S}}_{\text{in}} \tilde{\mathbf{S}}^\dagger[\omega] + \tilde{\mathbf{S}}[-\omega] \tilde{\mathbf{S}}_{\text{in}} \tilde{\mathbf{S}}^\dagger[-\omega]) \mathbf{T}^\dagger.$$

This gives us

$$\mathcal{S}_{x_1 p_2} = \frac{i}{4} \left[\bar{n}_1 (\tilde{\mathbf{S}}_{a_1 a_1}[\omega] \tilde{\mathbf{S}}_{a_2 a_1}^*[\omega] - \tilde{\mathbf{S}}_{a_1^\dagger a_1^\dagger}[\omega] \tilde{\mathbf{S}}_{a_2^\dagger a_1^\dagger}^*[\omega] + \tilde{\mathbf{S}}_{a_1 a_1}[-\omega] \tilde{\mathbf{S}}_{a_2 a_1}^*[-\omega] - \tilde{\mathbf{S}}_{a_1^\dagger a_1^\dagger}[-\omega] \tilde{\mathbf{S}}_{a_2^\dagger a_1^\dagger}^*[-\omega]) \right. \quad (\text{E4})$$

$$\left. + \bar{n}_2 (\tilde{\mathbf{S}}_{a_1 a_2}[\omega] \tilde{\mathbf{S}}_{a_2 a_2}^*[\omega] - \tilde{\mathbf{S}}_{a_1^\dagger a_2^\dagger}[\omega] \tilde{\mathbf{S}}_{a_2^\dagger a_2^\dagger}^*[\omega] + \tilde{\mathbf{S}}_{a_1 a_2}[-\omega] \tilde{\mathbf{S}}_{a_2 a_2}^*[-\omega] - \tilde{\mathbf{S}}_{a_1^\dagger a_2^\dagger}[-\omega] \tilde{\mathbf{S}}_{a_2^\dagger a_2^\dagger}^*[-\omega]) \right. \quad (\text{E5})$$

$$\left. + \bar{n}_3 (\tilde{\mathbf{S}}_{a_1 a_3}[\omega] \tilde{\mathbf{S}}_{a_2 a_3}^*[\omega] - \tilde{\mathbf{S}}_{a_1^\dagger a_3^\dagger}[\omega] \tilde{\mathbf{S}}_{a_2^\dagger a_3^\dagger}^*[\omega] + \tilde{\mathbf{S}}_{a_1 a_3}[-\omega] \tilde{\mathbf{S}}_{a_2 a_3}^*[-\omega] - \tilde{\mathbf{S}}_{a_1^\dagger a_3^\dagger}[-\omega] \tilde{\mathbf{S}}_{a_2^\dagger a_3^\dagger}^*[-\omega]) \right]. \quad (\text{E6})$$

Since $\tilde{\mathbf{S}}_{a_i a_j}^*[\omega] = \tilde{\mathbf{S}}_{a_i^\dagger a_j^\dagger}[\omega]$, we can rewrite this as (for $\bar{n}_1 > 0$, $\bar{n}_2 = \bar{n}_3 = 0$)

$$\mathcal{S}_{x_1 p_2} = -\frac{\bar{n}_1}{2} \Im \left\{ \tilde{\mathbf{S}}_{a_1 a_1}[\omega] \tilde{\mathbf{S}}_{a_2 a_1}^*[\omega] + \tilde{\mathbf{S}}_{a_1 a_1}[-\omega] \tilde{\mathbf{S}}_{a_2 a_1}^*[-\omega] \right\}, \quad (\text{E7})$$

which is a real and ω -symmetrized expression, encoding the phase-difference between mode and adjoint scattering amplitudes of the ports of interest. This has big implications: This tells us, that (in absence of squeezing), the imaginary part in thermal-correlations tell us how different thermal noise of modes and adjoints will scatter through the system. If they are asymmetric (which is maximized for the reciprocal limit), an imaginary part starts to appear for correlations. If modes and adjoints are scattered the same way, the correlation between different quadratures $\mathcal{S}_{x_i p_j} = \mathcal{S}_{p_i x_j} = 0$ will vanish, which means that the noise-matrix will only have real elements.

f. Rectification

As stated in the beginning of the thesis, see Sec. II A, only the ratio of scattering probabilities needs to be conserved for reciprocity. In a more quantitative manner, we can thus define two functions, the *scattering rectification* (in the mode-basis)

$$\tilde{\xi}_{a_i a_j}[\omega] \equiv \frac{|\tilde{\mathbf{S}}_{a_j a_i}|^2 - |\tilde{\mathbf{S}}_{a_i a_j}|^2}{|\tilde{\mathbf{S}}_{a_j a_i}|^2 + |\tilde{\mathbf{S}}_{a_i a_j}|^2}, \quad (\text{E8})$$

and the *noise rectification* (in the mode-basis)

$$\tilde{\zeta}_{ij}[\omega] \equiv \frac{|\tilde{\mathcal{S}}_{a_i^\dagger a_i}^{\text{out}}|^2 - |\tilde{\mathcal{S}}_{a_j^\dagger a_j}^{\text{out}}|^2}{|\tilde{\mathcal{S}}_{a_i^\dagger a_i}^{\text{out}}|^2 + |\tilde{\mathcal{S}}_{a_j^\dagger a_j}^{\text{out}}|^2}, \quad (\text{E9})$$

which both track when the system is reciprocal. The scattering rectification just tests the unevenness between both transmission directions. Consider Fig. 38, where in (a) the scattering rectification is shown in the mode basis $\tilde{\xi}_{a_1 a_2}[\omega]$ and in (b) in the quadrature basis $\xi_{x_1 x_2}[\omega]$, for varying values of Φ plotted against ω/κ . Comparing both, it becomes clear that modes are tilted in that space, whereas quadratures are not. This re-enforces our observations regarding the asymmetry in ω for modes. The last figure (c) shows the noise rectification $\tilde{\zeta}_{12}$ in the mode basis for inputs $\bar{n}_1 = \bar{n}_2 = 0$, and $\bar{n}_3 \neq 0$. Sending in thermal fluctuations in port 3, will either end up at output 1 (for $\Phi = \phi_L$), or output 2 (for $\Phi = \phi_R$), or both (in reciprocal limits), thus we can observe the difference between the transport limits with input 3. For $\Phi = \phi_R$ we get $\tilde{\zeta}_{12}[0] = +1$, and for $\Phi = \phi_L$ we get $\tilde{\zeta}_{12}[0] = -1$. This figure looks the same for modes and quadratures, and shows that the output-noise is an always symmetric quantity.

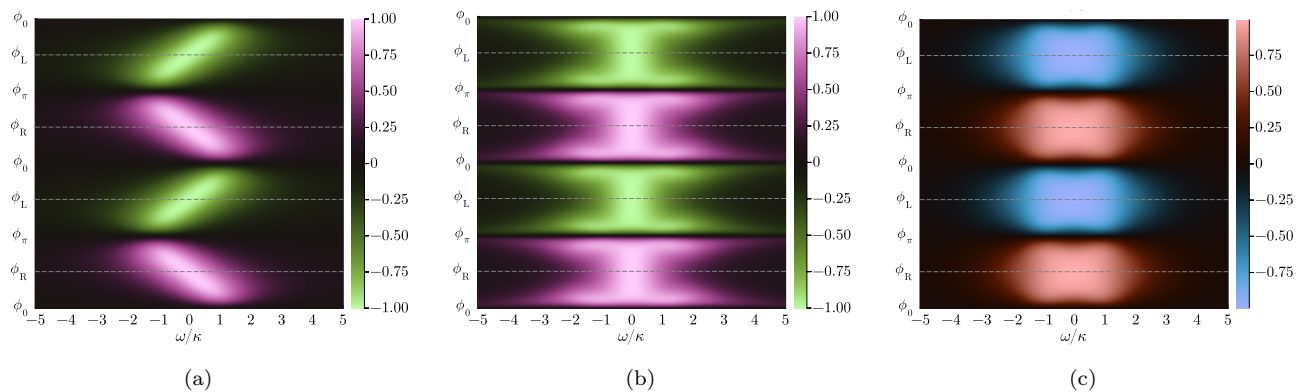


FIG. 38. Rectifications for $\kappa \equiv \kappa_i/2$ plotted against Φ and ω/κ . (a) Asymmetric look of the scattering rectification $\tilde{\xi}_{12}$ in the mode basis. (b) Symmetric look of the scattering rectification ξ_{12} in the quadrature basis. (c) Symmetric noise rectification $\tilde{\zeta}_{12}$ in the mode basis for $\bar{n}_{1,2} = 0$, $\bar{n}_3 \neq 0$.

2. Dissipative directional transistor

a. Isolating the gauge-invariant phases for the directional transistor

From the interaction scheme we see that there are only three relevant phases

$$\tau_1 \equiv \alpha_{31} - \alpha_{41} + \alpha_{43}, \quad (\text{E10a})$$

$$\tau_2 \equiv -\alpha_{32} + \alpha_{42} - \alpha_{43}, \quad (\text{E10b})$$

$$\tau_3 \equiv \alpha_{12} + \alpha_{41} - \alpha_{42}, \quad (\text{E10c})$$

where the Aharonov-Bohm phase of the three-mode model can be trivially reconstructed by summing up these new phases

$$\Phi = \tau_1 + \tau_2 + \tau_3 = \alpha_{12} + \alpha_{31} - \alpha_{32}, \quad (\text{E11})$$

which is not relevant phase, but is consistent to the idea of "splitting up the phase Φ " in this model. We then perform the gauge-transformation $\langle a_j \rangle \rightarrow \langle a'_j \rangle = e^{i\gamma_j}$, giving us the following terms

- | | |
|--|--|
| 1. $\alpha_{12} + \gamma_2 - \gamma_1$, | 4. $\alpha_{32} + \gamma_2 - \gamma_3$, |
| 2. $\alpha_{31} + \gamma_1 - \gamma_3$, | 5. $\alpha_{42} + \gamma_2 - \gamma_4$, |
| 3. $\alpha_{41} + \gamma_1 - \gamma_4$, | 6. $\alpha_{43} + \gamma_3 - \gamma_4$, |

where three of these can be set to zero, since we only have three relevant phases. We choose to set 1., 4., and 5. to zero. This implies

1. $\stackrel{!}{=} 0 \implies \gamma_1 = \gamma_2 + \alpha_{12}$,
4. $\stackrel{!}{=} 0 \implies \gamma_2 = \gamma_3 - \alpha_{32}$,
5. $\stackrel{!}{=} 0 \implies \gamma_2 = \gamma_4 - \alpha_{42}$,

where we make the choice $\gamma_2 = \alpha_{41} - \alpha_{42}$, giving us

$$\begin{aligned} \gamma_1 &= \alpha_{12} + \alpha_{41} - \alpha_{42} = \tau_3, \\ \gamma_2 &= \alpha_{41} - \alpha_{42}, \\ \gamma_4 &= \alpha_{41}, \\ \gamma_3 &= \alpha_{32} + \alpha_{41} - \alpha_{42}. \end{aligned}$$

The remaining equations can then be expressed as

2. $= \tau_1 + \tau_2 + \tau_3$,
3. $= \tau_3$,
6. $= -\tau_2$.

Now we would be finished, but since we aim to have a specific form of the EOMs (for aesthetic and didactic purposes), we can apply a last additional gauge $\langle a_1 \rangle \rightarrow e^{i\tau_3} \langle a_1 \rangle$, which we will simply denote with $\langle a_1 \rangle$, since this action leaves the physics invariant. With this, the interaction parameters become

$$J_{12} \rightarrow |J_{12}| e^{i\tau_3}, \quad J_{31} = |J_{31}| e^{i(\tau_1 + \tau_2)}, \quad J_{32} = |J_{32}|, \quad (\text{E12})$$

$$J_{41} \rightarrow |J_{41}|, \quad J_{42} = |J_{42}|, \quad J_{43} = |J_{43}| e^{-i\tau_2}, \quad (\text{E13})$$

b. *Derivation of the effective model of the transistor and explicit formulas*

Here, we Fourier transform the EOMs of the full model, see Eq. (6.19d), and eliminate the third and the fourth mode, similar to three-mode model to get an effective model for the modes a_1 and a_2 . Consider the following solutions

$$\langle a_3[\omega] \rangle = \frac{1}{i\omega + \kappa_3/2} (-iJ_{31} \langle a_1[\omega] \rangle - iJ_{32} \langle a_2[\omega] \rangle - iJ_{43}^* \langle a_4[\omega] \rangle), \quad (\text{E14})$$

$$\langle a_4[\omega] \rangle = \frac{1}{i\omega + \kappa_4/2} (-iJ_{41} \langle a_1[\omega] \rangle - iJ_{42} \langle a_2[\omega] \rangle - iJ_{43} \langle a_4[\omega] \rangle), \quad (\text{E15})$$

where we introduce the susceptibility $\chi_i[\omega] \equiv 1/(i\omega + \kappa_i/2)$, $\bar{\chi}[\omega] \equiv \chi_3[\omega]\chi_4[\omega]$, and the unit-less scaling factor

$$\bar{d}[\omega] \equiv \frac{1}{1 + |J_{43}|^2 \bar{\chi}[\omega]}$$

to get

$$\langle a_3[\omega] \rangle = (-i\chi_3[\omega]\bar{d}[\omega]J_{31} - \bar{\chi}[\omega]\bar{d}[\omega]J_{43}^*J_{41}) \langle a_1[\omega] \rangle + (-i\chi_3[\omega]\bar{d}[\omega]J_{32} - \bar{\chi}[\omega]\bar{d}[\omega]J_{43}^*J_{42}) \langle a_2[\omega] \rangle, \quad (\text{E16})$$

$$\langle a_4[\omega] \rangle = (-i\chi_4[\omega]\bar{d}[\omega]J_{41} - \bar{\chi}[\omega]\bar{d}[\omega]J_{43}J_{31}) \langle a_1[\omega] \rangle + (-i\chi_4[\omega]\bar{d}[\omega]J_{42} - \bar{\chi}[\omega]\bar{d}[\omega]J_{43}J_{32}) \langle a_2[\omega] \rangle, \quad (\text{E17})$$

leading to

$$\begin{aligned} i\omega \langle a_1[\omega] \rangle = & \left(-\frac{\kappa_1}{2} - \chi_3[\omega]\bar{d}[\omega]|J_{31}|^2 - \chi_4[\omega]\bar{d}[\omega]|J_{41}|^2 + i\bar{\chi}[\omega]\bar{d}[\omega] (J_{31}^*J_{41}J_{43}^* + J_{31}J_{41}^*J_{43}) \right) \langle a_1[\omega] \rangle \\ & (-iJ_{12} + \chi_3[\omega]\bar{d}[\omega] (-J_{31}^*J_{32} + i\chi_4[\omega]J_{31}^*J_{42}J_{43}^*) + \chi_4[\omega]\bar{d}[\omega] (-J_{41}^*J_{42} + i\chi_3[\omega]J_{41}^*J_{32}J_{43})) \langle a_2[\omega] \rangle, \end{aligned} \quad (\text{E18})$$

$$\begin{aligned} i\omega \langle a_2[\omega] \rangle = & \left(-\frac{\kappa_2}{2} - \chi_3[\omega]\bar{d}[\omega]|J_{32}|^2 - \chi_4[\omega]\bar{d}[\omega]|J_{42}|^2 + i\bar{\chi}[\omega]\bar{d}[\omega] (J_{32}^*J_{42}J_{43}^* + J_{32}J_{42}^*J_{43}) \right) \langle a_2[\omega] \rangle \\ & (-iJ_{12}^* + \chi_3[\omega]\bar{d}[\omega] (-J_{31}J_{32}^* + i\chi_4[\omega]J_{41}J_{32}^*J_{43}^*) + \chi_4[\omega]\bar{d}[\omega] (-J_{41}J_{42}^* + i\chi_3[\omega]J_{31}J_{42}^*J_{43})) \langle a_2[\omega] \rangle, \end{aligned} \quad (\text{E19})$$

for the EOMs in the effective picture. By also introducing

$$|\delta| := |J_{12}|, \quad \chi_i[\omega] := \frac{1}{i\omega + \kappa_i/2}, \quad \bar{\chi}[\omega] := \chi_3[\omega]\chi_4[\omega] \quad \bar{d}[\omega] := \frac{1}{1 + \bar{\chi}[\omega]|J_{43}|^2}, \quad (\text{E20})$$

$$\lambda_1[\omega] := \chi_3[\omega]\bar{d}[\omega]|J_{31}J_{32}|, \quad \lambda_2[\omega] := \chi_4[\omega]\bar{d}[\omega]|J_{41}J_{42}|, \quad \mu_1[\omega] := \bar{d}[\omega]|J_{31}J_{42}J_{43}|, \quad \mu_2[\omega] := \bar{d}[\omega]|J_{41}J_{32}J_{43}|, \quad (\text{E21})$$

and

$$\bar{\sigma}_i[\omega] := 2\bar{\chi}[\omega]\bar{d}[\omega]|J_{3i}J_{4i}J_{43}|, \quad \frac{\bar{\gamma}_i[\omega]}{2} := \frac{\kappa_i + 2\chi_3[\omega]\bar{d}[\omega]|J_{3i}|^2 + 2\chi_4[\omega]\bar{d}[\omega]|J_{4i}|^2}{2}, \quad (\text{E22})$$

as new damping rates of the shared effective reservoir, we get

$$\begin{aligned} i\omega \langle a_1[\omega] \rangle = & \left(-\frac{\bar{\gamma}_1[\omega]}{2} + i\bar{\sigma}_1[\omega] \cos \tau_1 \right) \langle a_1[\omega] \rangle \\ & - \left(\lambda_1[\omega]e^{-i(\tau_1+\tau_2)} + \lambda_2[\omega] - i(\mu_1[\omega]\bar{\chi}[\omega]e^{-i\tau_1} + \mu_2[\omega]\bar{\chi}[\omega]e^{-i\tau_2} - |\delta|e^{i\tau_3}) \right) \langle a_2[\omega] \rangle, \end{aligned} \quad (\text{E23})$$

$$\begin{aligned} i\omega \langle a_2[\omega] \rangle = & \left(-\frac{\bar{\gamma}_2[\omega]}{2} + i\bar{\sigma}_2[\omega] \cos \tau_2 \right) \langle a_2[\omega] \rangle \\ & - \left(\lambda_1[\omega]e^{i(\tau_1+\tau_2)} + \lambda_2[\omega] - i(\mu_1[\omega]\bar{\chi}[\omega]e^{i\tau_1} + \mu_2[\omega]\bar{\chi}[\omega]e^{i\tau_2} - |\delta|e^{-i\tau_3}) \right) \langle a_1[\omega] \rangle, \end{aligned} \quad (\text{E24})$$

for the non-Markovian effective model. The Markovian regime is reached for $\chi_i[\omega = 0] \in \mathbb{R}_{>0}$. This implies, that $\lambda_1 \equiv \lambda_1[0], \lambda_2 \equiv \lambda_2[0], \mu_i \equiv \mu_i[0], \bar{d} \equiv \bar{d}[0], \bar{\sigma}_i \equiv \bar{\sigma}_i[0], \bar{\gamma}_i \equiv \bar{\gamma}_i[0] \in \mathbb{R}_{>0}$ are all positive real numbers. Thus, the effective EOMs in the Markovian regime are

$$i\omega \langle a_1[\omega] \rangle = \left(-\frac{\bar{\gamma}_1}{2} + i\bar{\sigma}_1 \cos \tau_1 \right) \langle a_1[\omega] \rangle - \left(|\lambda_1| e^{-i(\tau_1 + \tau_2)} + |\lambda_2| - i \left(|\mu_1| \bar{\chi} e^{-i\tau_1} + |\mu_2| \bar{\chi} e^{-i\tau_2} - |\delta| e^{i\tau_3} \right) \right) \langle a_2[\omega] \rangle, \quad (\text{E25})$$

$$i\omega \langle a_2[\omega] \rangle = \left(-\frac{\bar{\gamma}_2}{2} + i\bar{\sigma}_2 \cos \tau_2 \right) \langle a_2[\omega] \rangle - \left(|\lambda_1| e^{i(\tau_1 + \tau_2)} + |\lambda_2| - i \left(|\mu_1| \bar{\chi} e^{i\tau_1} + |\mu_2| \bar{\chi} e^{i\tau_2} - |\delta| e^{-i\tau_3} \right) \right) \langle a_1[\omega] \rangle, \quad (\text{E26})$$

which concludes our short derivation.

c. Different scattering probabilities for the directional transistor

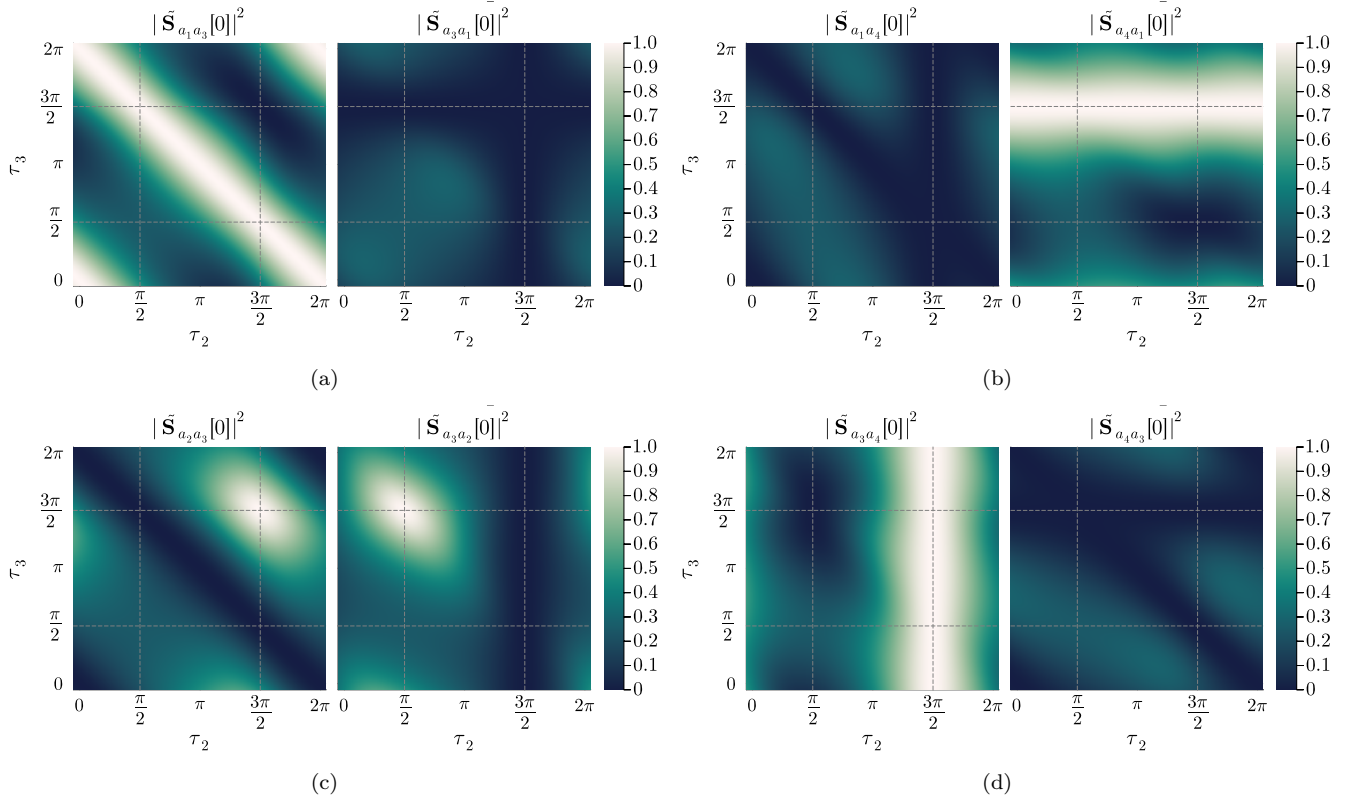


FIG. 39. Comparison between scattering probabilities of the directional transistor for $\omega = 0$, $\kappa \equiv \kappa_i/2$, a fixed phase $\tau_1 = \pi/2$, plotted against $\tau_{2,3}$. This Figure supplements Fig. 29.

d. Comparison scattering between two-ports with the noise of all ports for the directional transistor

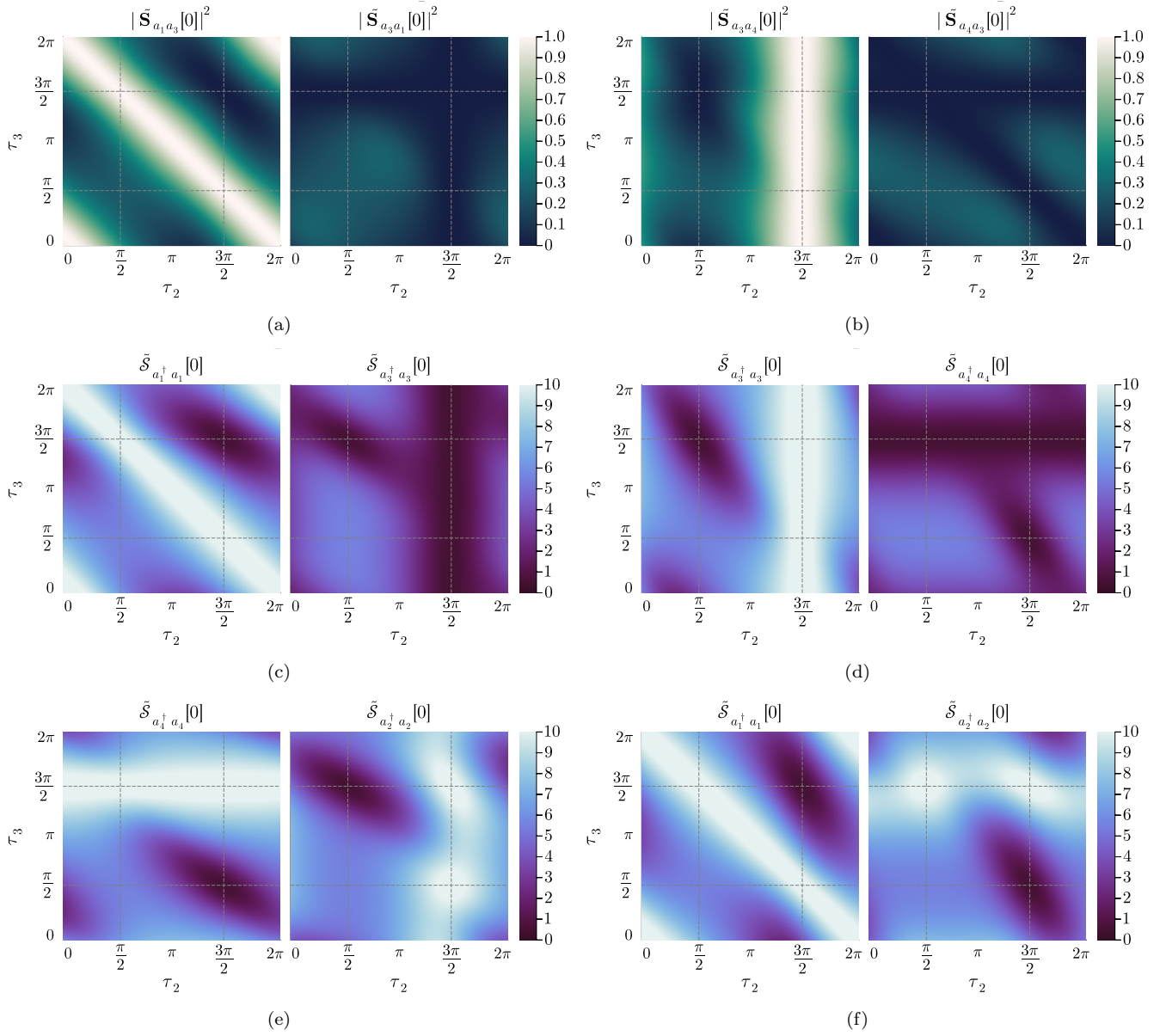
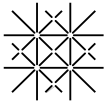


FIG. 40. Comparison between scattering probabilities and fluctuations at outputs for $\omega = 0$, $\kappa \equiv \kappa_i/2$, a fixed phase $\tau_1 = \pi/2$, plotted against $\tau_{2,3}$, with varying input-noise. This Figure shows the input $\mathbf{n}_{\text{th}} = (10, 0, 10, 0)$ in the left column, and $\mathbf{n}_{\text{th}} = (0, 0, 10, 10)$ for the right column. This Figure supplements Fig. 29.



Declaration on Scientific Integrity
(including a Declaration on Plagiarism and Fraud)
Translation from German original

Title of Thesis: Nonreciprocity and noise in few mode bosonic systems

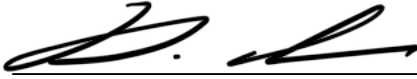
Name Assessor: Patrick Potts

Name Student: Danial Chughtai

Matriculation No.: 13-058-508

I attest with my signature that I have written this work independently and without outside help. I also attest that the information concerning the sources used in this work is true and complete in every respect. All sources that have been quoted or paraphrased have been marked accordingly.

Additionally, I affirm that any text passages written with the help of AI-supported technology are marked as such, including a reference to the AI-supported program used. This paper may be checked for plagiarism and use of AI-supported technology using the appropriate software. I understand that unethical conduct may lead to a grade of 1 or "fail" or expulsion from the study program.


Place, Date: Basel, 08.07.2024 Student: 

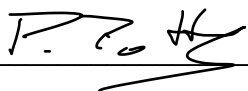
Will this work, or parts of it, be published?

No

Yes. With my signature I confirm that I agree to a publication of the work (print/digital) in the library, on the research database of the University of Basel and/or on the document server of the department. Likewise, I agree to the bibliographic reference in the catalog SLSP (Swiss Library Service Platform). (cross out as applicable)

Publication as of: _____

Place, Date: Basel, 08.07.2024 Student: 

Place, Date: Basel, 08.07.2024 Assessor: 

Please enclose a completed and signed copy of this declaration in your Bachelor's or Master's thesis.